Sheffield Hallam University

A Sheffield Hallam University thesis

2612

ProQuest Number: 10697228

ProQuest 10697228

THE INFLUENCE OF STRAIN RATE AND THE EFFECT OF FRICTION ON
THE FORGING LOAD IN SIMPLE UPSETTING AND CLOSED DIE FORGING

Francis Bland Klemz
MPhil, CEng, MIMechE

A thesis submitted to the COUNCIL FOR NATIONAL ACADEMIC
AWARDS in partial fulfilment for the degree of DOCTOR OF
PHILOSOPHY

Department of Mechanical and Production Engineering
Sheffield City Polytechnic (Sponsoring Establishment)

The Drop Forging Research Association
Sheffield S3 7BA (Collaborating Establishment)

December 1984

ACKNOWLEDGEMENTS

DECLARATION

The author declares that no part of this work has been submitted in support of another degree or qualification to this or any other establishment. The author further declares that he has not been a registered candidate or enrolled student for another award of the CNAA or other academic or professional institution during the course of the research programme.

F B Klemz

ABSTRACT

THE INFLUENCE OF STRAIN RATE AND THE EFFECT OF FRICTION
ON THE FORGING LOAD IN SIMPLE UPSETTING AND CLOSED DIE
FORGING.

F B Klemz

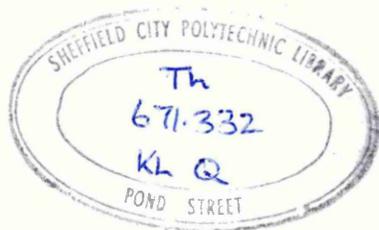Forging provides an elegant solution to the problem of
producing complicated shapes from heated metal. This study
attempts to relate some of the important parameters involved
when considering, simple upsetting, closed die forging and
extrusion forging.

A literature survey showed some of the empirical graphical
and statistical methods of load prediction together with
analytical methods of estimating load and energy. Investi-
gations of the effects of high strain rate and temperature
on the stress-strain properties of materials are also
evident.

In the present study special equipment including an
experimental drop hammer and various die-sets have been
designed and manufactured. Instrumentation to measure
load/time and displacement/time behaviour, of the deformed
metal, has been incorporated and calibrated. A high speed
camera was used to record the behaviour mode of test
pieces used in the simple upsetting tests.

Dynamic and quasi-static material properties for the
test materials, lead and aluminium alloy, were measured
using the drop hammer and a compression-test machine.

Analytically two separate mathematical solutions have been developed: A numerical technique using a lumped-mass model for the analysis of simple upsetting and closed-die forging and, for extrusion forging, an analysis which equates the shear and compression energy requirements to the work done by the forging load.

Cylindrical test pieces were used for all the experiments and both dry and lubricated test conditions were investigated. The static and dynamic tests provide data on Load, Energy and the Profile of the deformed billet. In addition for the Extrusion Forging, both single ended and double ended tests were conducted. Material dependency was also examined by a further series of tests on aluminium and copper.

Comparison of the experimental and theoretical results was made which shows clearly the effects of friction and high strain rate on load and energy requirements and the deformation mode of the billet. For the axisymmetric shapes considered, it was found that the load, energy requirement and profile could be predicted with reasonable accuracy.

CONTENTS

LIST OF FIGURES

1.1 Background

In recent years there has been an urgent need to increase the rate at which forgings can be produced in order to reduce manufacturing costs. This has led to a study of the dynamic behaviour of metals in order to exploit to the full the potential of high rate forming methods.

Manufacturers with existing forging equipment need reliable information regarding the load and energy needed to make particular forgings. It should be noted that the numerical technique, such as the finite element method and other techniques based on the upper bound method have successfully been employed to solve very complex forming processes. However these techniques require large computer facilities and are not easily accessible to everyday Engineers. Hence there would always be room for analytical solutions, for specific problems, based on simpler and easily understandable principles.

1.2 Literature Survey

1.2.1 Empirical Graphical and Statistical Methods of Load Prediction

A number of empirical methods have been formulated [1-5] to determine the forging load under dynamic conditions. However, these are applicable to a limited number of cases only.

Graphs relating the area of forging including flash to the forging load for different degrees of die complexity have been used. Examples are given in a

Drop Forging Research Association report[11].

BALOGUN[6] measured forging loads on presses to produce axisymmetric and plane strain forgings. Using multiple linear regression analysis, equations for estimating forging load were then developed.

NEUBERGER and PANNASCH[7] plotted values of mean effective yield strength vs mean height and deriving equations for the upper and lower curves which encompassed their experimental data, obtained expressions for the mean effective yield stress in terms of forging weight and forging area. They have also extended their analysis to produce nomograms for predicting load and energy requirements. Other investigators [8-10] have also compiled similar design nomograms.

In the Drop Forging Research Association report[11] on Load and Energy estimation in Forging, results calculated using Neuberger and Pannasch's[9] method were used to obtain equations for relative yield strength and forging load. The load equations were based on a multiple linear regression analysis of experimental results on completely axisymmetric for-gings with external flash. The load equation is in terms of the area of forging including flash, the ratio of the flash land width to flash land thick-ness and the mean height of the forging including flash.

1.2.2 Analytical Methods for Estimating Load and Energy

SIEBEL[12] produced an analysis for the load estimation for the free upsetting of a cylinder or prism.

SCHROEDER and WEBSTER[13] have given a more detailed analysis of free upsetting in which they recognise a limiting value for frictional resistance. Once this resistance exceeds the material yield strength they argue that deformation proceeds by internal shearing of the deformed metal.

FOSTER[14] modified SIEBEL'S[12] analysis to extend to complex forging shapes. His method is to divide the forging into sections, and having found the stress required to induce metal flow in each section, determines the value of the load in each section by integration of the stress throughout the section.

DEAN[15], in a paper discussing the effect of flash land geometry on die stresses, evolved a method of calculating forging load based on an interpretation of the Schroeder-Webster[13] analysis.

Dean assumed that, in the final stage of forging, deformation is confined to a disc whose thickness is that of the flash gap. Within the body of the forging sticking friction is assumed, whilst the conditions in the flash land are decided by calculating the radius of the sticking region. The parameters involved in Dean's equations are: radius

to the entrance to the flash, radius to which sticking extends, radius to edge of flash land, coefficient of friction, normal stress on forging section, load, flash land width and mean yield strength.

DIETRICH and ANSELL[16] have considered the forging of plane symmetrical sections. As with the Siebel-Foster[14] method the forging is divided into sections and calculations begin with the flash and proceed towards the centre. Frictional resistance is accounted for by means of a 'back-pressure' term and the extrusion effect when metal flows into a reduced section is also allowed for.

BISWAS and ROOKS[17] have adapted an original analysis by ALTAN[18] to predict forming load and energy. In analysing the forging load for axisymmetric shapes they assumed that, free upsetting, extrusion into cavities and the formation of flash occur as three discrete forming stages.

McDERMOTT[19] has extended the upper bound elemental technique first suggested by KUDO[25] to calculate forging energy. In applying the method a forging is split into a number of regions and for each region an equation is set up relating the rate of energy dissipation to the strain rate of the forging in various principal directions. By developing admissible velocity fields for metal flow, the mean

yield strength in a section can be determined, allowing load and energy to be calculated.

1.2.3 <u>Stress-Strain Properties at High Strain Rates</u>

A number of workers have attempted to derive a single equation expressing the stress in terms of strain, strain rate and temperature. LUBAHN[20] obtained such an equation containing six constants from three empirical relationships. He assumed that for large strains the true stress/strain curve could be represented by a simple power law. This assumption was supported by tensile test data obtained on a number of materials by FUSFELD[21] and by LOW and GAROFALO[22] but was in poor agreement with the results of DORN et al.[23]

ALDER and PHILLIPS[24] used a cam plastometer to produce constant true strain rates in the range 1-40 sec^{-1} during compression to 50% reduction of height on (a) commercial-purity aluminium from -190°C to 550°C, (b) phosphorus-dioxidized copper from 18°C to 900°C and (c) a 0.17% carbon steel from 930°C to 1200°C. They found that of the three materials tested only aluminium, at room temperature, had a stress strain relationship that could be represented by a power law. This power law had an index of approximately 0.2. The effect of strain rate on the stress for a given strain was better expressed by a power law than by the semi-logarithmic formula of

LUDWIK[26].

SOKOLOV[27-31] also concluded from tests on lead, tin,
zinc, aluminium, copper, nickel, brass and several
steels, over a range of strain rates from 10^{-3} to
10^2 sec^{-1} and at temperatures from 20°C to their
respective melting points, that the power law
provided a better interpretation of the effect of
strain rate. However, a number of American
workers[32-36] found from compression tests at
10^2-10^3 sec^{-1} on copper at room temperature that the
stress was proportional to the logarithm of the
strain rate for a given strain (up to 25% compression).

Other workers who have been concerned with the
effect of strain rate on the tensile properties are:
GINNS[37], ELAM[38], JONES and MOORE[39], and MANJOINE and
NADAI[40]. Nadai, working on aluminium, copper, and
steel at strain rates of 10^2-10^3 sec^{-1} and at
elevated temperatures, found that the ultimate true
stress varied approximately linearly with the
logarithm of the strain rate, in agreement with the
results of JONES and MOORE[39] on the yield strength of
fourteen metals tested at room temperature and at strain
rates up to 10^{-1} sec^{-1}.

SLATER, JOHNSON and AKU[40] derived approximate
equations to account for the compressive engineering
strain-time, dimensionless compressive engineering
strain-rate, compressive engineering strain and

7

dynamic force-time characteristics for the fast
compression of prismatic blocks of strain-
hardening, strain-rate-sensitive material using a
drop hammer. Within the limits of maximum strain
rate of 250 sec^{-1}, maximum engineering compressive
strain of 0.4 and a constant ambient temperature of
approximately 20°C experimental and theoretical
results were compared. Agreement between experi-
mental and theoretical results was found, with the
exception of the force-time relationship, where the
theoretical prediction underestimates the maximum
force by between 10 and 15 per cent. They concluded
that lead at ambient temperature was not particular-
ly strain-rate sensitive for strain rates of up to
250 sec^{-1}.

1.2.4   Use of a 'Model-Material' Technique

DANCKERT and WANHEIM[58] have used a model-material
technique in the analysis of a rotational symmetrical
forging. These results were then compared with an
actual forging made from aluminium. This technique
makes it possible to investigate the effect of
different preforms and billet sizes on:

(a) the filling capacity of the final dies

(b) the flow pattern in the final product

(c) the extent of die wear quantitatively.

They demonstrated the use of 'the plane analogy' as

a means of using the material model to get an overall idea of material flow in the dies. More accurate information about the flow pattern was obtained by way of a "three-dimensional model-material experiment" in which the model is geometrically similar to the original process. To determine the stress distribution in the dies a special rubber model technique was used. In this technique the die to be investigated is made of transparent rubber which has a grid placed in its plane of symmetry. The transparent rubber die is placed in a liquid with the same refraction index as the rubber and the forging is carried out with the billet made of wax, simulating the metal billet. The distortion of the grid that occurs during forging is recorded photographically. By measuring the displacement of the grid points during the deformation of the wax billet it is possible to calculate stress values and to locate stress concentrations in the die.

1.2.5   Extrusion Forging

JAIN, BRAMLEY, LEE and SHIRO KOBAYASHI[6] looked at the effect of friction and die hole geometry on the total height of axisymmetric extrusion forgings, for a range of billet and hole sizes. These results were then compared with theoretical

9

predictions, which were based on an assumed velocity field. They concluded that to achieve a maximum amount of rise (extrusion) and minimum load and energy, a billet with a high aspect ratio should be used in conjunction with a radiused and drafted die hole. Their analysis did not take account of the taper in the flange profile.

NEWNHAM and ROWE[62] applied a slip-line field theory analysis to the problem of compound metal flow in a simple extrusion/forging process. They tested their predictions experimentally and confirmed the transition from simple forging to rigid-core forging and hence to extrusion with forging. Their analysis also did not take account of the taper in the flange profile.

1.3 Present Work

1.3.1 Simple Upsetting and Closed Die Forging

A theoretical and experimental study of the load requirements associated with the upsetting and closed die forging of cylindrical billets, which takes into account the effects of interface friction, axial

inertia, strain rate and strain hardening properties of the material, was made.

A theoretical analysis has been developed based on a numerical technique which enables the billet profile, the tup load and velocity to be determined at any stage during the in-process time. The stress and strain-time history at any point within the billet can also be determined. This method uses a lumped mass model for the actual cylindrical billet. Each mass was considered in turn and the associated dynamic force equilibrium equation was expressed in finite difference form. This related the displacement of each mass to the strain in the corresponding link after each time increment. The stress in each link, and hence the axial force, was then calculated from the material stress strain characteristics.

Various dies, to enable axisymmetrical shapes to be formed from lead cylinders, were made. These dies allow for radial expansion only and no provision was made for flash. Split dies were used for the more complicated shapes.

For the simple upsetting tests high speed photo-graphs were taken of the billet as it was deformed. A Hi-cam high speed camera working at 2400 frames per second was used. The processed film was then projected on to a screen using a 16 mm cine-

projector with single frame movement facilities and analysed for instantaneous profiles and tup-displacement-time curves.

For the upsetting tests only, tests were also carried out on aluminium alloy billets heated to forging temperature.

1.3.2   Extrusion/Forging

As the flow of metal in this process is only partially radial the lumped-mass method outlined in Chapter 3 was found to be inapplicable and a different theoretical approach was developed. This approach considers the plastic work done in compression together with the work done in radial and circumferential shear. By equating the forces involved and assuming that the material deforms in a mode associated with the least work done, the shape of the profile during deformation can be predicted.

Dies with three different extrusion ratios were manufactured for experimental work in order to check the extrusion/forging theory. The majority of tests were carried out using lead billets. A few tests on aluminium and copper billets were also carried out to check for material dependency. Double-ended extrusion tests were also carried out using lead and copper billets.

A drop hammer was designed specifically for the

experimental work associated with this study. Its

energy capacity enables lead billets to be

deformed easily. The fact that lead is hot-worked at

temperature means that it can be used to simulate

the behaviour of other stronger materials that need

to be heated to a suitable hot working temperature.

The drop hammer incorporates instrumentation which

enables load/time and displacement time behaviour

to be measured and recorded.

13

CHAPTER 2

EXPERIMENTAL EQUIPMENT, INSTRUMENTATION

AND BILLET MATERIAL PROPERTIES

2.1 Equipment

2.1.1 Drop Hammer

The drop hammer frame was made from 80 x 80 x 10 mm angle iron and is of welded construction. See Fig. 1.

The framework provides the upper support for the tup guide rails, and support for a motorised hoist which is used to raise the tup to the required height. A cord release mechanism allows the tup to be separated from its lifting cradle. The tup (see Fig. 2 and 3) has a mass of 15.64 kg with a maximum free fall height of 4.32 m. This is equivalent to a maximum impact velocity of 9.2 m/sec.

At the base of the drop hammer an inner framework made from 50 x 50 x 6 mm angle iron is used to contain the load cell unit and to provide support for the tup guide rails. The load cell housing is encased in concrete to provide an additional mass of material to absorb the shock load which occurs at impact.

In the interest of safety the lower 1 m of the drop hammer framework is encased in 3 mm thick duralumin plate. The remainder of the framework is encased in 25 x 25 mm wire mesh. Access for the removal of test pieces is by means of a hinged door which is pivoted in such a way that when in the open position

15

it will arrest the tup should it fall accidentally.

2.1.2 Displacement Measurement

The displacement/time behaviour of the material
under test is measured using infra red light beams
which are activated by means of a grid attached to
the drop hammer tup (see Fig. 4). A complete
layout of the instrumentation is shown in a photo-
graph (Fig. 5).

2.2 Instrumentation

2.2.1 Load Cell

A schematic block diagram of the load cell instru-
mentation is shown in Fig. 6. The signal from the
load cell is fed into a Mini-balance and a Mini-
amplifier unit, the strain gauges being activated
by a 5 volt d.c. supply. The signal from the strain
gauge is balanced so that its output will be zero
at zero load.

Because the output voltage from the load cell was in
milli-volts a Mini-amplifier was used to increase
the signal strength by a gain of 200. This
amplified signal was then fed to a Digital storage
Oscilloscope OS4040. Later this stored signal was
used to produce a load time trace on an X,Y plotter.
The digital storage oscilloscope was also used to
record and display simultaneously the signals from

the infra-red switch unit.

2.2.2 Calibration of Load Cell

Before the load cell was assembled, in the base of
the drop hammer, it was calibrated using a 500 kN
Denison Tensile testing machine. The calibration
curve is shown in Fig. 7.

A further calibration was necessary when all the
instrumentation was in place and a series of tests
with the drop hammer were to be made. The
calibration took the following form:

(a) The load-cell was disconnected

(b) A known voltage of 0.5 mV was applied to the
    load cell input terminals

(c) The resulting display on the oscilloscope was
    copied using the XY plotter (see Fig. 8).

The 'step' on the XY plotter print out is equivalent
to 65.57 kN (Fig. 8). The size of the step can be
changed by altering the 'Y' axis settings on either
the oscilloscope or XY plotter. (A large 'step'
size was used when low impact forces were measured.)

The 0.5 mV output from the load cell was amplified
200 times. With the digital storage oscilloscope
set to display a step of 1 cm per 20 mV a 'step' of
50 mm would have been obtained if there were no
errors in the instrumentation.

2.2.3 Infra-Red Switch Unit

The velocity of the falling tup just before impact was obtained by an electronic counter which was activated and stopped by an infra-red switch unit. See Fig. 4. The signals were generated from the switch unit by interrupting the passage of light passing between two light emitting and light sensitive heads, the interrupting device being a strip of clear plastic sheet on which there had been drawn a series of equally spaced black, parallel, horizontal lines of equal thickness.

This switch was also used to trigger the displacement/time display on the Digital storage oscilloscope OS4040, together with the load time display. A ten per cent pre-trigger was used.

Copies of the load/time, displacement/time traces were obtained from an XY plotter which had been connected directly to the digital storage oscilloscope.

2.3 Load and Displacement Recordings

2.3.1 Load Recordings

A typical load/time trace is shown in Fig. 9. It is possible to read off values of load and time direct from this trace (see page 31)

2.3.2   Displacement Recordings

For each test using the drop hammer three traces are required, see Fig. 10.

Fig. 10(a) is obtained by lowering the tup gently on to the test piece and the resulting trace provides a datum which indicates the point of impact.

Fig. 10(b) shows how the tup decelerates as the metal is deformed.

Fig. 10(c) is obtained by lowering the tup gently on to the deformed test piece. Its function is to identify the total extent of deformation and will show clearly if there has been any rebound incorporated in Fig. 10(b).

Fig. 10(b) is used to provide displacement/time data from which the deceleration of the tup can be calculated. Since the mass of the tup is known the associated force (which is the forging force) can be calculated simply as the product of the deceleration and the mass of the tup.

2.4   Determination of Material Properties

2.4.1   Quasi-Static Tests

The true stress/log strain relationships for the lead used to produce all the test pieces for this study were obtained using a Denison testing machine for

the static tests, and an Experimental Drop Hammer
for the dynamic tests. The test pieces were cyl-
inders 24 mm ± 0.13 mm diameter and 24 mm ± 0.13 mm
high. In each case a paste of graphite in
petroleum jelly was used to lubricate the surfaces
in contact to reduce barrelling of the specimen.

In the quasi static test the Denison testing
machine was set to compress the test piece at its
slowest rate, a constant speed of 3.5 mm/min. The
test was interrupted at each true strain interval of
0.1 in order that the surfaces in contact could be
relubricated. Results from three identical tests
were averaged.

2.4.2 Dynamic Tests

For the complete deformation to occur at a constant
strain rate, using a drop hammer, it would be
necessary for the ratio, tup velocity/height of test
piece, to be constant. In practice the strain rate
will usually decrease as the deformation progresses.
To allow for this only the initial 10% of data
associated with a particular load/time, displacement/
time output was used to calculate strain rate. By
altering the height through which the tup had to
fall the impact velocity was accurately controlled.
By precompressing the test piece to the required
thickness a strain rate could be applied to the test
piece where its initial strain condition was known.

In this way successive steps were used to obtain stress/strain data at constant strain rate.

A computer program   was used to help analyse load/time and displacement/time data.

The relationship between stress and strain for different strain rates is shown in Fig. 11. These curves, based on experimental results were found to fit closely the strain rate sensitivity equation

$$\sigma = \sigma_1[1 + (\frac{\dot{e} + \dot{e}_1}{D})^{\frac{1}{p}}]$$

where σ is the dynamic flow stress corresponding to strain rates $\dot{e}$ of up to 500 per second and σ_1 is the flow stress corresponding to strain rate $\dot{e}_1$ equal to 1 per second. The constants of strain rate sensitivity D and p were found to be $1000s^{-1}$ and 0.65 respectively.

2.4.3   Quasi-static tests on lead and idealised diagram
From the quasi-statically obtained stress-strain characteristics shown in Fig. 11 it was found reasonable to assume that for direct comparison with quasi-static tests, the lead billets behaved as a bilinearly elastic-perfectly plastic material with a constant flow stress of 17 N/mm^2, after a strain of about 14%. This is shown in Fig. 12 and was incorporated in the numerical technique. For the

extrusion forging analysis outlined in Chapter 6
lead billets were assumed to be rigid-perfectly
plastic with a yield stress of 17 N/mm^2.

2.4.4   Quasi-Static Tests on Aluminium Alloy and Idealised
Diagram

The diagram shown in Fig. 13 was also obtained from
quasi-static tests. In its idealised form it is
suitable for analysis involving the finite difference
numerical techniques used in this study.

ARRANGEMENT OF DROP HAMMER

EXISTING STEELWORK

MOTORISED HOIST

TUP

FABRICATED MAIN FRAME

CORD ATTACHED TO

RELEASE MECHANISM

WIRE MESH

HINGED DOOR

LOAD CELL

FIG. 1.

23

LIFTING COLLAR

STEEL TUBE 100mm DIA.
LEAD FILLED

BRACKET USED TO
SECURE DISPLACEMENT
MEASURING GRID

GUIDES SET AT 300 mm.

DROP HAMMER TUP

FIG. 2

24

FIG. 3

25

STAND CARRYING

INFRA-RED

SWITCHES

TUP

GRID
(Black lines on
clear plastic)

TEST PIECE

BASE OF DROP
HAMMER
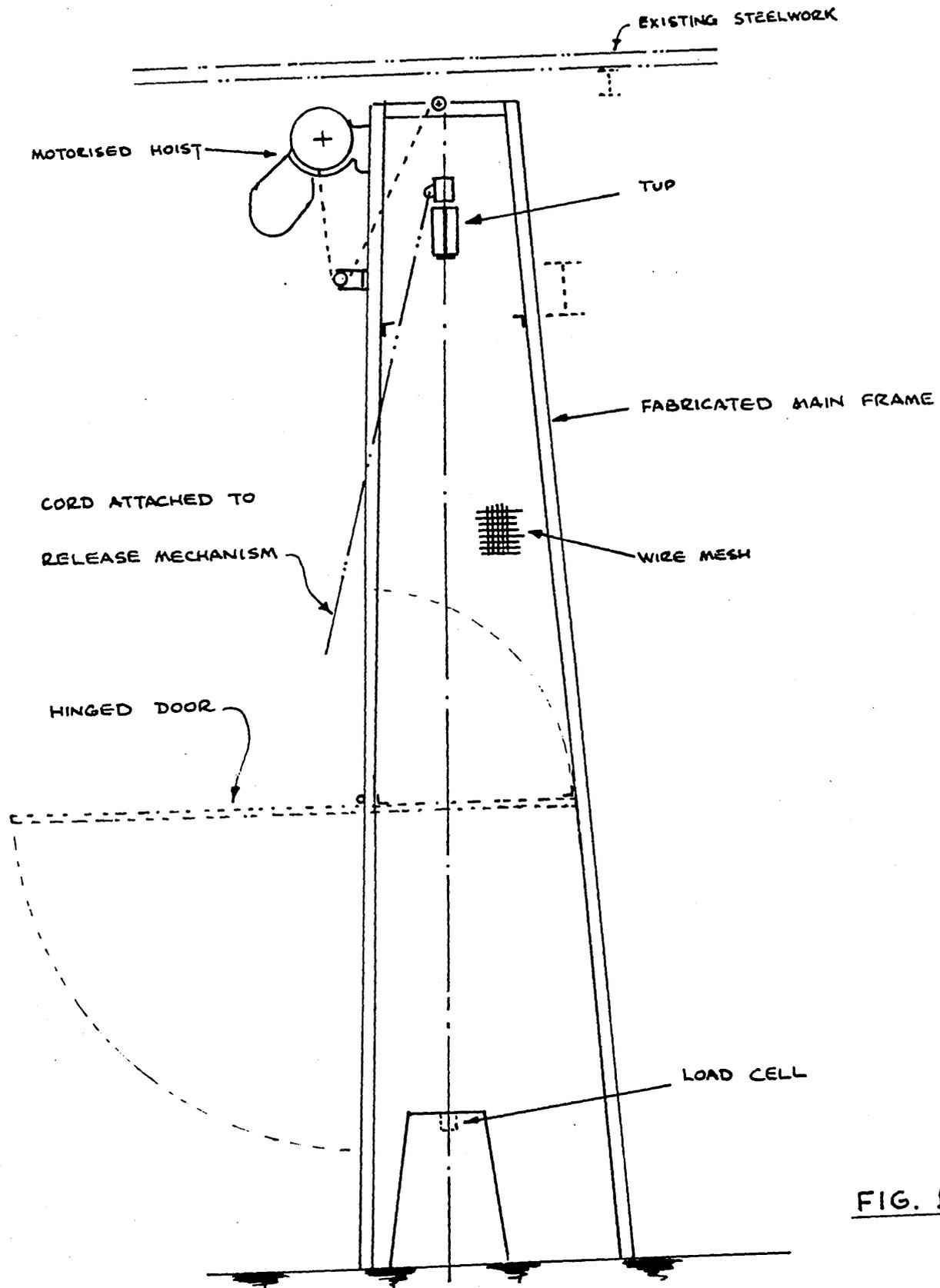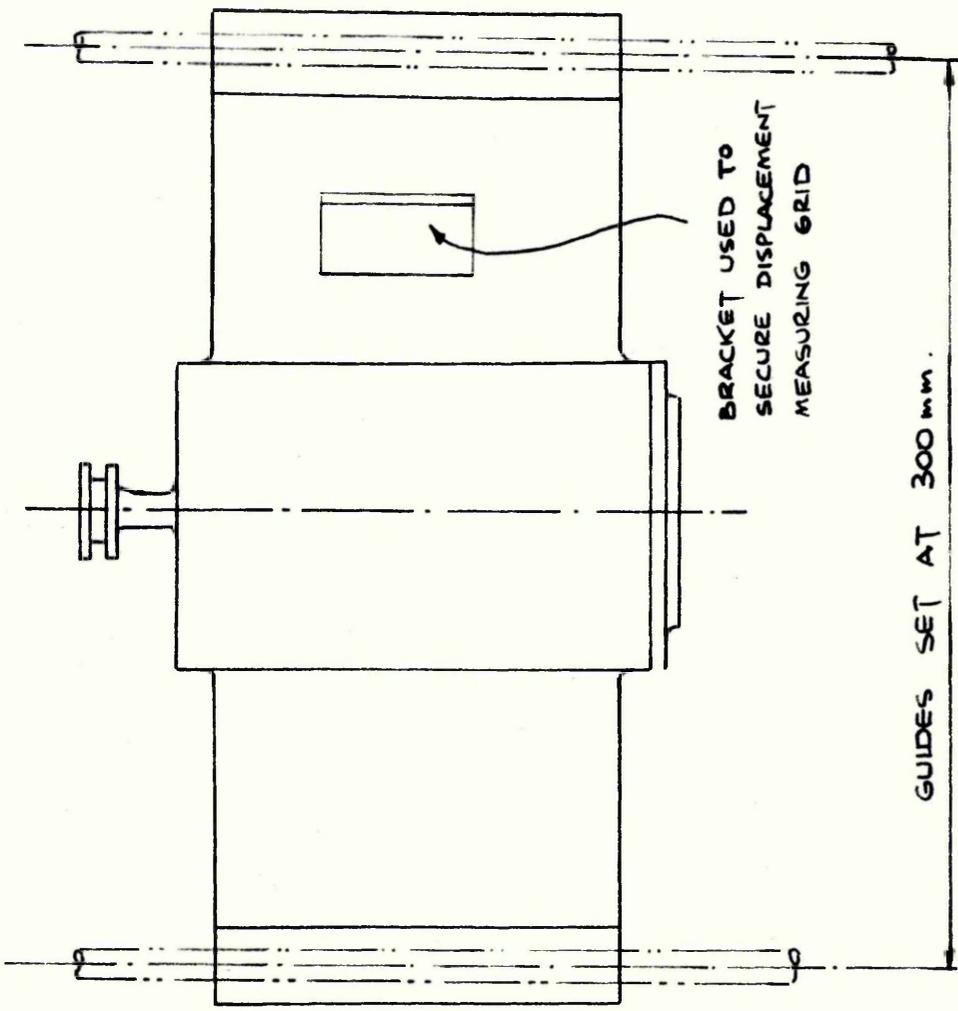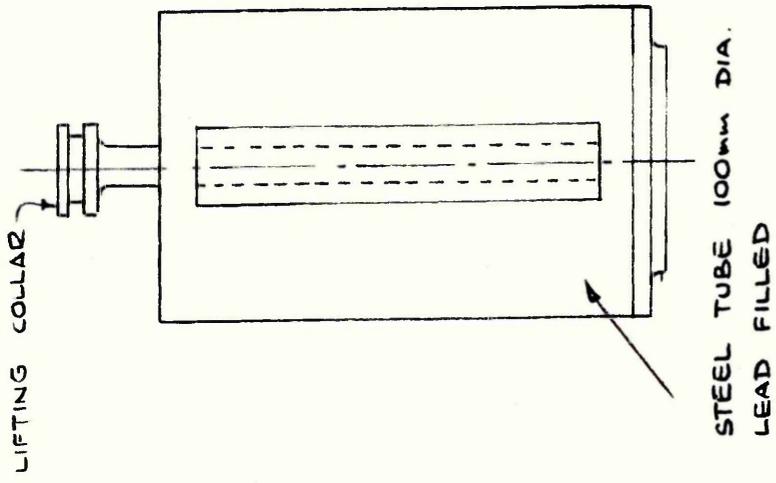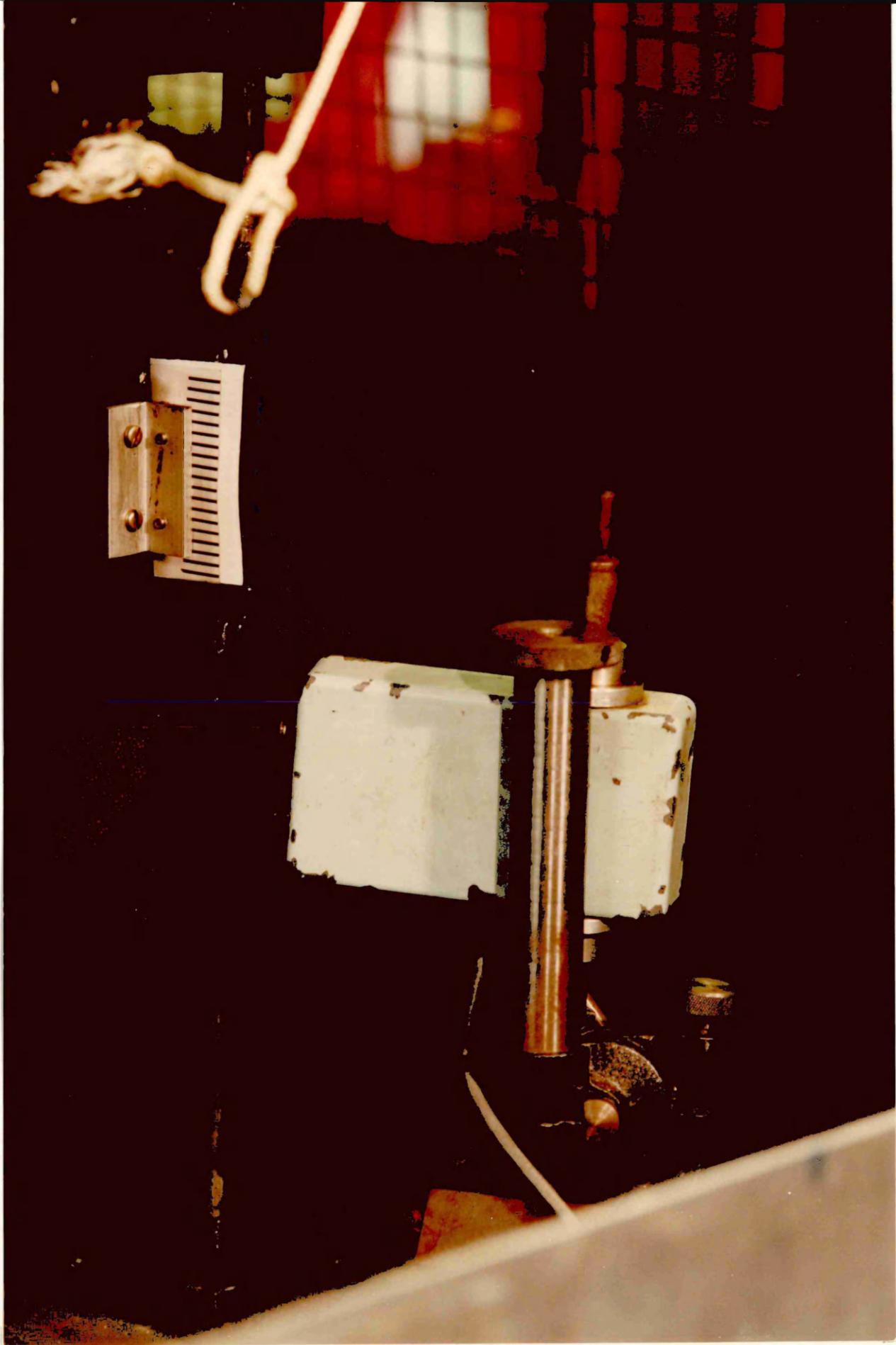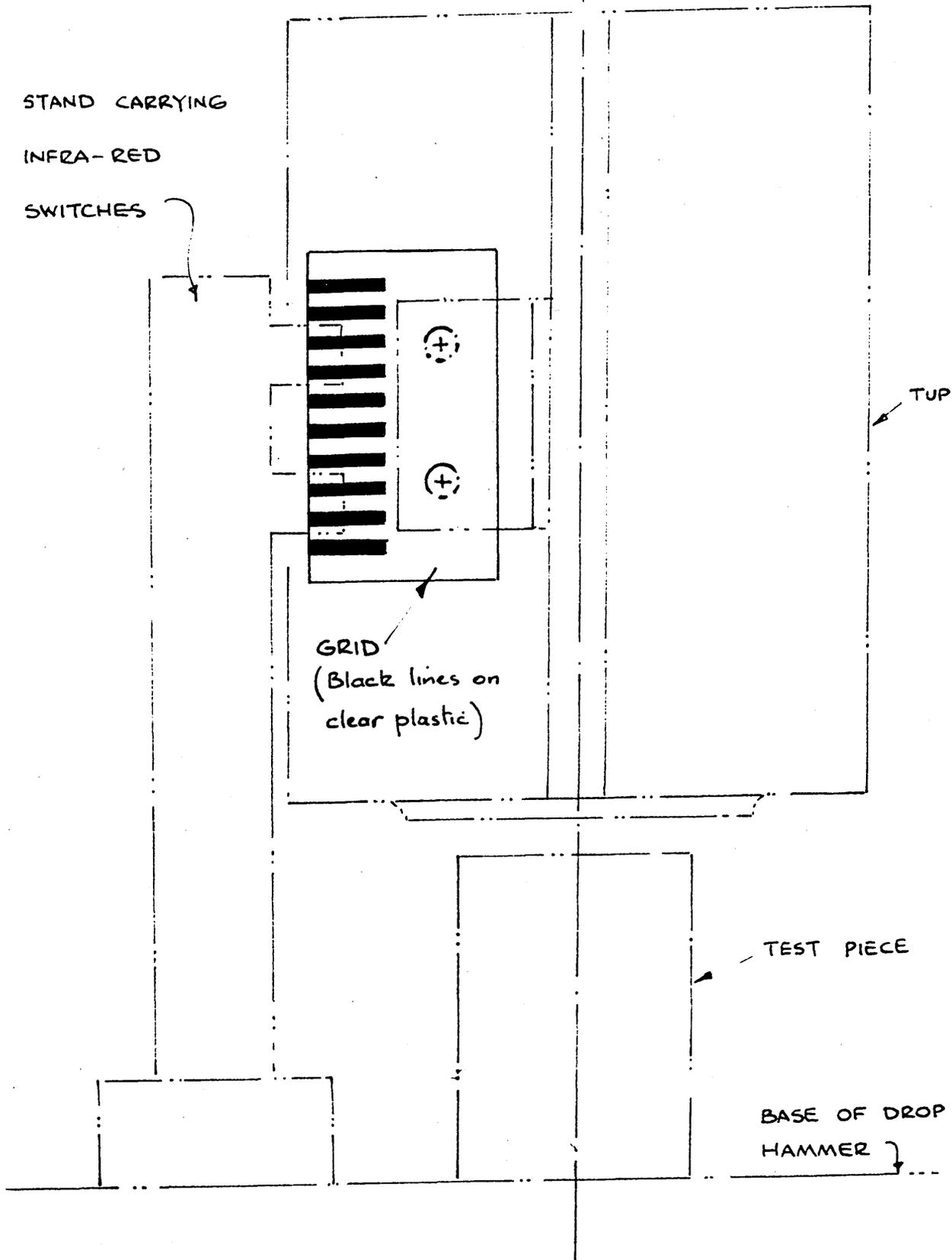
MEASUREMENT OF DEFORMATION

FIG. 4

26

FIG. 5

27
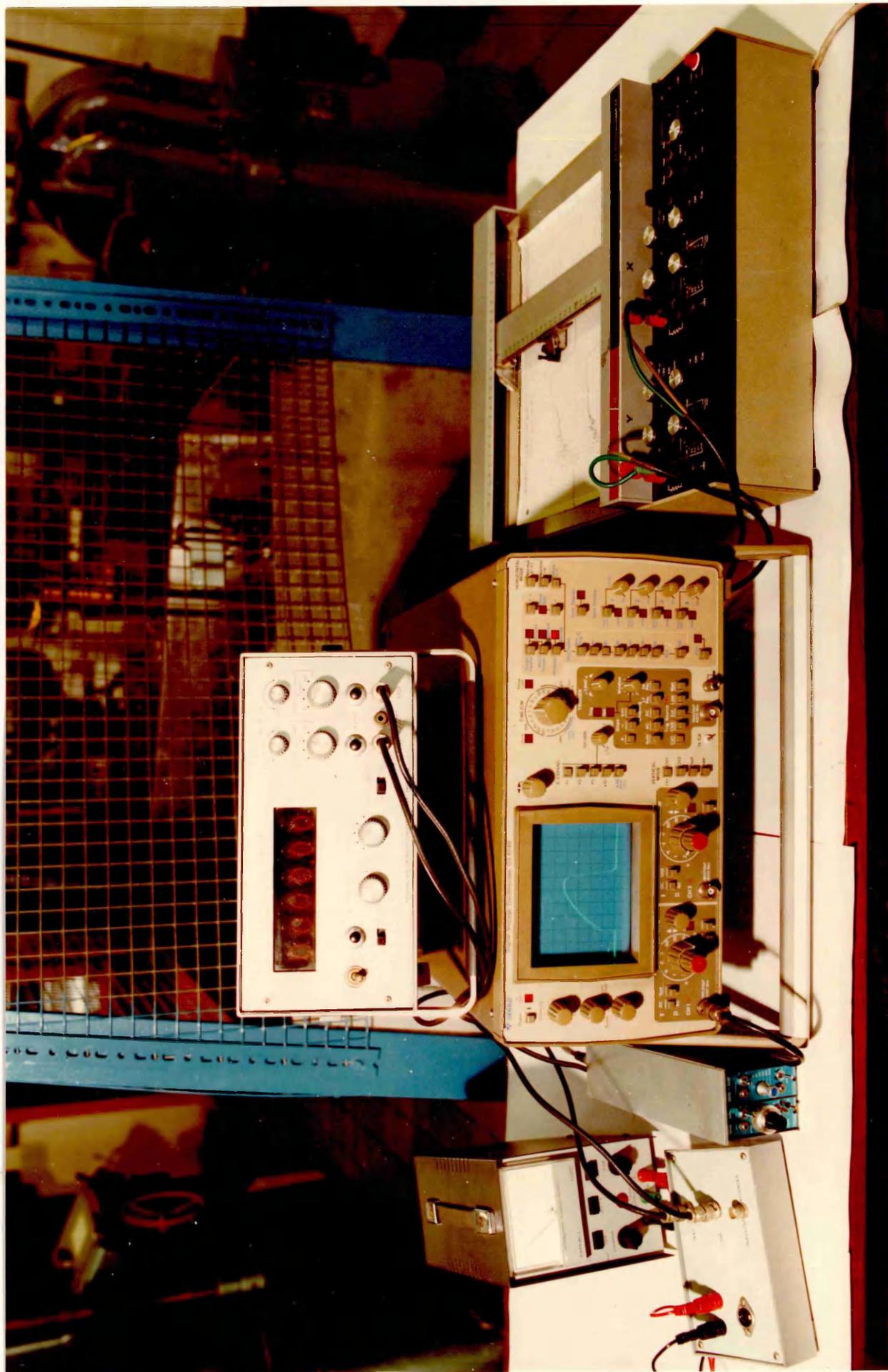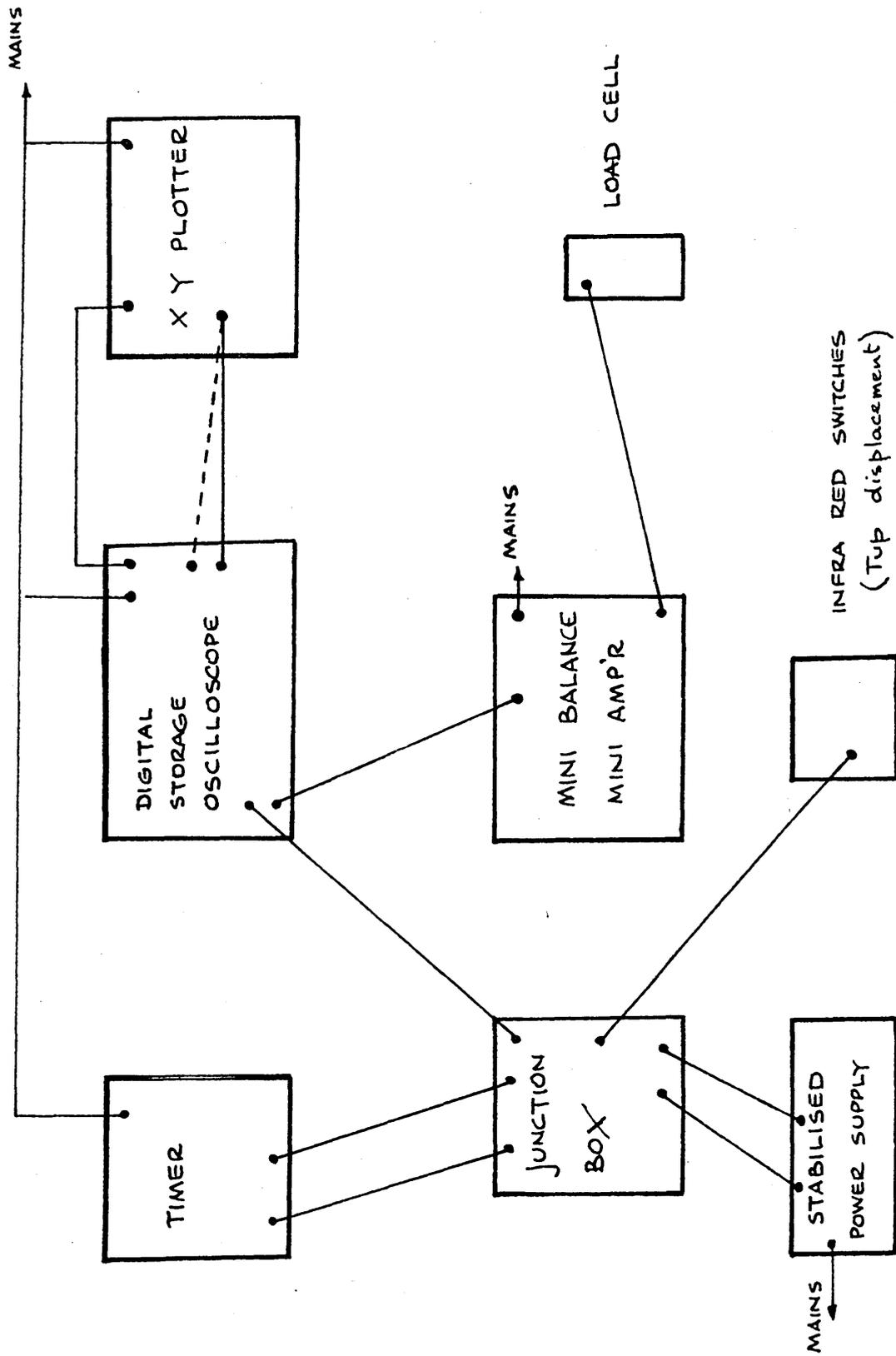
SCHEMATIC BLOCK DIAGRAM OF INSTRUMENTATION

FIG. 6

28

OUTPUT FROM LOAD CELL IN mVolts.

DEAD LOAD kN.

$1mV \equiv 133kN$

CALIBRATION OF LOAD CELL   FIG. 7

29

52 mm DISPLACEMENT EQUIVALENT TO 65.8 kN

10 m seconds
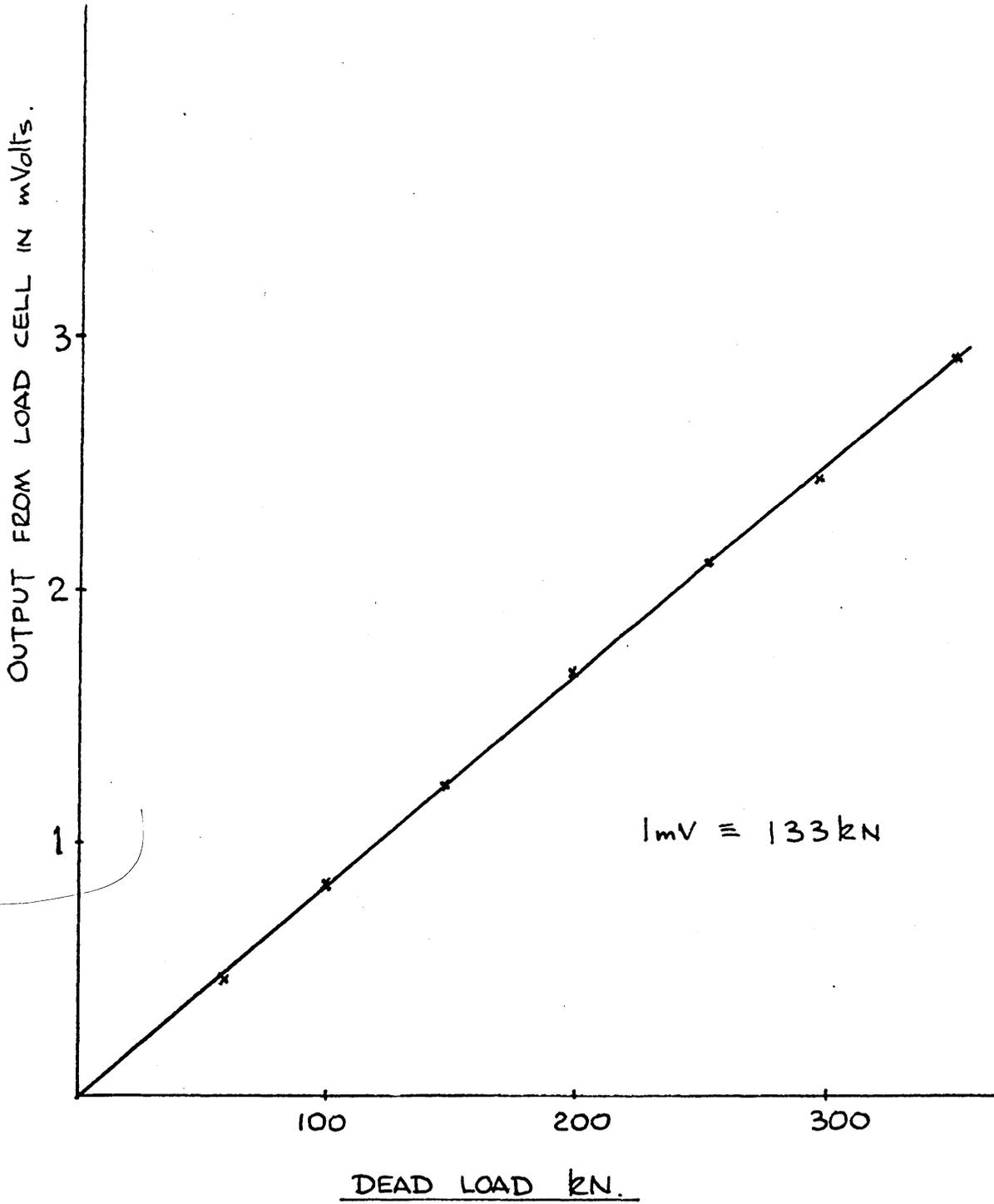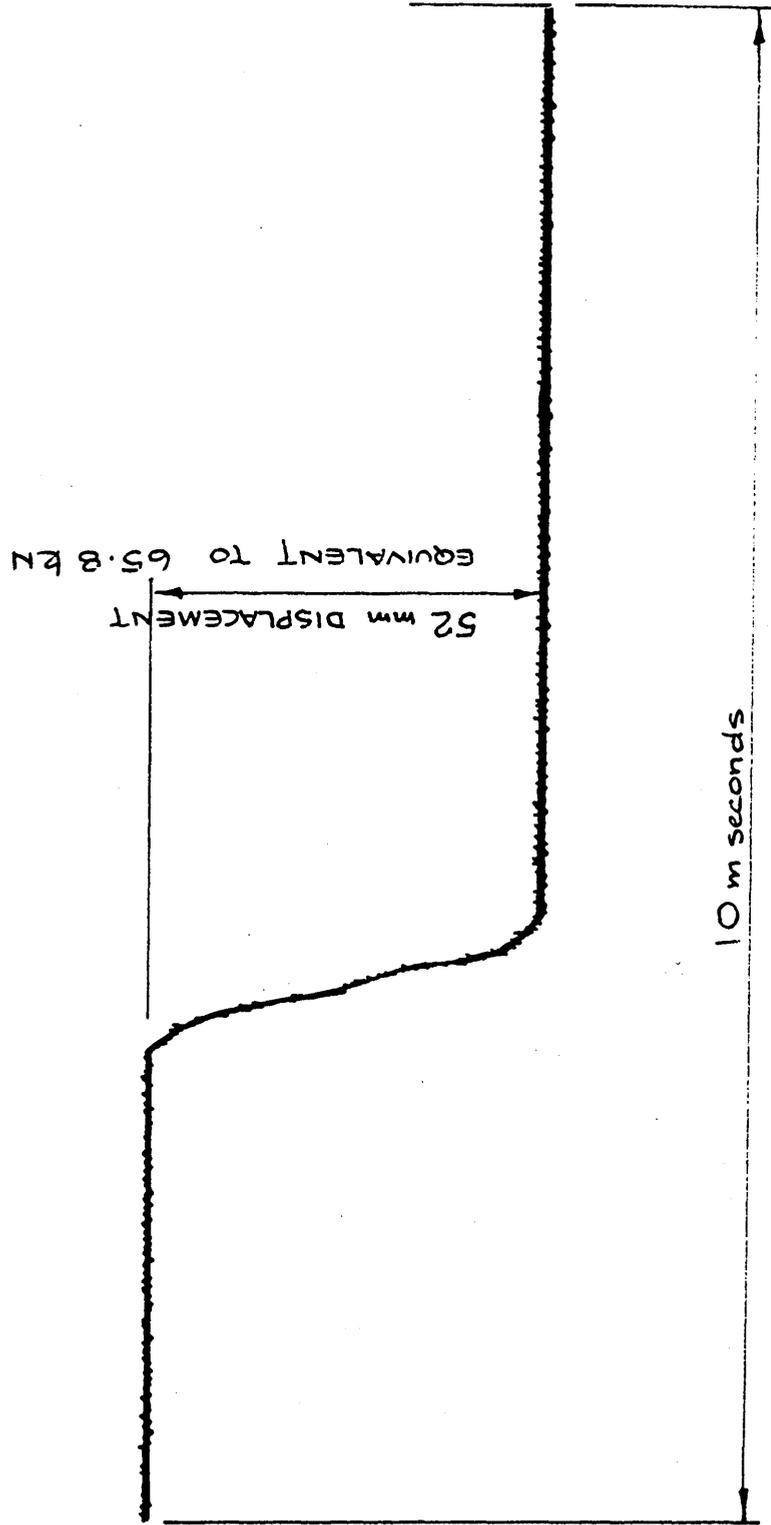
CALIBRATION OF INSTRUMENTATION USED TO MEASURE LOAD.

FIG. 8.

30

3.8 msec
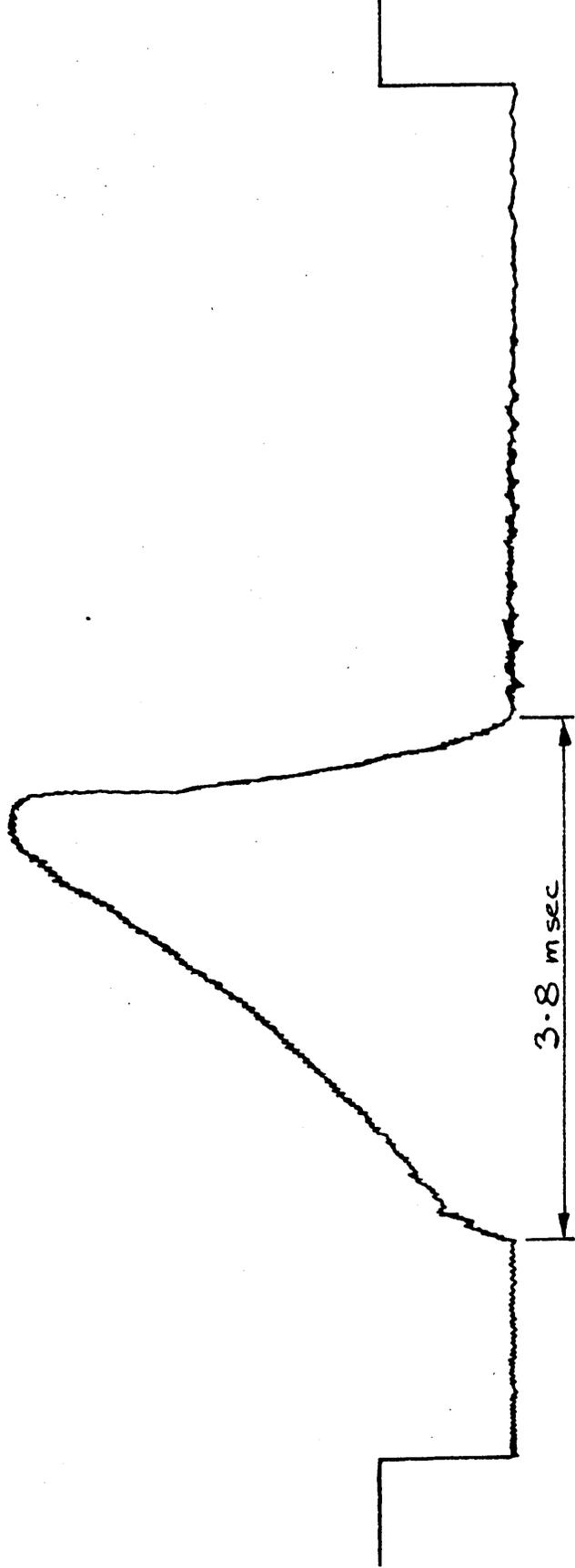
TYPICAL LOAD-TIME TRACE

FIG. 9.

31

DATUM (Before impact)

POINT OF IMPACT

FIG. 10(a)

DROP PLUS REBOUND

REBOUND

DEFORMATION

FIG. 10(b)

32

DATUM (After impact)

DEFORMATION

10 msec

FIG. 10(c)

DISPLACEMENT RECORDINGS.

FIG. 10

$$\sigma = \sigma_1 \left[1 + \left(\frac{\dot{e} + \dot{e}_1}{D} \right)^{\frac{1}{P}} \right]$$

$\dot{e} = 500 \ s^{-1}$

$\dot{e} = 250 \ s^{-1}$

$\dot{e} = 1 \ sec^{-1}$

static

STRESS, σ N/mm^2
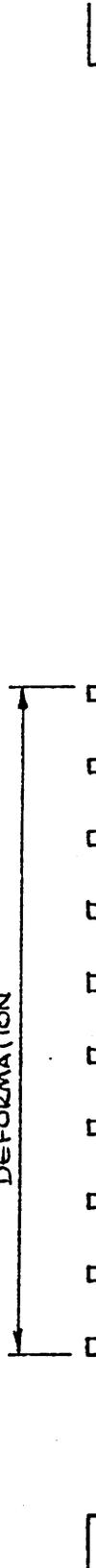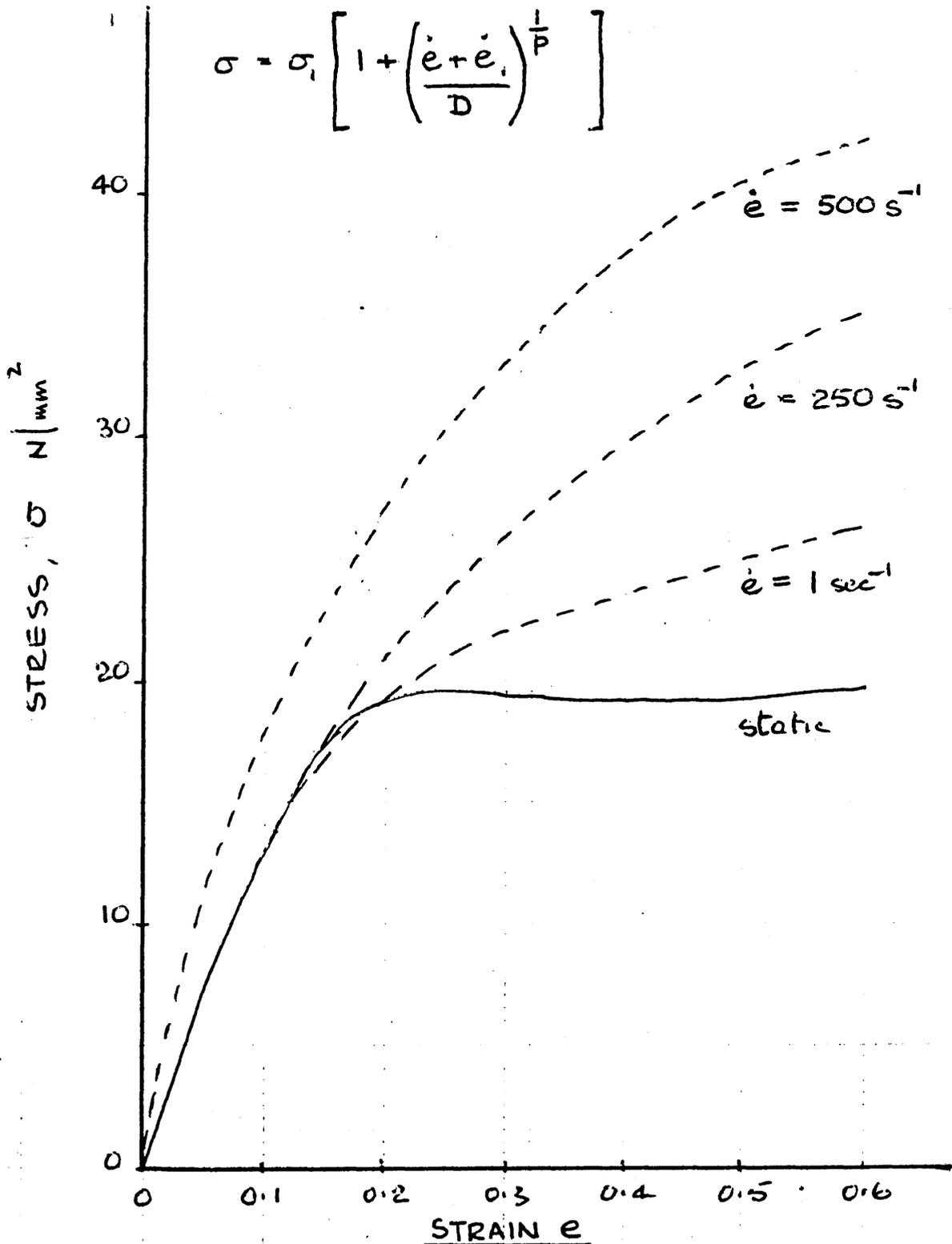
STRAIN e

STRESS STRAIN RESULTS FOR DIFFERENT STRAIN RATES

FIG. 11   33
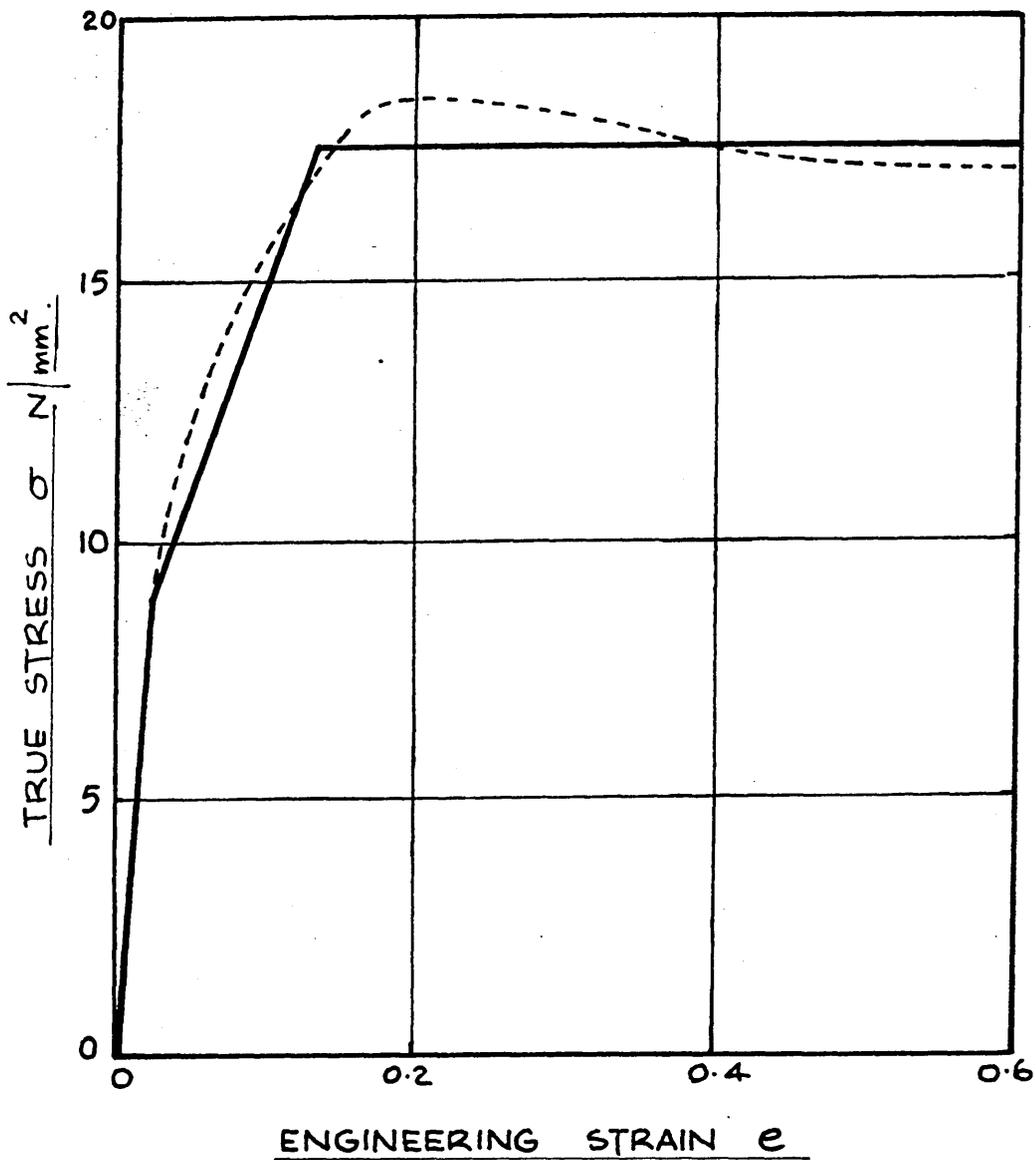
STRESS — STRAIN CHARACTERISTICS FOR LEAD.

FIG. 12.

34
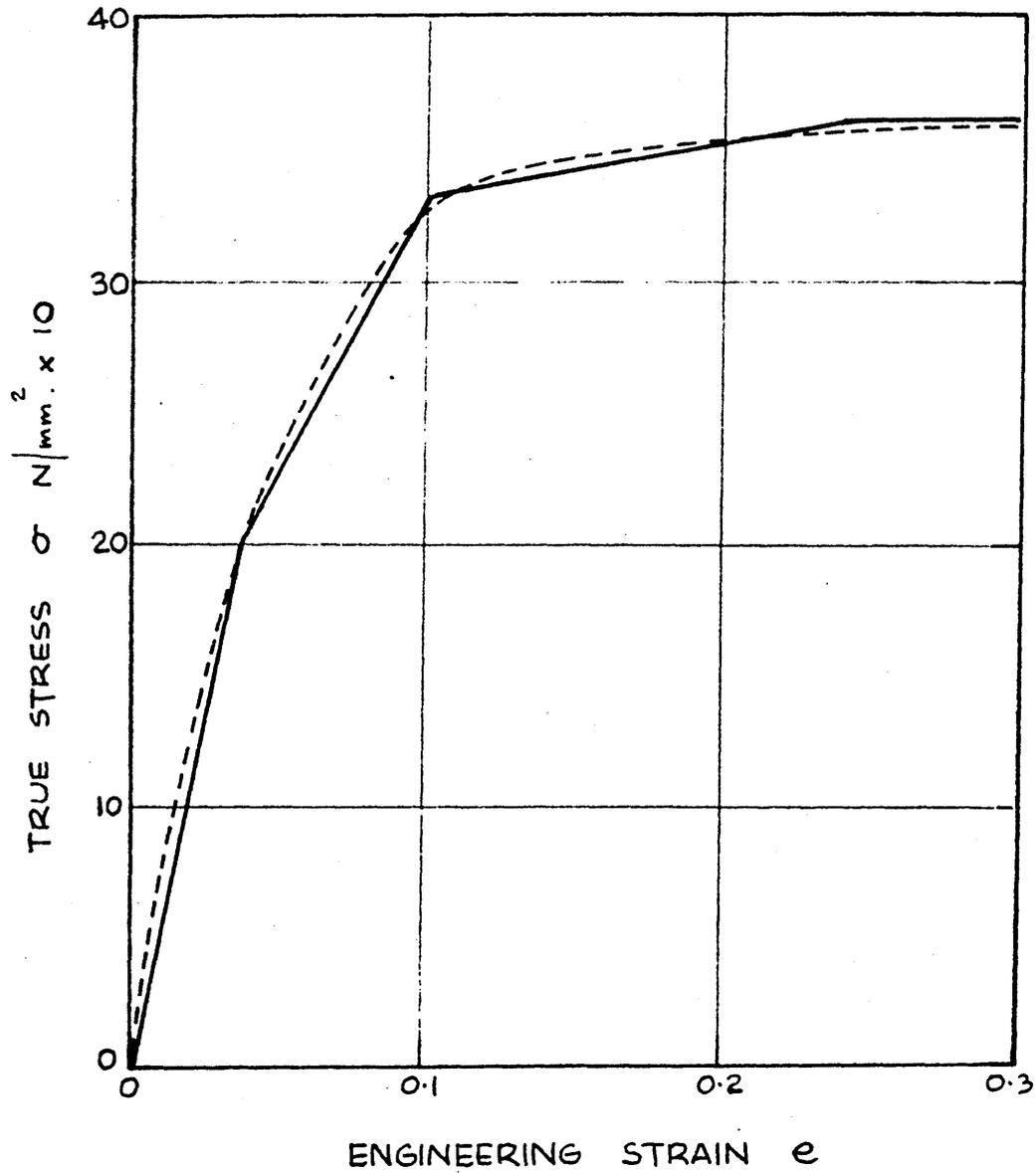
STRESS-STRAIN CHARACTERISTICS FOR ALUMINIUM ALLOY.

FIG. 13

35

CHAPTER 3

ANALYSIS USING A NUMERICAL TECHNIQUE

3.1 Introduction

In order to study theoretically the deformation mode and hence assess the influence of friction, material inertia, and strain rate sensitivity on the forging load in simple upsetting, a numerical technique has been employed. From this the billet profile, the tup load and velocity can be determined at any stage during the in-process time associated with the simple upsetting of cylindrical billets. The stress and strain time history at any point within the billet can also be determined.

3.2 The Numerical Technique

In this technique a lumped-mass model is used for the actual billet and is based on the following assumptions:

(a) The billet is made up of a number of concentrated connected masses connected to each other by massless links of circular cross section which possess the same strength properties as the material of the billet.

(b) The plane sections remain plane throughout the deformation process.

(c) Uniform axial straining occurs within each individual link.

(d) The frictional stress in the billet-tup interface is proportional to the normal stress in the face of the billet.

37

(e) The radial expansion for each connecting link is
      governed by the condition of volume constancy.

(f) There is no resistance to radial expansion of
      any link from the neighbouring link except for the
      links in contact with the top and bottom platens
      in which case interface frictional force resists
      radial expansion.

The procedure amounts to expressing the dynamic force
equilibrium equations for each concentrated mass point
in finite-difference form and relating the displace-
ment of each mass point to the strain in the corres-
ponding link after each time increment. The stress
in each link, and hence the axial force, is then
determined from the material stress-strain
characteristics.

SYMBOLS

A   annular area in the cross-section model

D   material strain-rate constant

E   elastic modulus

N   axial force

P   material strain rate constant

R   current billet radius

m   mass per unit length

Δs link length in the numerical model

Δt time increment

u,v   displacement

x,y   co-ordinate axis

ε   engineering strain

σ   stress

Subscripts

i   this refers to the mass point number and the
    preceeding link

j   time position

l   refers to the subannulus number

r   refers to the annulus number

Superscripts

m   modified value

t   trial value

(·) single differentiation with respect to time

(¨) double differentiation with respect to time

The general equation of motion for an element of the
billet, soon after the tup strikes the top face, can
be derived by considering the internal forces acting
on the element as shown in Fig. 14(a) and is given by

$$\frac{\delta N}{\delta s} - m\ddot{u} = 0 \makebox[3cm]{\hrulefill}(1)$$

Fig. 14(b) shows the lumped parameter model for a
number of elemental lengths of the billet shown in
Fig. 14(a). For convenience each elemental length Δs
will be considered to consist of one concentrated mass
and a massless link and initially all elemental
lengths to be equal. This model replaces the actual
billet by a mass-link system. Under the action of the

internal and inertia forces the position of each
concentrated mass in the model identifies the
position of a corresponding elemental length of the
actual billet. The finite-difference equation for
the elemental length at the ith location of the model
in Fig. 14(b) is given by

$$N_{i+1,j} - N_{i,j} - \Delta s_o m.\ddot{u}_{ij} = 0 \quad\text{——————(2)}$$

Equation (2) applies to all the elemental lengths
along the billet and gives the instantaneous value of
the acceleration $\ddot{u}_{i,j+1}$ for any instant of time t_{j+1}.

Using finite difference notation the relation between
displacement and time takes the form shown in Fig. 15.

$$\ddot{u}_{ij} = \frac{1}{\delta t}[(\frac{u_{i,j+1} - u_j}{\delta t}) - (\frac{u_{ij} - u_{i,j-1}}{\delta t})]$$

$$u_{ij+1} = \ddot{u}_{ij}(\delta t)^2 + 2u_{ij} - u_{ij-1} \quad\text{——————(3)}$$

where $\delta t = t_{j+1} - t_j$ ——————————————(4)

When equation (2) is combined with equation (3)
instantaneous values of $u_{i,j+1}$ for any instant of time
t_{j+1} can be determined.

In order to facilitate the calculation of stress which
may vary across the cross section of the billet, it is
necessary to idealise the actual cross section to an
equivalent cross section model which consists of a
number of annuli across each of which the stress is

40

assumed to be uniform. The circular cross section of
the billet is assumed to consist of n discrete annuli
of material which can carry normal stresses. These
annuli are considered to be separated by a material
which can not carry any normal stress but has infinite
shear rigidity.

With this simplified model the stress in the billet
can be defined by the individual normal stresses at the
n separate annuli without having to contravene the
assumption that plane sections remain plane throughout
the deformation process. The cross sectional area of
each tubular layer can be calculated by equating the
fully plastic pure axial load carrying ability, with
that of the actual cross section of the billet. A
typical cross section model is shown in Fig. 17.

In order to describe the elastic-plastic stress state
in an annulus of the section-model, further idealisation
is made and each annulus is assumed to consist of
subannuli the number of which is determined by the
number of positive sloped sides in the approximated
polygonal stress-strain diagram shown in Fig. 18.

Fig. 19 is used in establishing a relationship between
subannular area and its parent annular area

Assume that the deformation has reached stage B, ie
sublayer $A_{r(\ell-1)}$ is loaded elastically to the
condition $\sigma_1 \epsilon_1$ and the remaining subannular areas are

loaded to the condition $\sigma_2\varepsilon_2$.

The stress σ_B is the hypothetical stress that the **subannular** area A_{rl} would have to be subjected to if it were stressed elastically to a strain value of ε_2. σ_C is similarly related to ε_3 for the subannular area $A_{r(1+1)}$.

Equating forces   NOTE: $A_r = A_{r(l-1)} + A_{rl} + A_{r(l+1)}$

$$\sigma_2 A_r = A_{(1-1)r}\sigma_1 + A_{1r}\sigma_B + A_{(1+1)r}\sigma_B \text{ ————————(5)}$$

$$= A_{(1-1)r}\sigma_1 + \sigma_B(A_{1r} + A_{(1+1)r})$$

$$= A_{(1-1)r}\sigma_1 + \sigma_B(A_r - A_{(1-1)r})$$

$$= A_{(1-1)r}\sigma_1 + \sigma_B A_r - \sigma_B A_{(1-1)r}$$

$$A_r(\sigma_2 - \sigma_B) = A_{(1-1)r}(\sigma_1 - \sigma_B)$$

$$A_{(1-1)r} = A_r\frac{(\sigma_2 - \sigma_B)}{(\sigma_1 - \sigma_B)}$$

$$= A_r\frac{(\sigma_B - \sigma_2)}{(\sigma_B - \sigma_1)}$$

If the slope of OA $= E_1 = \dfrac{\sigma_1}{\varepsilon_1} = E = $ Young's modulus

and the slope of AB $= E_2 = \dfrac{\sigma_2 - \sigma_1}{\varepsilon_2 - \varepsilon_1}$

and the slope of BC $= E_3 = \dfrac{\sigma_3 - \sigma_2}{\varepsilon_3 - \varepsilon_2}$

then

$$A_{r(1-1)} = A_r \left[\frac{(\varepsilon_2-\varepsilon_1)(E-E_2)}{E(\varepsilon_2-\varepsilon_1)} \right]$$

$$= \frac{A_r}{E}[E - E_2] \underline{\hspace{4cm}} (6)$$

Assume deformation has reached Stage C.

Equating forces

$$\sigma_3 A_r = A_{(1-1)r}\sigma_1 + A_{1r}\sigma_B + A_{(1+1)r}\sigma_C \underline{\hspace{2cm}} (7)$$

combining equations (5) and (6)

$$\sigma_3 A_r = \sigma_2 A_r - A_{(1+1)r}\sigma_B + A_{(1+1)r}\sigma_C$$

$$A_r(\sigma_3-\sigma_2) = A_{(1+1)r}(\sigma_C-\sigma_B)$$

$$A_{(1+1)r} = A_r \frac{(\sigma_3-\sigma_2)}{(\sigma_C-\sigma_B)}$$

$$= \frac{E_3}{E} \frac{(\varepsilon_3-\varepsilon_2)}{(\varepsilon_3-\varepsilon_2)} A_r$$

$$= \frac{E_3 A_r}{E} \underline{\hspace{4cm}} (7)$$

To find A_{1r}

$$A_{1r} = A_r - \frac{A_r}{E}[E_1-E_2] - \frac{A_r E_3}{E}$$

$$= \frac{A_r}{E}[E_2 - E_3] \underline{\hspace{4cm}} (8)$$

If the number of subannuli is reduced to two to be

compatible with stress strain diagram shown in

Fig. (16) then the two subannular areas A_{r1} and $A_{r(1+1)}$

are related to the parent annular area A_r by the

43

relationships

$$A_{rl} = \frac{A_r}{E_1}[E_1 - E_{1+1}] \text{————————} (9)$$

and

$$A_{r(1+1)} = A_r \frac{E_{1+1}}{E_1} \text{————————} (10)$$

When the number of positive sloped sides in the
approximated polygonal stress-strain diagram exceeds
two, the subannular areas, as a fraction of the annular
area, for any two adjacent positive sloped sides,
can be obtained using equations (9) and (10) where E_1
is as defined in Fig. (20).

Knowing the subannular stress $\sigma_{irl,j-1}$ at time t_{j-1} at
the 1th subannuli of the rth annulus at the ith link and
the strain increment $\delta\varepsilon_{ir,j}$ at time t_j at the rth annulus
of the ith link, the subannular stress $\sigma_{irl,j}$ at time
t_j, at the 1th subannuli is determined as follows.

First a trial value $\sigma^t_{irl,j}$ of the subannular stress
$\sigma_{irl,j}$ is calculated by assuming an elastic path,
thus

$$\sigma^t_{irl,j} = \sigma_{irl,j-1} + E\delta\varepsilon_{ir,j} \text{————————} (11)$$

Once the trial value is calculated, the correct value
can be ascertained by using the following conditions:
Let σ_{yl} be the subannular yield stress and be given by
$\sigma_{yl} = E\varepsilon_l$, where ε_1 is the strain defining the 1th
corner of the polygonal stress strain diagram.

44

Denoting $\sigma_{irl,j}$ as σ_1 for convenience,

$$\left.\begin{array}{ll}
\text{If } -\sigma_{y1} < \sigma_1^t < \sigma_{y1} & \text{then } \sigma_1 = \sigma_1^t \\[2ex]
\text{If } \sigma_1^t < -\sigma_{y1} & \text{then } \sigma_1 = -\sigma_{y1} \\[2ex]
\text{If } \sigma_1^t > \sigma_{y1} & \text{then } \sigma_1 = \sigma_{y1}
\end{array}\right\} \quad (12)$$

This procedure is applied to all subannuli of each annuli for all the links.

The values of the subannular stresses for the links in immediate contact with the tup and the anvil are then modified, to take into account the interface friction, by using the equation,

$$\sigma = \sigma_0[1 + 2\mu(R-r)/h] \quad\text{————————}\quad (13)$$

Following the terminology applied to the numerical model this equation could be written as

$$\sigma_{1,j}^m = \sigma_{1j}[1 + 2\mu(R_i-R_{ir})/h] \quad\text{——————}\quad (14)$$

where μ is the interface friction coefficient, and $\sigma_{1,j}$ is the subannular stress determined by equations (12). After this modification, the axial forces $N_{i,j}$ in each link are then obtained from the equation

$$N_{i,j} = \sum_{r=1}^{n} \sum_{1=1}^{k} \sigma_{irl,j} A_{1,j} \quad\text{——————}\quad (15)$$

where $A_{1,j}$ is the current subannular area.

If the links can be assumed to have the same mass

density as the billet, then further modification to the values of the subannular stresses can be made to take into account the effect of radial inertia of the billet material, by using the equation

$$\sigma = \sigma_o + 3\rho v^2 (R^2 - r^2)/8h^2 \qquad\qquad (16)$$

Equations (13) and (16) are detailed in appendices 1 and 2.

In its existing form, when using the present numerical approach the time increment cannot be chosen arbitrarily. The value of the time increment should be less than the time needed for the elastic stress wave to propagate through the length of the link.

3.2.1 Strain Rate Sensitivity

To take into account strain rate sensitivity the stress strain behaviour of the material, for different strain rates, must be known. Approximated stress strain diagrams are shown in Fig. 18, and referring to equations (3) and (4), namely

$$\delta t = t_{j+1} - t_j \qquad\qquad (4)$$

$$u_{ij+1} = \ddot{u}_{ij}(\delta t)^2 + 2u_{ij} - u_{ij-1} \qquad\qquad (3)$$

The change in length of the element $\delta(\Delta S)_{i,j+1}$ of the link occurring during the time interval δt is

$$\delta(\Delta S)_{i,j+1} = \Delta S_{i,j+1} - \Delta S_{i,j} \qquad\qquad (17)$$

46

The strain increment and strain rate occurring in the link during the time interval are:

$$\delta \varepsilon_{i,j+1} = \frac{\delta(\Delta S)_{i,j+1}}{\Delta S_{i,o}} \quad\text{————————————} \quad (18)$$

where $\Delta S_{i,o}$ is the original length of the link

and

$$\dot{\varepsilon}_{i,j+1} = \frac{\delta \varepsilon_{i,j+1}}{\delta t} \quad\text{————————————} \quad (19)$$

The total strain in the link can now be determined from:

$$\varepsilon_{i,j+1} = \varepsilon_{i,j} + (\dot{\varepsilon}_{i,j+1})\delta t \quad\text{——————} \quad (20)$$

$$\varepsilon_{i,j+1} = \varepsilon_{i,j} + \delta \varepsilon_{i,j+1} \quad\text{————————} \quad (21)$$

since the time interval and, hence, the strain increment are both small.

A computer simulation based on the lumped parameter model can be used and strain rate sensitivity incorporated into the analysis in the form of a stress-strain rate law. For lead the law $\sigma = \sigma_1 [1 + (\frac{\dot{e} - \dot{e}_1}{D})^{\frac{1}{p}}]$ was used as detailed in Chapter 2.
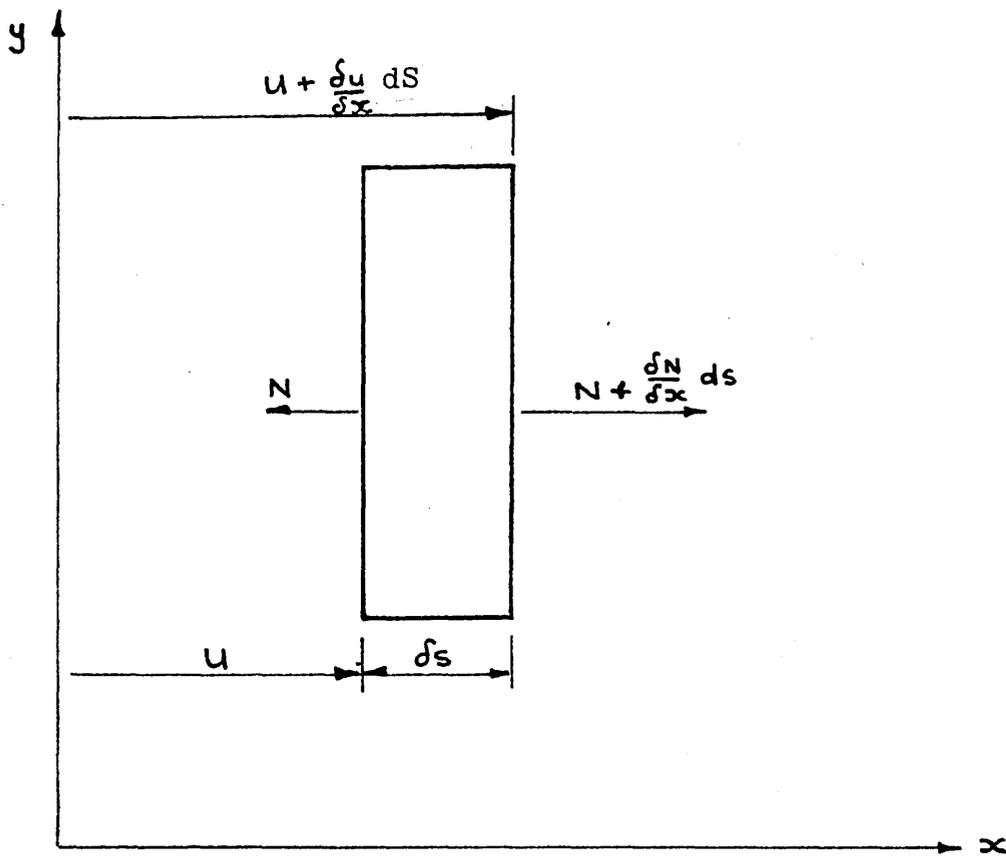
AN ELEMENT OF THE BILLET

FIG. 14a.
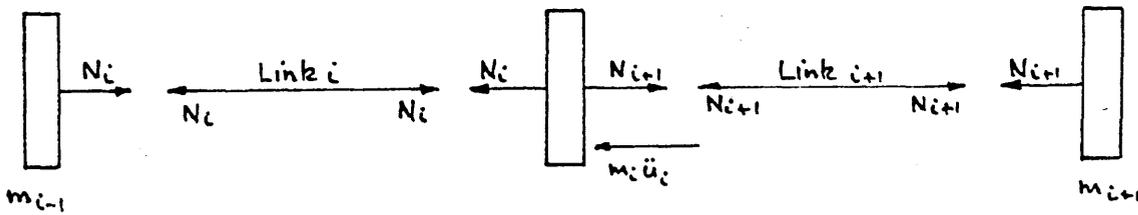
EQUIVALENT FINITE – DIFFERENCE MODEL

FIG. 14b.

48
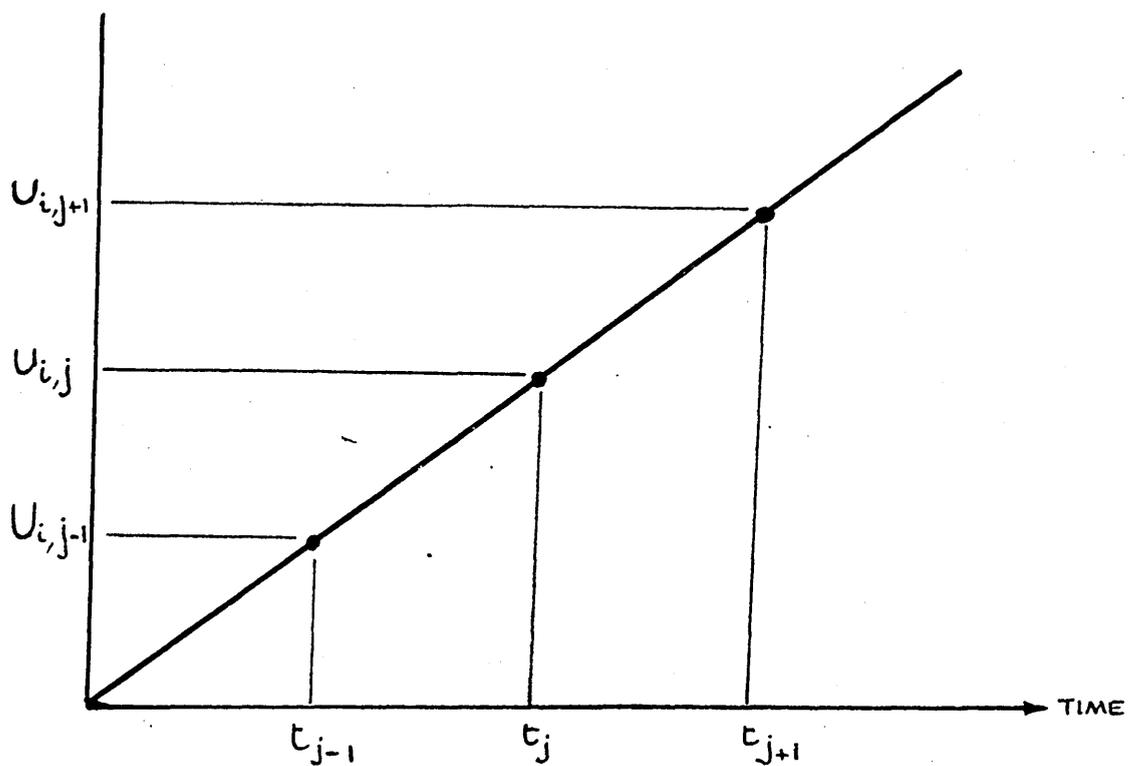
FINITE DIFFERENCE TIME/DISPLACEMENT RELATIONSHIP

FIG. 15.
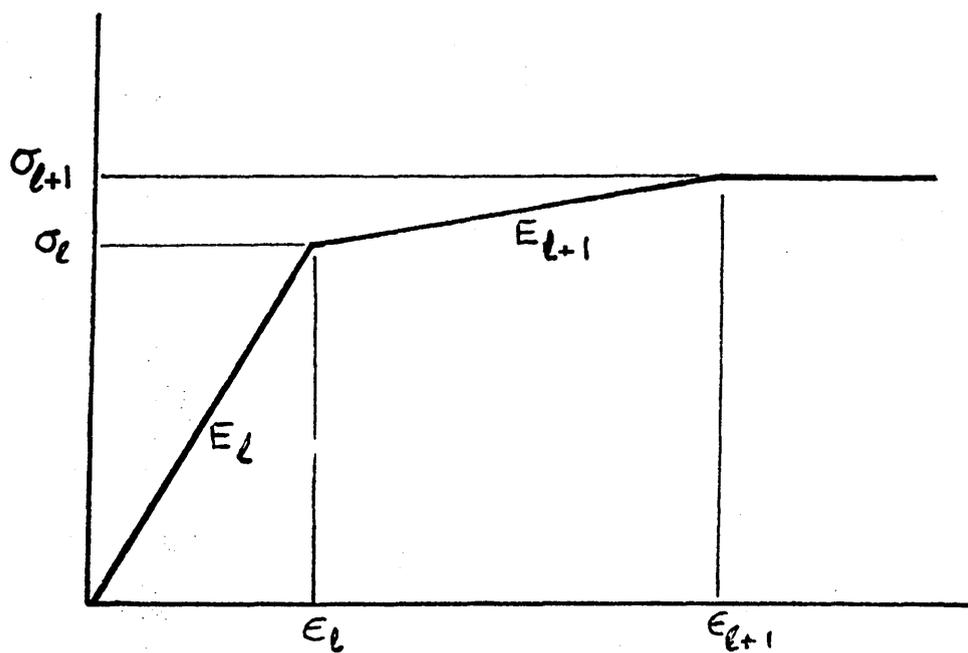
ELASTIC BINARY STRAIN HARDENING STRESS STRAIN PROPERTY

FIG. 16

49

ANNULUS AREA A_r
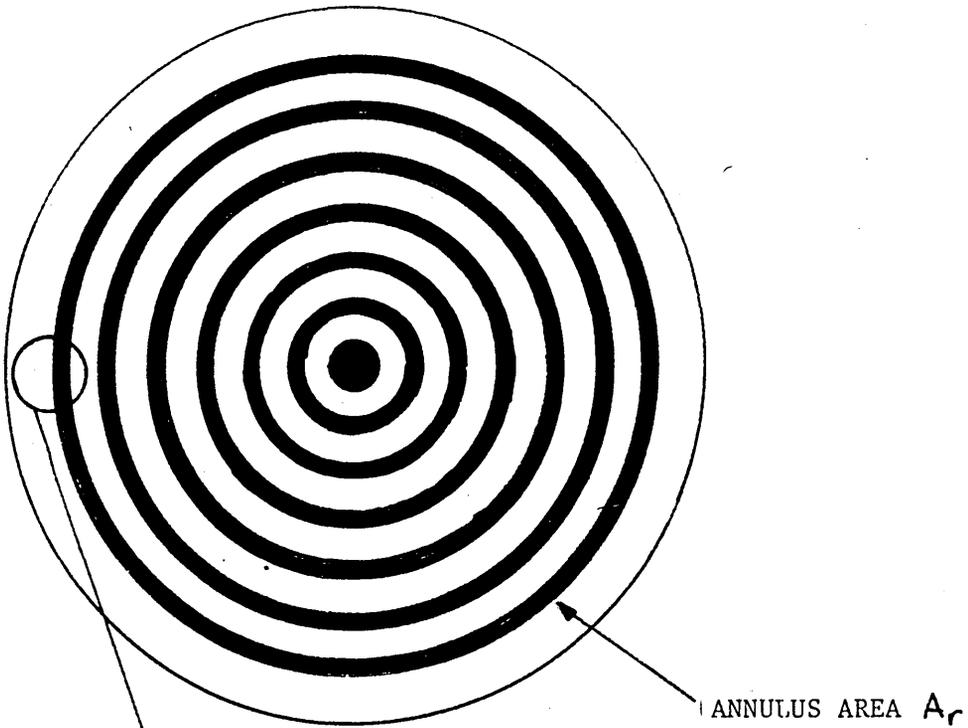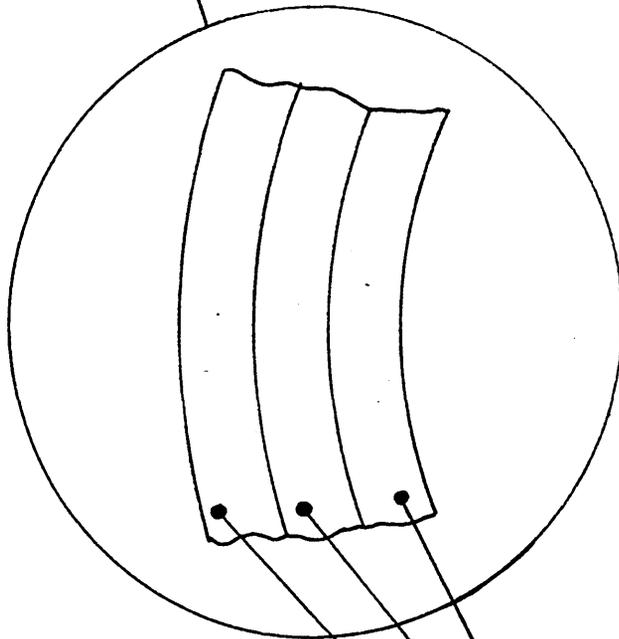
NOTE: $A_r = A_{r(\ell-1)} + A_{r\ell} + A_{r(\ell+1)}$

SUBANNULAR AREA $A_{r(\ell-1)}$

" " $A_{r\ell}$

" " $A_{r(\ell+1)}$

FIG. 17

CROSS SECTION MODEL OF BILLET

50

'NEST' OF GRAPHS SHOWING THE EFFECT
OF STRAIN RATE SENSITIVITY.

APPROXIMATED POLYGONAL STRESS STRAIN DIAGRAM

FIG. 18

For each positively sloped side
there is one sub-annular area.
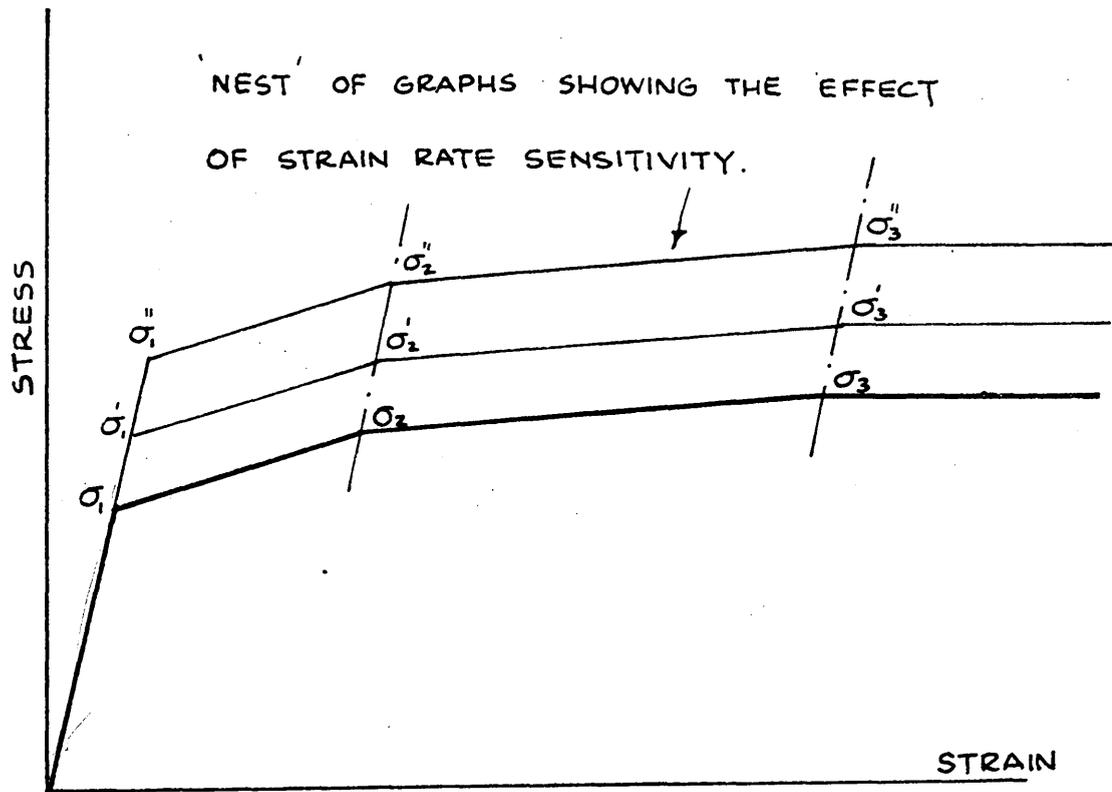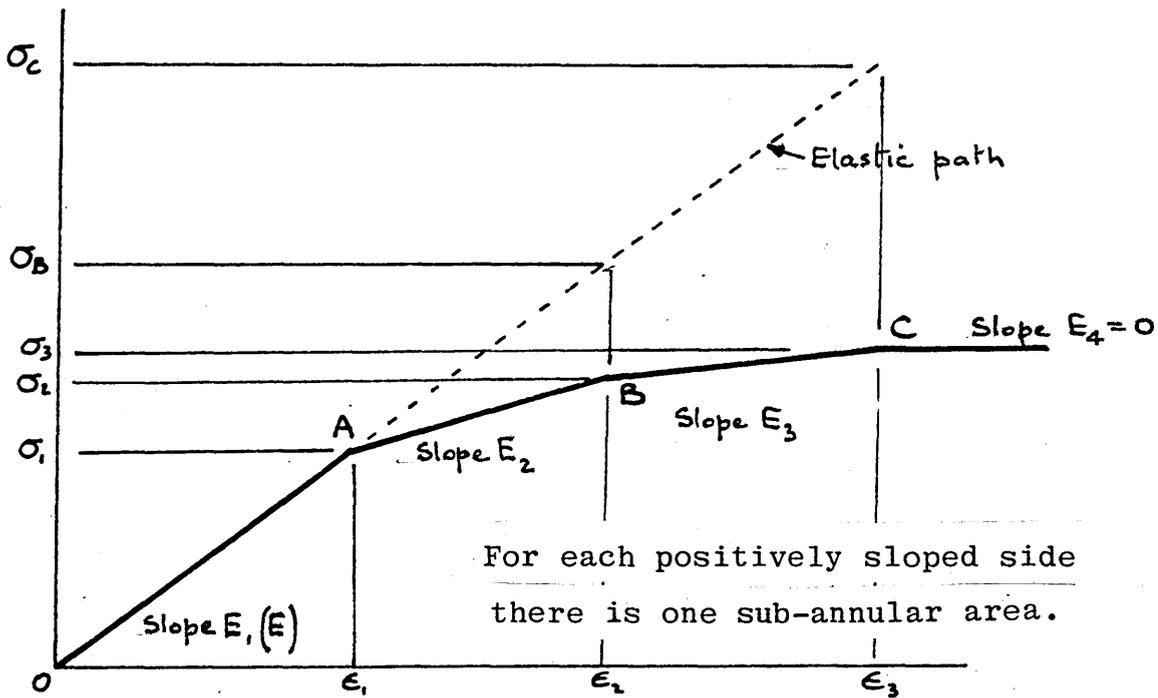
STRESS STRAIN DIAGRAM IDENTIFYING SYMBOLS USED

IN THEORETICAL ANALYSIS   FIG. 19

51

slope corresponding to subannulus ℓ

$$E_\ell = \frac{\sigma_\ell - \sigma_{\ell-1}}{\epsilon_\ell - \epsilon_{\ell-1}}$$
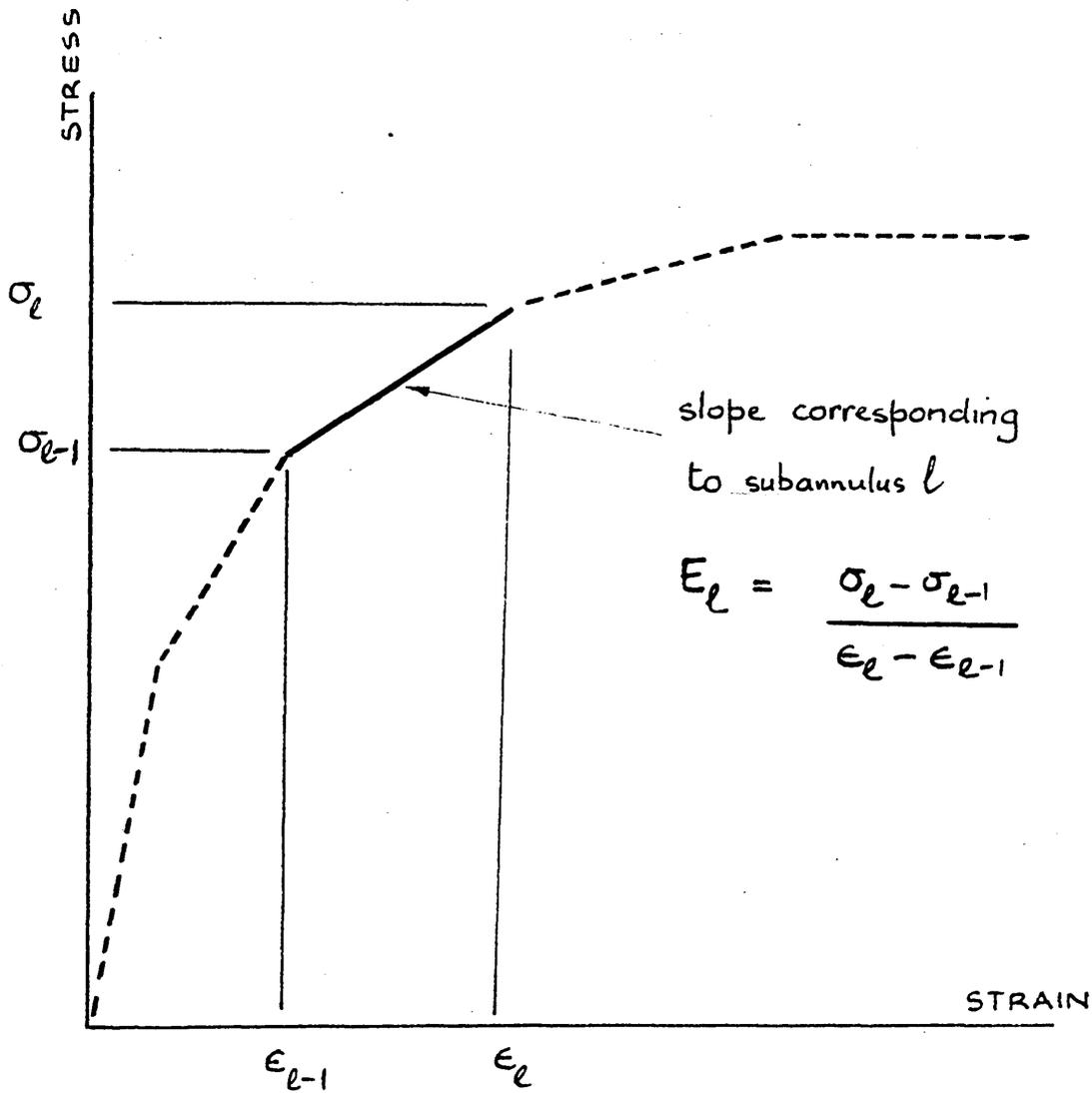
APPROXIMATED POLYGONAL STRESS STRAIN DIAGRAM

FIG. 20

52

4.1 Introduction

Simple upsetting or dynamic compression of cylindrical billets is one of the most commonly used and relatively simple operations used to increase the diameter of the billet. The dimensions of larger sized billets are usually changed by hot upsetting at moderately high speeds and hence the forging load is influenced by interface friction and strain-rate sensitivity of the material. The object of this part of the work is to investigate the effects of friction and strain rate sensitivity on the forging load and final shape of the billet, both experimentally and theoretically.

4.2 Experimental Work

Simple upsetting tests were carried out under the drop hammer and a different degree of deformation was imparted to each billet by releasing the tup from different heights. For each test the following data were obtained:

(a) the forging load

(b) impact velocity

(c) deformation-time history.

The deformation sequence of a number of test specimens were recorded using a Hi-Cam high speed camera.

Using the drop hammer set to give maximum impact, velocity tests were carried out on lead billets

54

25 mm diameter x 24 mm long and aluminium alloy billets
19 mm diameter x 19 mm long. Two types of friction
condition were studied, one, using a paste of graphite
in petroleum jelly as lubricant to induce low friction
and the other, without any lubricant, to induce dry
friction conditions. High speed photographs were
used to obtain experimental data giving instantaneous
billet profiles and tup-displacement-time curves.
Elastic strain hardening and stress-strain character-
istics of the billet material were obtained from quasi-
static tests. The dynamic stress-strain properties
were established from drop hammer tests (described in
Chapter 2).

The load time variation was obtained from the tracings
recorded on the oscilloscope. A typical photograph of
such a trace for an aluminium alloy billet is shown in
Fig. 21.

4.3 Theoretical Predictions

In order to predict the results theoretically, the
numerical technique described in the previous Chapter
was employed. In predicting the results it was assumed
that a constant frictional coefficient $\mu = 0.06$ existed
for both lead and aluminium billets. This value of μ
was thought to be a reasonable estimate of what graphite
in jelly would induce. For dry test conditions the
value of $\mu = 0.577$ was incorporated in the analysis for

lead billets [51] while for aluminium billets
μ = 0.18 was used [59].

The actual loading configuration and its equivalent
numerical model, applied to both the lead and
aluminium billets, is shown in Fig. 22. The quasi-
statically obtained stress strain characteristics and
their polygonal approximations, as required by the
numerical technique, for lead and aluminium alloy used
for these tests are shown in Fig. 12 and Fig. 13
respectively.

4.4 Results and Discussions

The instantaneous profiles of a lead billet at various
instants of time after the onset of the process were
obtained from the high speed photographs and are
shown in Fig.23(a). This test was carried out under
lubricated conditions. The billet deformed in such a
manner that the profile shape remained right cylindri-
cal throughout the deformation process. The
theoretically predicted instantaneous profiles for the
same billet are shown in Fig.23(b) which shows profile
shapes having either upwards or downwards directed
slightly tapered sides. Slight barrelling also becomes
apparent in the profiles corresponding to higher
reductions in billet height. This slight discrepancy
is thought to have arisen due to instability in the
technique used. Experimentally it was not possible
to identify such behaviour.

The instantaneous profiles shown in Fig. 24(a) for a lead billet deformed under dry lubrication conditions are seen to compare reasonably well with those in Fig. 24(b), which were predicted using the numerical technique. The die load determined experimentally was plotted in Figs. 25 and 26 against reduction in billet height measured from the high speed photographs for lead and aluminium alloy billets respectively, both tests being carried out under lubricated conditions.

The theoretically predicted curves are also included in the respective figures for comparison. It can be seen that for the lead billet both theoretical curves predict lower die loads. For 14.4 mm reduction in height the curve excluding the strain rate term predicts a load which is 38% of the actual load, whereas the curve including the strain rate term predicts a load which is 60% of the actual load. The effect of strain rate is clearly shown by these two theoretical curves. During the initial stages of deformation the theoretical curve matches closely with the experimental curve when strain rate sensitivity is incorporated in the analysis. For greater deformation the frictional effect becomes predominant. The discrepancy between the theory and experiment for larger deformation may thus be attributed to frictional effect. Although the effect of friction has been

incorporated in the analysis, in reality the coefficient
of friction may change from what was assumed
originally, generally becoming much higher and
approaching that of sticking friction in hot forging.

Since aluminium alloy is not a strain rate sensitive
material, only a single theoretical load curve is shown.
The load predicted is comparable with that obtained
experimentally, being slightly higher during the
initial part of the deformation and slightly lower
thereafter.

In order to compare the effect of friction the die
load/deformation curves obtained experimentally for the
aluminium alloy billets under lubricated and dry
conditions are plotted in Fig. 27. The corresponding
predicted curves are also shown in this figure. It
is seen that a maximum increase in die load of less than
10% occurs for reductions of billet height of up to 3 mm
(16%). The increase in die load due to friction as
predicted using the numerical technique is much
less than that obtained experimentally.

The increase in friction, when the billet is deformed
under dry test conditions, results in increased
barrelling of the billet. Fig. 28 shows the increase
in radii at the middle and top section of the aluminium
alloy billet. The extent of barrelling can be readily
appreciated from this figure. The theoretically
predicted results suggest slightly less barrelling of

the billet.

Tup displacement-time curves were obtained using
high-speed photographs which upon graphical differen-
tiation enabled a velocity time curve to be used to
calculate the kinetic energy of the tup still unused
at any time instant during the deformation process.
Figs. 29 and 30 show the variation in percentage
kinetic energy absorbed with deformation for lead
and aluminium billets respectively both deformed under
lubricated test conditions. The theoretical curve for
the lead billet shows that much less energy is
required where more than 55% reduction in height is
obtained. This is again an underestimation of the
actual energy requirement due to the exclusion of the
strain-rate sensitivity. On the other hand, it is evi-
dent from Fig. 30, which shows similar kinetic energy
vs. deformation curves for the aluminium alloy billet,
that there is close agreement between the experimental
results of predictions obtained theoretically, despite
the exclusion of the strain rate sensitivity.

The deformation vs. time curves for lead and aluminium
alloy billets deformed under lubricated test conditions
are shown in Fig. 31 and 32 respectively. The experi-
mental and theoretical correlation is very good for
lead billets when the theoretical curve which takes
into account strain rate is used. The theoretical curve
which does not take strain rate into account gave good

results for up to 55% deformation.

For aluminium alloy billets, close agreement exists during the whole of the deformation process.
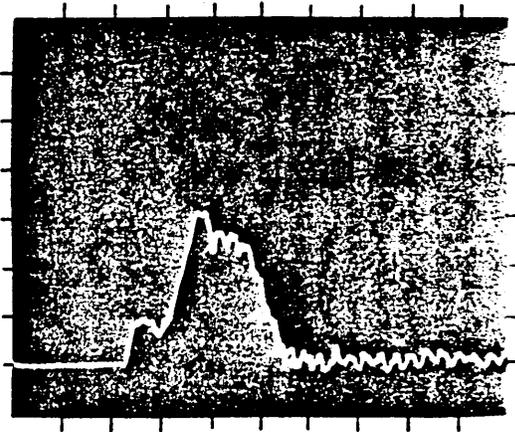
TYPICAL LOAD-TIME TRACE FOR ALUMINIUM BILLET.

FIG. 21.
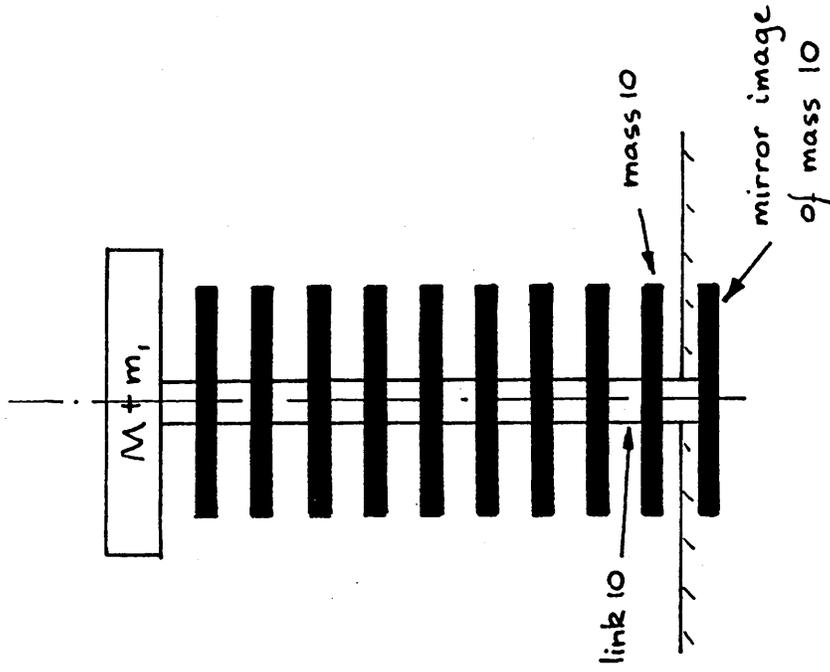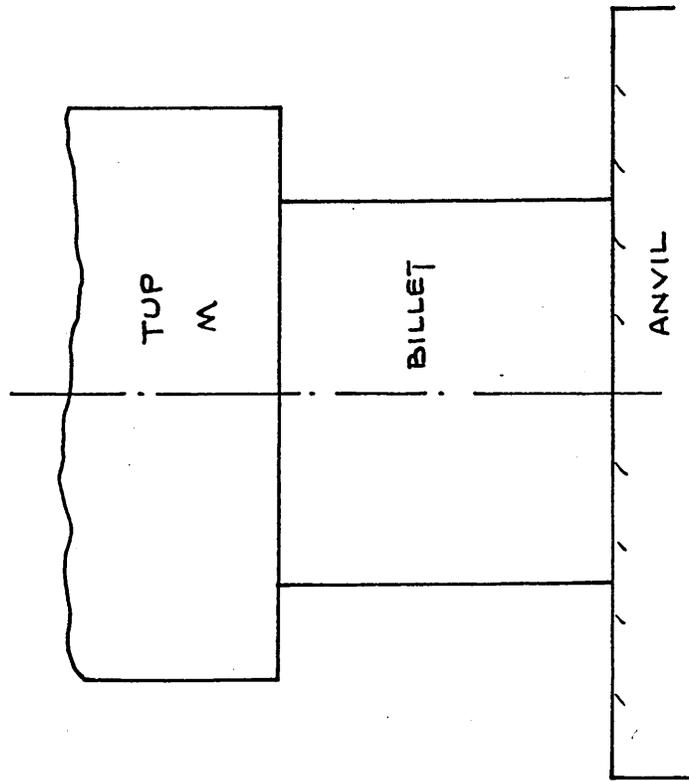
FIG. 22

ACTUAL LOAD CONFIGURATION AND THE
CORRESPONDING NUMERICAL MODEL

62

(a)

0.417 msec
0.834 "
1.251 "
1.668 "
2.083 "

(b)

0.43 msec
0.86 "
1.29 "
1.72 "
2.15 "
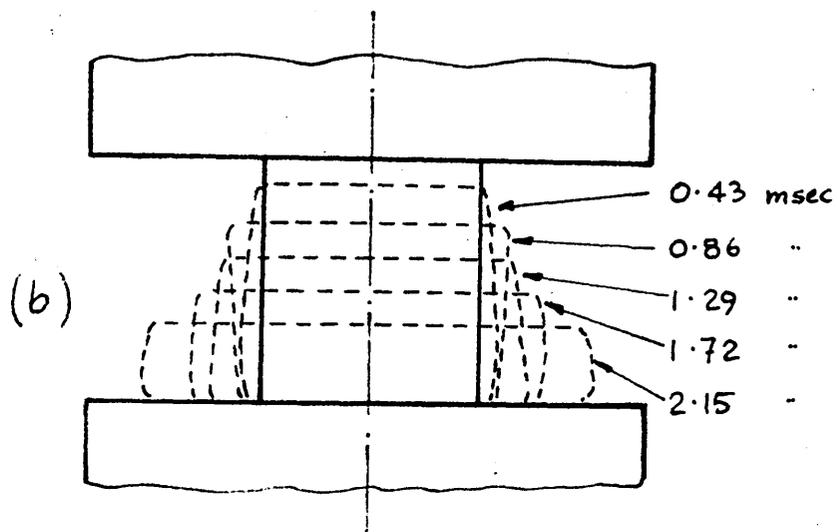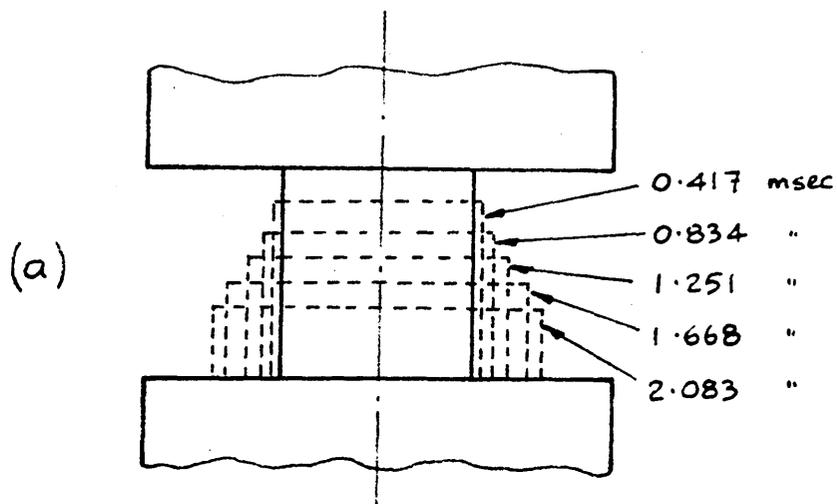
FIG. 23(a) SHOWING THE INSTANTANEOUS PROFILES OF A LEAD BILLET
(b) FORMED UNDER LUBRICATED TEST CONDITION AND

(b) CORRESPONDING INSTANTANEOUS PROFILES PREDICTED
THEORETICALLY.

(a)

0.435 msec
0.870 "
1.305 "
1.739 "

(b)

0.43 msec
0.86 "
1.29 "
1.72 "
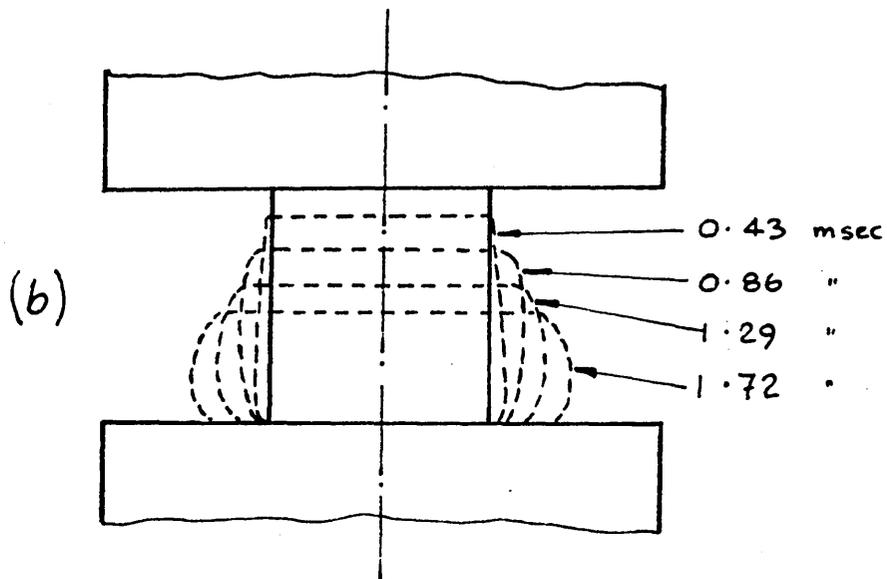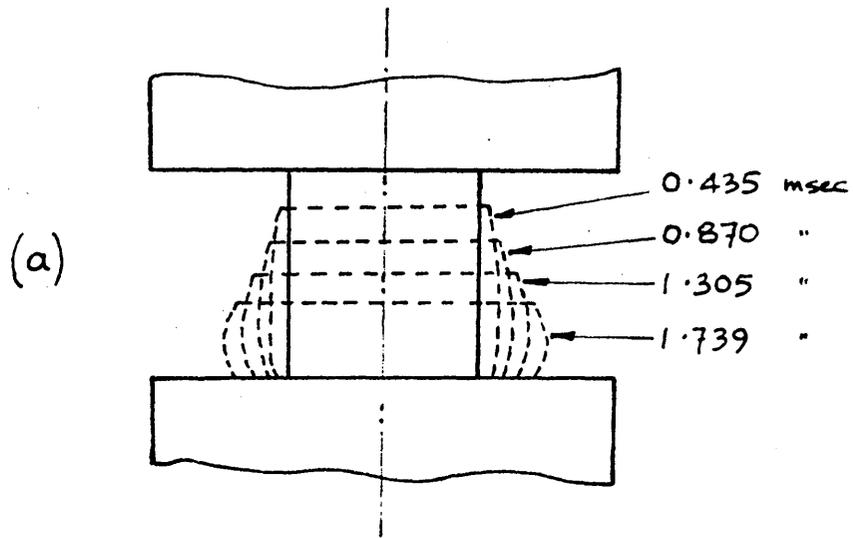
FIG.24(a) SHOWING THE INSTANTANEOUS PROFILES OF A LEAD BILLET DEFORMED UNDER DRY TEST CONDITIONS, AND

(b) CORRESPONDING INSTANTANEOUS PROFILES PREDICTED THEORETICALLY

64

THEORETICAL CURVES
   CURVE 'A' WITHOUT STRAIN RATE
   CURVE 'B' WITH STRAIN RATE
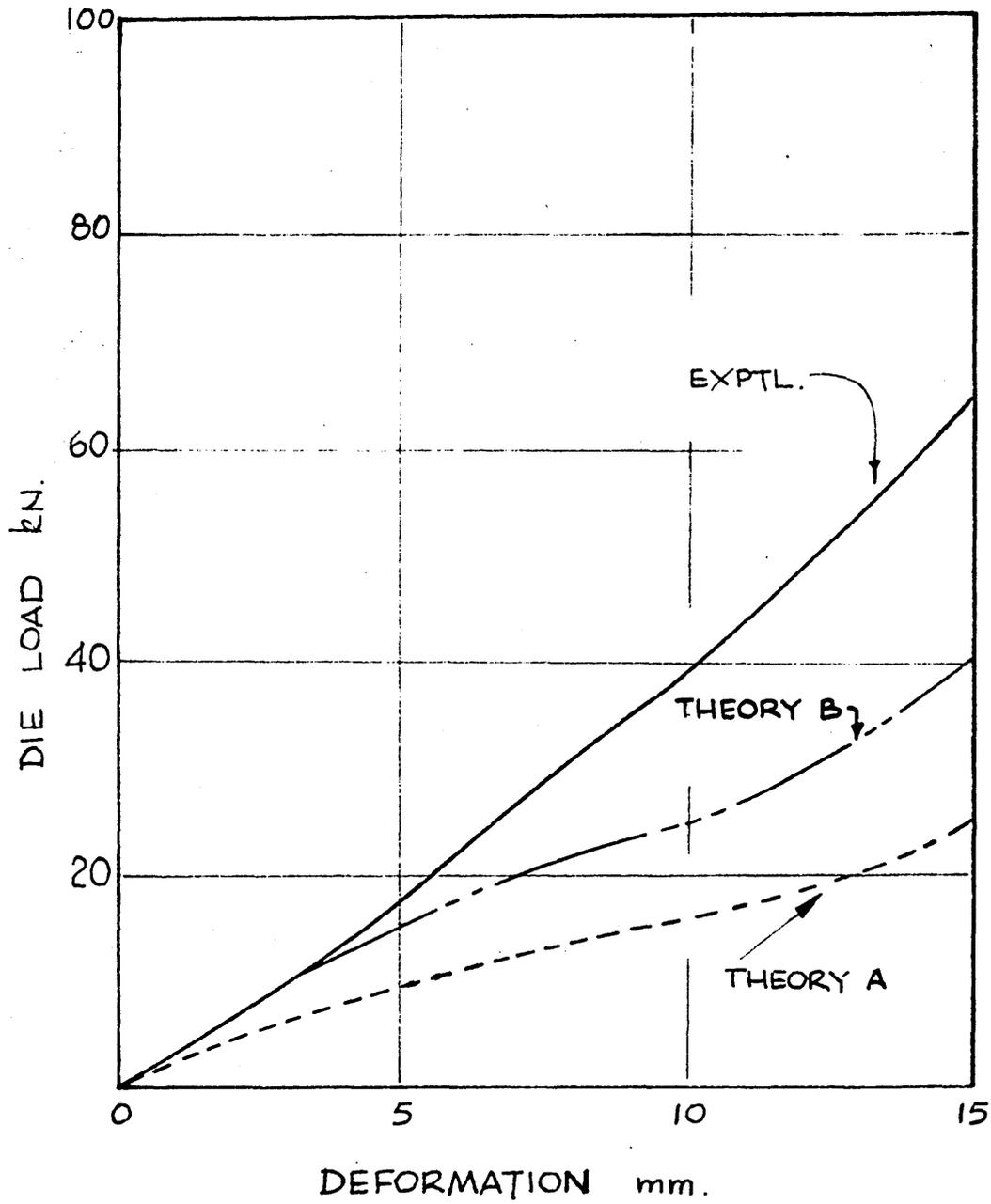
UPSETTING OF LEAD CYLINDER (LUBRICATED)

FIG. 25.
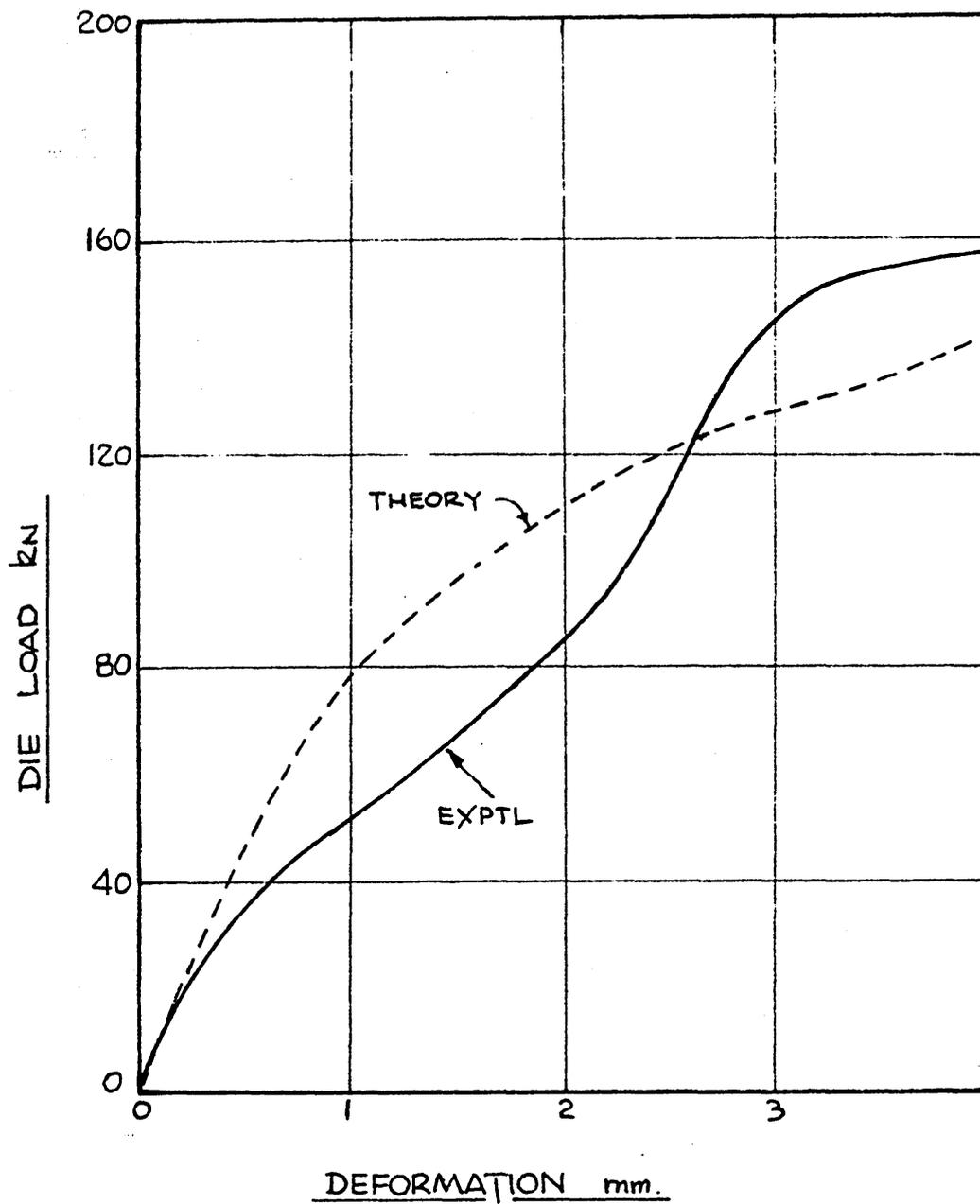
UPSETTING OF ALUMINIUM ALLOY CYLINDER
(LUBRICATED)

FIG. 26.
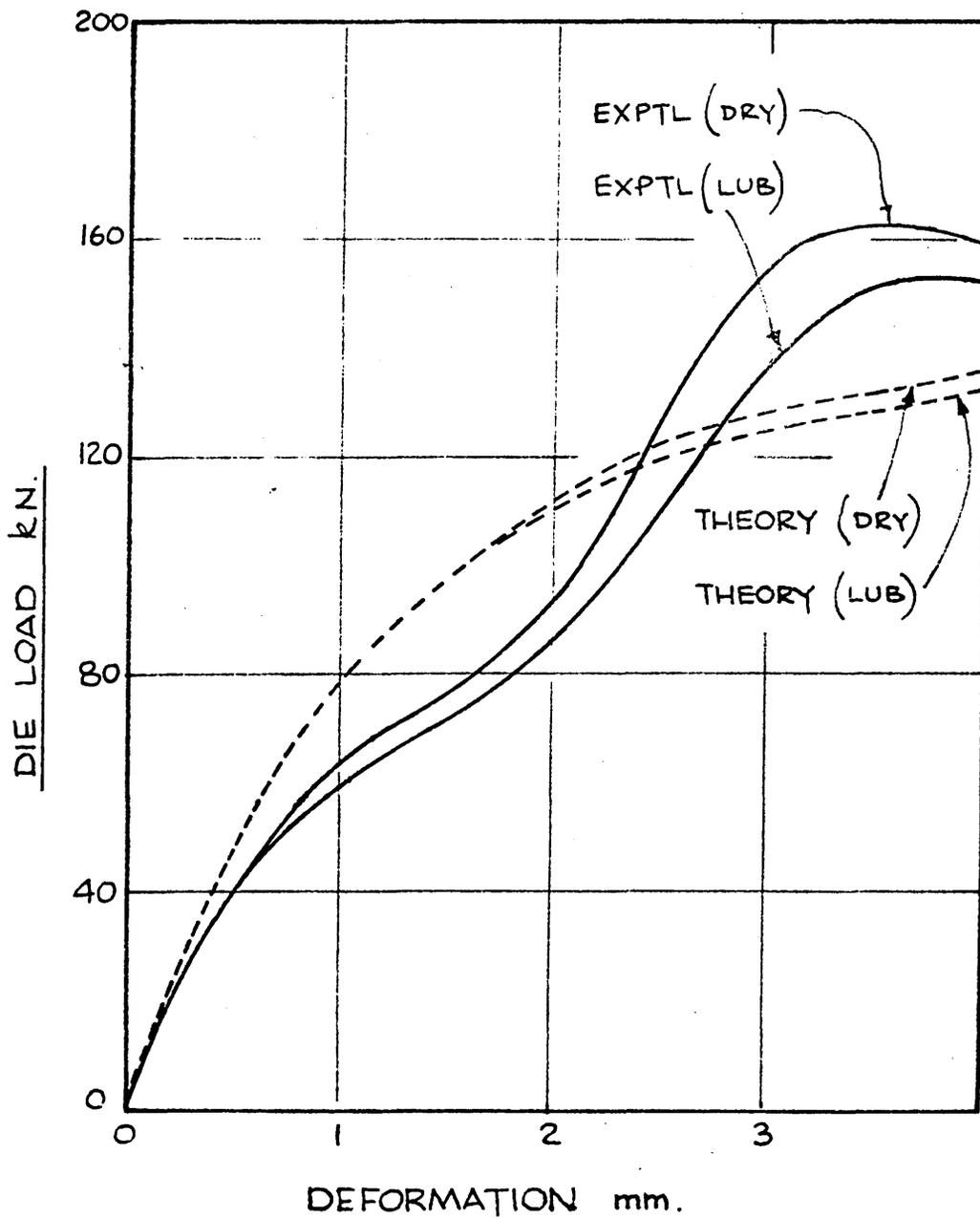
UPSETTING OF ALUMINIUM ALLOY CYLINDER
DEFORMED UNDER LUBRICATED AND DRY
TEST CONDITIONS.

FIG. 27
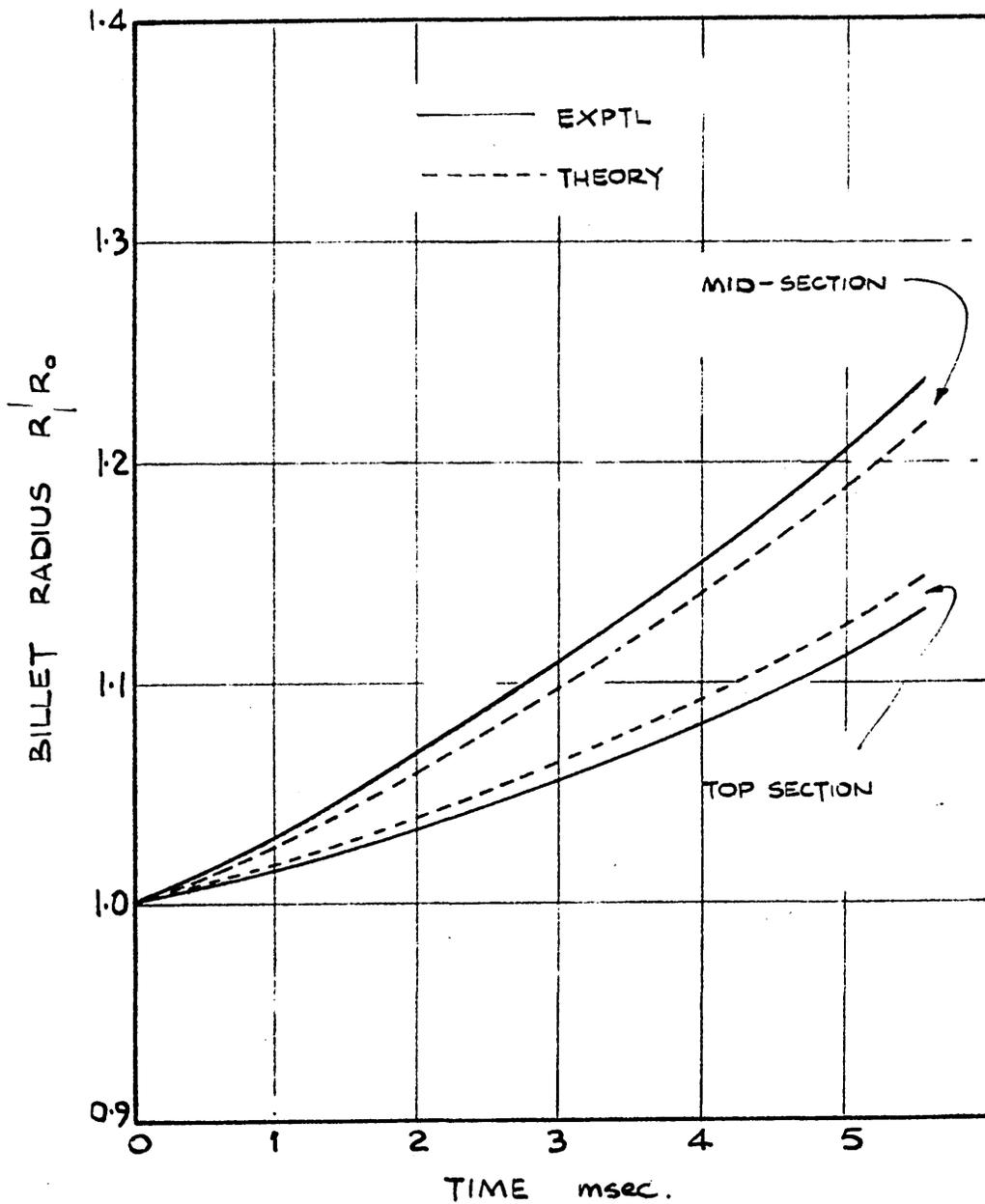
UPSETTING OF ALUMINIUM ALLOY CYLINDER
UNDER DRY TEST CONDITIONS.

FIG. 28.

THEORETICAL CURVES
    CURVE 'A' WITHOUT STRAIN RATE
    CURVE 'B' WITH STRAIN RATE.
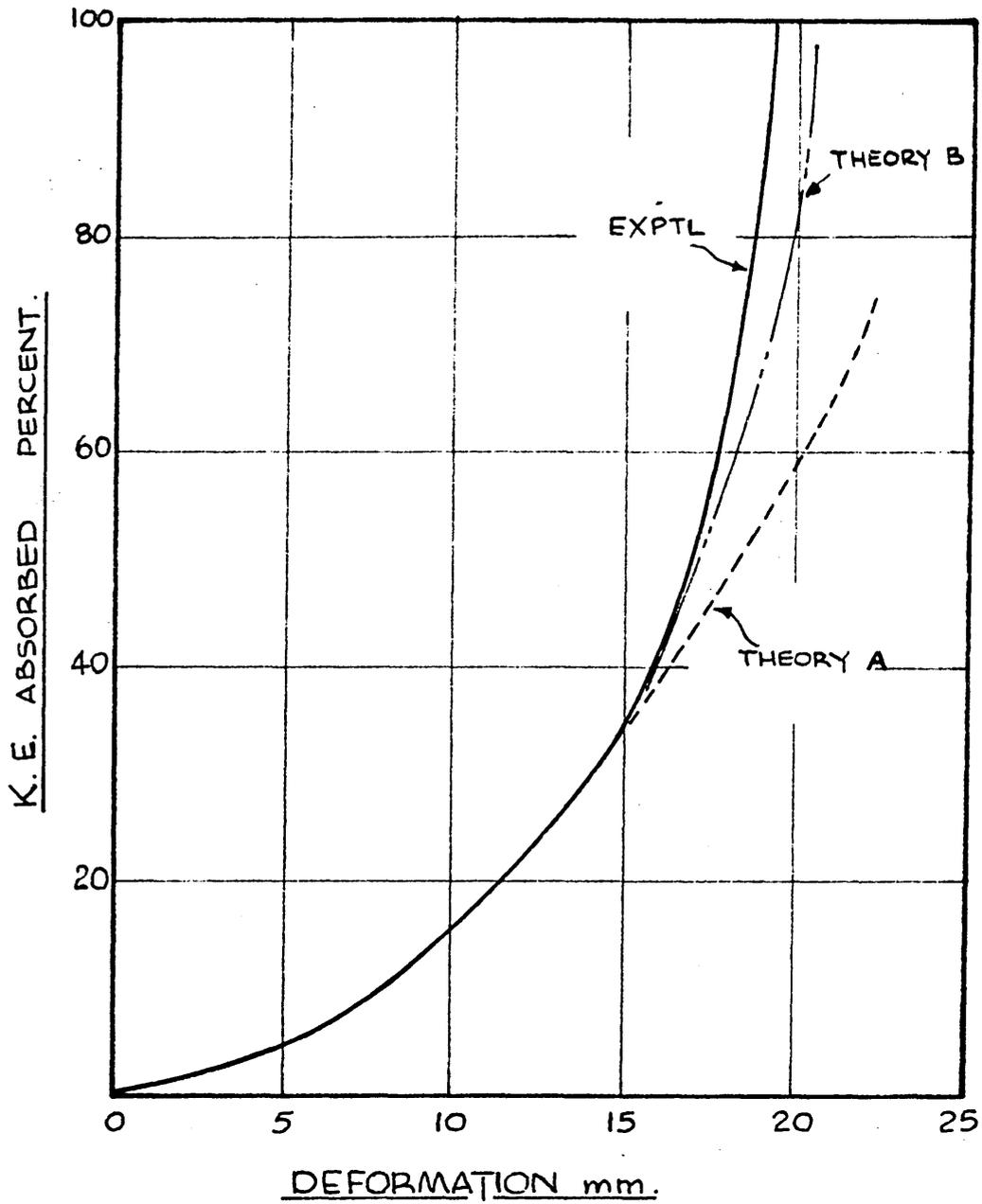
PERCENTAGE KINETIC ENERGY ABSORBED vs. DEFORMATION CURVES FOR LEAD BILLETS DEFORMED UNDER LUBRICATED TEST CONDITIONS.

FIG. 29
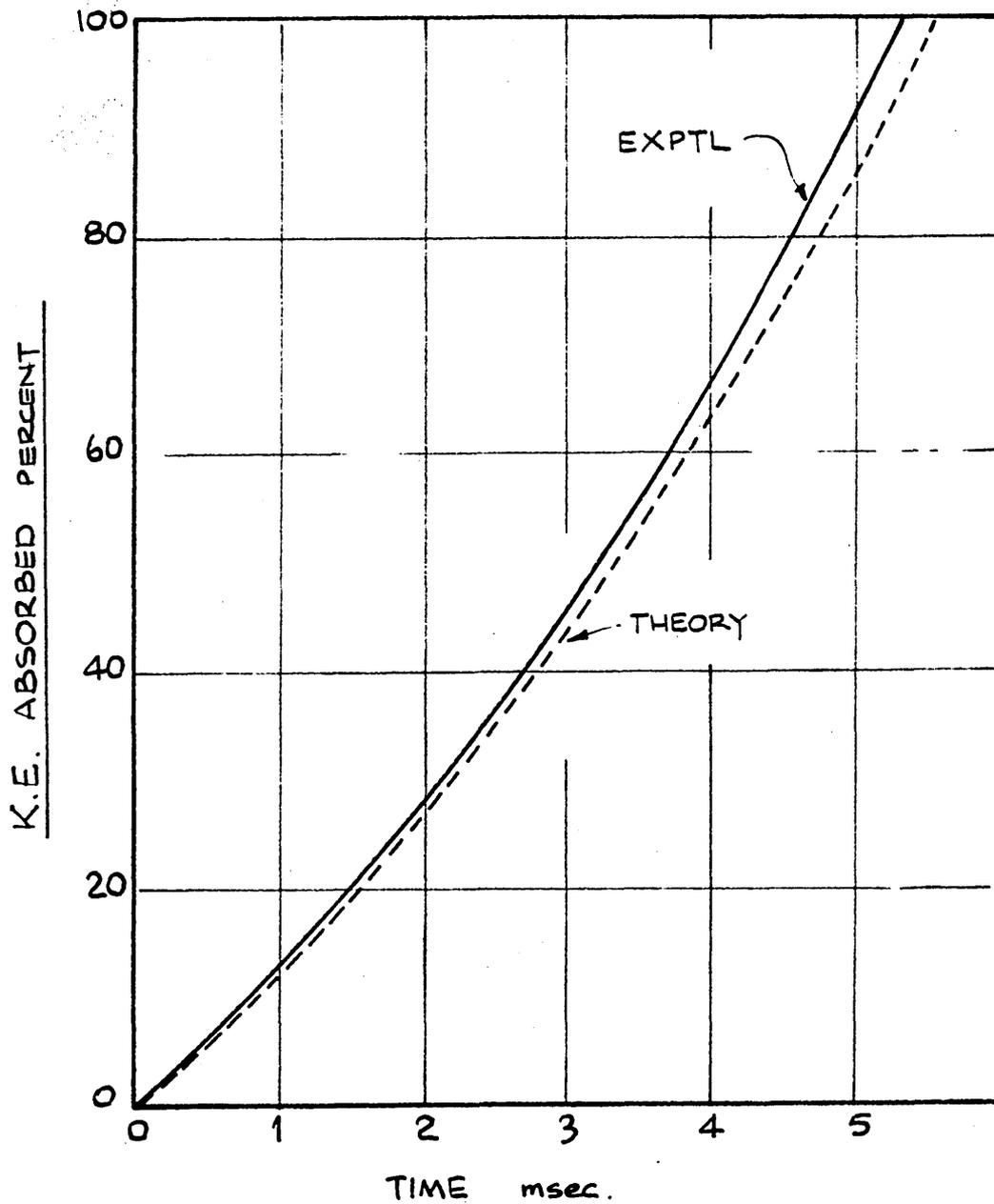
UPSETTING OF ALUMINIUM ALLOY CYLINDER UNDER
LUBRICATED TEST CONDITIONS.

FIG. 30

THEORETICAL CURVES
  CURVE 'A' WITHOUT STRAIN RATE.
  CURVE 'B' WITH STRAIN RATE.
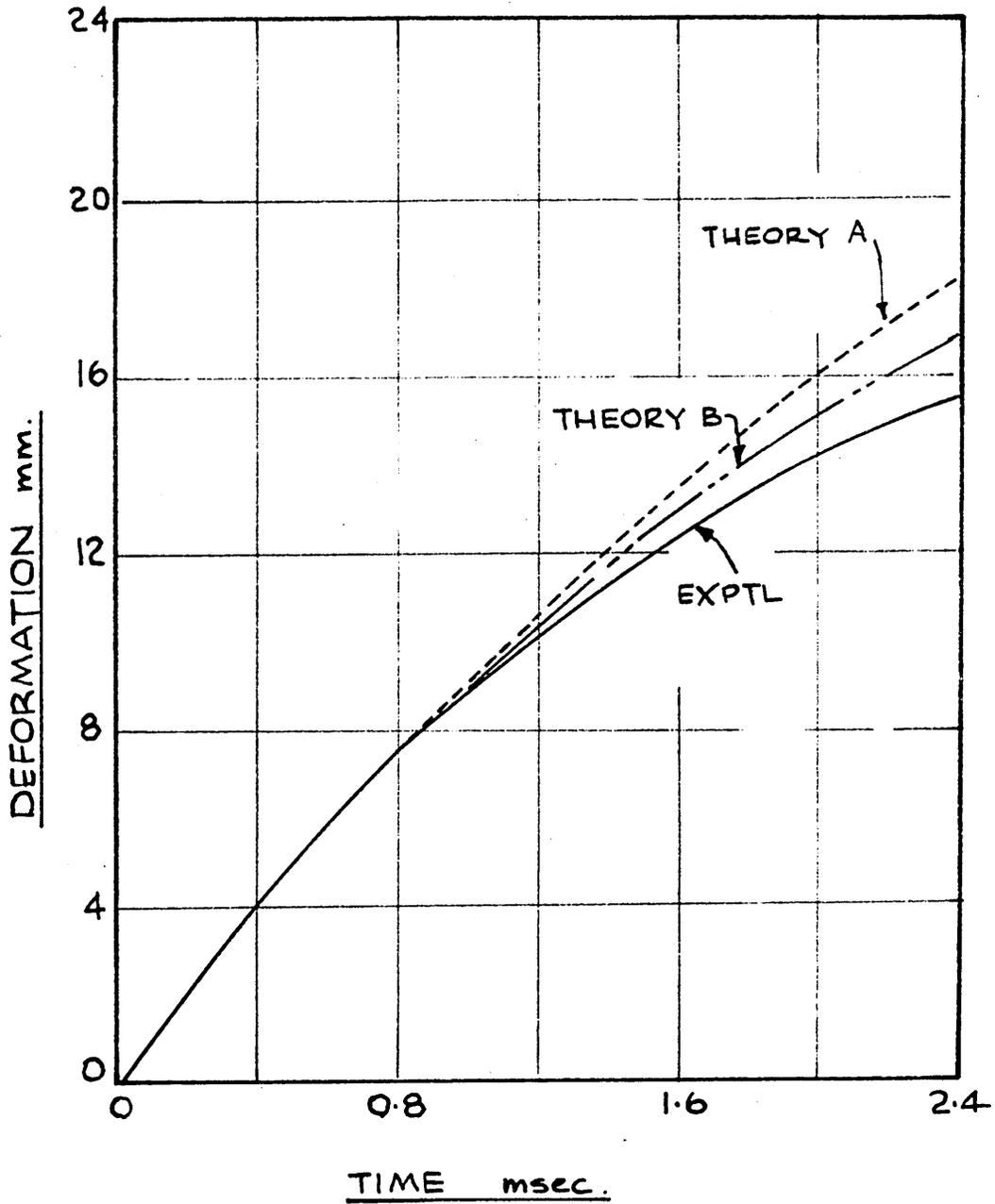
UPSETTING OF LEAD CYLINDER
(LUBRICATED)

FIG. 31

71
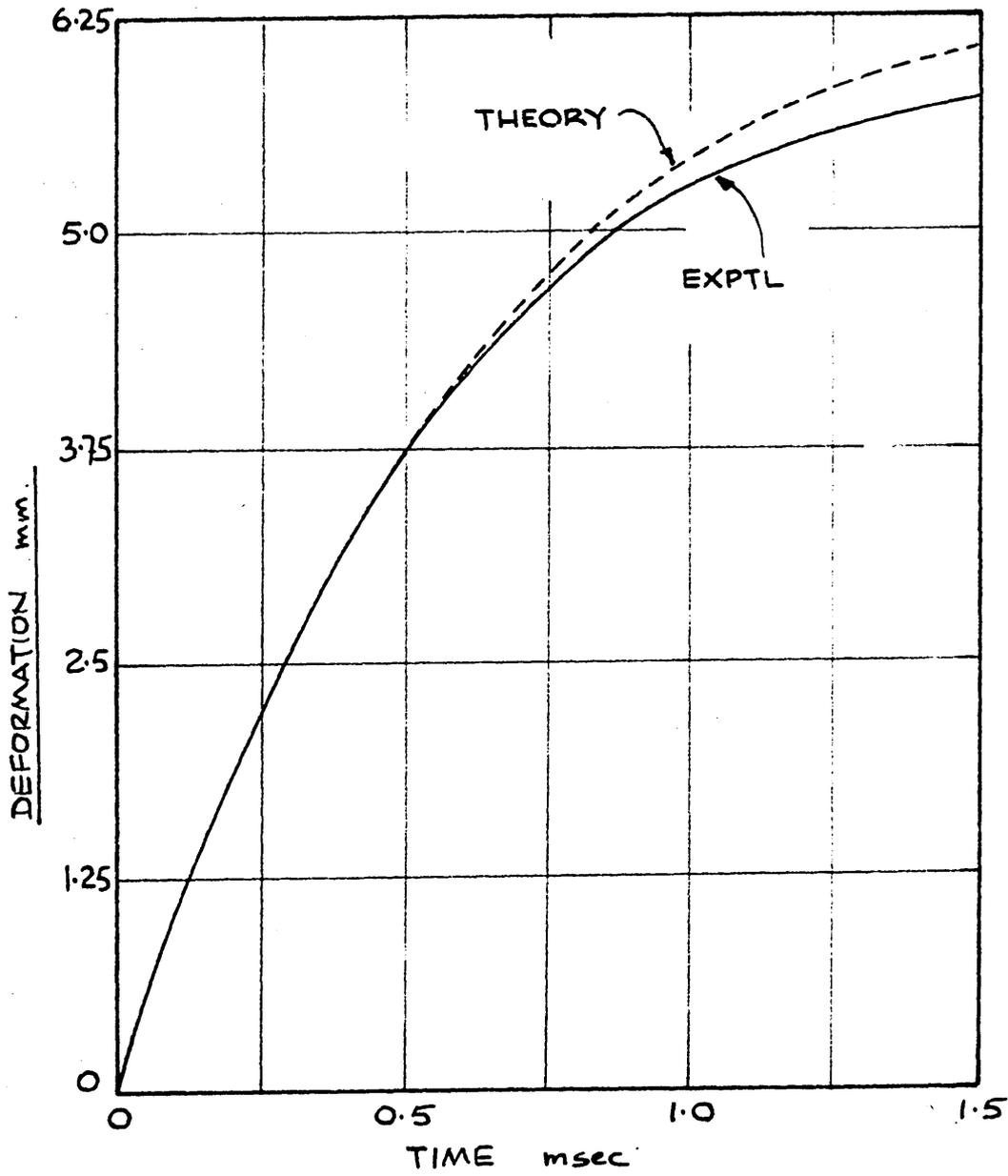
UPSETTING OF ALUMINIUM ALLOY CYLINDER
(LUBRICATED)

FIG. 32

5.1 Introduction

Apart from upsetting tests on cylindrical billets closed die forming tests were also carried out using lead billets of 24 mm diameter and 46 mm in height. These were formed into axisymmetric shapes. Unlike simple upsetting it was not possible to photograph the deformation mode of the billet. The load time history was recorded and the impact velocity was measured. Tests were carried out under both dry and lubricated conditions.

5.2 Experimental Work

Experiments were conducted using the drop hammer. The tup was dropped from its highest position so that the velocity at impact reached its maximum value of 9 m/s. The actual loading configuration of the billet is shown in Fig. 33(a). Billet details are shown in Fig. 34.

Experimental results were obtained in terms of the load deformation history, final shape of the billet, kinetic energy and friction effects.

5.3 Theoretical Prediction

The numerical technique detailed in Chapter 3 was applied to predict theoretically the deformation mode for each loading situation. The finite-difference equivalent model of the actual loading situation is shown in Fig. 33(b). The stress strain properties shown in Fig. 11 were incorporated in the analysis.

74

The effects of material inertia and interface friction at the die-billet constraint were also taken into account. The die load, instantaneous billet profiles, die pressure and strain rate within the billet, for both the lubricated and dry friction condition, were predicted theoretically and compared with experimental results where appropriate. In the analysis, the friction factor for the dry friction condition was taken as unity whilst for the lubricated condition it was taken as zero along the die-billet interfaces. For shearing friction within the billet at the die-billet constraint the friction factor was again taken as unity to simulate sticking friction. Fig. 35 shows theoretically predicted instantaneous profiles at various times during the deformation process for a billet forged under lubricated condition. The instantaneous profiles for a billet forged under dry friction conditions are shown in Fig. 36. It was not possible to record the experimental instantaneous profiles due to the nature of the forming process. Therefore only the corresponding experimentally obtained final profiles are shown in these figures. It is clearly evident that forging under dry friction condit- ions gives rise to considerable barrelling of the billet during the development process. This causes the billet material to get into the flash land rela- tively earlier than under lubricated forging conditions.

5.4 Results and Discussions

In Fig. 37 the variation in forging loads with tup displacement measured experimentally are compared with those predicted theoretically for forging under lubricated and dry friction conditions. The effect of strain rate and material inertia on the forging load was found to be significant when the experimentally established dynamic stress strain properties shown in Fig.11 were incorporated in the analysis. The agreement between the theoretical and forging load under both frictional conditions show close agreement. Fig. 37 also shows the quasi-static forging load under dry friction conditions. This static load is seen to be considerably lower than both the experimental and theoretically predicted dynamic forging loads. This discrepancy may be explained by the apparent strain hardening of the lead, used for these experiments, under dynamic loading conditions. The instantaneous profiles in Fig. 35 and 36 showed barrelling of the billet in a qualitative manner. In Fig. 38 this is shown in a quantitative manner in terms of the variation in the billet radius at mid-section and at the die-billet constraints. It is clearly evident from this figure that forging under dry friction conditions causes the billet radius at mid-span to increase at a relatively faster rate with deformation than under lubricated forging conditions. This may result in appreciable loss of material as flash.

The theoretically predicted variation in strain
rate at mid-section and at the section along the die-
billet constraint is shown in Fig. 39 for lubricated
and dry friction conditions. This figure shows that
during most of the deformation process the maximum
strain rate within the billet remains above about $200/sec$
for an impact velocity of 9 m/s and hence makes appre-
ciable difference in the forging load even during the
later stages of deformation.

Comparing the theoretically estimated die pressures
with those obtained experimentally as shown in Fig.40.
shows close agreement under both forging conditions.
It is evident, however, that in the case of dry friction,
the theoretically predicted die pressure is slightly
greater than that obtained experimentally whilst this
trend is reversed when a lubricant is used. The main
reason for this behaviour could be the fact that for
dry friction conditions the friction factor, taken as
unity, was too high and that the use of graphite
in petroleum jelly as a lubricant did not result in
a friction factor of zero.

Feasibility tests were carried out on shapes involving
the use of split dies, Fig. 41. Photographs showing
the different shapes produced are shown in Fig. 42.
These shapes have not been investigated analytically
but could serve as a basis for further work.
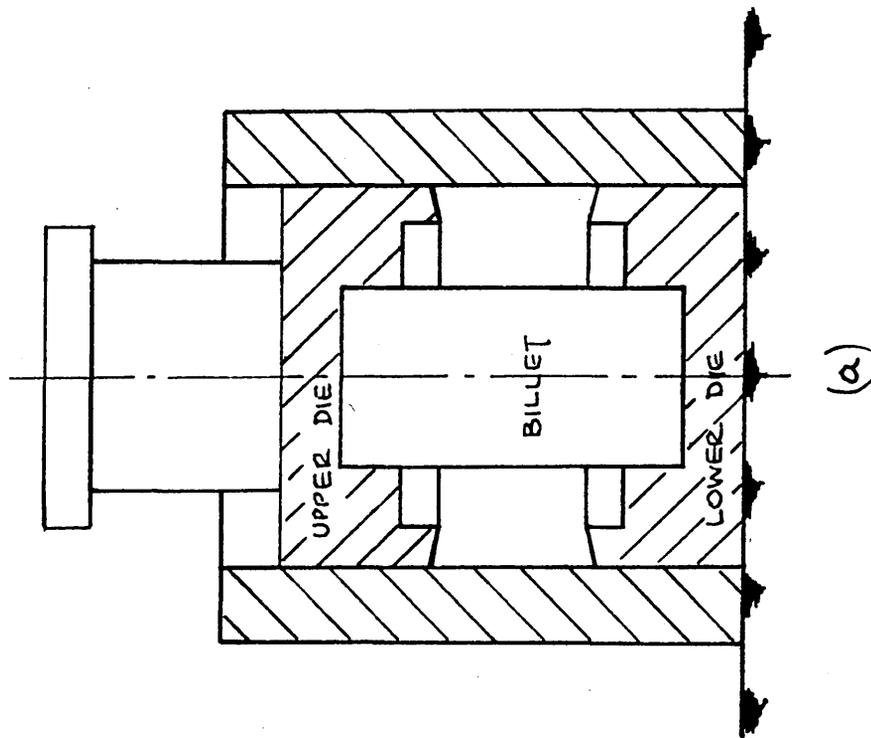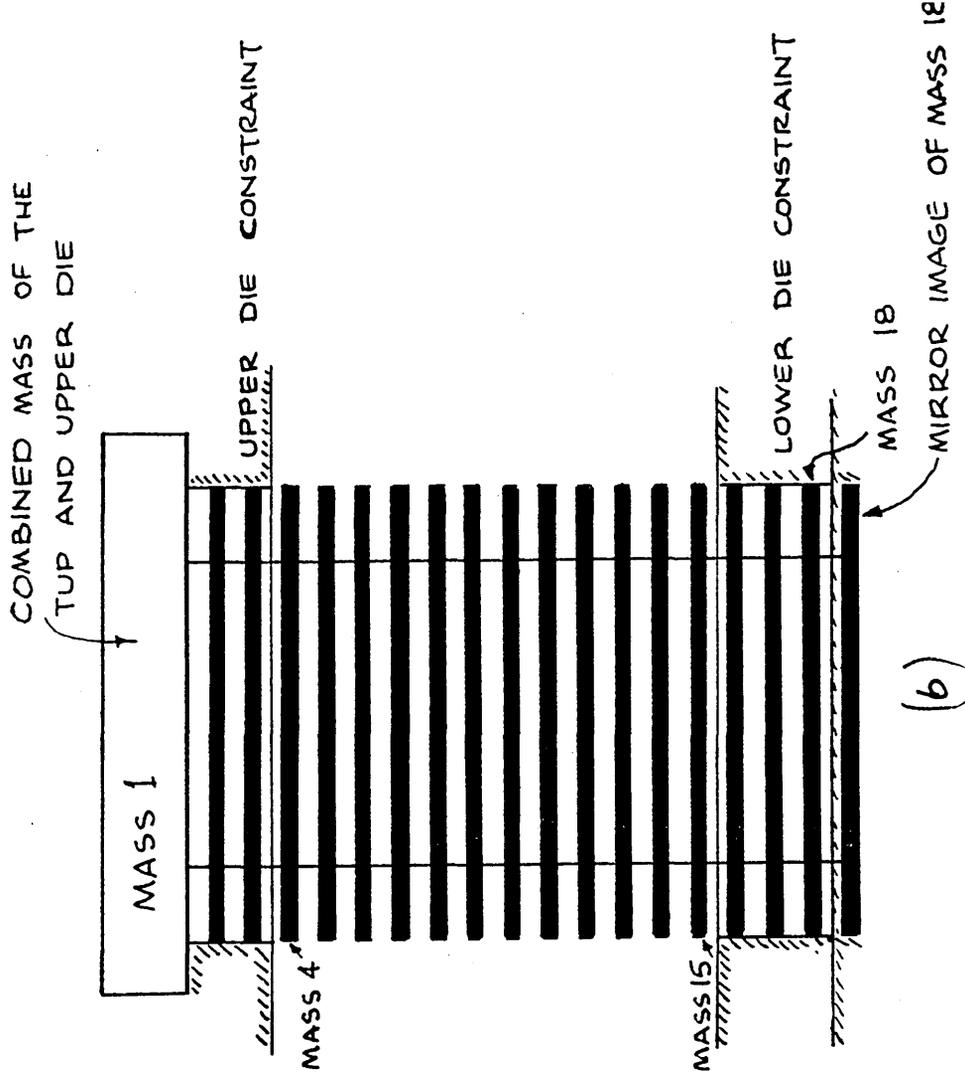
COMBINED MASS OF THE TUP AND UPPER DIE

UPPER DIE CONSTRAINT

LOWER DIE CONSTRAINT

MASS 18

MIRROR IMAGE OF MASS 18

MASS 1

MASS 4

MASS 15

(b)

EQUIVALENT NUMERICAL MODEL

UPPER DIE

BILLET

LOWER DIE

(a)

ACTUAL LOADING CONFIGURATION

OF THE BILLET

FIG. 33.

78

CYLINDRICAL LEAD
BILLET

24 mm ϕ

46 mm

FINAL DEFORMED SHAPE

24 mm ϕ

40 mm ϕ

8

10

8

FIG. 34.

79

ORIGINAL PROFILE

$t = 85\mu$ sec

$t = 145\mu$ sec

$t = 175\mu$ sec
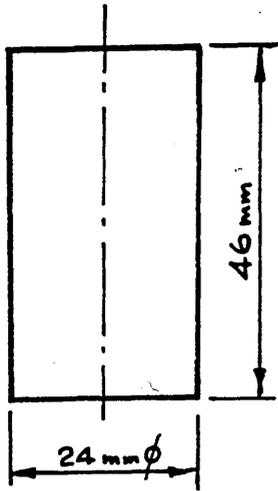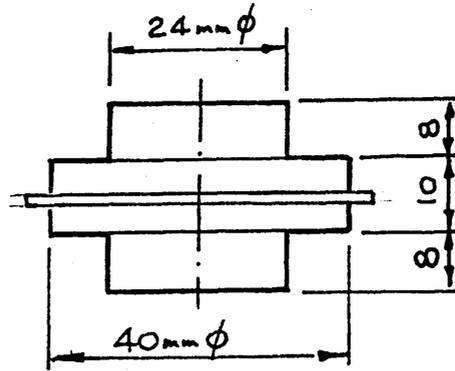
FINAL PROFILE
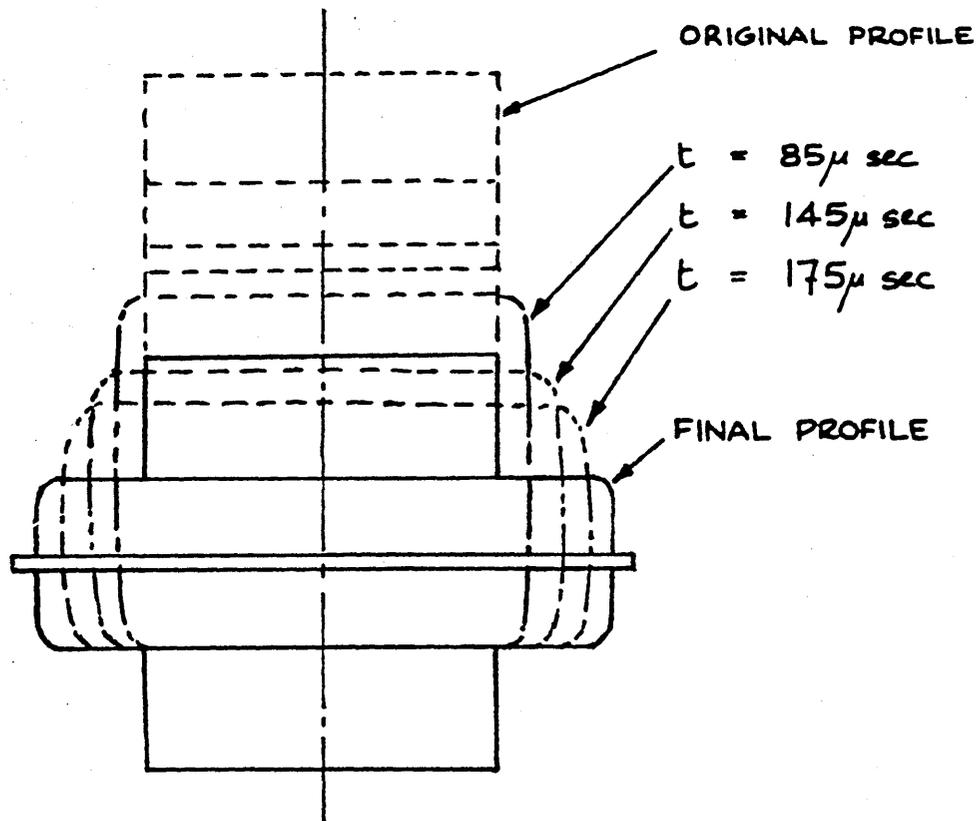
THEORETICALLY PREDICTED INSTANTANEOUS
PROFILES UNDER LUBRICATED CONDITIONS.

FIG. 35

ORIGINAL PROFILE

t = 85μ sec.

t = 145μ sec.

t = 175μ sec.

FINAL PROFILE
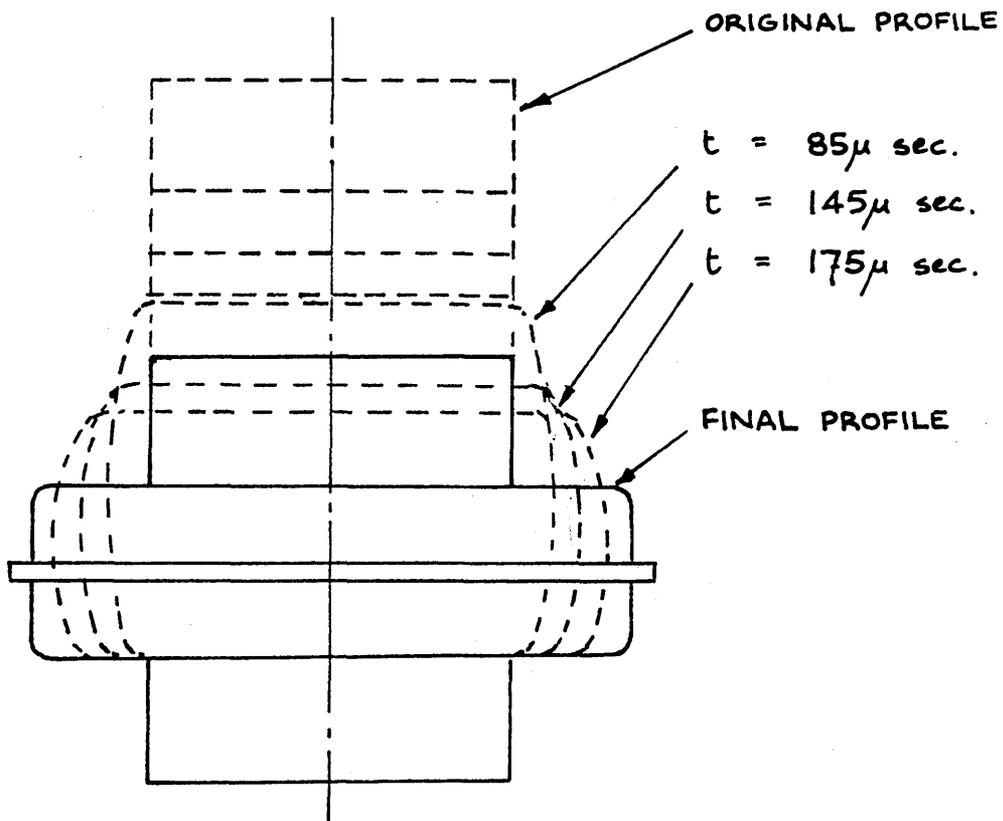
THEORETICALLY PREDICTED INSTANTANEOUS
PROFILES UNDER DRY FRICTION CONDITIONS

FIG. 36

81
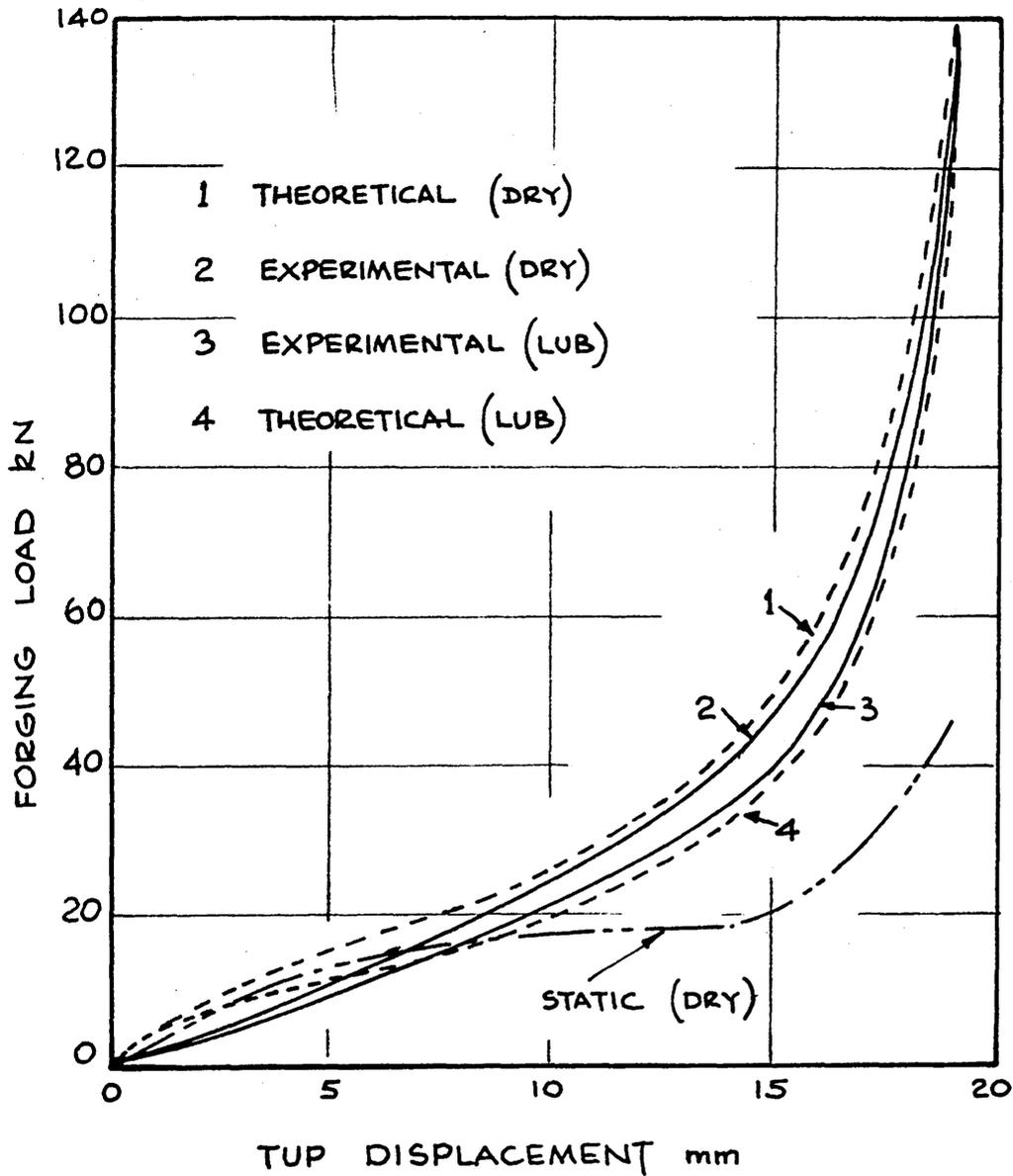
COMPARISON OF THEORETICAL AND EXPERIMENTAL
FORGING LOAD Vs TUP-DISPLACEMENT CURVES.

FIG. 37
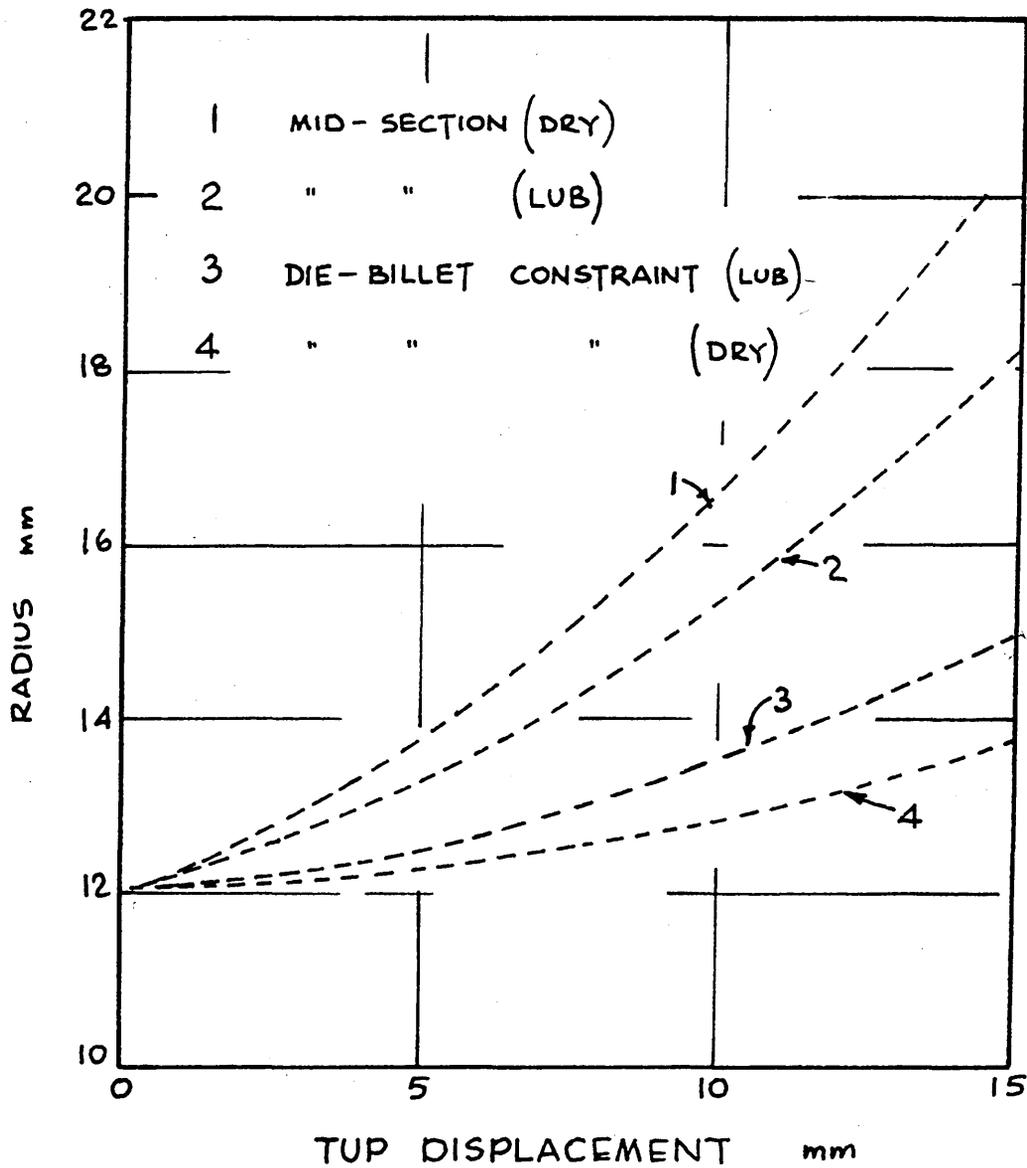
VARIATION IN BILLET RADIUS WITH TUP
DISPLACEMENT AT MID-SECTION AND
DIE-BILLET CONSTRAINT.

FIG. 38
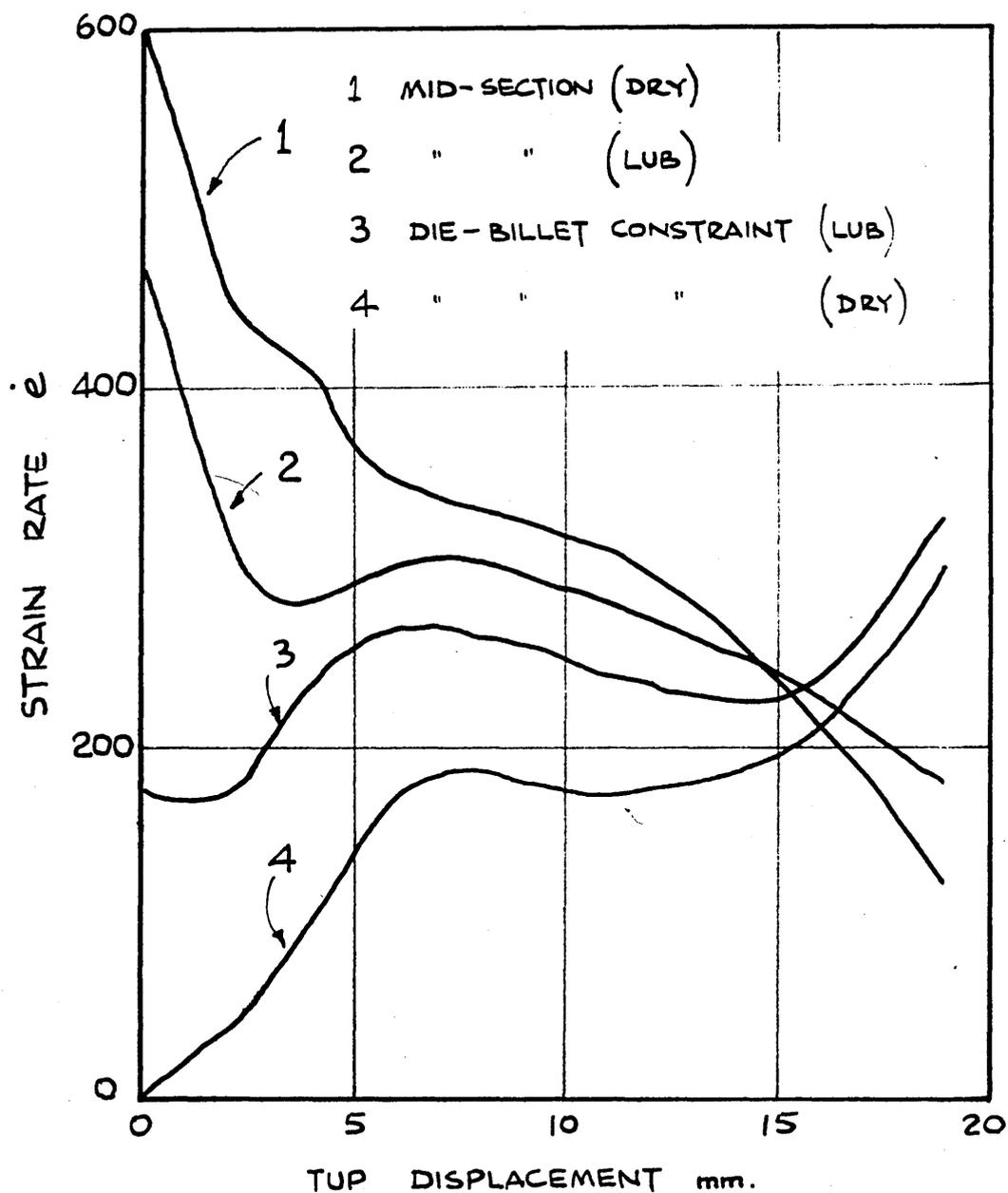
83

VARIATION IN STRAIN RATE WITH TUP DISPLACEMENT
AT MID-SECTION AND DIE BILLET CONSTRAINT.

FIG. 39
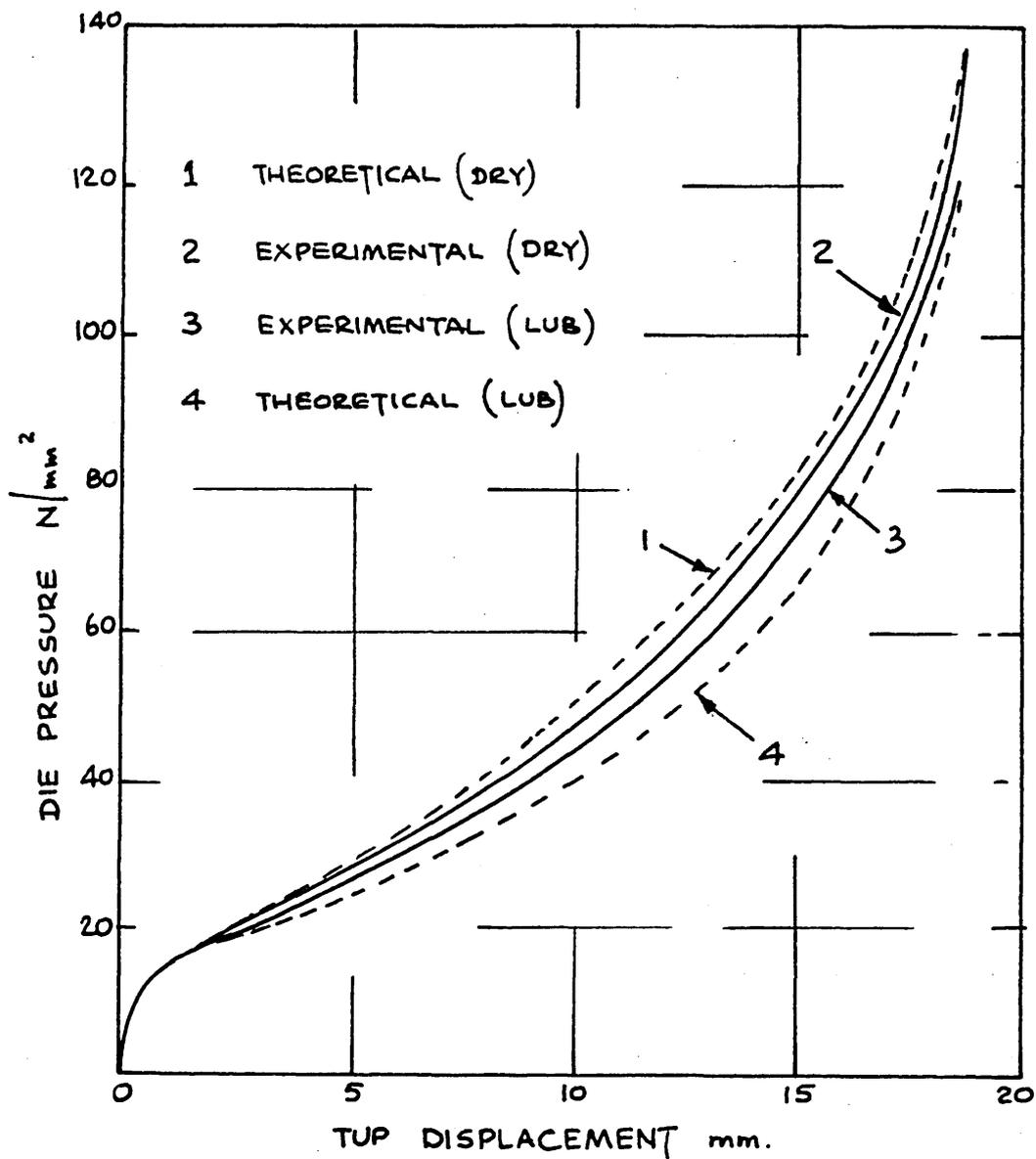
SHOWING DIE PRESSURE Vs TUP DISPLACEMENT
CURVES PREDICTED THEORETICALLY AND
OBTAINED EXPERIMENTALLY.

FIG. 40.

85

SPLIT DIES.   FIG. 41

CLOSED DIE FORGINGS.   FIG. 42.

6.1 Introduction

In chapter 3 the mathematical model used was formulated to take into account forging conditions where the flow of metal during deformation was entirely radial. A more complex material flow situation is where flow is partly radial and partly axial i.e. extrusion forging. In this chapter extrusion forging is analysed by assuming that the energy absorbed during deformation is used to deform the material plastically, while being strained axially, and at the same time shear energy is required as the boss is being formed.

A relevant analysis has been presented earlier in reference [6l] in which the equations for predicting various parameters during extrusion forging were formulated based on an assumed velocity field. In this analysis attempts were taken to take into account the influence of billet and tool geometry speed and frictional conditions. However, the analysis, which appears to be very complex was derived on the basis of the assumption that the billet deformed in a purely cylindrical manner throughout the deformation period. Furthermore the frictional effect on the total height of the deformed specimen was found to be exaggerated and the correspondence between the theoretical and experimental shapes of the billet for deformations up to about 70% have never been demonstrated. This aspect of the product shape during the earlier stages

of deformation which shows significant deviation
from the assumption of purely cylindrical deformation,
should be taken into account in formulating an analysis.

In this work such an analysis has been attempted,
initially under frictionless condition, which
predicts the shape during the first 70% of the deforma-
tion which shows severe tapering of the flange during
the deformation especially when the boss to billet
ratio is more than 40%. Very good agreement between
the theoretically predicted and experimentally observed
flange shapes was predicted over a large range of
boss to billet diameter ratios. This is thought to be
the main contribution of this work towards the study
of extrusion forging. Subsequently an attempt has
been made to incorporate the effect of friction in
the analysis in an approximate and simple manner, and
has been outlined in Section 6.2.4.

In the analysis outlined in the following sections
the deformation is shown to be in two stages. In the
first stage deformation of the top surface begins
when the applied load is just sufficient to cause
local yielding of the billet. This yielding causes
the top surface to spread radially while the lower
portion of the billet retains its original radial
dimension. However the lower portion of the billet
begins to expand radially when the applied load is
large enough to cause yielding in that area. This

marks the beginning of the second stage. At the end
of the first stage the overall depth at which
plastic yielding occurs is shown to be equal to half
the boss diameter.

From the commencement of the second stage any increase
in load causes deformation such that axial
compression becomes directly related to a simultaneous
increase in the billet diameter.

Equations have been derived which enabled the tup load,
total energy absorbed, boss and flange heights and
profile of the deformed billet to be calculated.

90

SYMBOLS

D   billet diameter at depth h

H   depth *
k   shear yield stress = ($\frac{\tau}{2}$ for Tresca Yield Criterion)
K   constant

Y   yield stress

h   axial depth *

w   plastic work done per unit volume

D_B billet diameter

D_C boss diameter

P_H load at depth H

P_O load required to initiate formation of boss

W_S shear work done

W_P plastic work done

W_T total work done

H_1 depth of shear zone

H_2 depth of flange taper

H_0 depth of plastic yield zone

L_0 original length of billet

h_0 depth of flange taper

h_1 flange dimension *

h_2 depth of flange with constant diameter

x_1 axial displacement

H' depth *

D_B' bottom diameter of flange

P_H' load *

ε true strain

* defined in text

6.2.1 First Stage

In formulating the equations it is assumed that the material of the billet is rigid perfectly plastic with a yield stress Y. Referring to Fig. 43 D_B is the diameter of the billet, D_C is the diameter of the die cavity and L_O is the height of the undeformed billet. Let P_O be the load which is just sufficient to initiate plastic deformation to the ring area of the billet. Thus:

$$P_O = \frac{\pi}{4}Y(D_B{}^2 - D_C{}^2) \hspace{2cm} (1)$$

Let P be the applied load which is greater than P_O and which is sufficient just to cause plastic yielding to the ring area at a location H_O. At any other intermediate location the compressive load available to deform the ring area is given by:

$$P_H = P_O + \pi D_C k H \hspace{2cm} (2)$$

where H is the distance as shown in Fig. 43 and k is the shear yield stress of the material which may be taken as equal to Y/2. Substituting for k in equation (2) we have

$$P_H = P_O + \frac{\pi}{2}D_C Y H \hspace{2cm} (3)$$

when $H = H_O$ (denoting the top contact surface), P_H is simply given by the applied force P. Thus

$$P = P_O + \frac{\pi}{2}D_C Y H_O \hspace{2cm} (4)$$

which upon substitution for P_O becomes

$$P = \frac{\pi}{4}Y(D_B{}^2 - D_C{}^2) + \frac{\pi}{2}D_C Y H_O \quad\text{———— ————} \quad (5)$$

when P reaches a value P_1 which is sufficient to
cause plastic yielding of the billet as a whole, then

$$P = P_1 = \frac{\pi}{4}D_B{}^2 Y \quad\text{————————} \quad (6)$$

substituting for P in equation (5) we get

$$\frac{\pi}{4}D_B{}^2 Y = \frac{\pi}{4}(D_B{}^2 - D_C{}^2)Y + \frac{\pi}{2}D_C Y H_O$$

which upon rearrangement and simplification gives the
depth, H_O, of the plastically yielded zone before the
billet starts to deform, thus:

$$H_O = D_C/2 \quad\text{————————————} \quad (7)$$

Hence during the first stage of deformation, the
plastic zone will extend to a depth equal to half the
diameter of the boss.

Assuming that the billet deforms under the action of
P in the manner shown in Fig (43), let an element at
a location H before deformation correspond to an ele-
ment at a location h of the deformed billet. P_H will
thus be the load just sufficient to deform
plastically the new element of outer diameter D. Thus:

$$P_H = \frac{\pi}{4}Y(D^2 - D_C{}^2) \quad\text{————————————} \quad (8)$$

Substituting for P_H in equation (3) and noting that
$P_O = \frac{\pi}{4}Y(D_B{}^2 - D_C{}^2)$ and $k = \frac{Y}{2}$ we get,

$$\frac{\pi}{4}Y(D^2 - D_C{}^2) = \frac{\pi}{4}Y(D_B{}^2 - D_C{}^2) + \frac{\pi}{2}YD_CH$$

which upon simplification and rearrangement becomes:

$$H = (D^2 - D_B{}^2)/2D_C \hspace{3cm} (9)$$

Equation (9) gives the relationship between the diameter of the deformed shape and the parameter H which locates the position of the element of the undeformed billet. During this first stage of deformation the total work done may be expressed in terms of the plastic work and shear work done in the billet.

The plastic work per unit volume may be given by:

$$w = \int_0^\varepsilon \sigma d\varepsilon \hspace{3cm} (10)$$

since for a rigid plastic material

$$\sigma = Y \text{ (constant)}$$

hence, $w = Y\varepsilon$, which for the small element of original thickness 'dH' becomes:

$$w = Y\ln(\frac{dH}{dh}) \hspace{3cm} (11)$$

Plastic work done on the element is thus given by

$$w_d = dVY\ln(\frac{dH}{dh})$$

where dV is the volume of the element.

Thus

$$w_d = \frac{\pi}{4}(D^2 - D_C{}^2)dh\,Y\ln\left(\frac{dH}{dh}\right) \quad\text{——————————}\quad (12)$$

Total work done on the outer sleeve

$$p = \frac{\pi}{4}Y\int_O^{h_O}(D^2 - D_C{}^2)\ln\left(\frac{dH}{dh}\right)dh \quad\text{——————————}\quad (13)$$

From volume constancy of the element

$$dH(D_B{}^2 - D_C{}^2) = dh(D^2 - D_C{}^2)$$

$$\text{or}\quad \frac{dH}{dh} = \frac{D^2 - D_C{}^2}{D_B{}^2 - D_C{}^2} \quad\text{——————————}\quad (14)$$

and

$$dh = dH\left(\frac{D_B{}^2 - D_C{}^2}{D^2 - D_C{}^2}\right) \quad\text{——————————}\quad (15)$$

so that combining equations (13), (14) and (15)

$$W_p = \frac{\pi}{4}Y\int_O^{H_O}(D^2 - D_C{}^2)\ln\left(\frac{D^2 - D_C{}^2}{D_B{}^2 - D_C{}^2}\right)\times\left(\frac{D_B{}^2 - D_C{}^2}{D^2 - D_C{}^2}\right)dH$$

or

$$W_p = \frac{\pi}{4}\int_O^{H_O}(D_B{}^2 - D_C{}^2)\ln\left(\frac{D^2 - D_C{}^2}{D_B{}^2 - D_C{}^2}\right)dH \quad\text{——————}\quad (16)$$

From equation (9)

$$H = (D^2 - D_B{}^2)/2D_C \quad\text{——————————————}\quad (17)$$

$$\text{or}\quad \frac{dH}{dD} = \frac{2D}{2D_C}$$

and

$$dH = \frac{D}{D_C}dD \quad\text{——————————————}\quad (18)$$

Combining equations (18) and (16)

$$W_p = \frac{\pi}{4}Y\int_{D_B}^{D_1}(D_B{}^2 - D_C{}^2)\ln\left(\frac{D^2 - D_C{}^2}{D_B{}^2 - D_C{}^2}\right)\frac{D}{D_C}dD$$

or

$$W_p = \frac{\pi}{4}Y(\frac{D_B{}^2 - D_C{}^2}{D_C})\left[\int_{D_B}^{D_1} \ln(D^2 - D_C{}^2)DdD -\right.$$

$$\left.\int_{D_B}^{D_1} \ln(D_B{}^2 - D_C{}^2)DdD\right] \text{——} (19)$$

Now the integral:

$$\int_{D_B}^{D_1} \ln(D_B{}^2 - D_C{}^2)D.dD = \ln(D_B{}^2 - D_C{}^2)(\frac{D_1{}^2 - D_B{}^2}{2})$$

$$\text{——} (20)$$

and the integral

$$\int_{D_B}^{D_1} \ln(D^2 - D_C{}^2)DdD \text{——————} (21)$$

may be carried out as follows:

let $\ln(D^2 - D_C{}^2) = Z$

$\therefore \quad D^2 - D_C{}^2 \quad\;\; = e^Z$

or $\quad \dfrac{dZ}{dD} \quad\qquad = \dfrac{2D}{D^2 - D_C{}^2}$

hence $DdD \quad\qquad = (\dfrac{D^2 - D_C{}^2}{2})dZ = \dfrac{e^Z}{2} dZ$

Back substitution into equation (21) and integrating
we have:

$$\tfrac{1}{2}\int_{D_B}^{D_1} Ze^Z dZ = \frac{e^Z}{2}(Z - 1)$$

hence

$$\int_{D_B}^{D_1} \ln(D^2 - D_C{}^2)DdD = \tfrac{1}{2}\left[(D^2 - D_C)\{\ln(D^2 - D_C{}^2) - 1\}\right]_{D_B}^{D_1}$$

$$= \tfrac{1}{2}\left[(D^2 - D_C{}^2)\{\ln(D_1{}^2 - D_C{}^2) - 1\}\right] - \tfrac{1}{2}\left[(D_B{}^2 - D_C{}^2)\right.$$

$$\left.\{\ln(D_B{}^2 - D_C{}^2) - 1\}\right] \text{——} (22)$$

combining equations (19), (20) and (22)

$$W_p = \frac{\pi}{4}Y(\frac{D_B^2 - D_C^2}{2D_C})[(D_1^2 - D_C^2)\{\ln(D_1^2 - D_C^2) - 1\} - $$

$$(D_B^2 - D_C^2)\{\ln(D_B^2 - D_C^2) - 1\} - (D_1^2 - D_B^2)$$

$$\ln(D_B^2 - D_C^2)]$$

which after simplification and rearrangement becomes

$$W_p = [(D_1^2 - D_C^2)\{\ln(D_1^2 - D_C^2) - 1 - \ln(D_B^2 - D_C^2)\} +$$

$$(D_B^2 - D_C^2)]\frac{\pi}{4}Y(\frac{D_B^2 - D_C^2}{2D_C}) \quad\text{———————} \quad (23)$$

The shear work done along the interface of the outer sleeve and inner core material gives:

$$W_S = \frac{\pi}{2}D_C\frac{Y}{2}(H_o - x_o)x_o \quad\text{———————}\quad (24)$$

Total work done

$$W_T = W_P + W_S$$

The total work done by the **tup** load = average tup load x displacement

$$(\frac{P_o + P_1}{2})x_o = W_P + W_S \quad\text{———————}\quad (23b)$$

When the tup load reaches P_1

$$P_1 = \frac{\pi}{4}(D_1^2 - D_C^2)Y = \frac{\pi}{4}D_B^2Y$$

which gives the diameter of the billet at the tup interface. Thus,

$$D_1 = \sqrt{D_B{}^2 + D_C{}^2}$$

To determine the shape of the billet profile at the end of the first stage of deformation we have, from equation (15)

$$dh = dH\frac{(D_B{}^2 - D_C{}^2)}{(D^2 - D_C{}^2)} \tag{24}$$

let $(D^2 - D_C{}^2) = Z$

then $DdD = \dfrac{dZ}{2}$ \hspace{2cm} (25)

from equation (18)

$$DdD = D_C dH \tag{26}$$

combining equations (24), (23) and (26)

$$dh = \frac{DdD}{D_C}\left(\frac{D_B{}^2 - D_C{}^2}{Z}\right)$$

$$dh = \left(\frac{D_B{}^2 - D_C{}^2}{2D_C}\right)\frac{dZ}{Z}$$

$$dh = K\frac{dZ}{Z} \tag{27}$$

where $K = \left(\dfrac{D_B{}^2 - D_C{}^2}{2D_C}\right)$

integrating equation (27)

$$h + C = K\ln(D^2 - D_C{}^2)$$

when $h = 0$, $C = K\ln(D_B{}^2 - D_C{}^2)$

hence $h = K\ln(D^2 - D_C{}^2) - K\ln(D_B{}^2 - D_C{}^2)$ \hspace{0.5cm} (28)

98

6.2.2 Second Stage

During this stage, any increase in load will cause deformation such that the outer sleeve will be compressed axially with a simultaneous increase in the billet diameter.

Let the load P be greater than P_1 such that

$$P = \frac{\pi}{4}(D_B{}')^2 Y \quad\text{——————————}\quad (29)$$

where $D_B{}'$ is the expanded billet diameter at the lower end. Equation (5) is equally applicable to this new situation. Thus

$$P_H{}' = \frac{\pi}{4}Y(D_B{}_1^2 - D_C{}^2) + \frac{\pi}{2}D_C Y H' \quad\text{——————}\quad (30)$$

where H' locates an element of the deformed sleeve as shown in Fig. 44.

In this case, at $H' = H_1$, $P_{H'} = P$
so that $P = \frac{\pi}{4}Y(D_B{}_1^2 - D_C{}^2) + \frac{\pi}{2}D_C Y H_1$ ————— (31)

By combining equations (29) and (31) it can be seen that

$$H_1 = \frac{D_C}{2} \quad\text{———————————————}\quad (32)$$

Thus the shear zone is extended axially by an amount H_1 and the lower part of the billet, of height $(L_1 - H_1)$, will deform in a pure compression mode.

For an axial compression of x_1 the shear zone changes from H_1 to H_2. Thus the axial strain

$$\varepsilon = \ln\left(\frac{L_1}{L_1 - x_1}\right) = \ln\left(\frac{H_1}{H_2}\right) \quad\text{————— (32a)}$$

$$\text{or} \quad H_2 = \frac{H_1}{L_1}(L_1 - x_1) = \left(H_1 - H_1\frac{x_1}{L_1}\right) \quad\text{————— (33)}$$

The mean shear zone is thus given by:
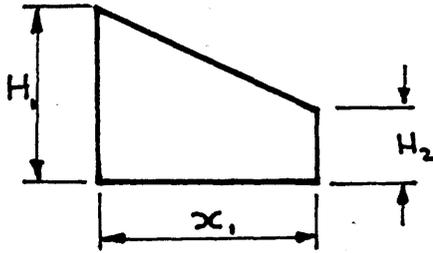
$$\frac{H_1 + H_2}{2} = \tfrac{1}{2}\left(H_1 + H_1 - \frac{H_1 x_1}{L_1}\right)$$

$$= \left(H_1 - \frac{H_1 x_1}{2L_1}\right)$$

The height of the section of the billet under pure compression may be obtained as follows:

$$\varepsilon = \ln\left(\frac{L_1}{L_1 - x_1}\right) = \ln\left(\frac{h_1}{h_2}\right)$$

$$\text{or} \quad h_2 = \frac{h_1}{L_1}(L_1 - x_1) \quad\text{——————————— (34)}$$

Total work done in the second stage

Plastic work done on the sleeve may be expressed as:

$$W_{ps} = \frac{\pi}{4}(D_B{}^2 - D_C{}^2)Y\ln\left(\frac{h_1}{h_2}\right)(H_1 + x_o) \quad\text{——— (35)}$$

and the shear work done between the sleeve and the inner core can be expressed as

$$W_S = \frac{\pi D_C Y}{2} x_1\left(H_1 - \frac{H_1 x_1}{2L_1}\right) \quad\text{——————— (36)}$$

SLEEVE   INNER CORE

100
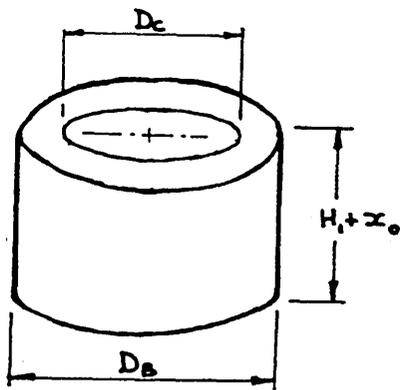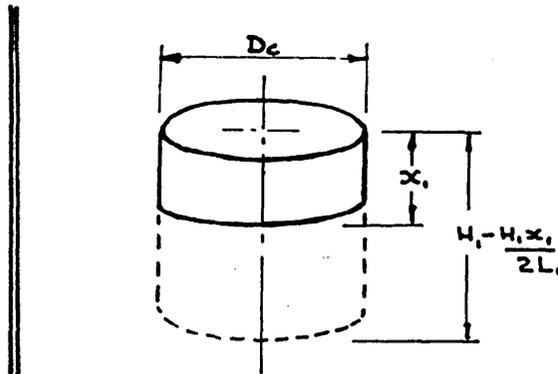
The shear work done at the junction of the boss and the lower part of the flange which is deforming in a pure compression mode

$$W_{S_1} = \frac{\pi D^2 Y_O}{8} (D_C{}' - D_C)$$

where $D_C{}'$ is the virtual increase in D_C due to an incremental compression x_1.

Also the plastic work done on the lower part of the billet is given by

$$W_P = (L_O - x_O - H_1)\frac{\pi}{4}D_B{}^2 Y \ln(\frac{h_1}{h_2}) \quad\text{————— (37)}$$

Total work done in the second stage is thus obtained by the sum total of all the works expressed by equations (35), (36) and (37). Thus,

$$W_t = \frac{\pi}{4}(D_B{}^2 - D_C{}^2)Y\ln(\frac{h_1}{h_2}) \times (H_1 + x_O) + \frac{\pi D_C Y}{2}$$

$$x_1(H_1 - \frac{H_1 x_1}{2L_1}) + (L_O - x_O - H_1)\frac{\pi}{4}D_B{}^2 Y \ln(\frac{h_1}{h_2})$$

$$+ \frac{\pi D^2 Y_O}{8} (D_C{}' - D_C) \quad\text{————— (37a)}$$

The tup load at the end of a small axial compression, x_1, can be calculated by equating the total plastic work done to the work done by the external load. Thus,

$$(\frac{P_1 + P_2}{2})x_1 = W_t$$

$$\text{hence } P_2 = \frac{2W_t}{x_1} - P_1 \quad\text{——————————————— (38)}$$

From Fig. 44 the boss height is given by

$$h_b = x_o + [x_1 - h_1 + h_2] \hspace{2cm} (39)$$

and the flange height is given by:

$$h_f = H_2 + h_2 \hspace{3cm} (40)$$

where H_2 and h_2 are given by equations (33) and (34) respectively.

The radial strain at the top of the sleeve may be expressed as

$$\varepsilon_r = \ln[\frac{(D_2 - D_C)}{(D_1 - D_C)}]$$

which is equal to half the axial strain ε given by equation (32a) hence,

$$D_2 - D_C = (D_1 - D_C) \exp(\frac{\varepsilon}{2})$$

so that

$$D_2 = D_C + (D_1 - D_C) \exp(\frac{\varepsilon}{2}) \hspace{2cm} (41)$$

Equation (41) thus enables calculation of the diameter at the top of the flange.

Similarly, the radial strain at the bottom of the sleeve may be expressed as

$$\varepsilon_1 = \ln[\frac{(D_B' - D_C)}{(D_B - D_C)}] = \frac{\varepsilon}{2}$$

which gives

$$D_B' = D_C + (D_B - D_C) \exp(\frac{\varepsilon}{2}) \hspace{2cm} (42)$$

Equation (42) thus gives the diameter at the bottom

of the flange.

These equations were used to obtain theoretical values for later comparison with those obtained experimentally. The results tabulated on pages A3.1 to A3.6 were calculated using a computer program given in Appendix 4. The foregoing equations were used in the following sequence in evaluating the theoretical results.

a) Equations (1) and (6) were used to calculate the values of P_o and P_1, the forces needed to initiate stages one and two respectively.

b) Equation (7) was used to obtain H_o, the amount of plastic deformation at the end of the first stage.

c) Equation (23) was used to calculate W_p, the plastic work done at the end of the first stage.

d) Equation (23a) was used to calculate W_s the amount of shear work done at the end of the first stage.

e) Equations (23), (23a) and (23b) together with equations (1) and (6) were used to find x_o, the boss height at the end of stage 1.

f) Equation (37a) was used to calculate W_t, the total work done during the second stage, for known values of x_1.

g) Equation (38) was used to calculate P_2, the maximum forging load for compression up to $(x_o + x_1)$.

h) Equations (39) and (40) were used to calculate h_b and h_f, the boss and flange heights at this stage.

Finally, equations (41) and (42) were used to calculate D_2 and D_B' the top and bottom flange diameters respectively. The procedure is repeated taking incremental values of x_1, each time the final values of the previous stage is taken as the starting value for the next stage. During this stage the energy requirement for deformation under the second and third modes are continuously compared until the extent of deformation is reached after which less energy is required to deform the billet in the third mode. The deformation there after carries on until the end of compression.

6.2.3 Third Stage

At some point during the deformation according to the mode prescribed in the second stage the billet will require less energy to deform in a mode in which only the outer sleeve is compressed and the central core remains rigid. The energy required is given by the sum of the energy to compress the outer sleeve and the shear energy at the sleeve-core interface. Thus, the plastic energy in the sleeve is given by:

$$W_{psi} = \frac{\pi}{4} Y L_o (D_B{}^2 - D_C{}^2) \ln\left(\frac{L_1}{L_1 - x_1}\right) \quad\text{————}\quad (43)$$

and the shear energy is given by:

$$W_{si} = \frac{\pi D_C}{2} Y x_1 (L_1 - \frac{x_1}{2}) \quad \text{———————} \quad (44)$$

6.2.4 Effect of Friction

The effect of friction at the die-billet interface on
the load and deformation modes in extrusion forging
may be accounted for in the above analysis in an
approximate but simple manner outlined below.

Assuming that the frictional shear stress can be
expressed in terms of mk where m is the friction
factor and k is the shear yield stress given by
k = Y/2 according to the Tresca yield criterion.
Equations (1) and (6) become:

$$P_O = \frac{\pi}{4} Y (D_B{}^2 - D_C{}^2)(1 + \frac{m D_B}{6 L_O}) \quad \text{———————} \quad (45)$$

and

$$P_1 = \frac{\pi}{4} Y D_B{}^2 (1 + \frac{m D_B}{6 L_O}) \quad \text{———————} \quad (46)$$

respectively. In the above equations it is assumed
that the mean forging pressure at the top and
bottom interfaces are modified by the friction
term $(1 + \frac{m D_B}{6 L_O})$ for $\frac{D_B}{L_O}$ ratios of about unity.

The depth H_O, of the initial plastic zone given by
equation (7) becomes

$$H_O = \frac{D_C}{2} + \frac{m}{12 L_O}(\frac{D_B}{D_C}) \quad \text{———————} \quad (47)$$

In calculating the boss height, x_O, at the end of
the first stage of deformation, equation (23b) needs

to be modified by the addition of frictional work done at the top die interface. No frictional work is done at the bottom interface during this stage. The frictional force at the top interface at the start of deformation is given by:

$$F_1 = 2\pi m K \int_{R_C}^{R_B} R dr$$

which after integrating and expressing in terms of the diameters and noting that $k = Y/2$, becomes

$$F_1 = \frac{\pi m Y}{8} (D_B{}^2 - D_C{}^2)$$

similarly, the friction force at the end of the first stage is given by

$$F_2 = \frac{\pi m Y}{8} (D_1{}^2 - D_C{}^2)$$

where D_1 is the top interface diameter and Y is assumed to remain constant during this stage.

The frictional work done during this stage may then approximately be expressed as

$$W_{f1} = \text{average frictional force x displacement}$$

or

$$W_{f1} = \frac{F_1 + F_2}{2} \times (D_1 - D_B)$$

which after substitution for F_1 and F_2 becomes:

$$W_{f1} = \frac{\pi m Y}{16} (D_1{}^2 + D_B{}^2 - 2D_C{}^2)(D_1 - D_B)$$

equation (23b) thus becomes

$$\left(\frac{P_0 + P_1}{2}\right) x_0 = W_p + W_s + W_{f1} \quad\text{————— (48)}$$

At the end of the first stage the lower end of the billet also starts to deform plastically and the second stage of deformation commences. For any increment, x_1, in compression the diameter D_1 at the top interface becomes D_2 and that at the bottom interface becomes D_B'.

The frictional force at the top interface at the start of the second stage is given by:

$$F_{2t} = \frac{\pi m Y}{8} (D_1{}^2 - D_C{}^2)$$

and that at the end of deformation is given by:

$$F_{3t} = \frac{\pi m Y}{8} (D_2{}^2 - D_C{}^2)$$

The frictional work done at the top interface during this stage is thus obtained in the same manner as before. Hence,

$$W_{ft} = \frac{\pi m Y}{16} (D_2 - D_1)(D_2{}^2 + D_1{}^2 - 2D_C{}^2) \quad\text{————(49)}$$

similarly, the frictional work done at the bottom interface is given by:

$$W_{fb} = \frac{\pi m Y}{16} (D_B' - D_B)(D_B'{}^2 + D_B{}^2) \quad\text{—————(50)}$$

Total frictional work done during this incremental compression, x_1, is thus,

$$W_{f2} = W_{ft} + W_{fb} \quad\text{————————— (51)}$$

The forging load P_2 is then given by equation (38) as:

$$P_2 = \frac{2}{x_1}(W_t + W_{f2}) - P_1$$

or the mean forging load P_m is given by:

$$P_{m2} = (W_t + W_{f2})/x_1 \quad\text{——————————}\quad (52)$$

The deformation mode changes at some stage during the second mode of deformation. In this changed mode the central core remains rigid and the outer sleeve deforms plastically. The forging load in this mode becomes less than that required for the previous mode. The plastic work done during this third stage is given by:

$$W_{3p} = \frac{\pi}{4}(D_B^2 - D_C^2)Y \; L_o \ln\left(\frac{L_1}{L_1 - x_1}\right) \quad\text{————}\quad (53)$$

where L_1 and x_1 are the current billet height and incremental compression respectively.

The shear work done between the inner rigid core and outer sleeve is given by:

$$W_{3s} = \frac{\pi}{2}D_C \; Y \; x_1\left(L_1 - \frac{x_1}{2}\right) \quad\text{——————————}\quad (54)$$

The frictional work at the top and bottom interfaces are given by equations (49) and (50) respectively.

The mean forging load during any incremental compression, x_1, is given by:

$$P_m = (W_{3P} + W_{3S} + W_{ft} + W_{fb})/x_1 \quad\text{————}\quad (55)$$

In the absence of friction, the deformation continues in this manner. However, due to the presence of friction, at some stage of deformation, which is dependent on the friction factor, m, the billet starts to deform in pure extrusion mode. This only happens when the frictional constraint is so high that the force required to extrude the billet becomes less than that to cause radial expansion. In reference [63] it has been suggested that the extrusion pressure for axisymmetric extrusion of lead may be expressed as

$$P = Y(0.8 + 1.5 \ln \frac{A_1}{A_2}) \qquad\qquad\qquad (56)$$

The extrusion force is thus given by

$$P_e = A_1 p \qquad\qquad\qquad\qquad\qquad (57)$$

where A_1 is the current area at the bottom end of the billet.

If at any point during the deformation the mean forging load P_m given by equation (55) becomes greater than P_e, the extrusion force, then the billet will start to deform in pure extrusion mode. In this mode, no further radial expansion of the billet will take place and axial compression will cause the boss height to increase obeying the rule of volume constancy. Hence the increase in the boss height for any incremental compression, x_1, is given by

109

6.3 Experimental Work

Cylindrical lead billets of 24 mm diameter and 24 mm
height were forged dynamically under the drop hammer
and quasi-statically using a compression testing
machine. Quasi-static tests were also carried out on
copper and aluminium billets of 24 mm diameter and
24 mm height. The tool and die arrangement is shown in
Fig. 45. Fig. 46 shows the use of a positioning ring
to centralise the billet over the die cavity. Two
types of friction conditions were investigated, one,
using acetone to dry the contacting surfaces and the
other, using a mixture of graphite in petroleum jelly
to induce low friction. Three different die cavities
of diameters 18, 12 and 9 mm were used to obtain
different billet to cavity diameter ratios. For double
ended extrusion tests die cavities of 18 mm diameter only
were used. The instrumentation used is as described in
Chapter 2. From the compression test results shown in
Fig. 12, it was found reasonable to assume that for
comparison with quasi-static tests, the lead billets
behaved as a rigid-perfectly plastic material with a
constant yield stress of 17 N/mm^2. Under dynamic test
conditions, of course, strain rate sensitivity and
material inertia effects would render this value
inapplicable as far as forging load is concerned.

6.4 Results and Discussions

The extrusion forging tests produced specimens with

a distinct profile irrespective of the material used
and of the method of deformation. The profile produced
lent itself to ready measurement using micrometers and
vernier calipers. Quasi-static and dynamic tests were
carried out, with and without lubrication, for
different billet to boss diameter ratios. These
results were compared with those calculated theoreti-
cally by applying the appropriate equations in the
analysis.

6.4.1 Single Ended Extrusion Forging

Fig. 47 and 48 shows a series of predicted profiles
of billets when dies of 18 mm and 9 mm diameter
cavities are used. The predicted profiles show
close similarity with those observed experimentally.
Where the boss diameter is small the deformed
billet will exhibit a small shoulder which quickly
tapers back to the original diameter. A die with a
large cavity diameter causes the deformed billet
to expand radially producing a large shoulder and
a considerable taper. Figs. 49 and 50 show a
number of photographs which depict the deformation
mode of lead billets. The shapes of the lead
specimens at different stages of deformation having
a boss diameter of 18 mm can be seen in the photo-
graph in Fig. 49. The shapes of lead specimens
having different billet to boss diameter ratios can
be seen in the photograph shown in Fig. 50. The

first photograph clearly demonstrates the tapering
nature of the profile of the flange. The second
photograph shows how this tapering effect is
influenced by the diameter of the boss.

The difference between the top and bottom flange
diameters gives a clear indication of the extent of
the flange taper. Fig. 51 shows experimental and
theoretically predicted variations in the top and
bottom diameters of the flange with the axial
compression under static lubricated condition. Both
the experimental and theoretical results show
significant difference between the top and bottom
diameters. A similar trend is demonstrated in
Fig. 52 in which the experimental results were
obtained under dynamic forging conditions. Figs.
53 and 54 demonstrate the tapering effect of the
flange profile when the boss diameter was 12 mm and
the billet was forged under quasi-static and dynamic
conditions respectively. The tapering effect is vis-
ibly less than that seen in Figs. 51 and 52.

Figs. 55 and 56 show this tapering effect of the
flange in terms of the ratio of the top and bottom
diameters for boss diameters of 12 mm and 18 mm
respectively. Fig. 57 shows the same diameter
ratio in a comprehensive manner for three
different boss diameters. It is evident that when
the boss diameter is 9 mm negligible tapering

occurs over the entire range of axial compression.

The effect of friction on the flange diameters is demonstrated experimentally when Figs.58, 59 and 60 are compared with Figs. 51, 52 and 53 respectively. The most revealing effect of friction is shown in Fig. 61 where the variation in the upper diameter with the axial compression, for a boss diameter of 18 mm, is clearly affected by the absence of lubrication. Without lubrication the upper diameter will be less and this will be reflected in the billet profile. Fig. 62 shows the effect of friction on the lower flange diameter, with a boss diameter of 18 mm. Here the effect of friction is minimal, possibly due to the small amount of radial material flow involved. Figs. 63 and 64 show the effect of friction on the top and bottom diameters respectively for a boss diameter of 12 mm. Here friction can be seen to marginally influence the upper diameter size but its effect on the lower diameter is again very small. Photographs showing the effect of friction on the upper flange diameters are shown in Fig. 65 the sharp ended profiles (a) should be compared with (b) where the profiles are rounded due to the absence of lubrication.

Although the profile of the billet is affected by friction it does not appear to be affected significantly by the rate of deformation. This can be

seen if reference is made to Figs. 66 and 67
which compares the flange diameters for both static
and dynamic tests. These show that for a boss
diameter of 18 mm equal amounts of deformation should
result in similar profiles under both quasi-static
and dynamic forging. The height of the boss obtain-
able for different billet lengths and different boss
diameters as predicted theoretically are shown in
Figs. 68, 69 and 70 for billet lengths of 18, 22 and
30 mm respectively. Results are shown for boss
diameters of 9, 12, 16 and 20 mm. It is evident that
for a given amount of axial compression and for a
given boss diameter the boss height is greater for the
smaller billet length. For a billet 24 mm
diameter and 24 mm long the boss height for boss
diameters of 9 and 18 mm is shown in Fig. 71 in which
experimentally observed results obtained from dynamic
and static tests carried out under lubricated
conditions are also plotted for comparison. It is
evident that for larger compressions, the boss
heights obtainable are predicted to be more than
those observed experimentally. For total axial
compression of up to 55 per cent the agreement bet-
ween the theory and experiment is very close.

Theoretical curves showing the variation in flange
thickness for billets of different lengths and boss
diameters are shown in Figs. 72, 73 and 74 for boss
diameters of 9, 16 and 22 mm respectively. The

billet diameter being 24 mm for all cases. Billet
lengths of 18, 24 and 30 mm were considered in
these figures. For a given displacement the flange
thickness is directly related to the billet length
and is independent of the boss diameter. As
illustrated in these figures, for an axial
compression of 12 mm the flange thickness is about
6 mm for a billet of length 18 mm, irrespective of the
boss diameter.

One of the most informative parameters in extrusion
forging is the ratio of the boss to flange height
obtainable for different boss diameters. This
parameter for boss diameters of 18 mm and 20 mm is
shown in Figs. 75 and 76 respectively for billet
diameter of 24 mm and billet lengths of 18, 20, 24
and 30 mm. These theoretical curves show that for
a given displacement the shorter the billet and
the larger the boss diameter - the greater the
height ratio. Fig. 77 shows the variation in boss
to flange height ratio with axial compression for
billet diameters of 24 mm and length of 24 mm and
boss diameters of 9, 12 and 18 mm as predicted
theoretically. Theoretical and experimental results
for boss diameters of 9 mm and 18 mm diameter are
compared in Fig. 78 for a billet diameter of 24 mm
and length 24 mm. It is evident that a more
reliable prediction for the height ratio is made for
the larger boss diameter. For smaller boss diameters

116

considerable discrepancy arises between the theoretical and experimental results. In Fig. 78(a) theoretical and experimental results show the variation in percentage total billet height with percentage deformation for boss sizes of 18, 12 and 9 mm, billet lengths of 24 mm were used and tests were undertaken under lubricated quasistatic and dynamic conditions. The transition from the second to the third deformation stage can be inferred from this figure. If allowance is made for 'scatter' there is a very reasonable correlation between the theoretical and experimental results for all three boss sizes, for both quasi-static and dynamic tests. Fig. 79 shows the theoretical relation between the height ratio and the diameter ratio for the forging loads of 14 kN and 13 kN applicable to a billet of diameter 24 mm and length 24 mm and constant flow stress of 17 N/mm². For a given billet size and material the load required to initiate axial displacement P_O will depend on the boss diameter. The variation of P_O with boss diameter for a lead billet of diameter 24 mm and length 24 mm is shown in Fig. 80.

The variation in forging load with axial compression for different boss diameters and billet lengths have been calculated for billet diameters of 24 mm. These results are shown in Figs. 81 to 86 for boss diameters ranging from 9 to 20 mm. For boss to

billet diameter ratios of up to 0.5 the forging
load is generally greater for smaller lengths of
the billet. This trend, however, reverses as the
ratio becomes as high as 0.8 (see Fig. 86) and the
axial compression is not more than about 60 per
cent. The forging load for a billet of length 24 mm
and diameter 24 mm but with boss diameters of
9, 12 and 18 mm are shown in Fig. 87. In Figs.
88(a) and 88(b) theoretically calculated forging
loads for a 24 mm long and 24 mm diameter billet
having a boss diameter of 18 mm and 12 mm are comp-
ared with those obtained experimentally from
static and dynamic forging tests. It is evident
that the load recorded from the quasi-static forging
tests, for both 18 mm and 12 mm boss diameters,
agrees reasonably well in terms of the magnitude
with that predicted theoretically. To predict the
load under dynamic conditions the flow stress
is modified and incorporated in the theory used for
the quasi-static forging condition to take into
account the effect of strain rate. For the boss
diameter of 18 mm there is an overestimation of the
forging load required when the billet is deformed
dynamically, whereas for the boss diameter of 12 mm
there is an underestimation . In both these cases
it is evident that the modified flow stress used
to predict forging load gives agreement between
theory and experiment similar to the static tests.

As the inertia effect has not been included in the
analysis some error in load prediction must be
expected. The effect of friction as observed
experimentally on the forging load for boss
diameters of 12 mm and 18 mm diameter is shown in
Figs. 89 and 90 respectively. It is evident that
friction adversely affects the forging load for a
given displacement and that the larger the boss
diameter the greater the influence of friction on
the forging load. The forging load calculations
were also carried out for mild steel at hot
working temperatures for providing a basis of compar-
ison with the forging loads predicted for lead used
in this study. Theoretical curves showing the
variation in forging load with axial compression
for different boss diameters and billet lengths
for steel at forging temperatures of 800, 1000
and 1200°C are shown in Figs. 91-96. These
results help estimation of the load requirement if
extrusion forging was to be carried out with steel
at hot working temperatures and show that the
temperature of the billet is of paramount importance
when calculating forging loads.

The total energy requirement predicted theoretically
and measured from quasi-static lubricated tests via
load displacement traces, are shown in Figs. 97-99 for
boss diameters of 9, 12 and 18 mm respectively with
a billet diameter of 24 mm. These values are again

shown in Figs. 100, 101 and 102 and are compared
with dynamic forging test results where the amount of
energy used was calculated from the tup mass and its
total displacement. Again it is clearly evident
that close agreement is demonstrated between
statically measured and theoretically predicted
results. Dynamically forged results show much
greater energy requirement for the same amount of
axial deformation.

The total energy curves, based on the theoretical
(dynamic) load results shown in Figs. 88(a) and
88(b), are shown in Figs. 101 and 102. In each
case there is an underestimation of the total energy
required. This could be due to the fact that not
all energy given up by the tup is actually used to
deform the billet. Energy losses occur by way of
elastic deformation of dies and the load cell
housing, together with losses due to impact noise.
A further improvement in predicting the dynamic for-
ging energy requirement could be obtained if allow-
ance for material inertia could be incorporated in the
analysis.

6.4.2   Tests on Materials other than Lead

To check if the profile of the deformed billet is
material dependent quasi-static lubricated extrusion
forging tests were carried out on copper and it was
found that the copper billets deform in just about
the same manner as the lead billets did. Fig. 103

shows a photograph of copper billets at different
stages of deformation with boss diameters of 18 mm.
These profiles are similar to those observed for lead
billets and shown in the photograph in Fig. 49.
It is evident from these tests that when different
billet materials are used similar profiles can be
expected from the same set of dies.

6.4.3   Double-Ended Extrusion Forging

To confirm that the analysis developed in this study
could be applied to cylindrical billets in which
forging was combined with extrusion at both ends,
static lubricated tests on lead billets 24 mm
diameter, 24 mm long with boss diameters of 18 mm
were carried out. Figs. 104, 105 and 106 show how
Displacement is related to Energy, Flange diameter
ratio and the Top and Bottom flange diameters
respectively. In each case a close relation between
theoretical and experimental results was found and
it is thus evident that the double ended extrusion
forgings could be analysed in the same way as the
single ended ones.

A further check on material dependency was made with
billets made from copper and aluminium. Fig. 107
shows photographs of copper billets at various
stages of deformation in double ended extrusion
forging modes for boss diameters of 18 mm. Fig.
108 shows a photograph of aluminium copper and lead

121

billets partially deformed in double-ended
extrusion forging mode. The deformation modes
appear to be independent of the billet material.

Dynamic forging also gives rise to increase in
forging load due to material inertia. Any influence
in the forging load observed in this study for
tests under the drop hammer is thus due to the
combined effects of strain rate sensitivity and
inertia.

Some unexpected results associated with these
tests is shown in the photograph in Fig. 109 which
shows a lead billet flanked by two aluminium billets.
In each case the flange profile is uneven. This
is thought to be due to the use of recast metal having
a large grain size. This phenomenon did not occur
when 'bar' material was used.

6.4.4   Discussion on the effect of friction
Figs. 110 and 111 show the effect of   friction
(m = 1) and (m = 0.5) on the variation in percentage
total height with percentage displacement for boss
sizes of 12, 15, 18 and 21 for lead billets 24 mm
diameter and 24 mm high. The onset of the third and
fourth stages can be seen clearly, but in practice
the abrupt changes shown would be more gradual. It
is clearly evident that the larger the boss size the
lower the percentage displacement needed to initiate
flow in the third mode. This would appear to be

in good agreement with earlier works[62,61] although
it is not possible to make a direct comparison
because of the difference in the size of die and
test piece used. The experimental results show close
agreement with the theory when deformation takes place
in the second and third modes for boss diameters of
12 and 18 mm.

Fig. 112 shows the effect of three different friction
factors in predicting the percentage total height
with percentage displacement for a boss size of
12 mm. Again the onset of the third and fourth
stages can be clearly seen and it is evident that the
larger the friction factor the earlier the fourth
mode of deformation is likely to occur. This is in
agreement with earlier works[62,61]. It is evident
from the results in Fig. 112 that the friction has
insignificant effect on the total height of the
deformed billet until the fourth mode of deformation
commences. The agreement between the theory and
experiment is very close. Fig. 113 shows the effect
of friction on the forging load with percentage
displacement for a die size of 12 mm. Theoretically
the higher the friction factor, m, the greater the
forging load required. The experimental curve
shown in the figure indicates that the predicted
load is an overestimation when forging was carried
out under lubricated condition. It is to be noted,

123

however, that experimentally the difference in for-

ging loads under lubricated and dry conditions was

found to be very small for deformation of up to

about 50 per cent (See Fig. 89).

124

FIRST STAGE OF DEFORMATION

FIG. 43

SECOND STAGE OF DEFORMATION

FIG. 44.

126

TOP DIE

TEST PIECE

BOTTOM
DIE.

LOAD CELL
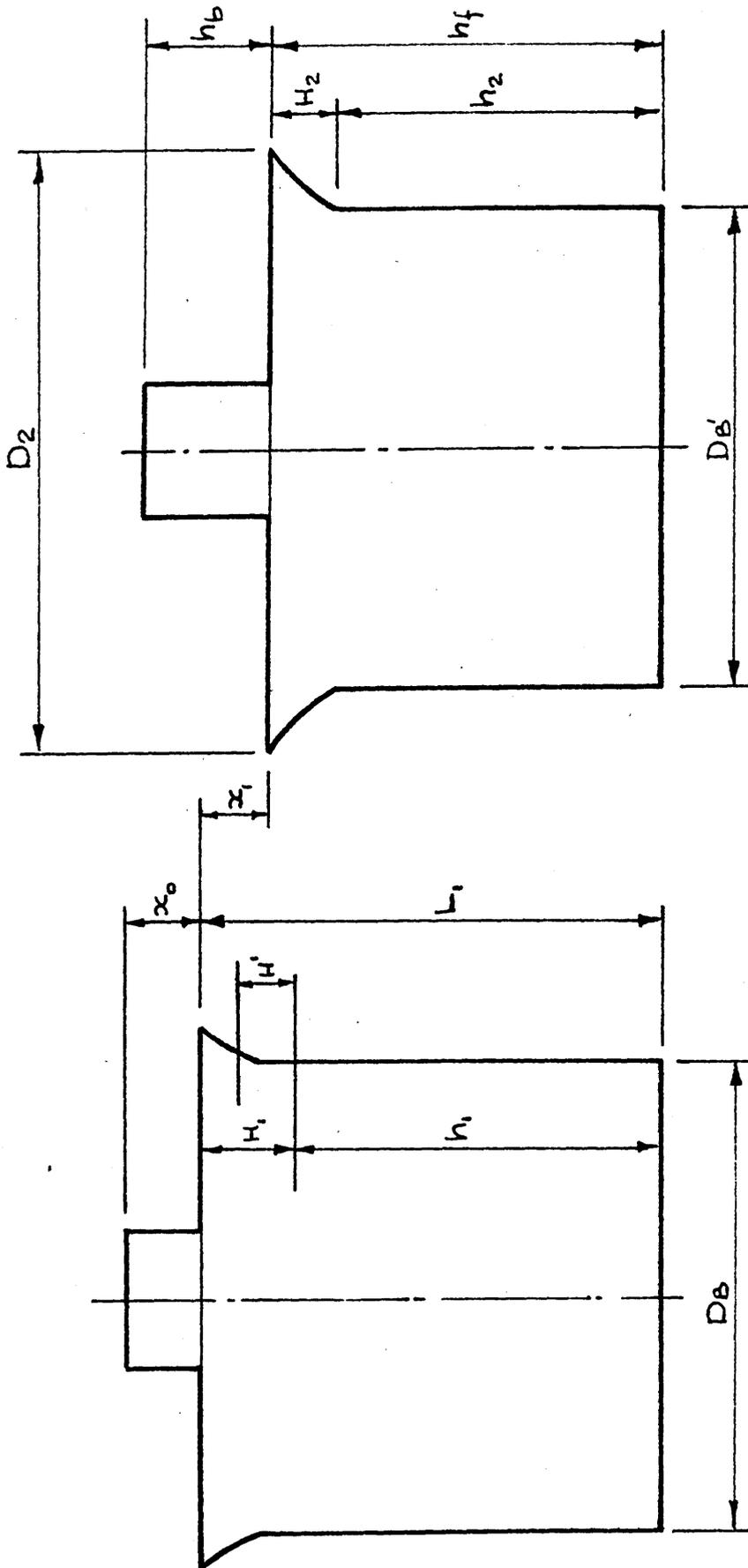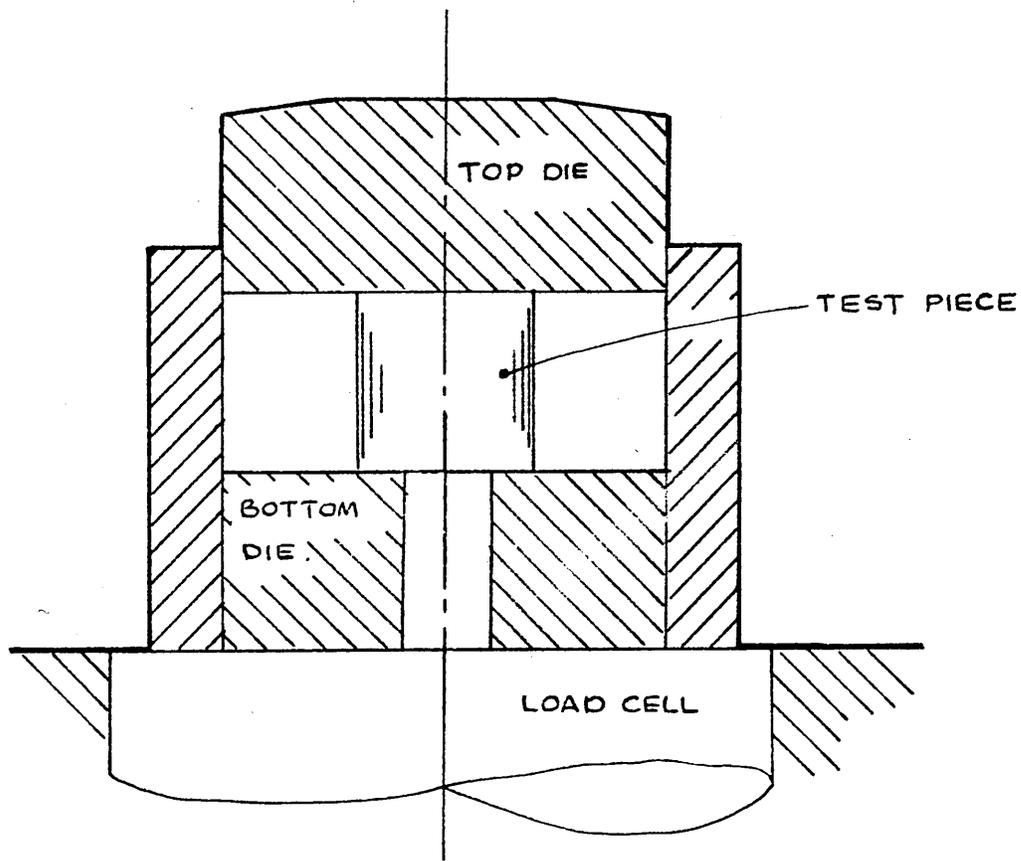
DIE - BILLET CONFIGURATION

FIG. 45.

127
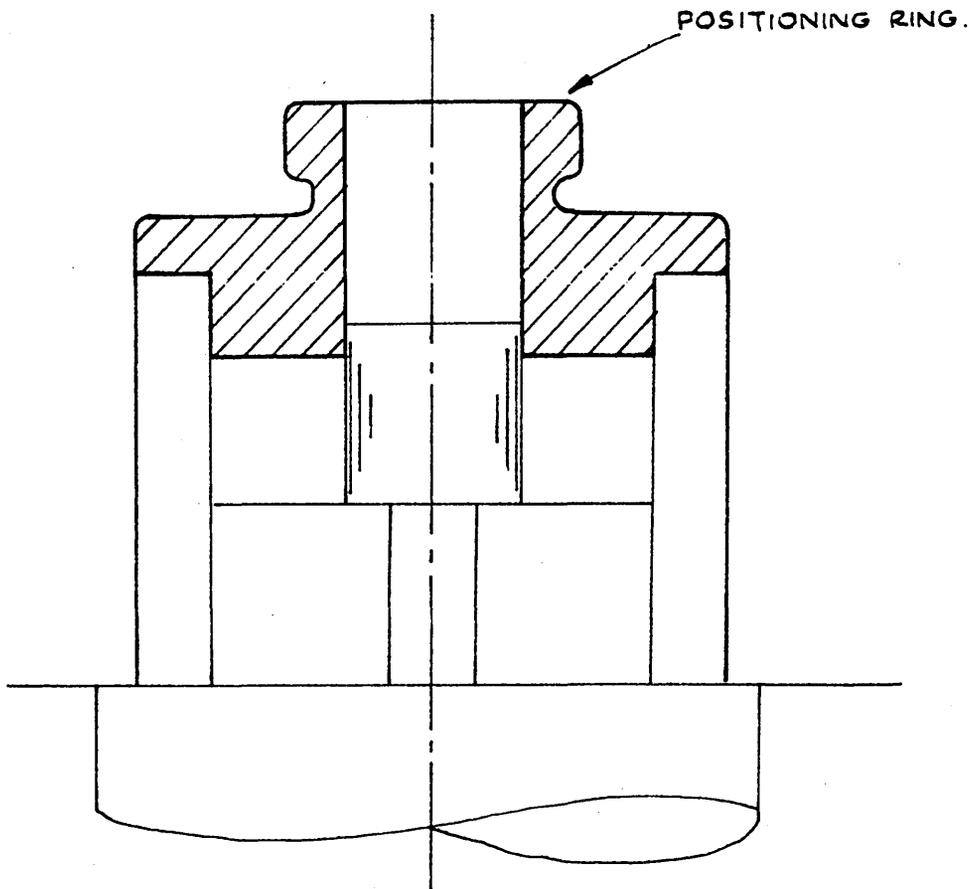
POSITIONING RING.

USE OF POSITIONING RING TO CENTRALISE TEST PIECE

FIG. 46

128

THEORETICAL PROFILES

$D_c = 18mm$

FIG. 47

129
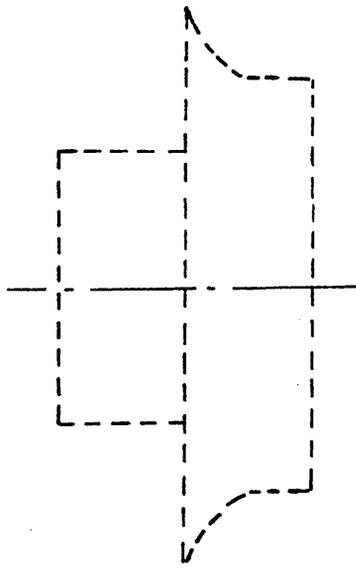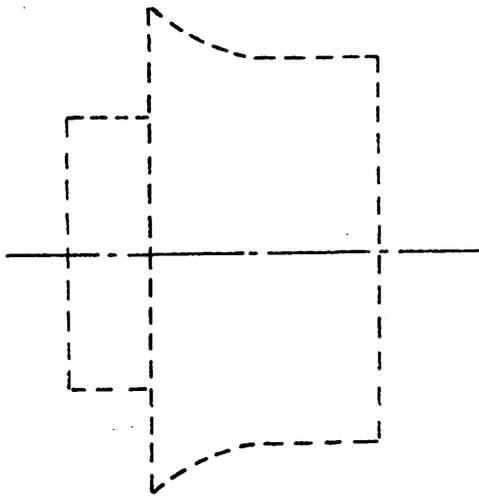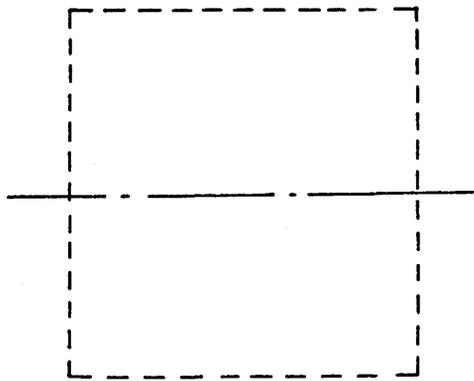
THEORETICAL PROFILES

$D_s = 9mm$
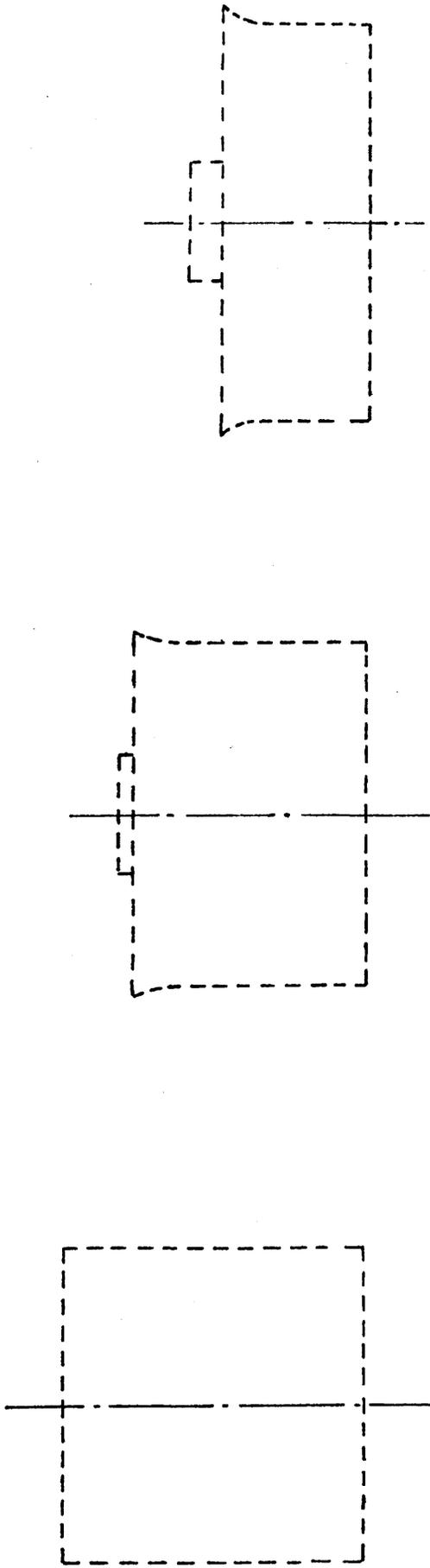
FIG. 48.
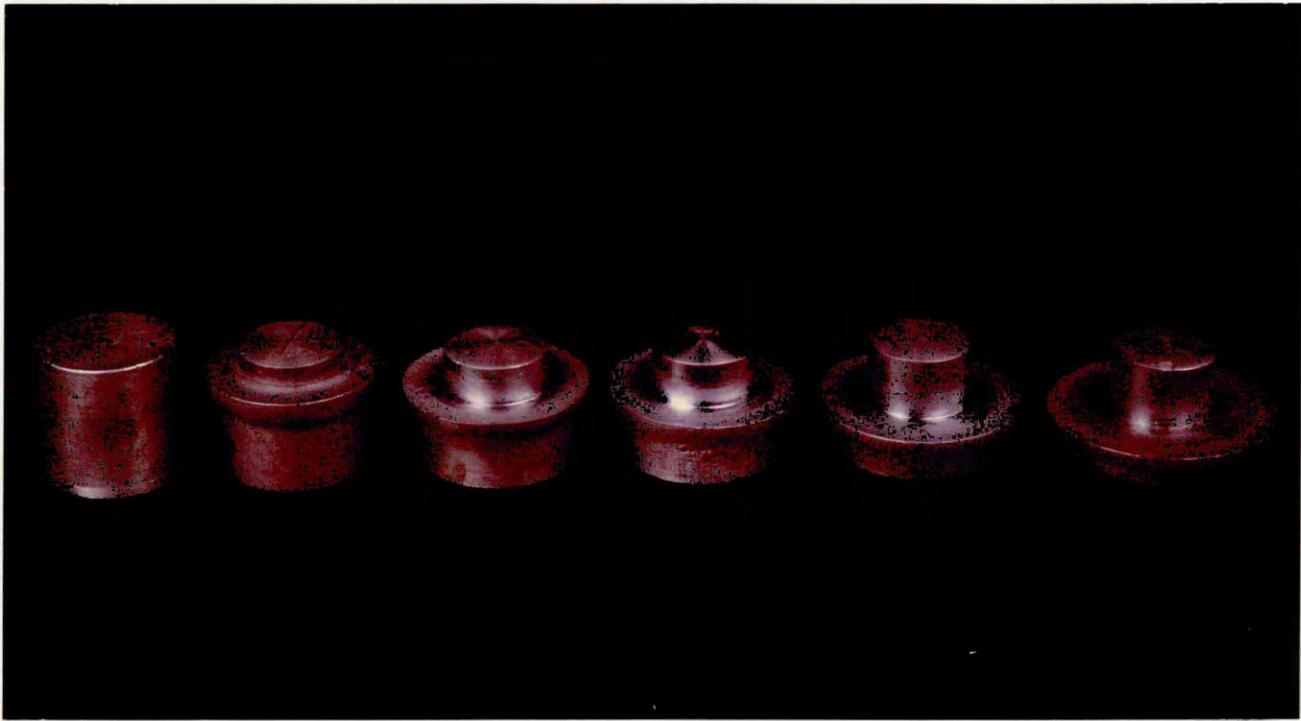
FIG. 49.

EXTRUSION FORGINGS.   THREE DIFFERENT SIZES.
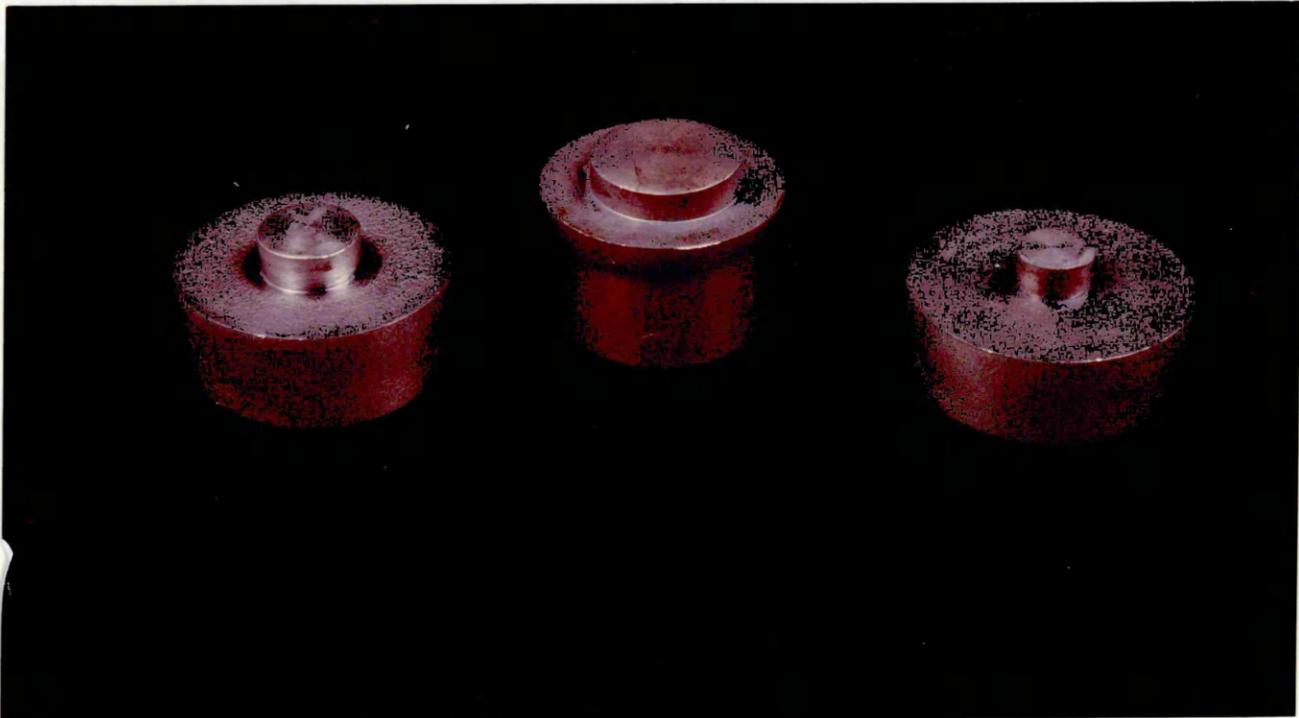
FIG. 50

THEORETICAL / EXPERIMENTAL CURVES
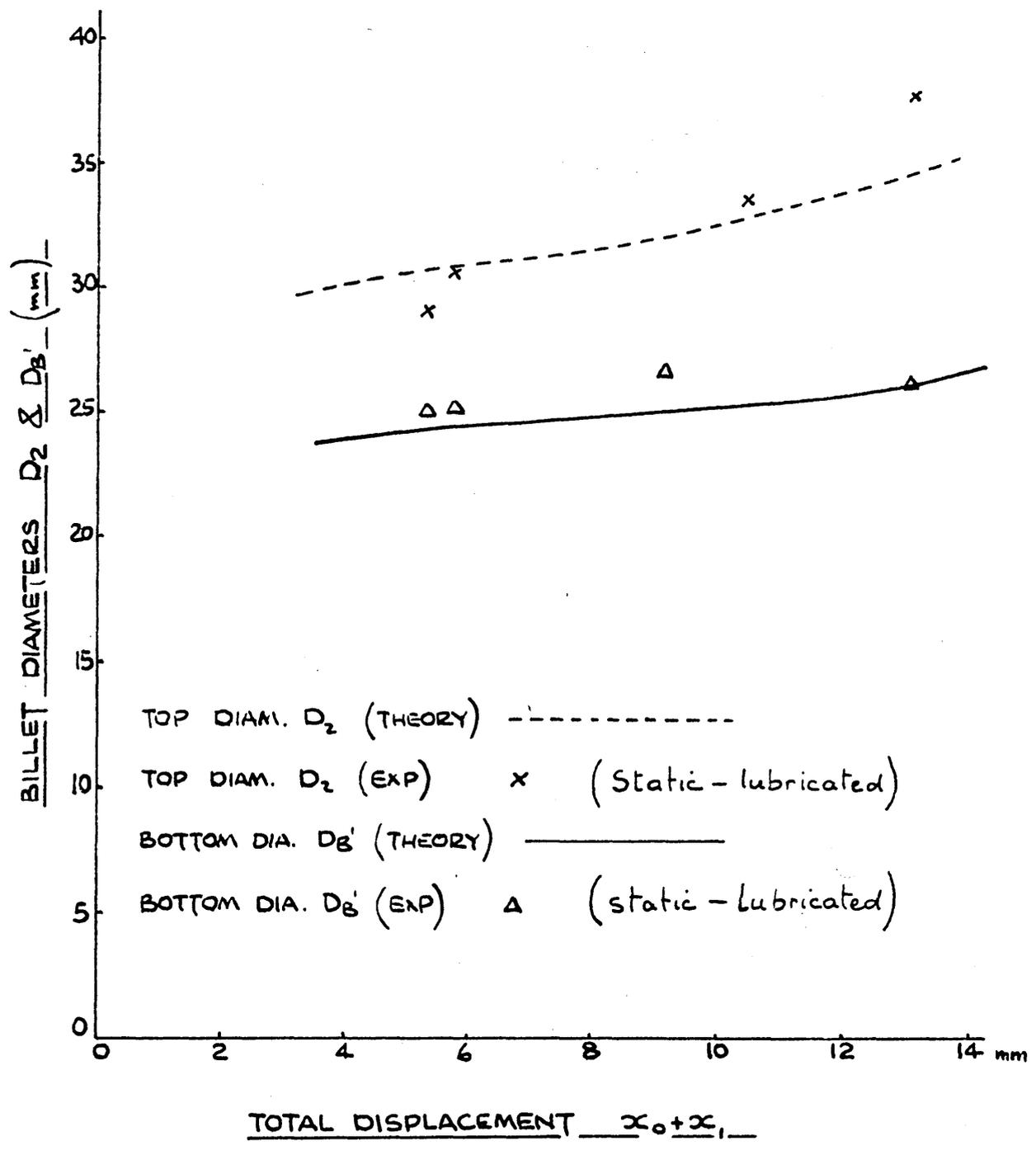
BOSS DIA. = 18 mm $Y = 17 \text{ N/mm}^2$.

TOP DIAM. D_2 (THEORY) - - - - - - - - -

TOP DIAM. D_2 (EXP) × (Static - lubricated)

BOTTOM DIA. D_B' (THEORY) ————

BOTTOM DIA. D_B' (EXP) △ (static - lubricated)

TOTAL DISPLACEMENT $x_0 + x_1$

FLANGE DIAMETERS v. TOTAL DISPLACEMENT.

FIG. 51.   132

THEORETICAL / EXPERIMENTAL CURVES

BOSS DIA. = 18mm $Y = 17 \ N/mm^2$

TOP DIAM. D_2 (THEORY) — — — — —

TOP DIAM. D_2 (EXP) ☐ (Dynamic – lubricated)

BOTTOM DIA. D_B' (THEORY) ————

BOTTOM DIA. D_B' (EXP) ■ (Dynamic – lubricated)

TOTAL DISPLACEMENT $x_0 + x_1$

FLANGE DIAMETERS v. TOTAL DISPLACEMENT

FIG. 52.   133

THEORETICAL / EXPERIMENTAL CURVES

BOSS DIA. = 12mm $Y = 17 \, N/mm^2$

TOP DIAM. D_2 (THEORY) ---------------

TOP DIAM. D_2 (EXP) x (Static - lubricated)

BOTTOM DIA. D_B' (THEORY) _____

BOTTOM DIA. D_B' (EXP) △ (Static - lubricated)

TOTAL DISPLACEMENT $x_0 + x_1 \, (mm)$
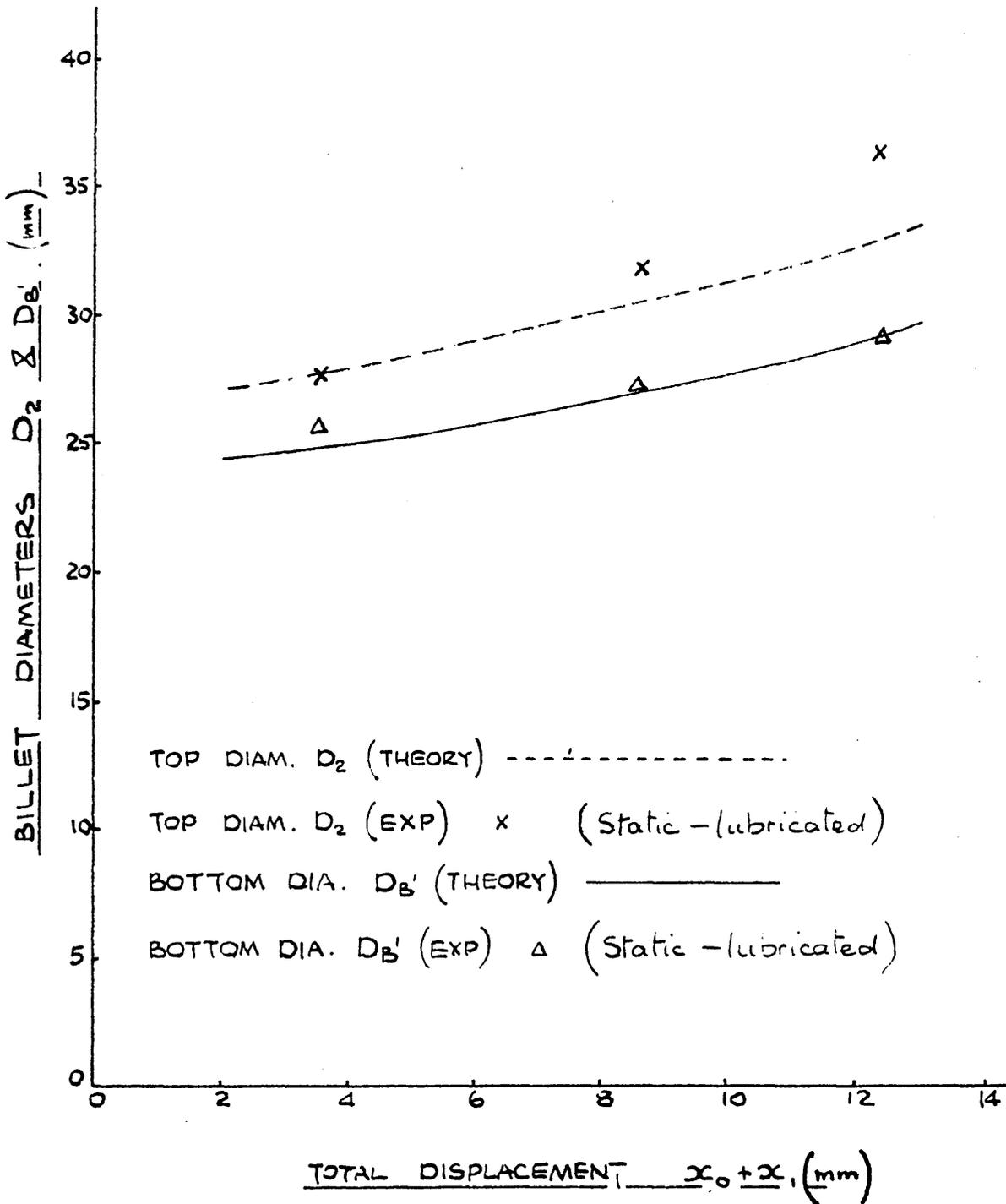
FLANGE DIAMETERS v. TOTAL DISPLACEMENT

FIG. 53.

134

THEORETICAL / EXPERIMENTAL CURVES

BOSS DIA = 12 mm $Y = 17 \, N/mm^2$

FLANGE DIAMETERS v. TOTAL DISPLACEMENT.

FIG. 54.   135

THEORETICAL / EXPERIMENTAL CURVES

BOSS DIA = 12mm $Y = 17 N/mm^2$.

THEORETICAL CURVE ——————

EXPERIMENTAL VALUES X
(Static - lubricated)

TOTAL DISPLACEMENT $x_0 + x_1$ (mm)

DIAMETER RATIO v. TOTAL DISPLACEMENT

FIG. 55.

136

THEORETICAL / EXPERIMENTAL CURVES

BOSS DIA = 18 mm   Y = 17 N/mm²

TOTAL DISPLACEMENT $x_0 + x_1$ (mm)

DIAMETER RATIO v. TOTAL DISPLACEMENT.

FIG. 56.

137

THEORETICAL / EXPERIMENTAL CURVES

$Y = 17 \, N/mm^2$.

THEORETICAL CURVES
D_c = 18 ----------
D_c = 12 ————
D_c = 9 ——-- ——

EXPERIMENTAL RESULTS (STATIC LUBRICATED)
D_c = 18 □
D_c = 12 △
D_c = 9 ○

Y-axis: DIAMETER RATIO D_2/D_B'

X-axis: TOTAL DISPLACEMENT $x_0 + x_1$ (mm)
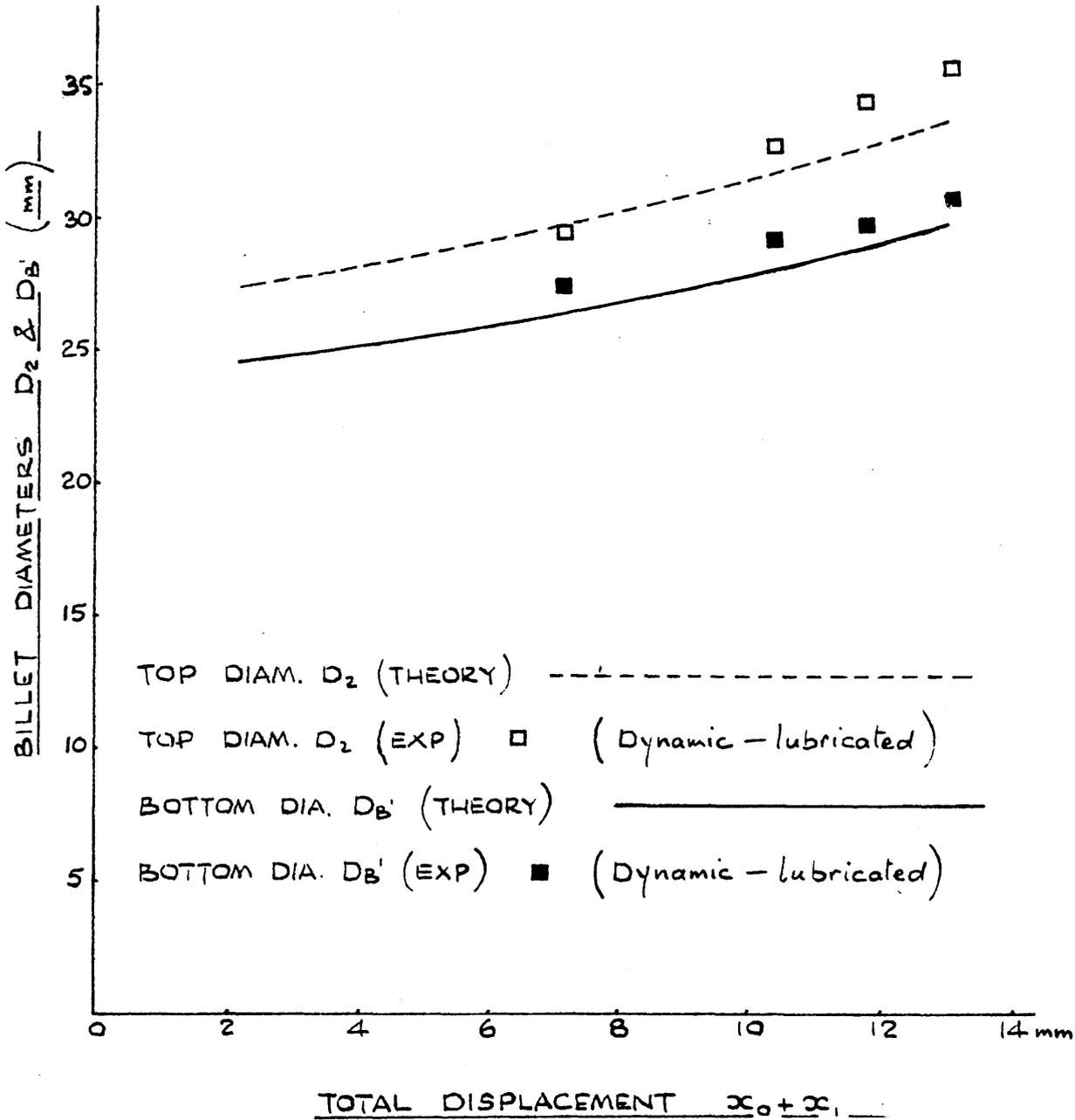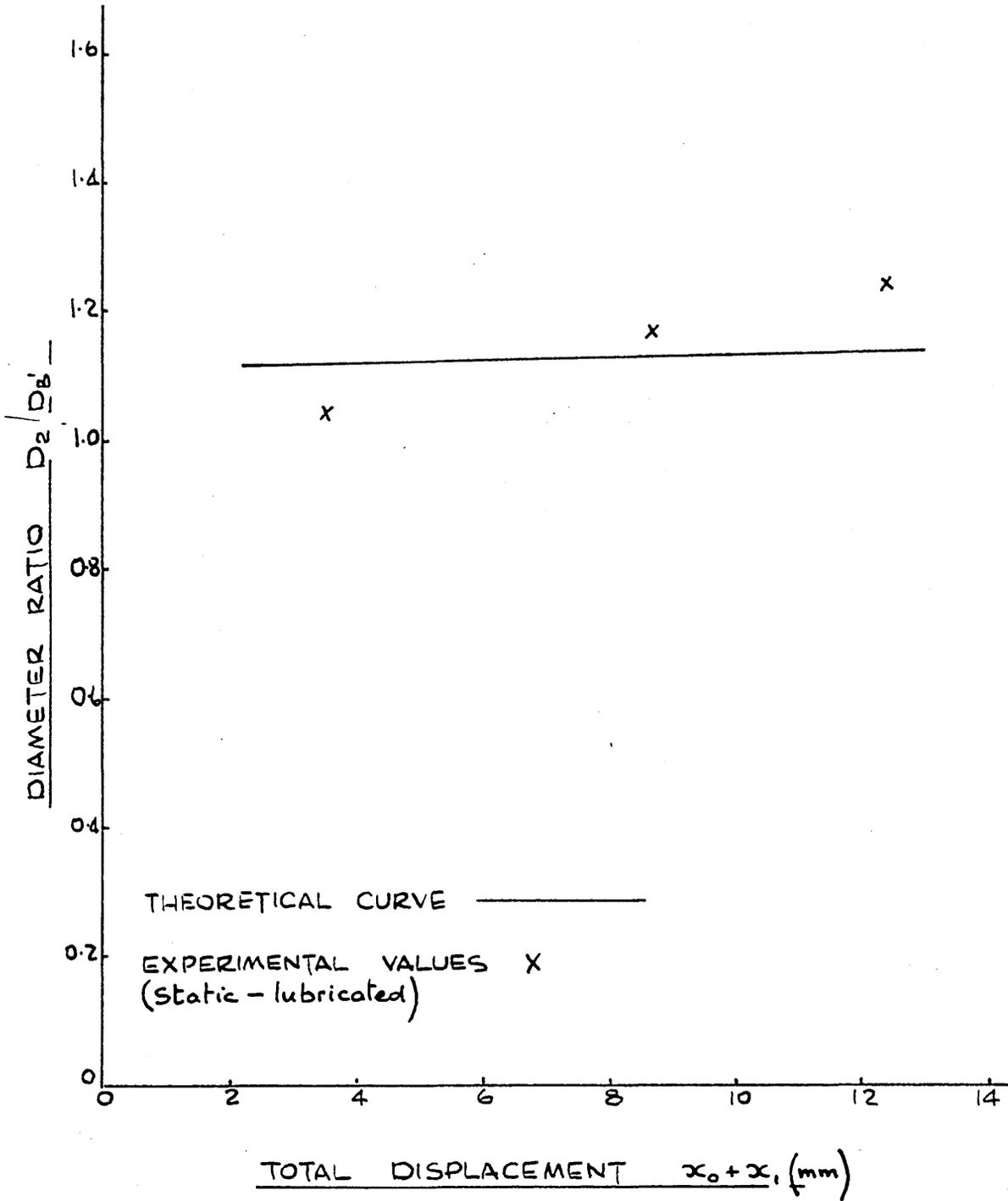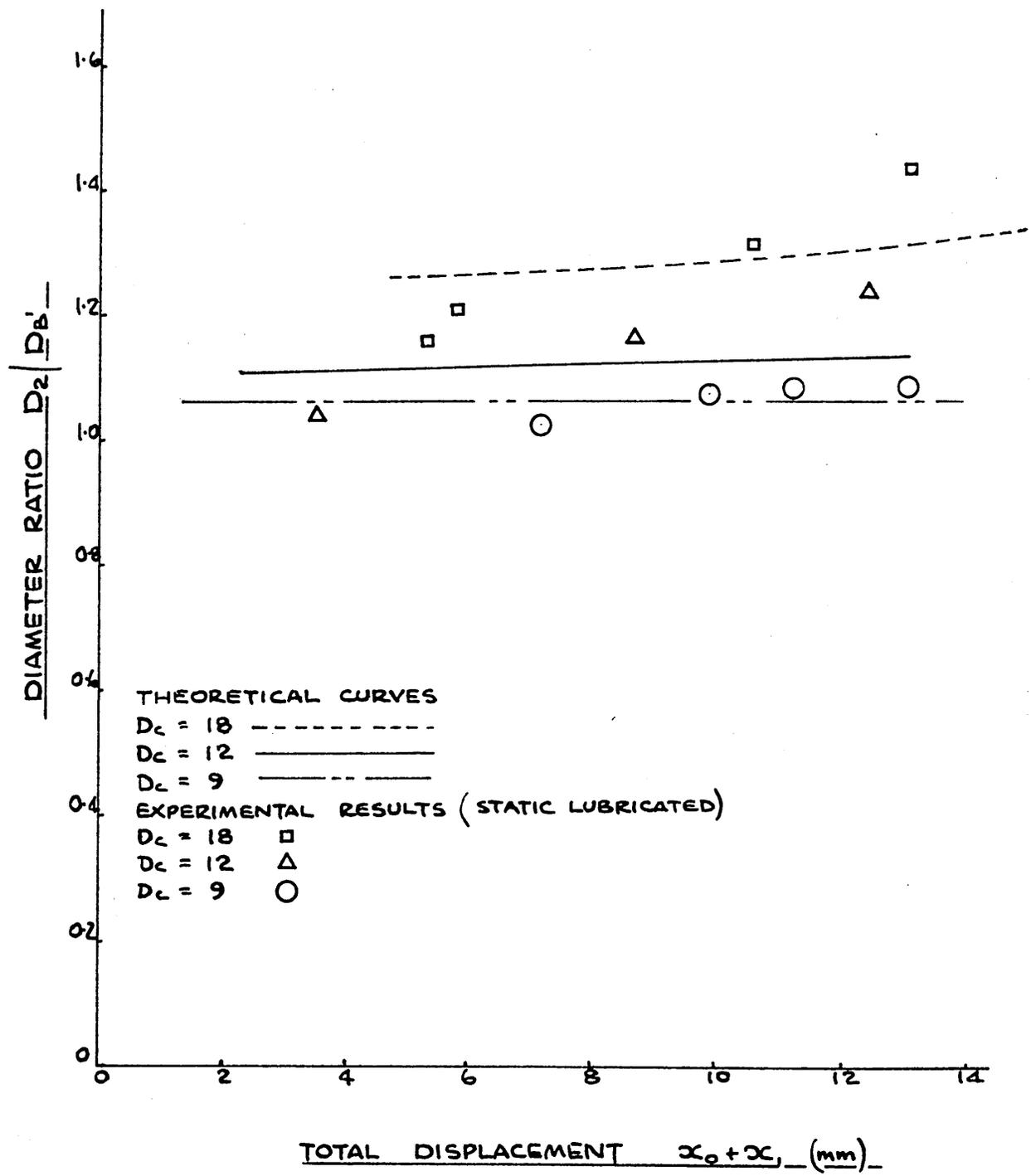
DIAMETER RATIO v. TOTAL DISPLACEMENT

FIG. 57.

138

THEORETICAL EXPERIMENTAL CURVES

BOSS D.A = 18mm   Y = 17 N/mm²
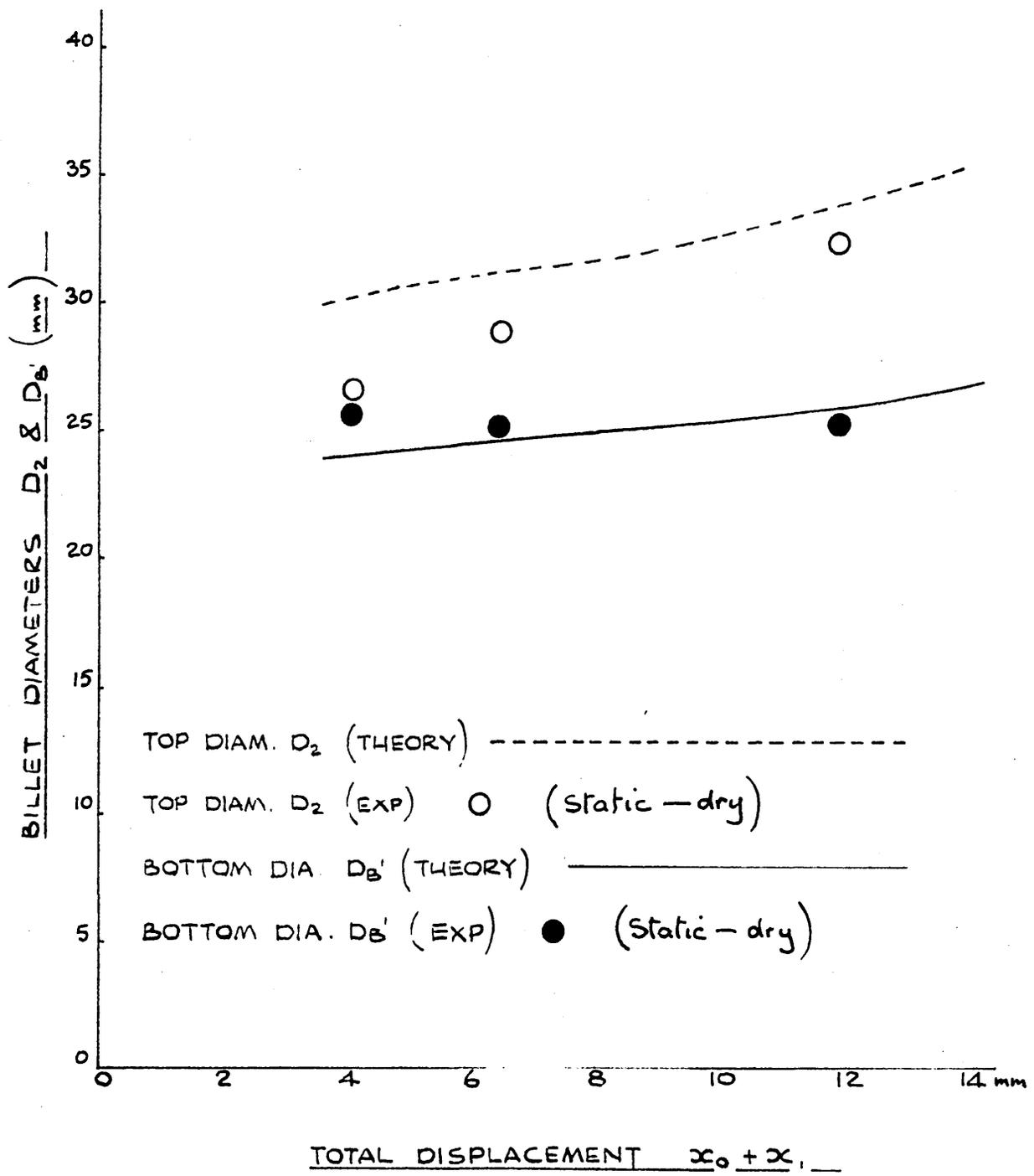
FLANGE DIAMETERS v. TOTAL DISPLACEMENT.

FIG. 58.
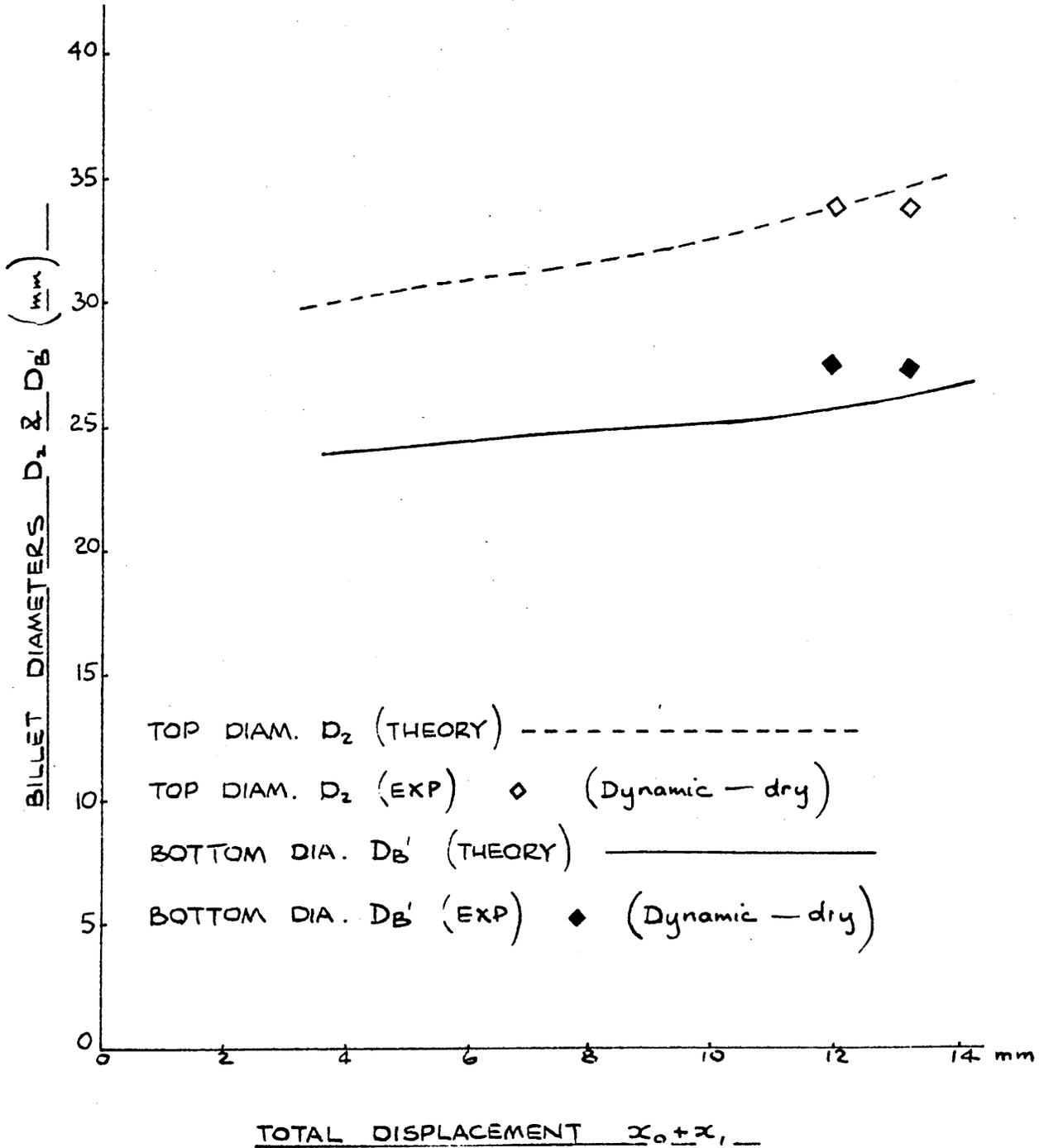
139

THEORETICAL EXPERIMENTAL CURVES

BOSS DIA. = 18mm $Y = 17 \text{ N/mm}^2$

TOP DIAM. D_2 (THEORY) — — — — — — — —

TOP DIAM. D_2 (EXP)   ◇   (Dynamic — dry)

BOTTOM DIA. D_B' (THEORY) ——————

BOTTOM DIA. D_B' (EXP)   ◆   (Dynamic — dry)

TOTAL DISPLACEMENT $x_0 + x_1$

FLANGE DIAMETERS v. TOTAL DISPLACEMENT

FIG. 59.

140

THEORETICAL / EXPERIMENTAL CURVES

BOSS DIA = 12 mm $Y = 17 \, N/mm^2$.

TOP DIAM. D_2 (THEORY) — — — — — — — —

TOP DIAM. D_2 (EXP) O (Static - dry)

BOTTOM DIA D_B' (THEORY) ————————

BOTTOM DIA D_B' (EXP) ● (Static - dry)

BILLET DIAMETERS D_2 & D_B' (mm)

TOTAL DISPLACEMENT $x_0 + x_1$ (mm)
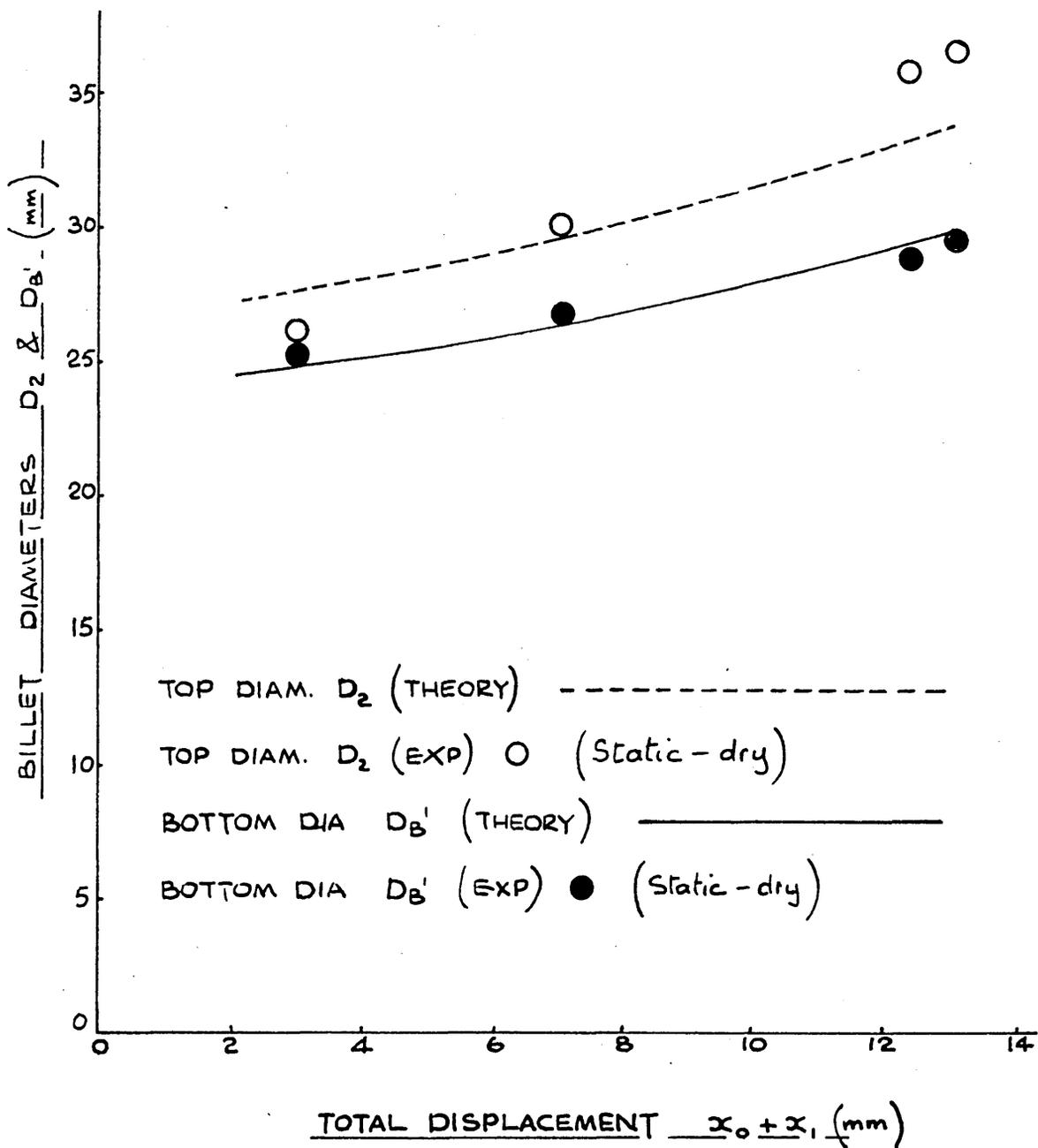
FLANGE DIAMETERS v. TOTAL DISPLACEMENT.

FIG. 60.

141

EXPERIMENTAL RESULTS

BOSS DIA = 18mm $Y = 17 N/mm^2$

TOP DIAMETER OF FLANGE v. TOTAL DISPLACEMENT.

FIG. 61.

14-2

EXPERIMENTAL RESULTS

BOSS D.A = 18mm   Y = 17 N mm²

FLANGE DIAMETER D₈' (mm)

EXPERIMENTAL 'STATIC' RESULTS

DRY ●

LUBRICATED △

TOTAL DISPLACEMENT $x_0 + x$, (mm)
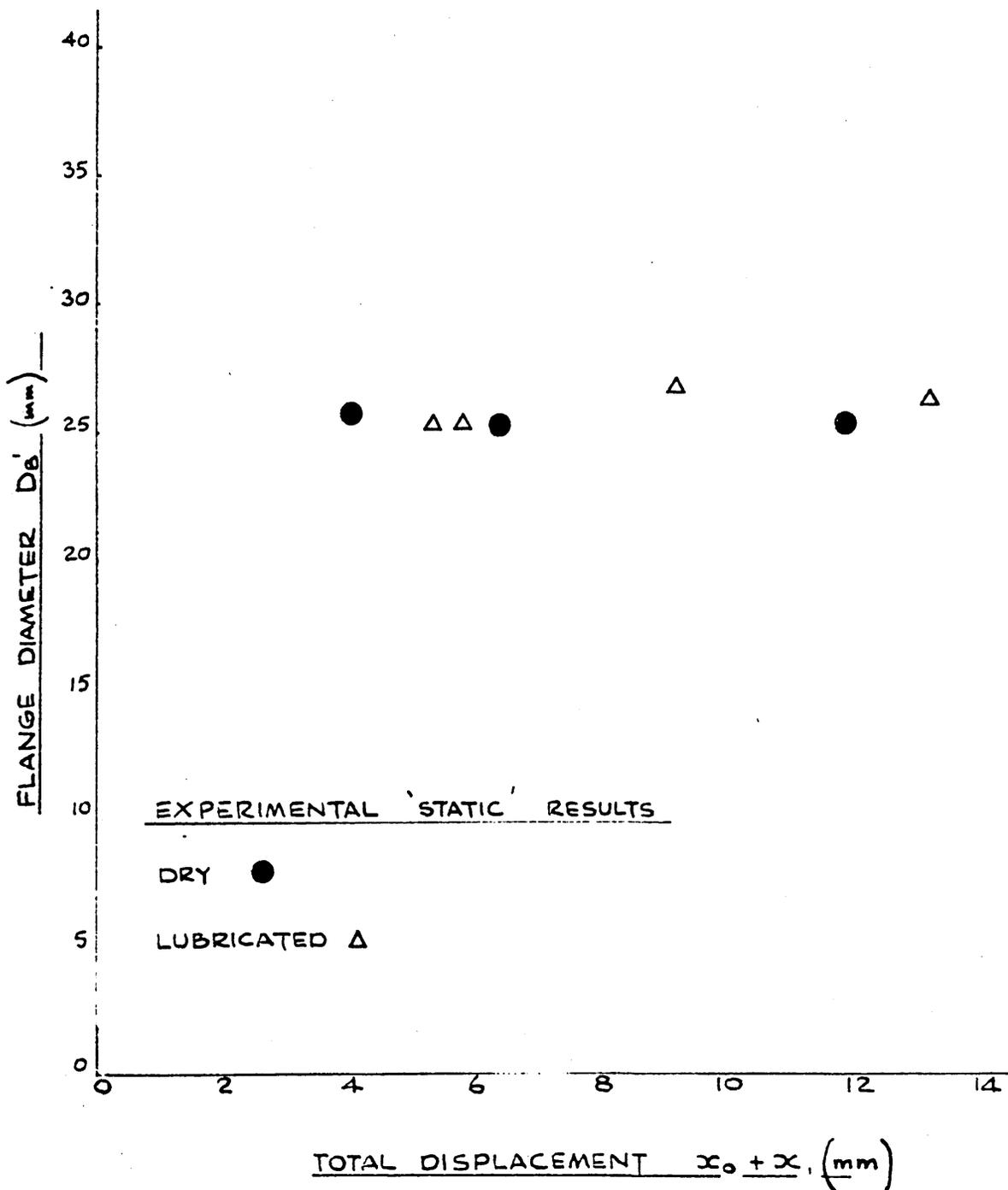
BOTTOM DIAMETER OF FLANGE v. TOTAL DISPLACEMENT

FIG. 62.

143

EXPERIMENTAL RESULTS

BOSS DIA = 12 mm   Y = 17 N/mm²
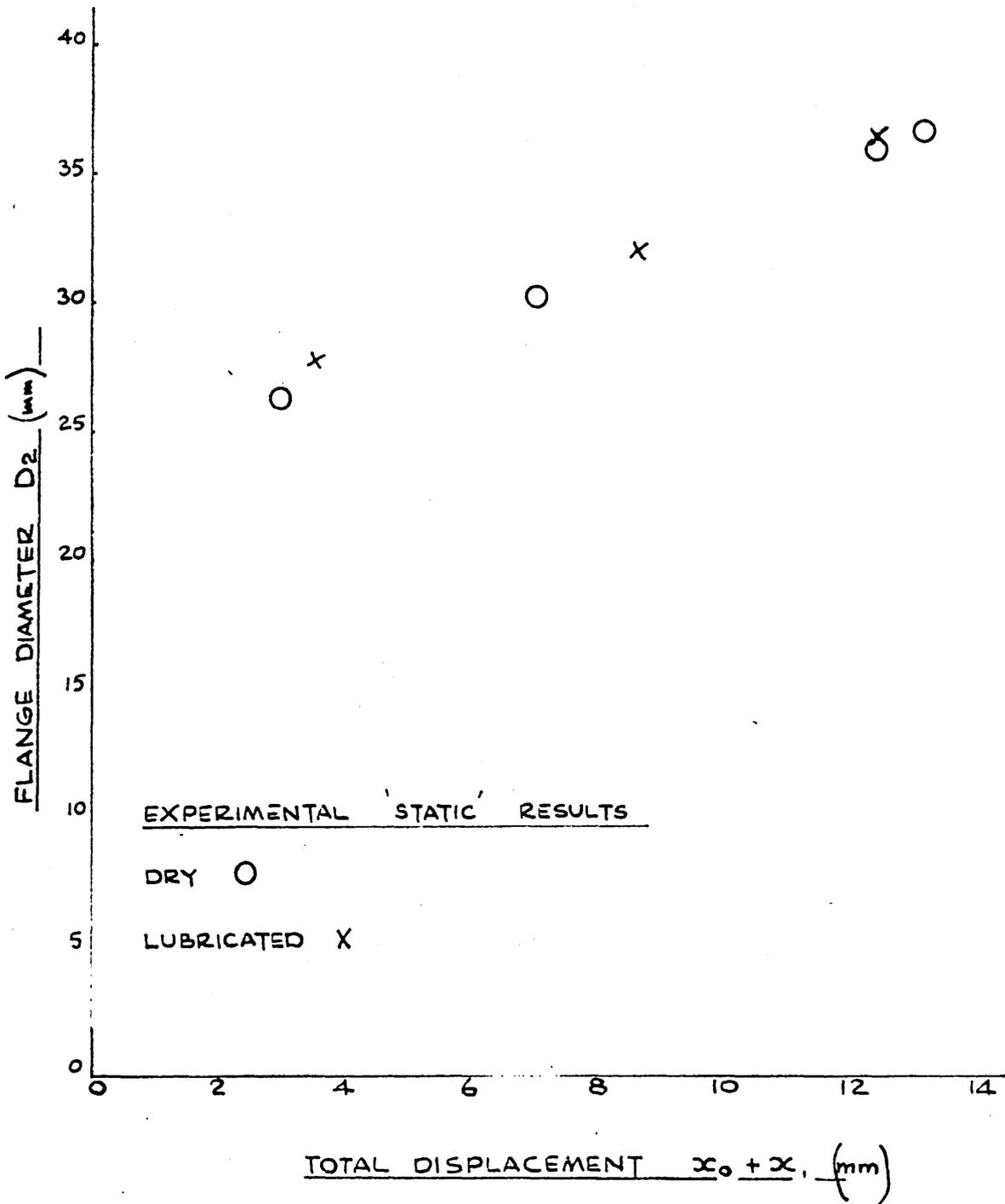
TOP DIAMETER OF FLANGE v. TOTAL DISPLACEMENT.

FIG. 63.   144

EXPERIMENTAL RESULTS

BOSS D.A = 12 mm   Y = 17 N/mm²
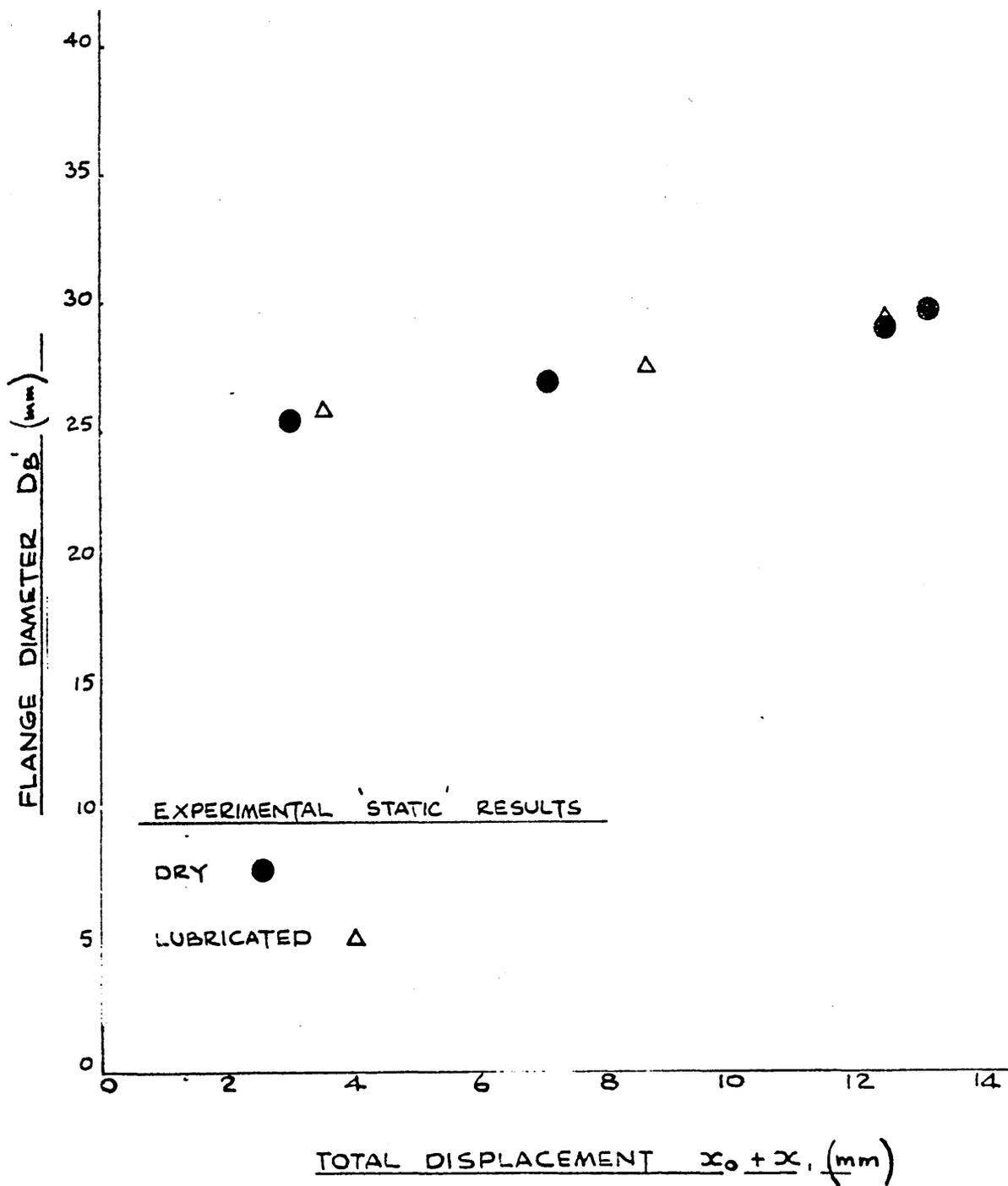
BOTTOM DIAMETER OF FLANGE v. TOTAL DISPLACEMENT.

FIG. 64.

145
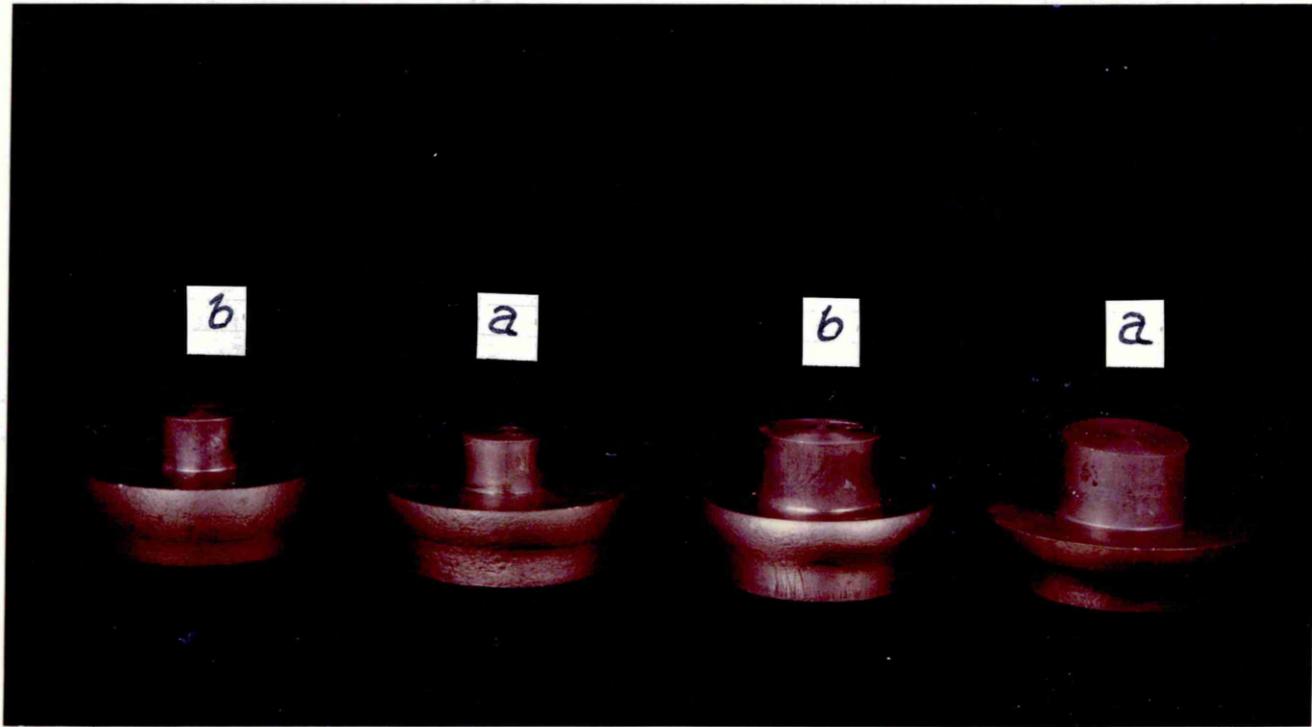
EFFECT OF FRICTION ON BILLET PROFILE

FIG. 65

BOSS DIA = 18 mm $Y = 17 \, N/mm^2$
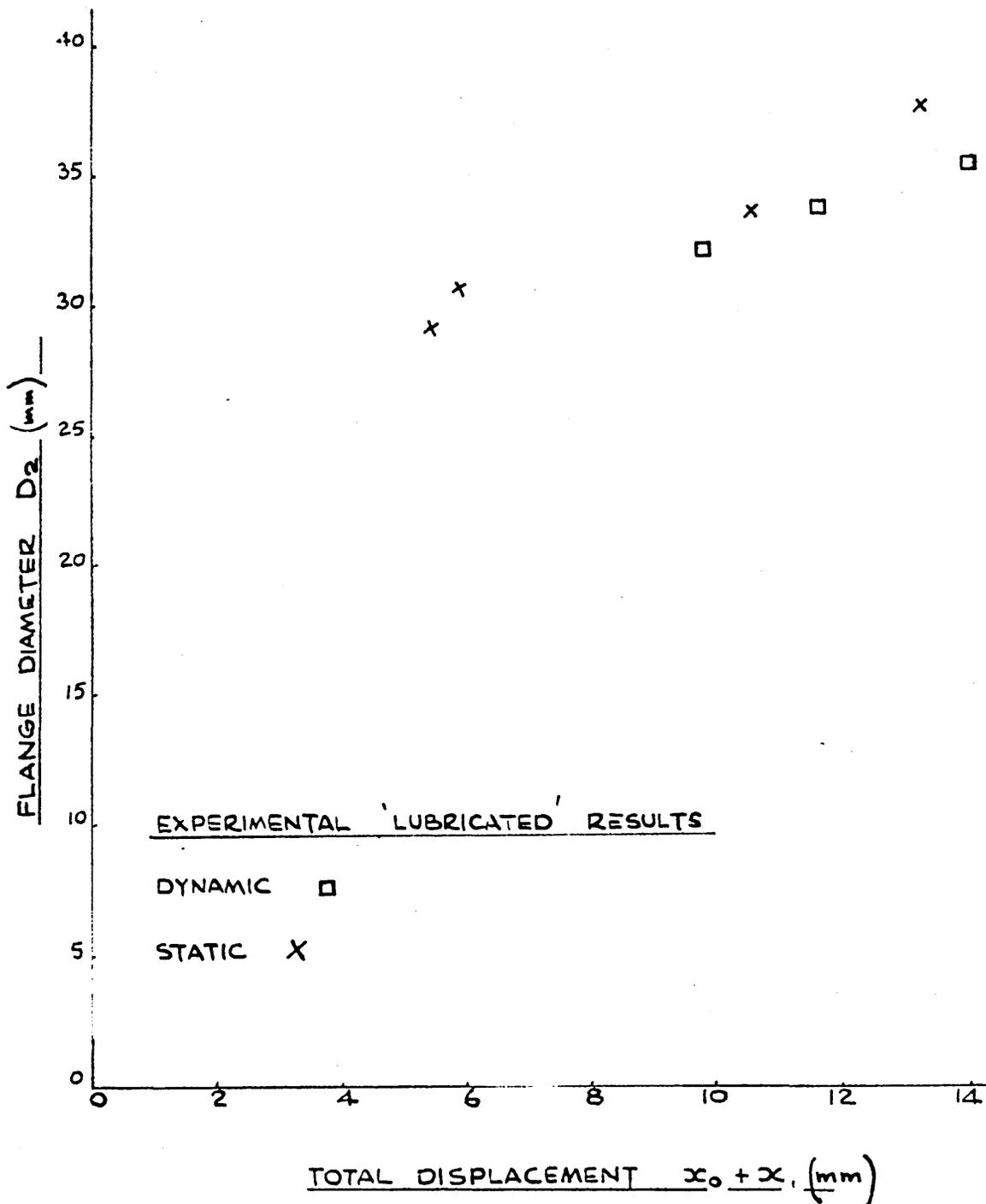
TOP DIAMETER OF FLANGE v. TOTAL DISPLACEMENT.

FIG. 66.

147

EXPERIMENTAL RESULTS

BOSS DIA = 18 mm $Y = 17 \text{ N/mm}^2$
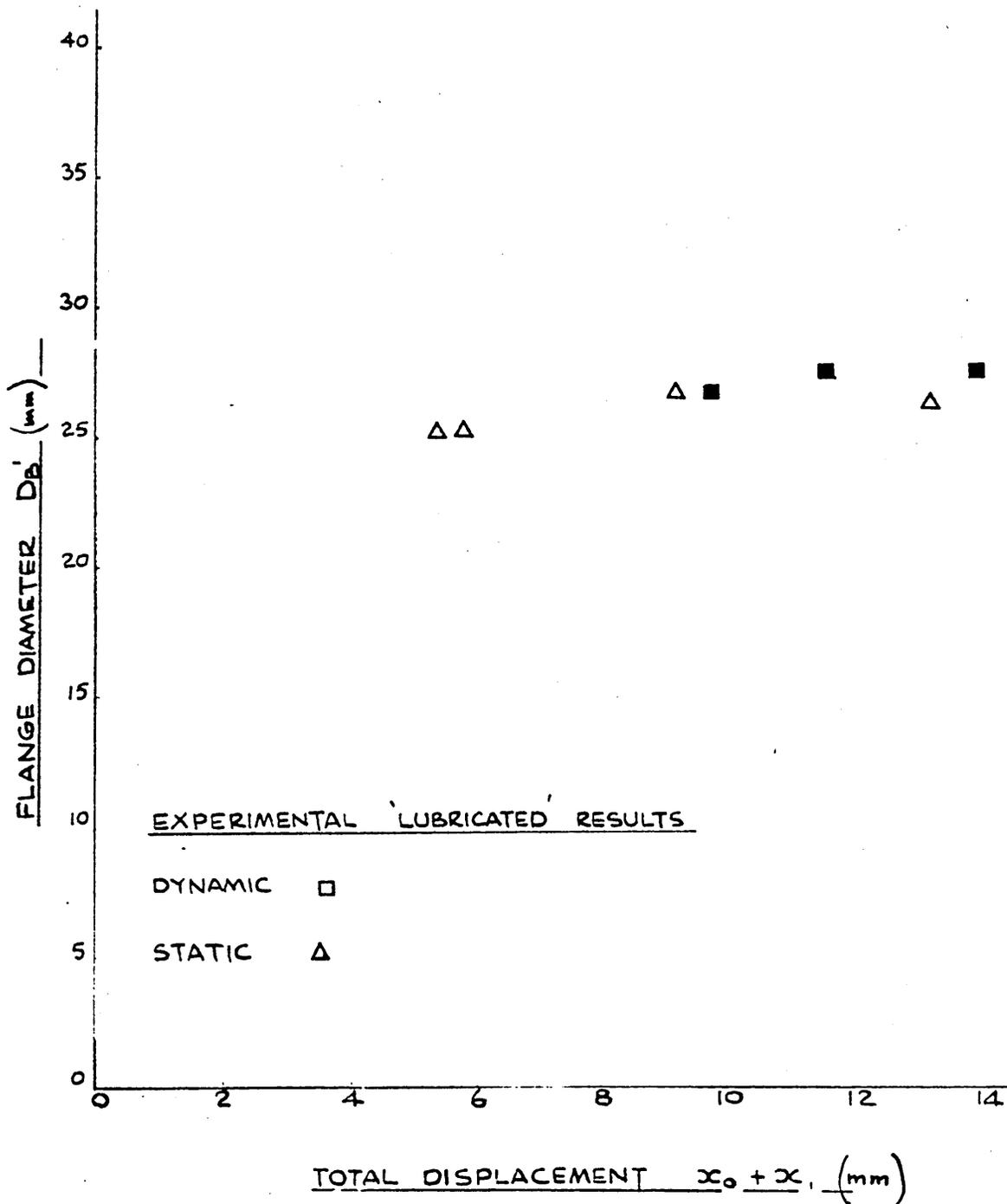
TOP DIAMETER OF FLANGE v. TOTAL DISPLACEMENT.

FIG. 67.

148

THEORETICAL CURVES

$L_0 = 18$ $Y = 17 \, N/mm^2$
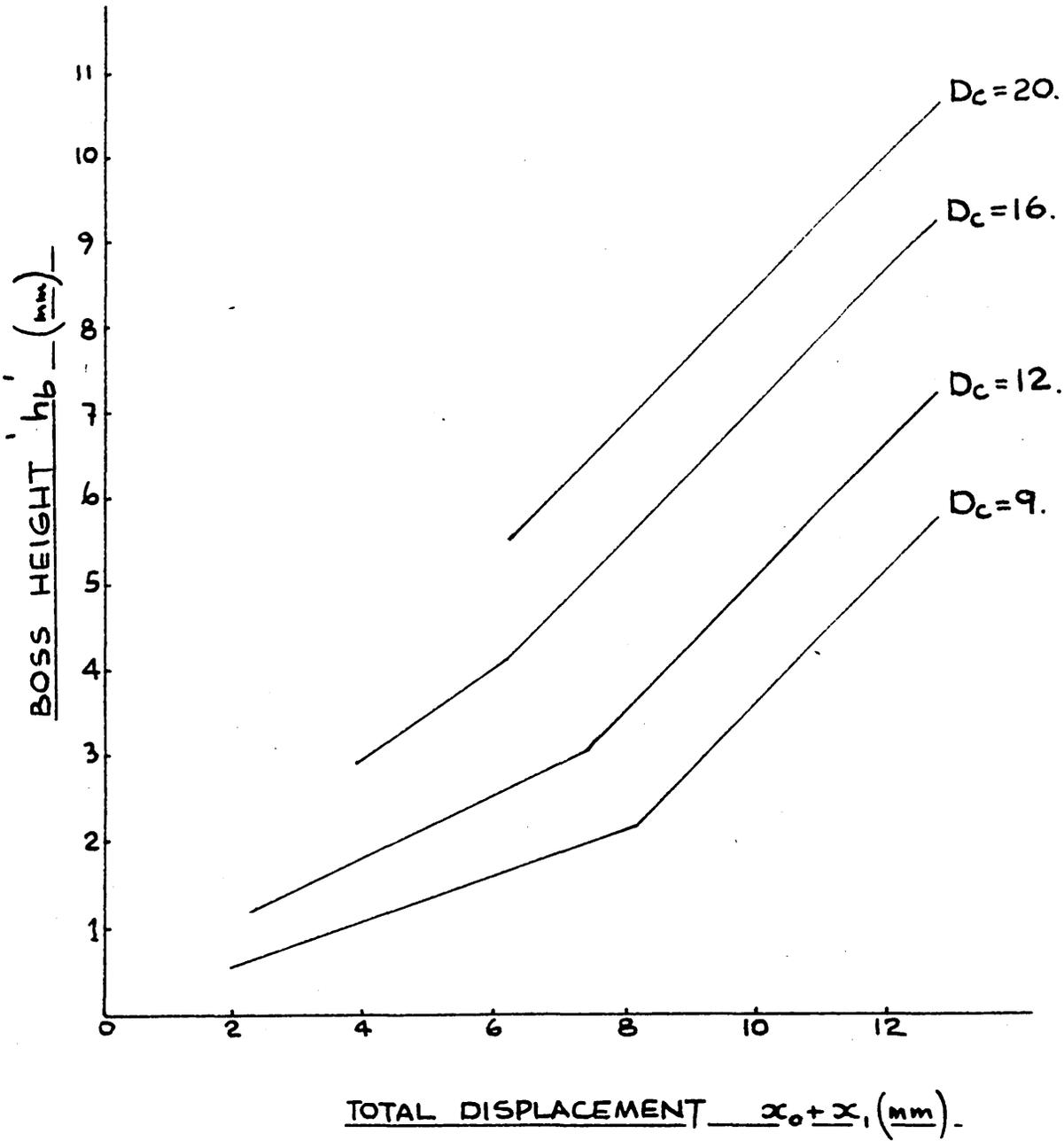
BOSS HEIGHT v. TOTAL DISPLACEMENT

FIG. 68.

149

THEORETICAL CURVES

$L_0 = 22 \, mm.$ $Y = 17 \, N/mm^2$
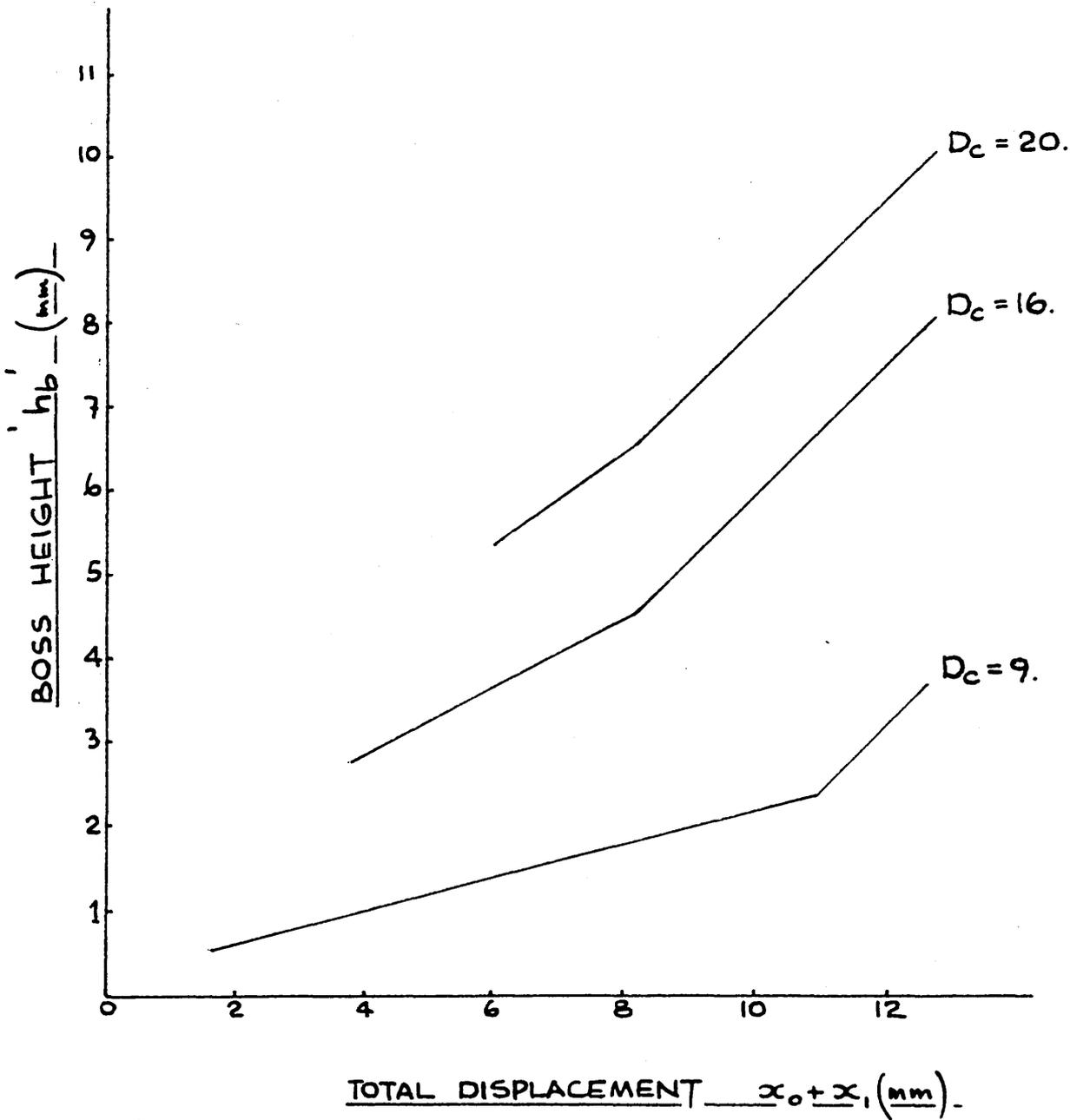
BOSS HEIGHT v. TOTAL DISPLACEMENT.

FIG. 69.

150
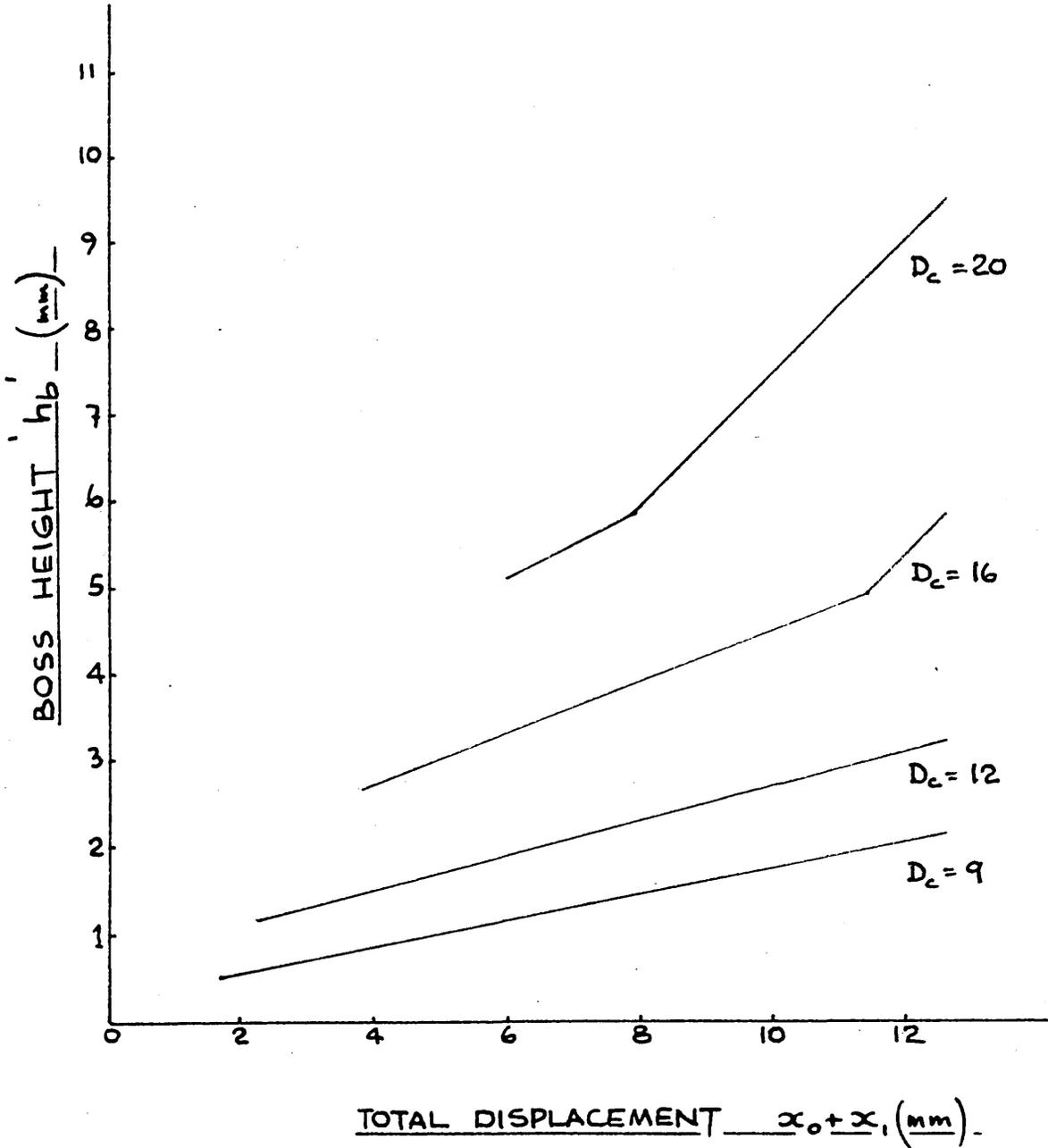
$L_0 = 30\,mm.$ $Y = 17\,N/mm^2.$

BOSS HEIGHT v. TOTAL DISPLACEMENT

FIG 70.

THEORETICAL / EXPERIMENTAL CURVES

$$Y = 17 \, N/mm^2 \qquad L_0 = 24 \, mm$$

THEORETICAL VALUES ————————

EXPERIMENTAL RESULTS STATIC LUBRICATED

$D_c = 18$ ——— ∎ ———— ∎ ———— ∎ ——

$D_c = 9$ ———— ▲ ———— ———— ——

EXPERIMENTAL RESULTS DYNAMIC LUBRICATED

$D_c = 18$ ——— ◻ ——— ——— ◻ ——— ——

$D_c = 9$ ———— △ ———— ———— ——

BOSS HEIGHT V. TOTAL DISPLACEMENT

FIG. 71.

152

THEORETICAL CURVES

BOSS DIA = 9 mm   Y = 17 N/mm²
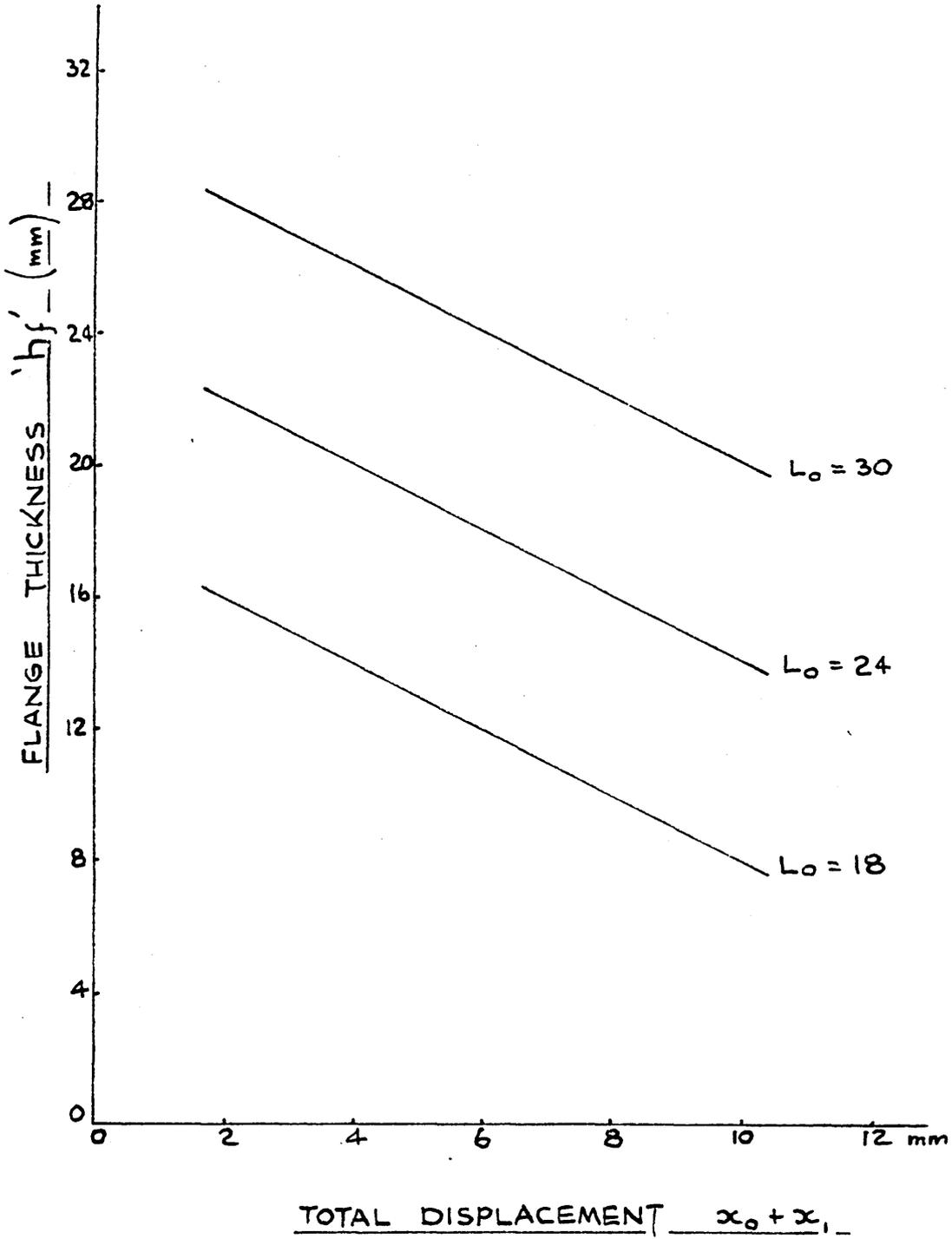
FLANGE THICKNESS V. TOTAL DISPLACEMENT

FIG. 72.

153

THEORETICAL CURVES

BOSS DIA = 16 mm $Y = 17 \, N/mm^2$
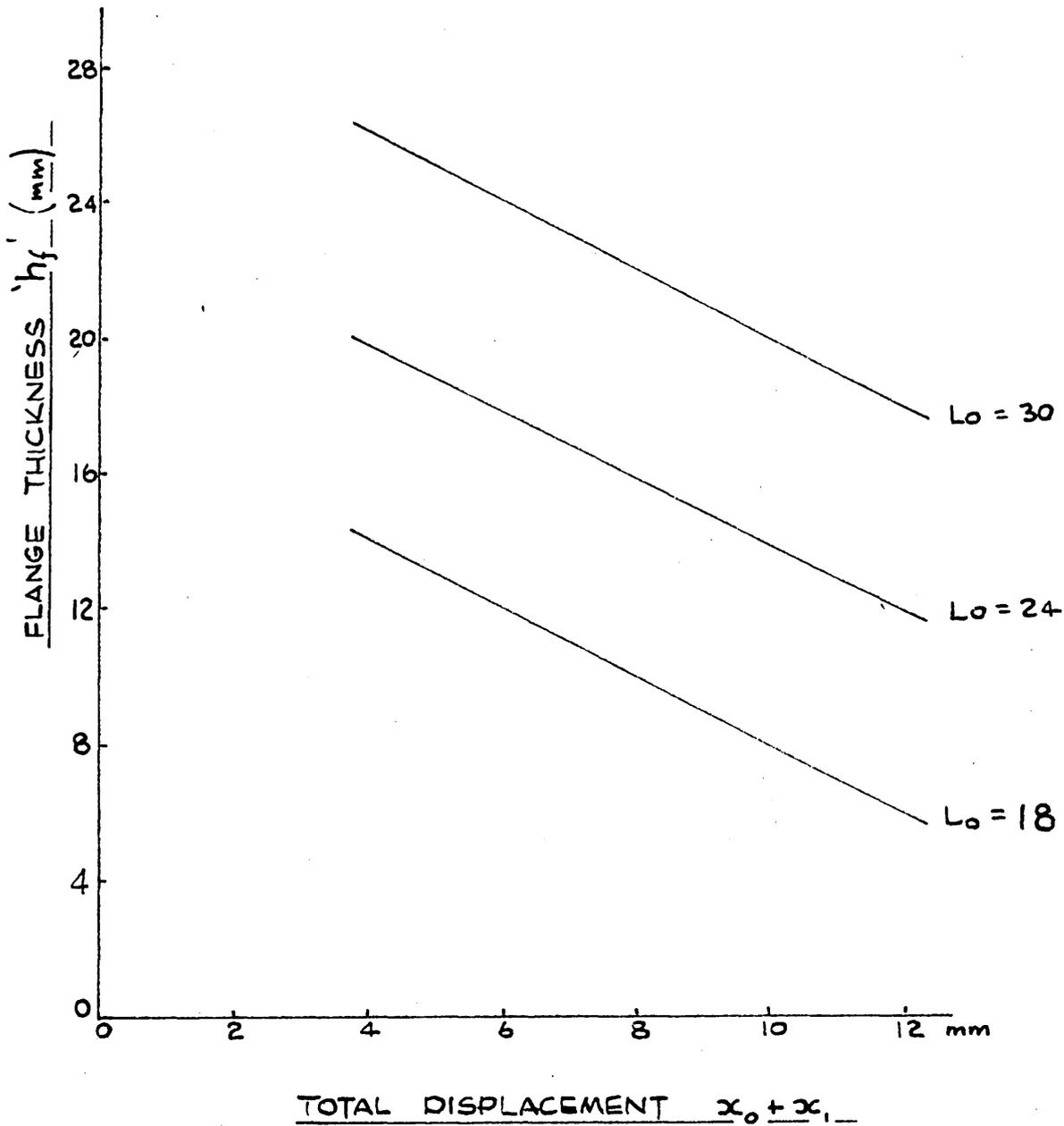
FLANGE THICKNESS v. TOTAL DISPLACEMENT.

FIG. 73.

154

THEORETICAL CURVES

BOSS DIA = 20 mm   Y = 17 N/mm²
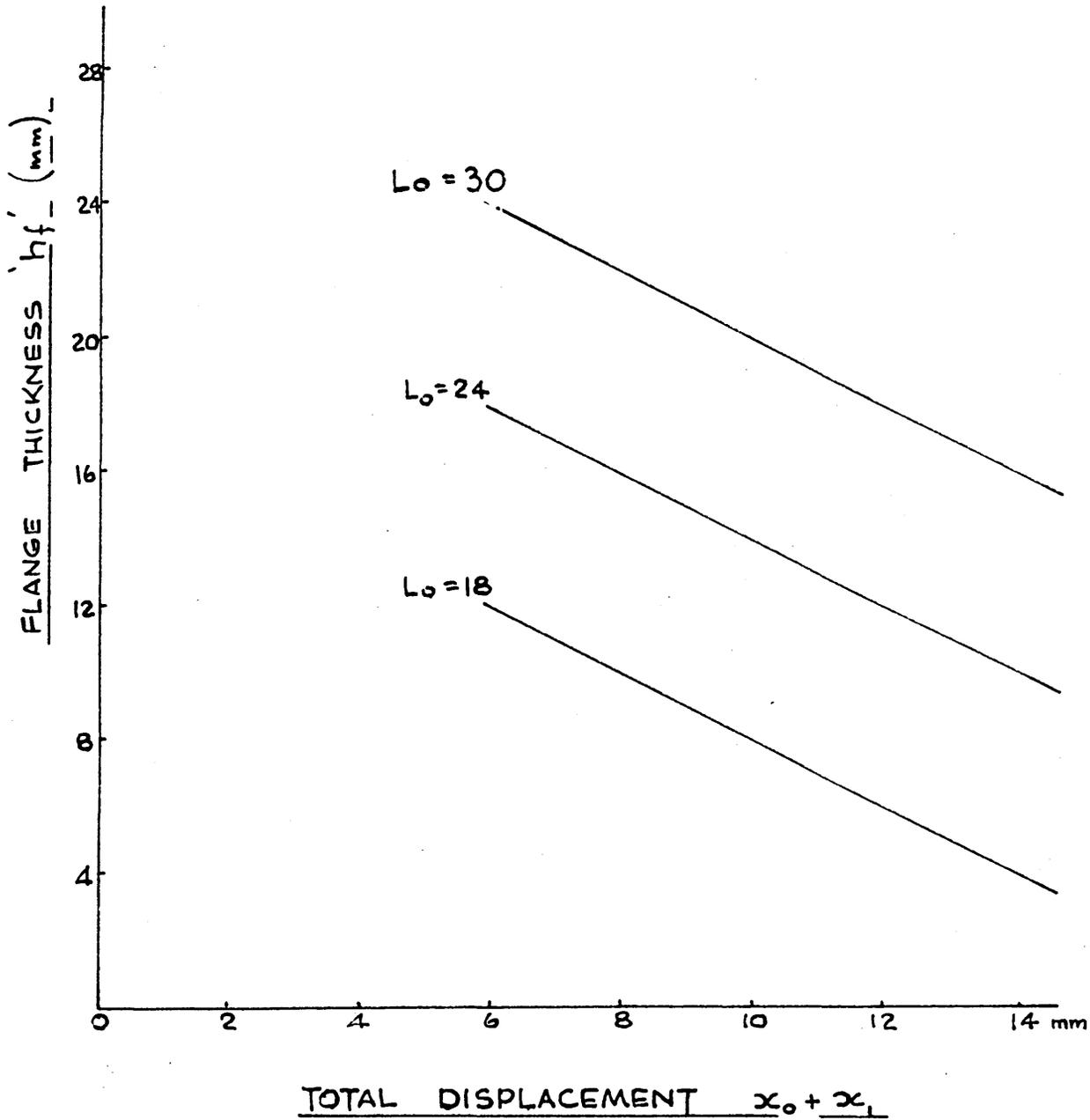
FLANGE THICKNESS v. TOTAL DISPLACEMENT

FIG. 74.

155

THEORETICAL CURVES

BOSS DIA = 18 mm $Y = 17 \, N/mm^2$
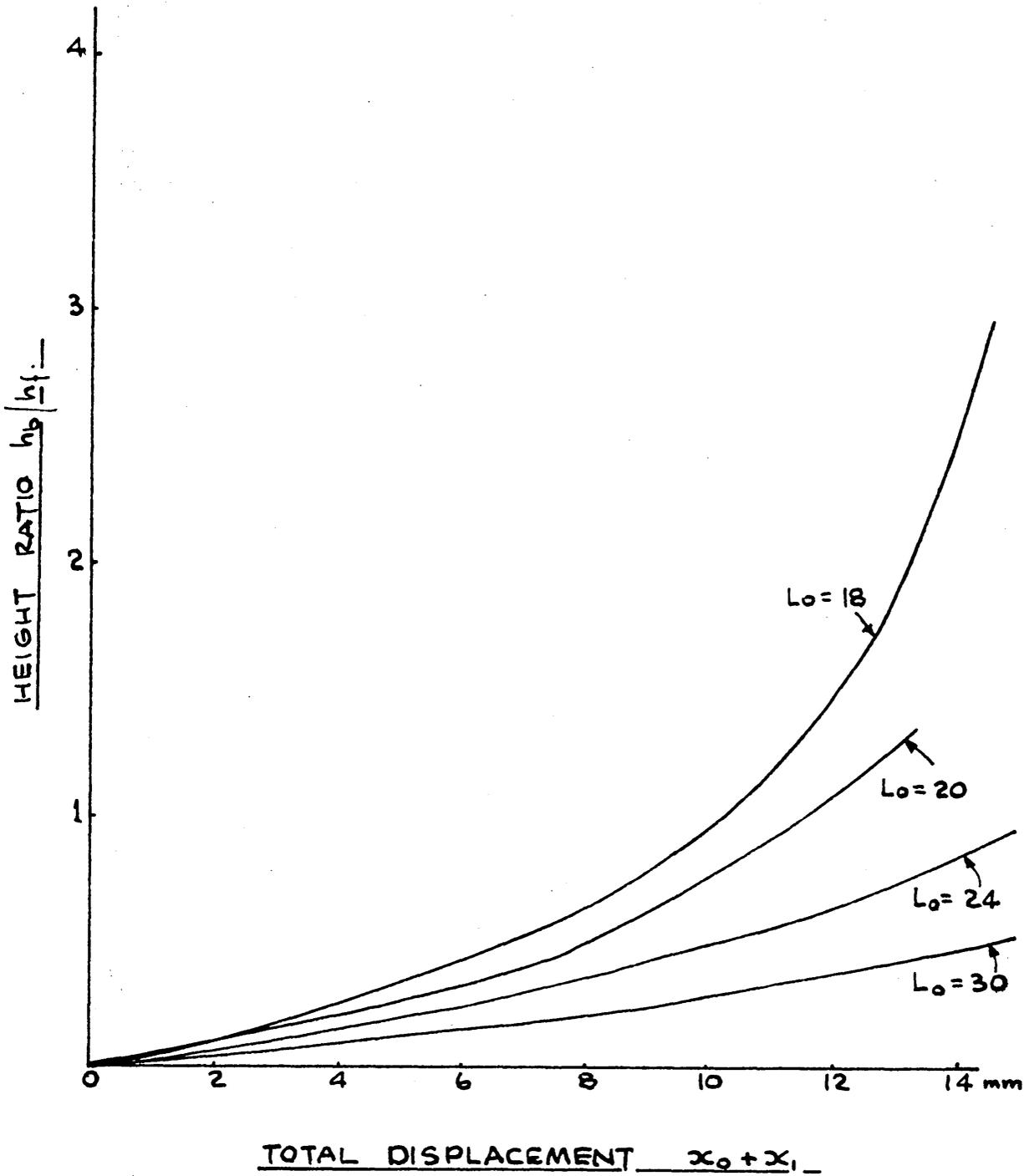
HEIGHT RATIO v. TOTAL DISPLACEMENT

FIG.75.

156

THEORETICAL CURVES

BOSS DIA. = 20 mm $Y = 17 \, N/mm^2$
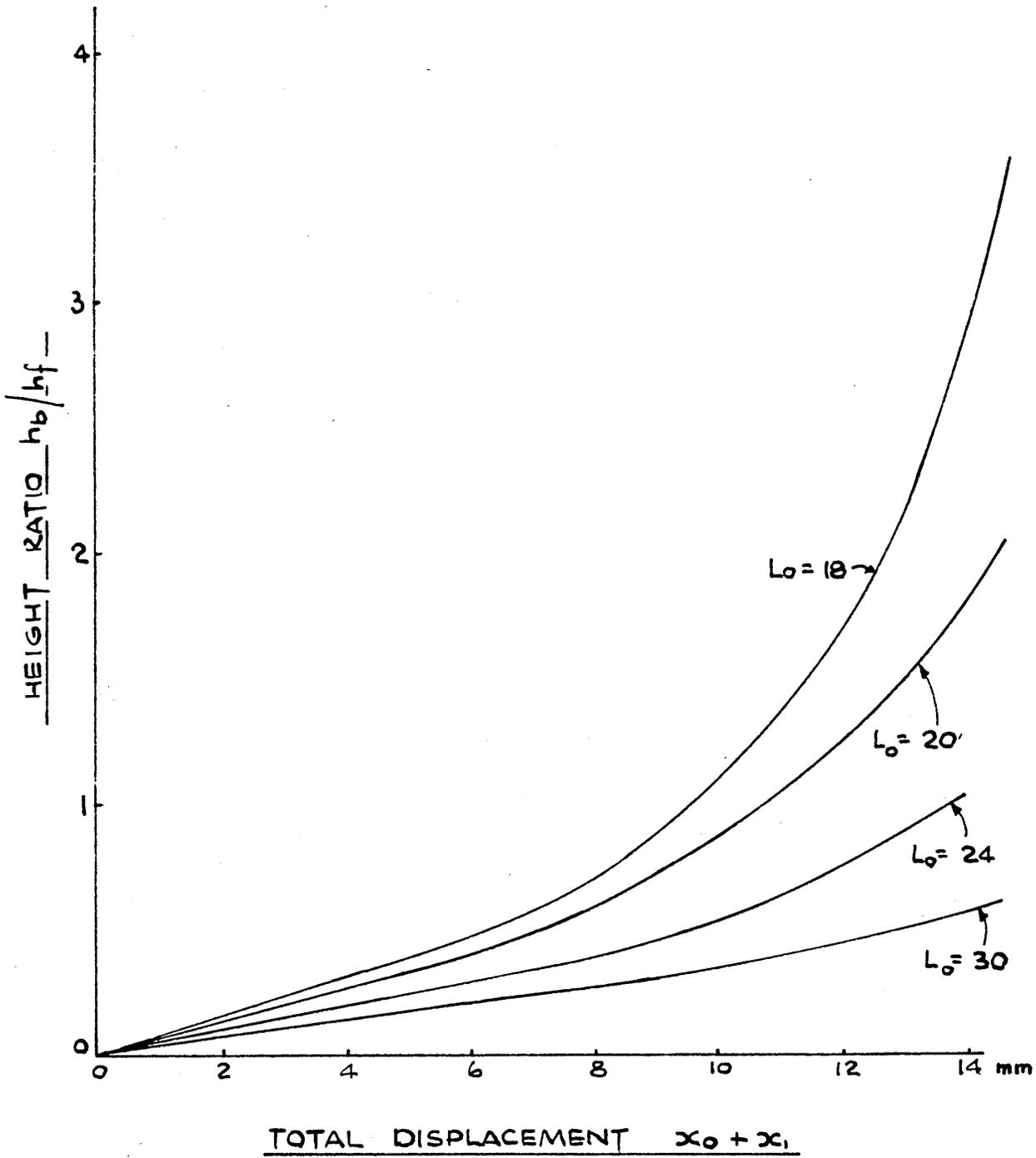
HEIGHT RATIO v. TOTAL DISPLACEMENT

FIG. 76.

157

THEORETICAL RESULTS

$L_0 = 24$ mm. $Y = 17$ N/mm^2.

HEIGHT RATIO h_b/h_f.

$D_c = 18$

$D_c = 12$

$D_c = 9$.

TOTAL DISPLACEMENT $(x_0 + x_1)$ mm.
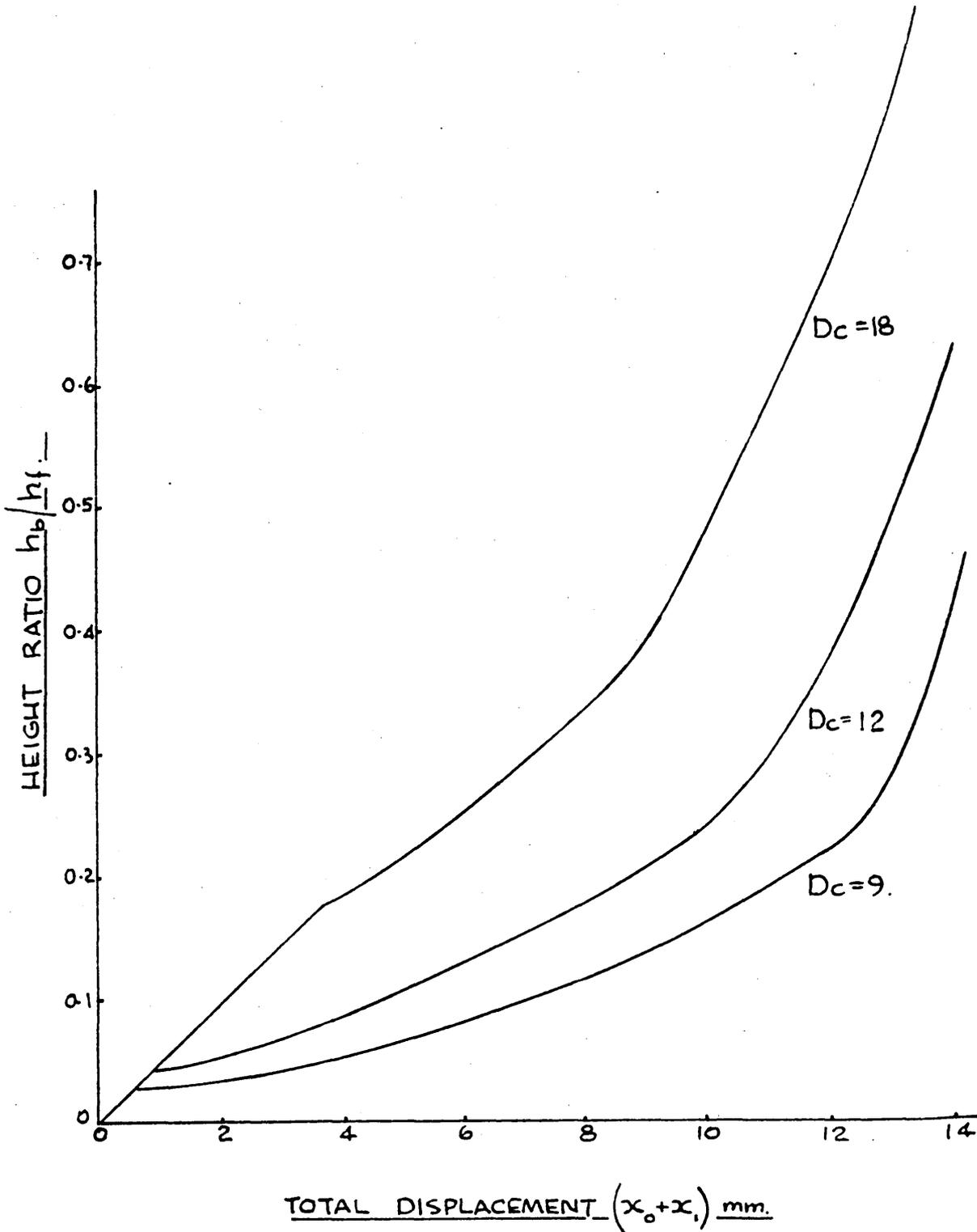
HEIGHT RATIO v. TOTAL DISPLACEMENT.

FIG. 77.

THEORETICAL / EXPERIMENTAL RESULTS

$L_0 = 24$ mm. $Y = 17$ N/mm^2.
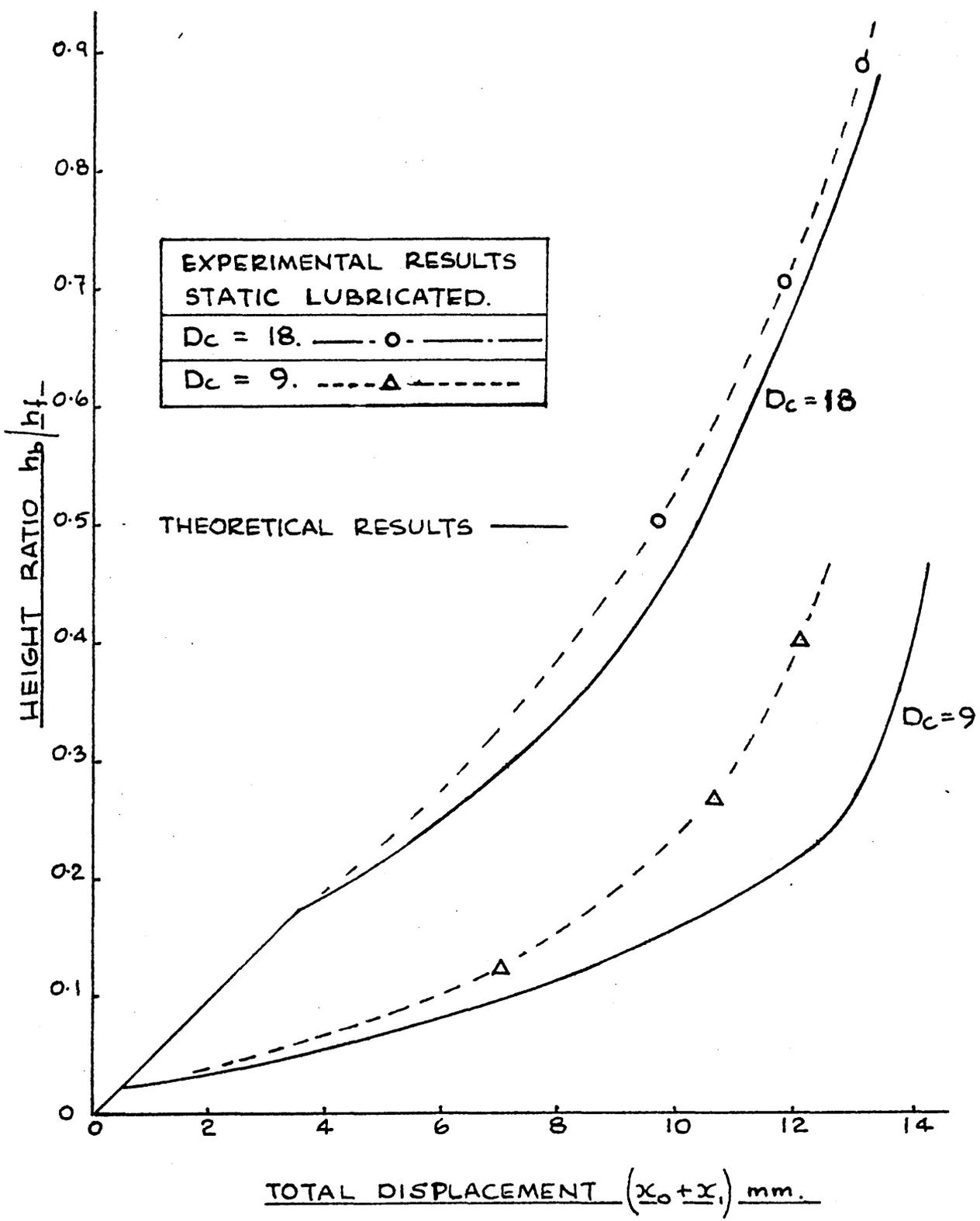
HEIGHT RATIO v. TOTAL DISPLACEMENT

FIG. 78.

159

THEORETICAL AND EXPERIMENTAL RESULTS

$L_o = 24$ mm $Y = 17 \, N/mm^2$
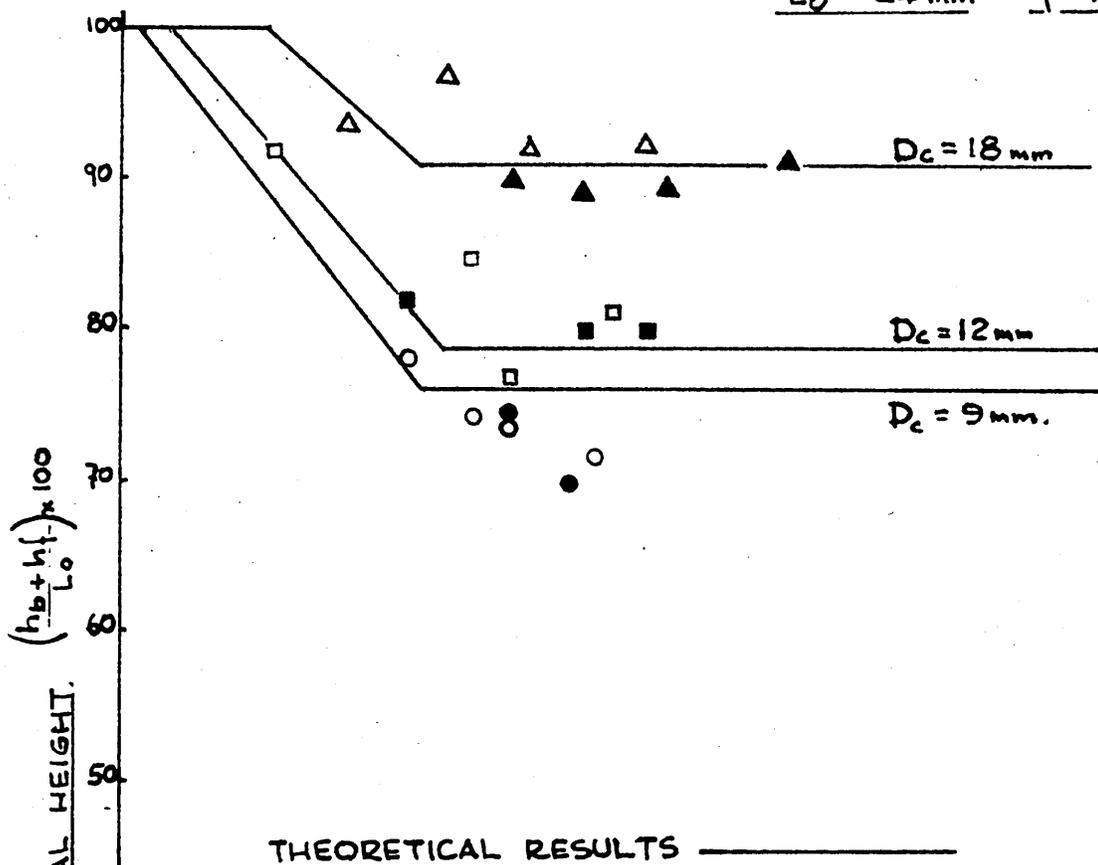
THEORETICAL RESULTS ———

EXPERIMENTAL RESULTS.		
D_c	MODE	SYMBOL
9	QUASI-STATIC —LUB.	○
	DYNAMIC — LUB.	●
12	QUASI-STATIC—LUB.	□
	DYNAMIC—LUB.	■
18	QUASI-STATIC—LUB.	△
	DYNAMIC —LUB.	▲

PERCENTAGE TOTAL HEIGHT. $\left(\dfrac{h_b + h_f}{L_o}\right) \times 100$

PERCENTAGE DISPLACEMENT $\left(\dfrac{x_o + x_i}{L_o}\right) \times 100$

RATIO OF TOTAL BILLET HEIGHT TO TOTAL DISPLACEMENT.

FIG. 78 (a)

160

$$L_o = 24 \, mm$$
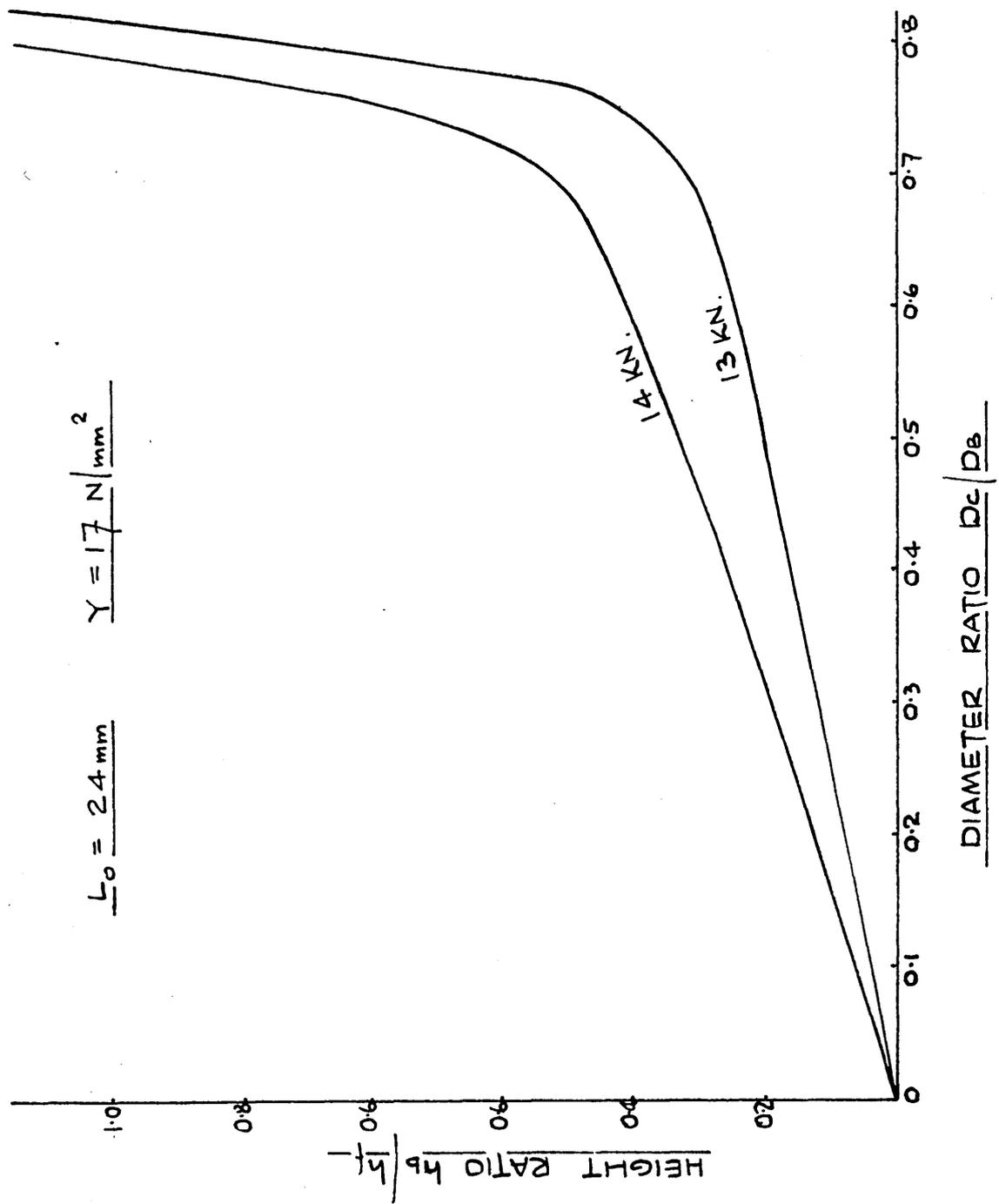
$$Y = 17 \, N/mm^2$$

HEIGHT RATIO v. DIAMETER RATIO.

FIG. 79.

DIAMETER RATIO D_c/D_B

HEIGHT RATIO h_b/h_t

14 KN.

13 KN.

161

THEORETICAL CURVE.

BILLET DIA. = 24 mm. $Y = 17 \, N/mm^2$.
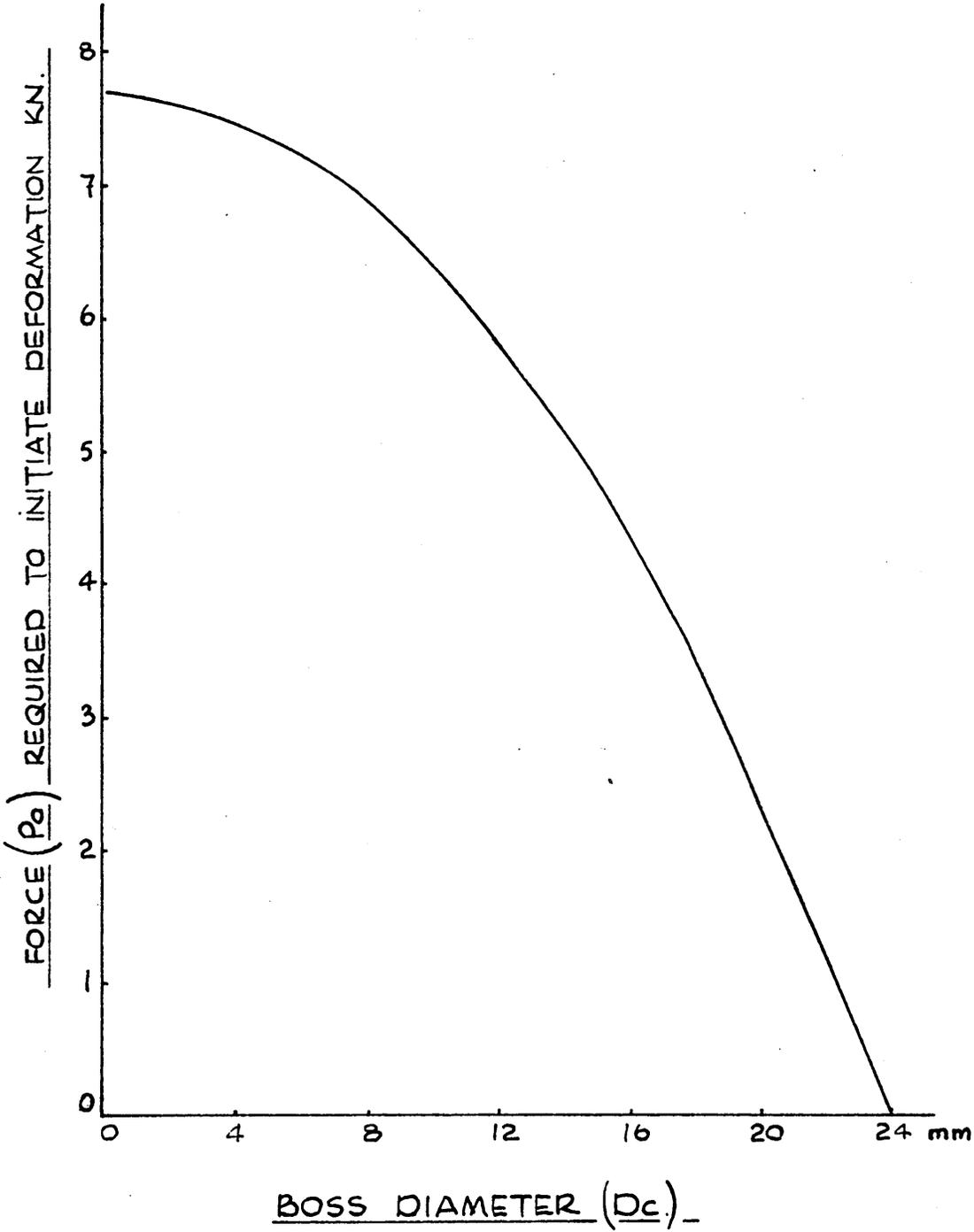
FORCE REQUIRED TO INITIATE DEFORMATION v. BOSS DIAMETER.

FIG.80.

162

THEORETICAL CURVES

BOSS DIA. = 9 mm $Y = 17 \, N/mm^2$
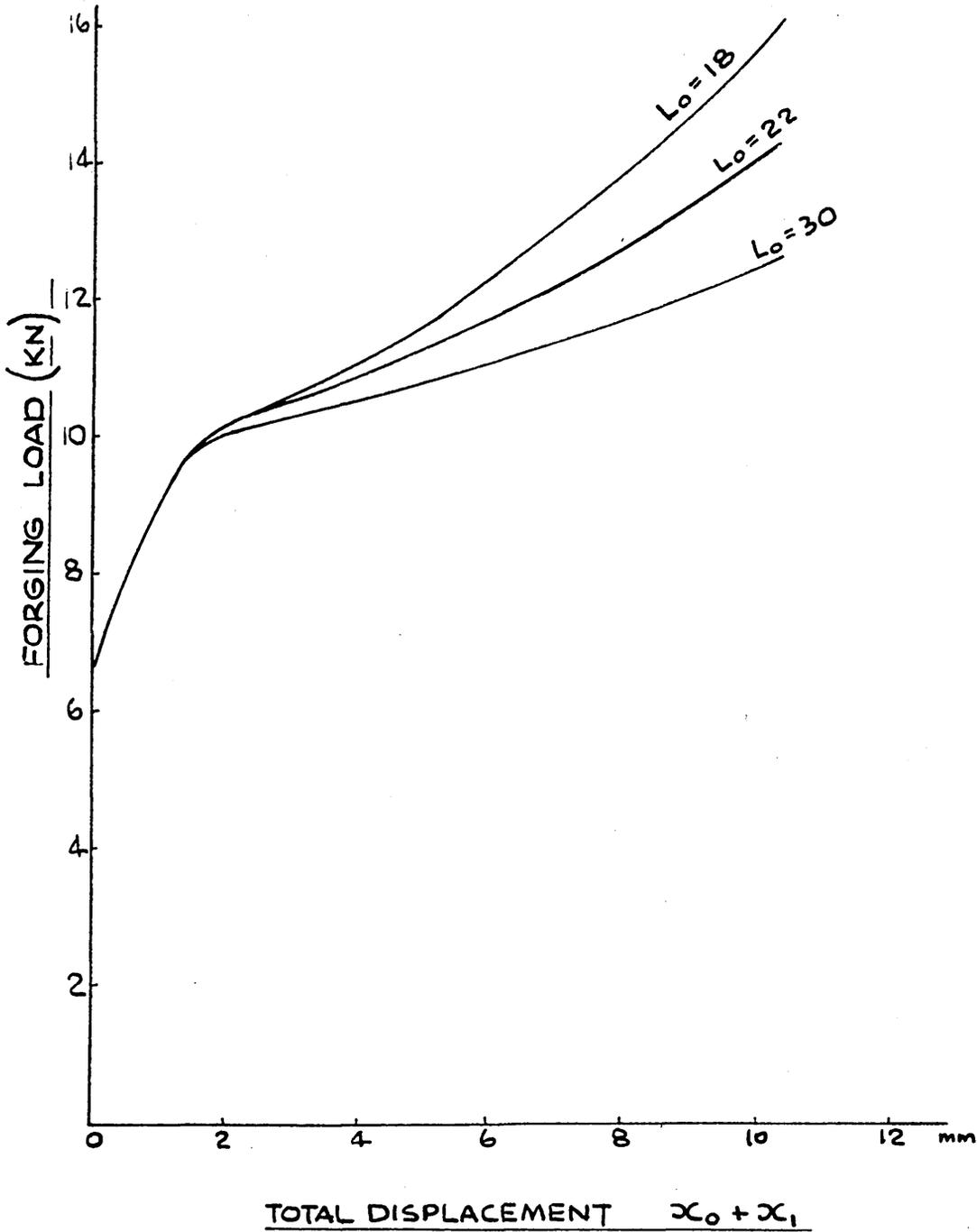
FORGING LOAD v. TOTAL DISPLACEMENT

FIG. 81

163

THEORETICAL CURVES

BOSS DIA = 12 mm $Y = 17 \text{ N/mm}^2$
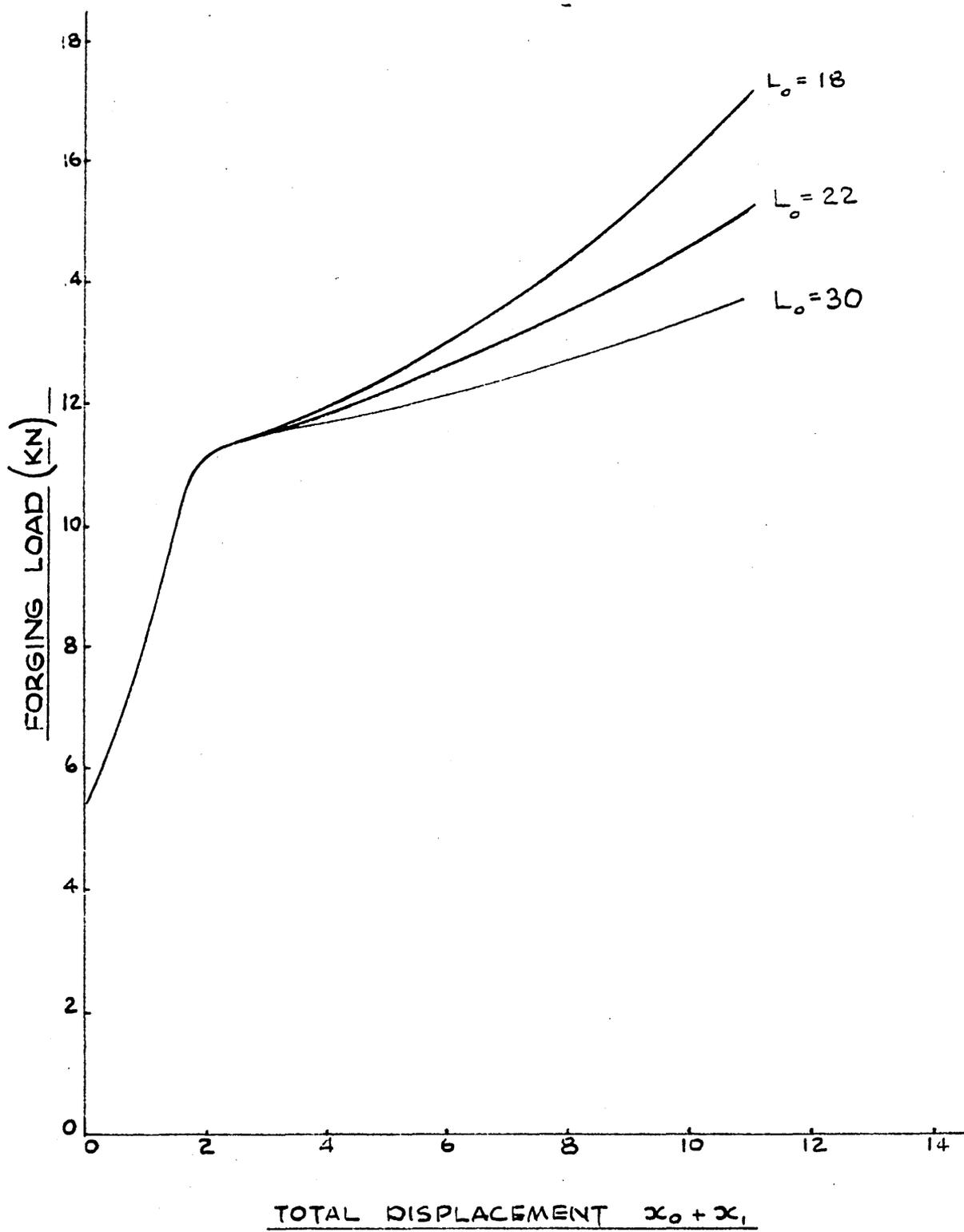
FORGING LOAD v. TOTAL DISPLACEMENT

FIG. 82

164

THEORETICAL CURVES

BOSS DIA = 14 mm   Y = 17 N/mm²
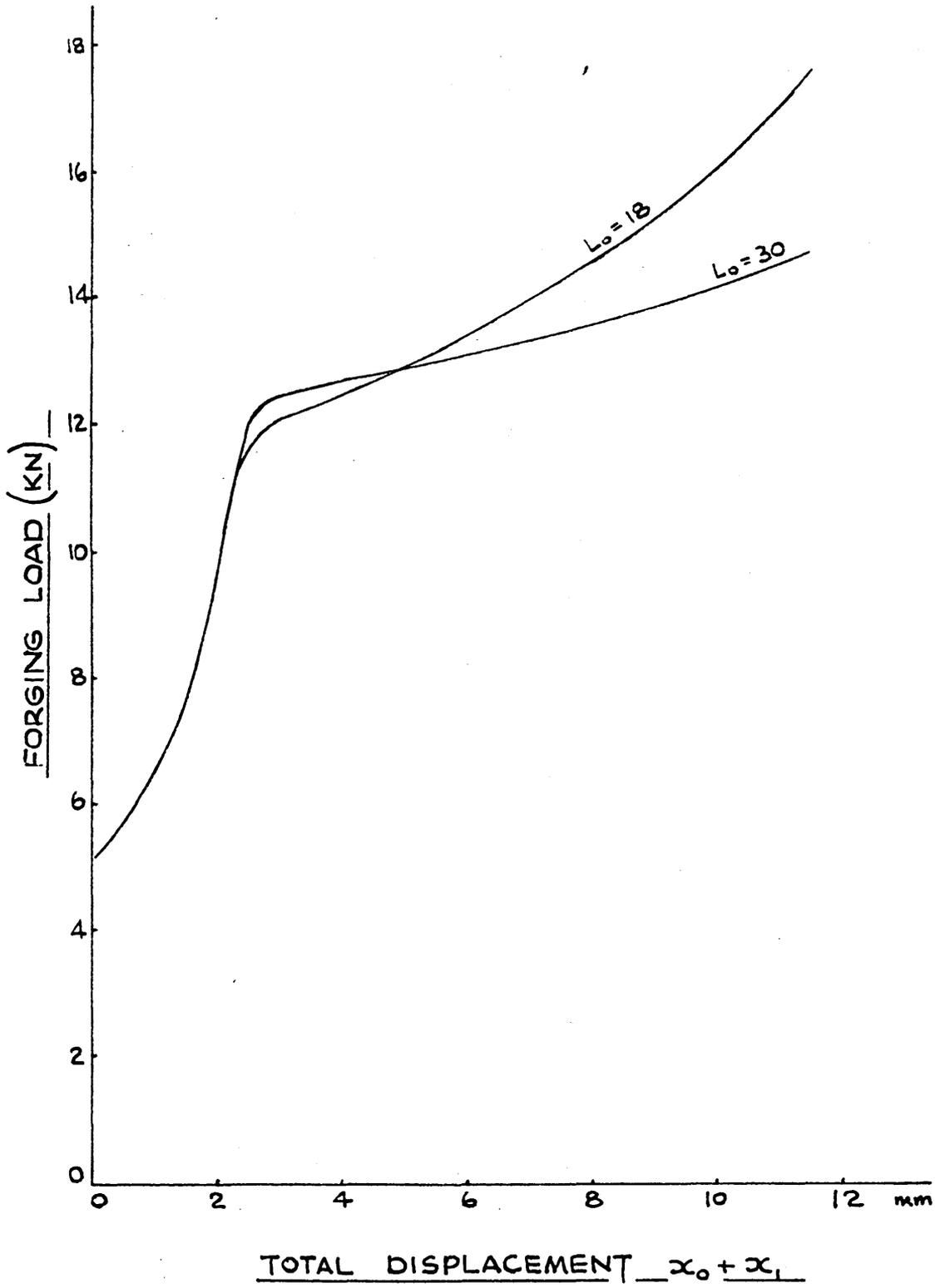
FORGING LOAD v. TOTAL DISPLACEMENT

FIG. 83

165
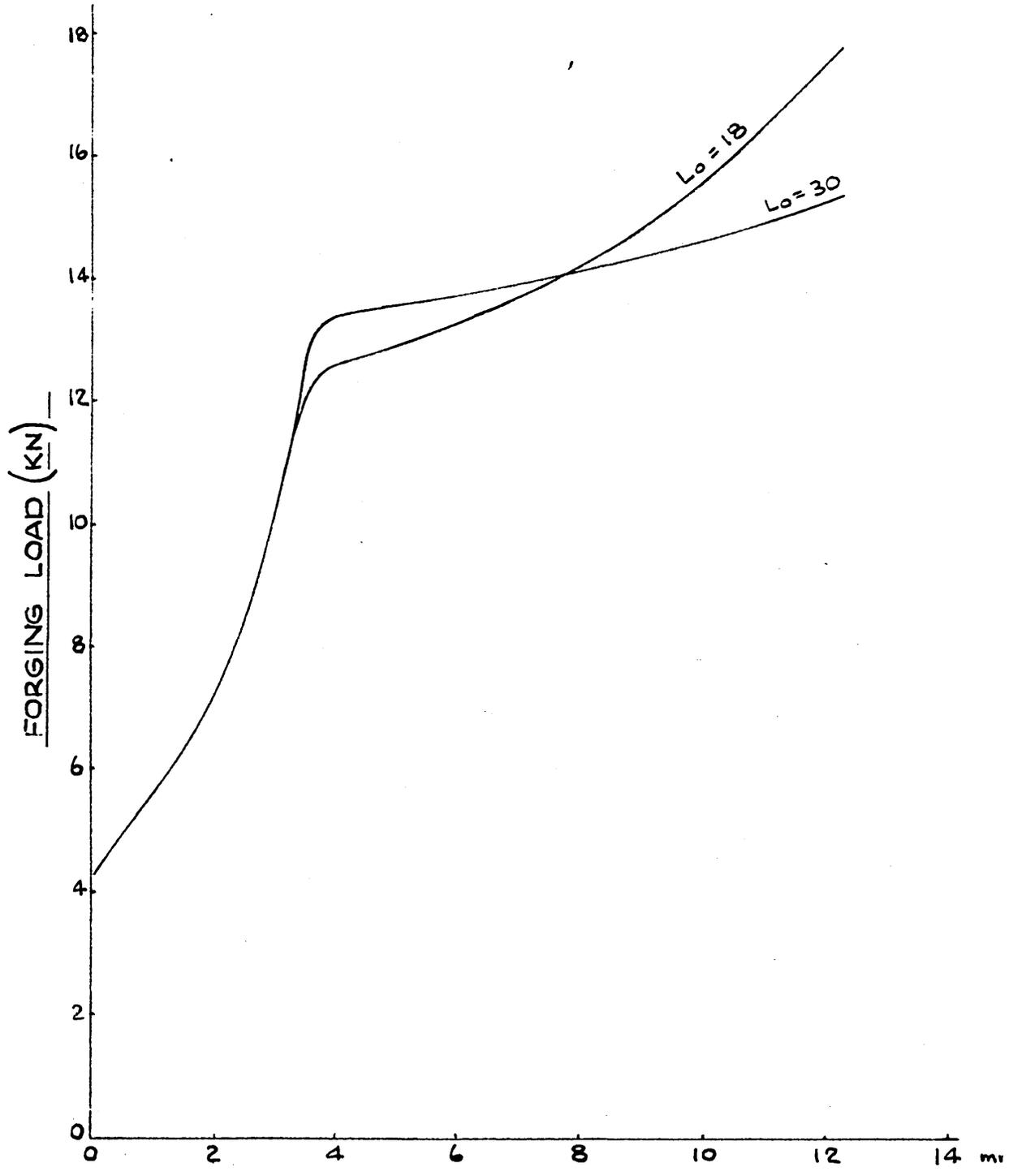
THEORETICAL CURVES

BOSS DIA. 16mm $Y = 17 \, N/mm^2$

FORGING LOAD v. TOTAL DISPLACEMENT

FIG.84   166

THEORETICAL CURVES

BOSS DIA = 18mm   Y = 17 N/mm²
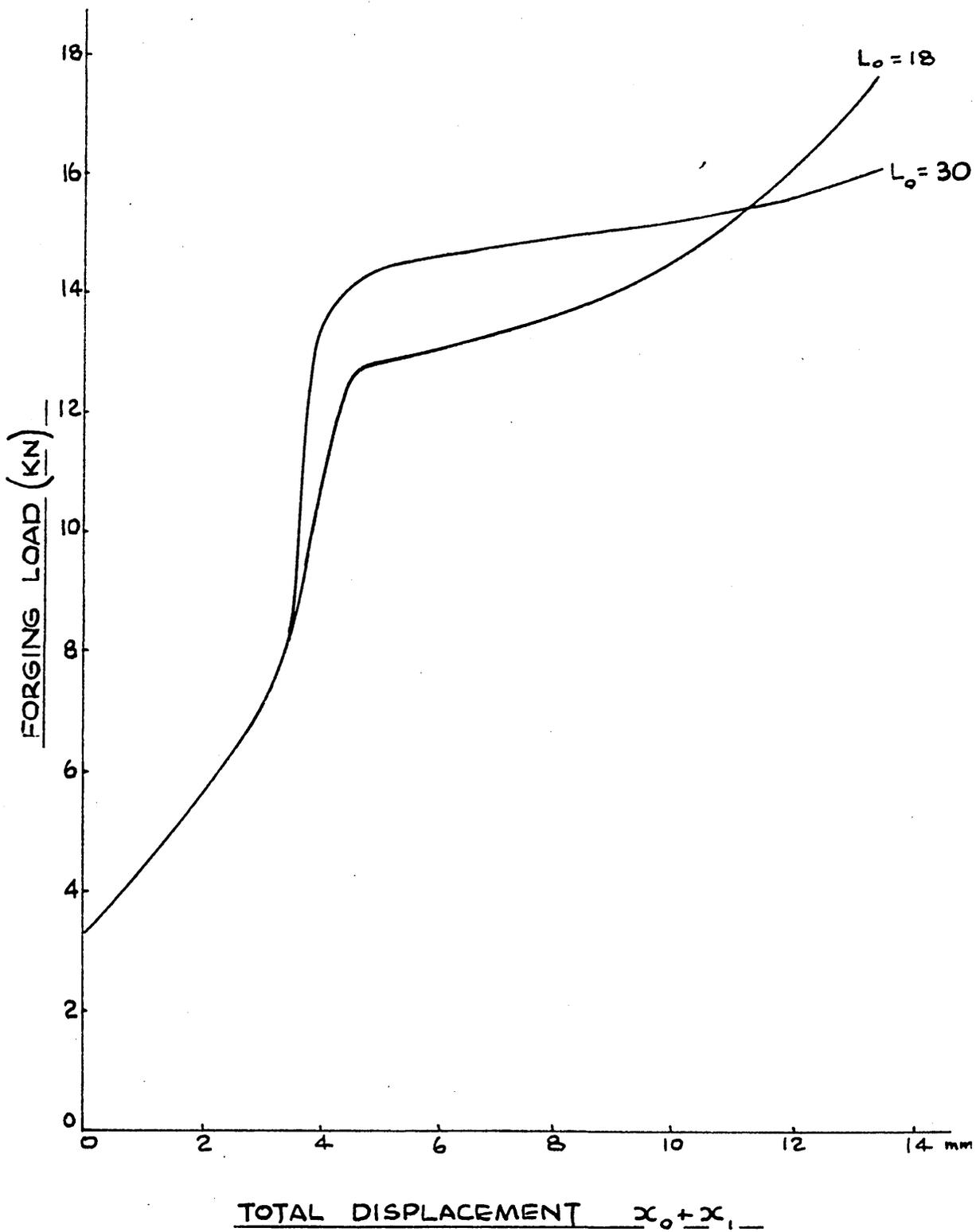
FORGING LOAD v. TOTAL DISPLACEMENT

FIG.85

167

THEORETICAL CURVES

BOSS DIA = 20mm   Y = 17 N/mm²
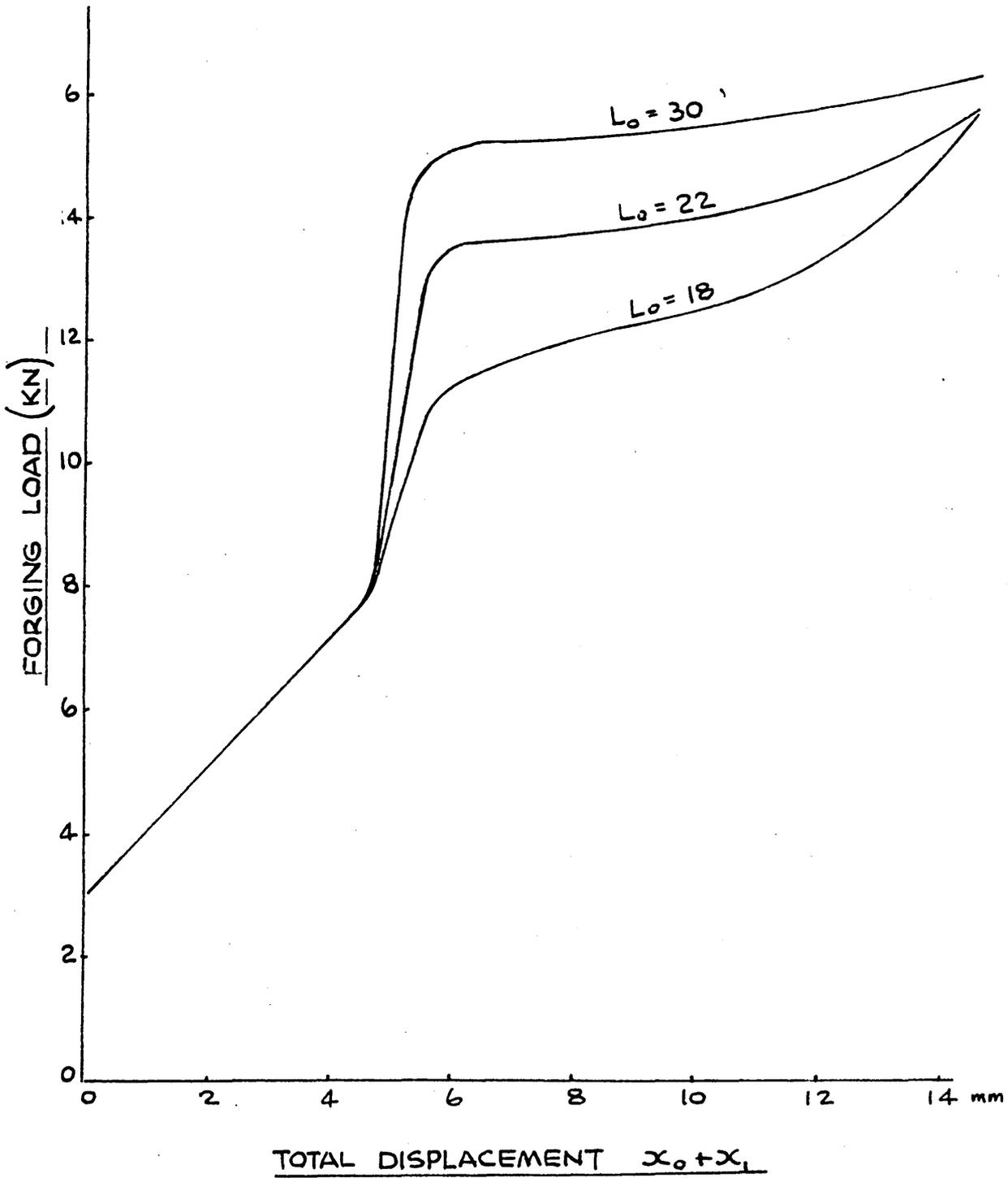
FORGING LOAD v. TOTAL DISPLACEMENT

FIG.86

168

THEORETICAL CURVES

$Y = 17 \, \text{N/mm}^2 \qquad L_0 = 24 \, \text{mm}.$
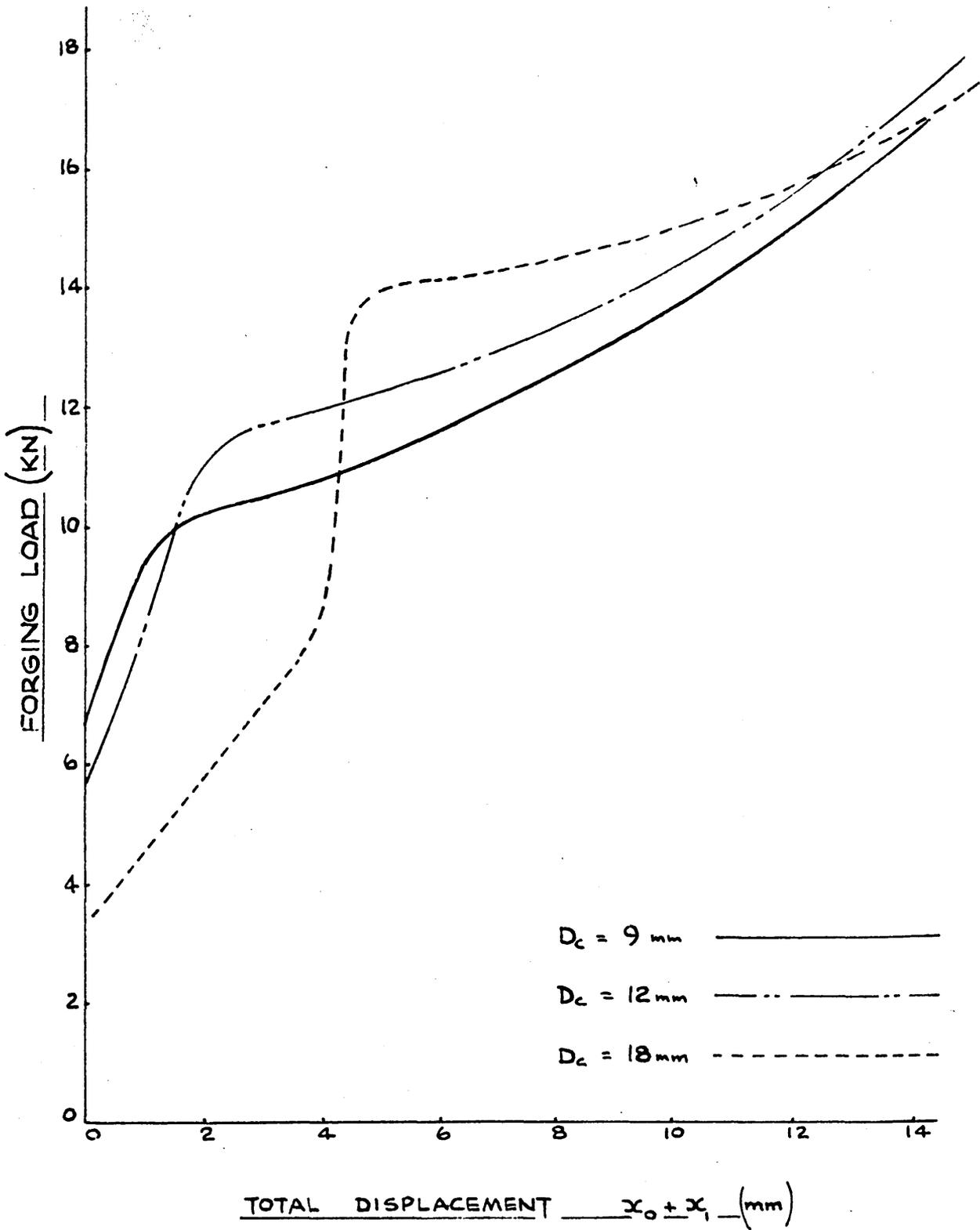
FORGING LOAD (KN)

TOTAL DISPLACEMENT $x_0 \pm x_1$ (mm)

$D_c = 9 \, \text{mm}$ ————

$D_c = 12 \, \text{mm}$ —·—·—

$D_c = 18 \, \text{mm}$ — — — —

FORGING LOAD v. TOTAL DISPLACEMENT

FIG.87

169

THEORETICAL | EXPERIMENTAL RESULTS.

$D_c = 18$ mm. $L_0 = 24$ mm. $Y = 17$ N/mm^2

EXPERIMENTAL DYNAMIC LUBRICATED. —·—

EXPERIMENTAL STATIC LUBRICATED ·······

THEORETICAL (STATIC) ————

THEORETICAL (DYNAMIC) —·—·—
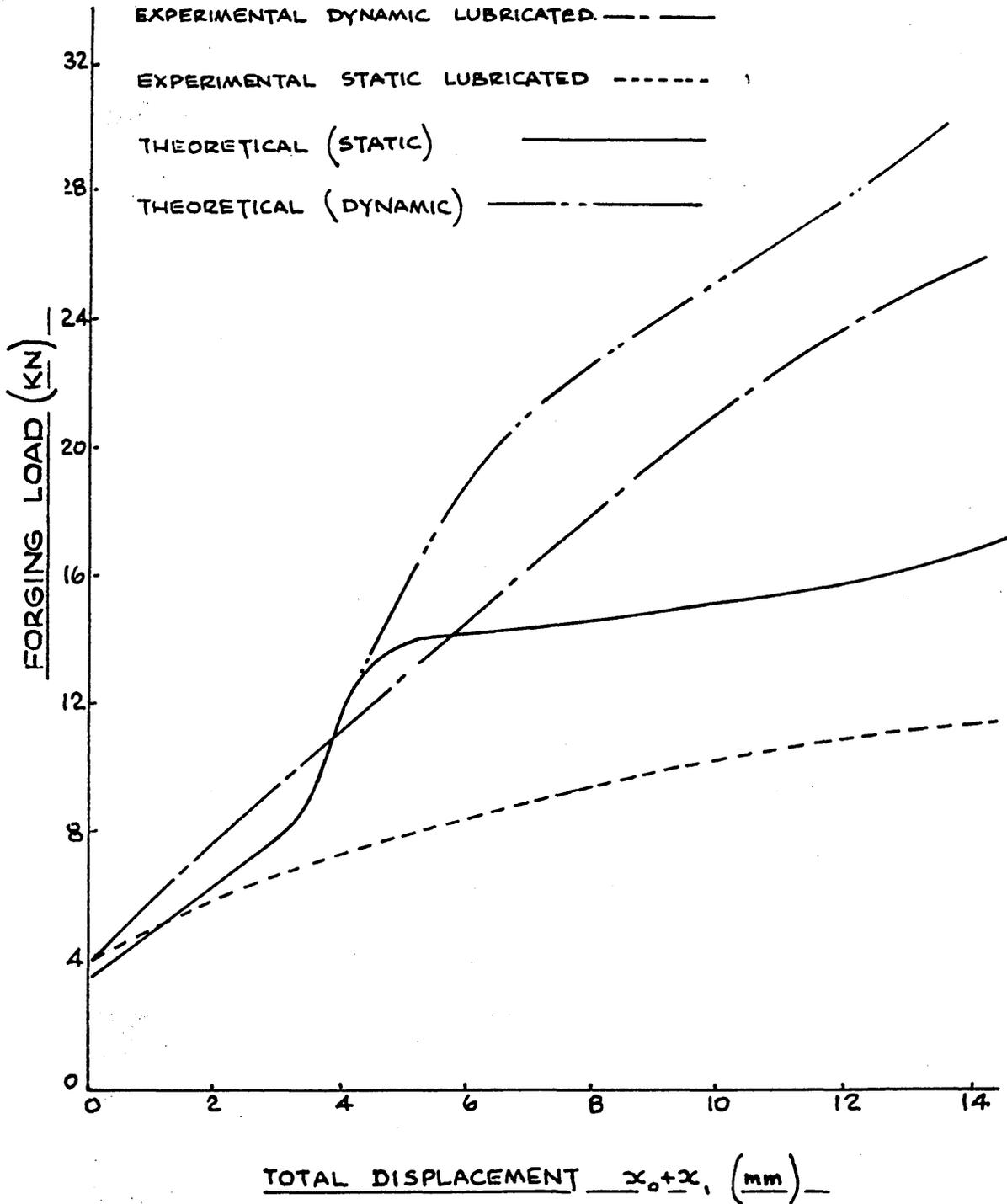
FORGING LOAD v. TOTAL DISPLACEMENT

FIG. 88(a)

170

THEORETICAL / EXPERIMENTAL RESULTS

$D_c = 12$ mm $L_0 = 24$ mm $Y = 17$ N/mm^2

EXPERIMENTAL DYNAMIC LUBRICATED

EXPERIMENTAL STATIC LUBRICATED

THEORETICAL (STATIC)

THEORETICAL (DYNAMIC)

FORGING LOAD (KN)

TOTAL DISPLACEMENT $x_0 + x_1$ (mm)
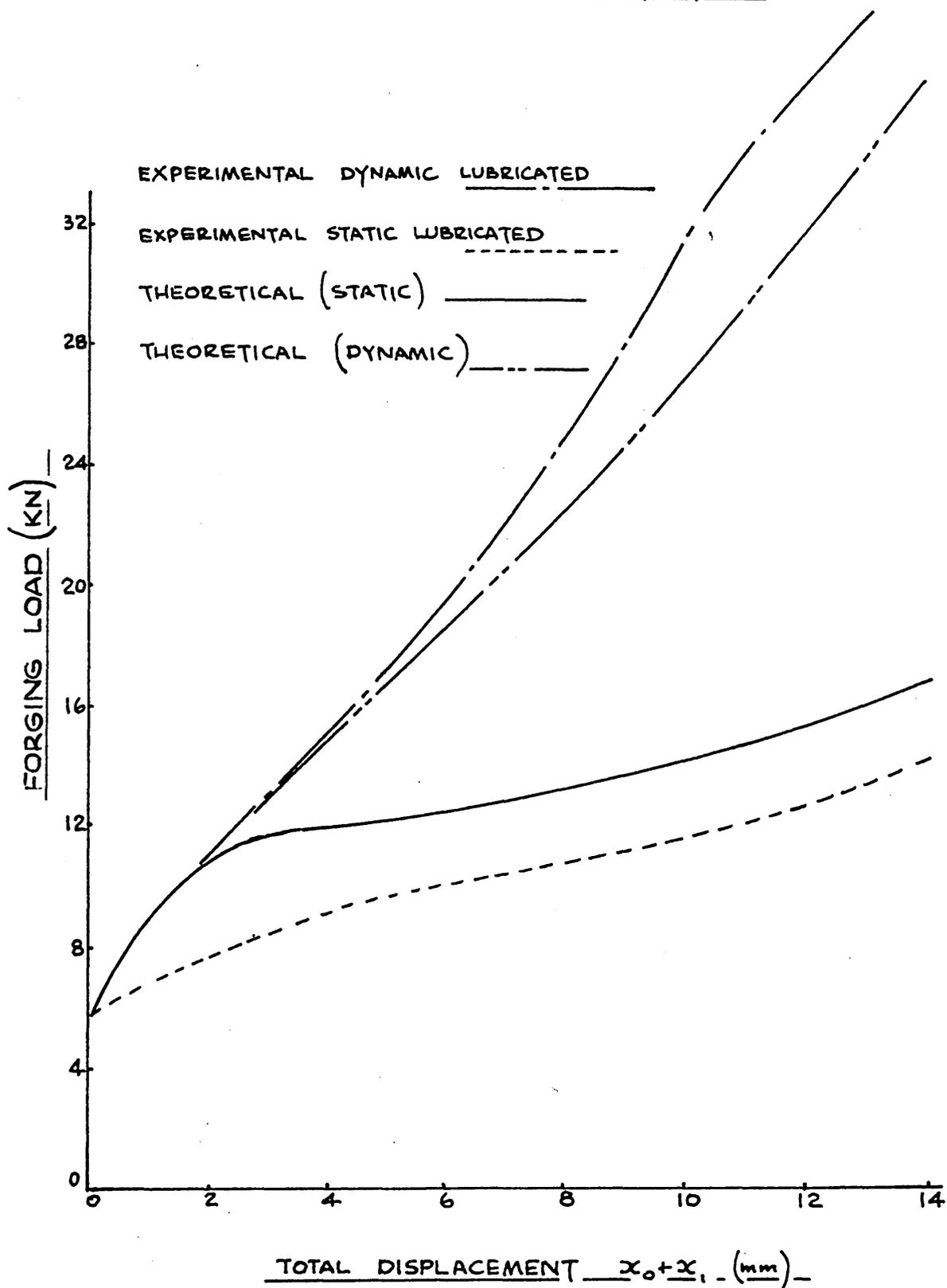
FORGING LOAD v. TOTAL DISPLACEMENT

FIG. 88(b)

171

EXPERIMENTAL RESULTS

$D_c = 12\,mm$ $Y = 17\,N/mm^2$

STATIC LUBRICATED $- \triangle$ — — — — — —
STATIC DRY — — — $\square$ — — — — — —
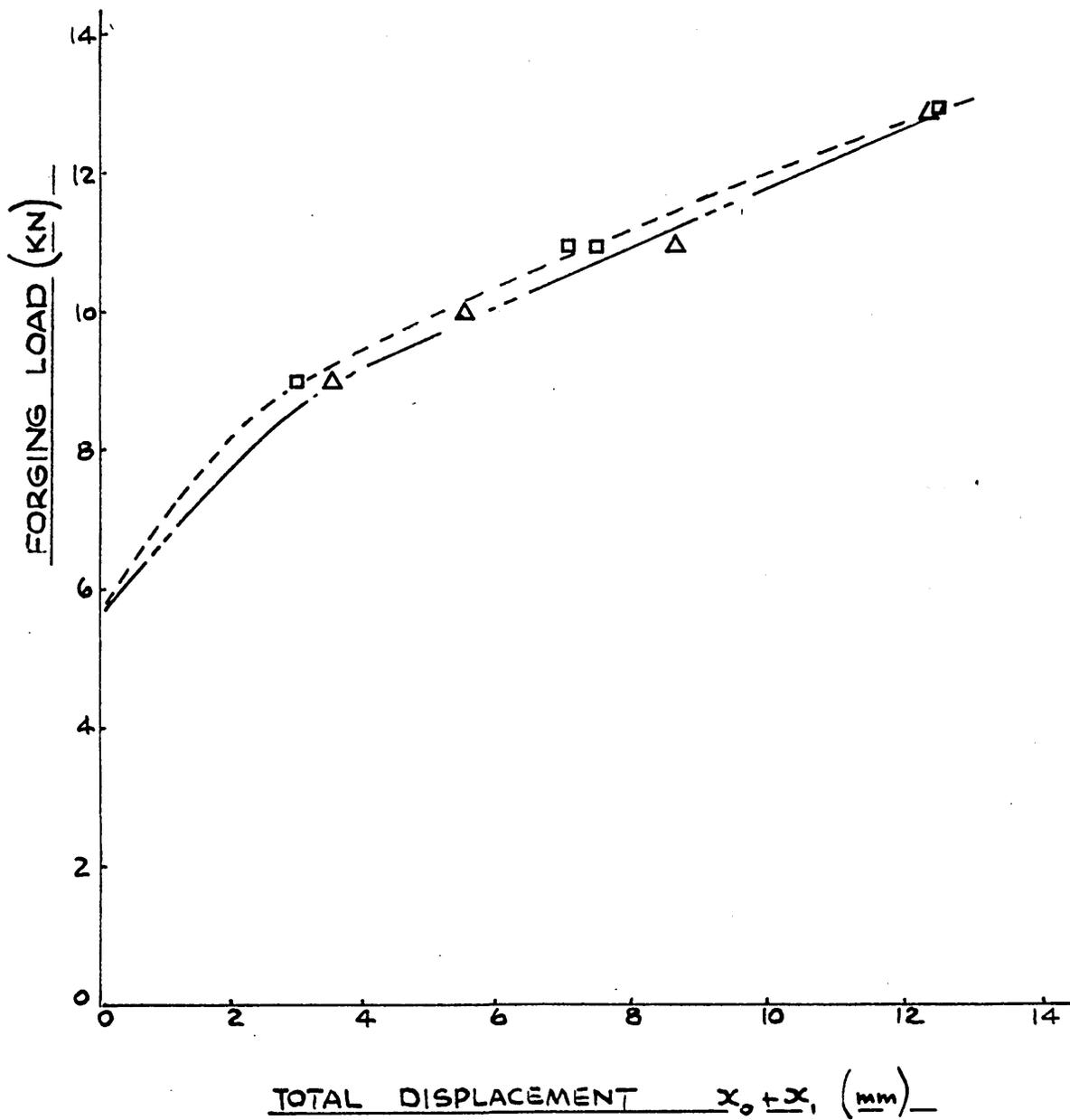
FORGING LOAD v. TOTAL DISPLACEMENT

FIG. 89

172

EXPERIMENTAL RESULTS

$D_c = 18\,mm$ $Y = 17\,N/mm^2$

STATIC LUBRICATED $-\triangle---------$
STATIC DRY $\quad\square\quad-\cdot-\cdot-$
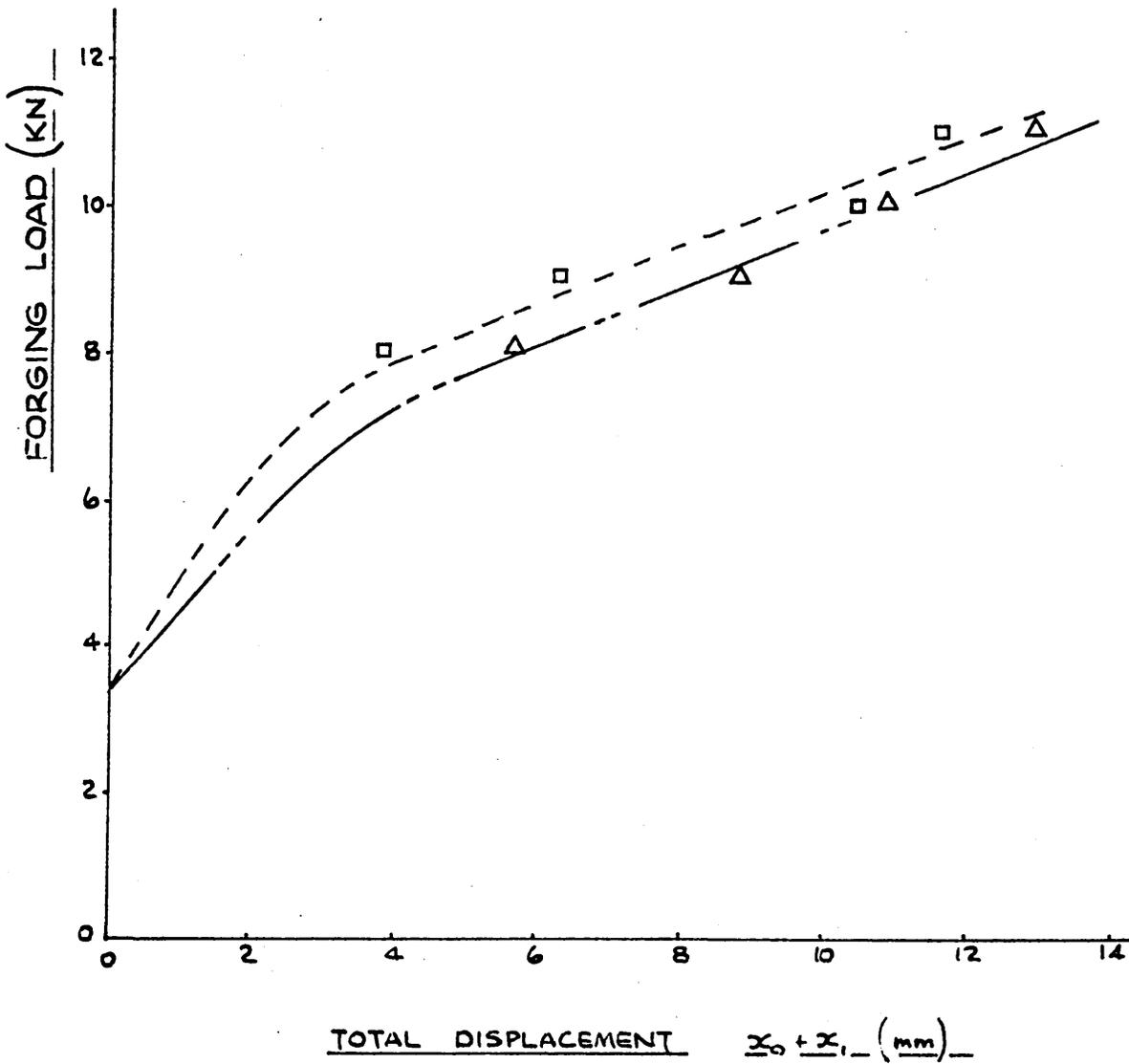
FORGING LOAD v. TOTAL DISPLACEMENT

FIG. 90

THEORETICAL CURVES

BOSS DIA = 9mm L_0 = 24 mm

* 0·08 % CARBON STEEL

* 800°C

* 1000°C

* 1200°C

LEAD AT ROOM TEMP.

TOTAL DISPLACEMENT $x_0 + x_1$
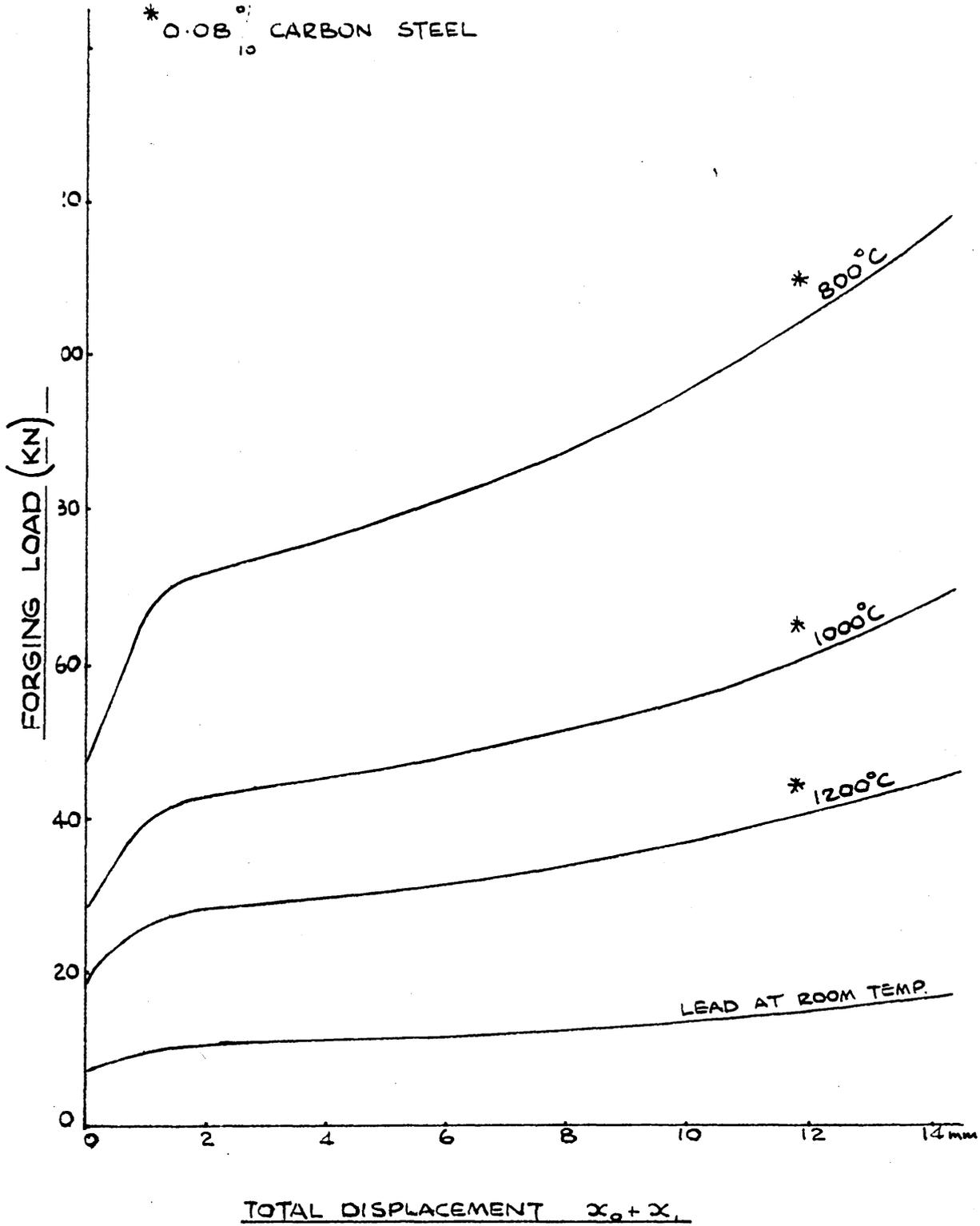
FORGING LOAD v. TOTAL DISPLACEMENT

FIG. 91

174

THEORETICAL CURVES

BOSS DIA = 12mm L_o = 24 mm
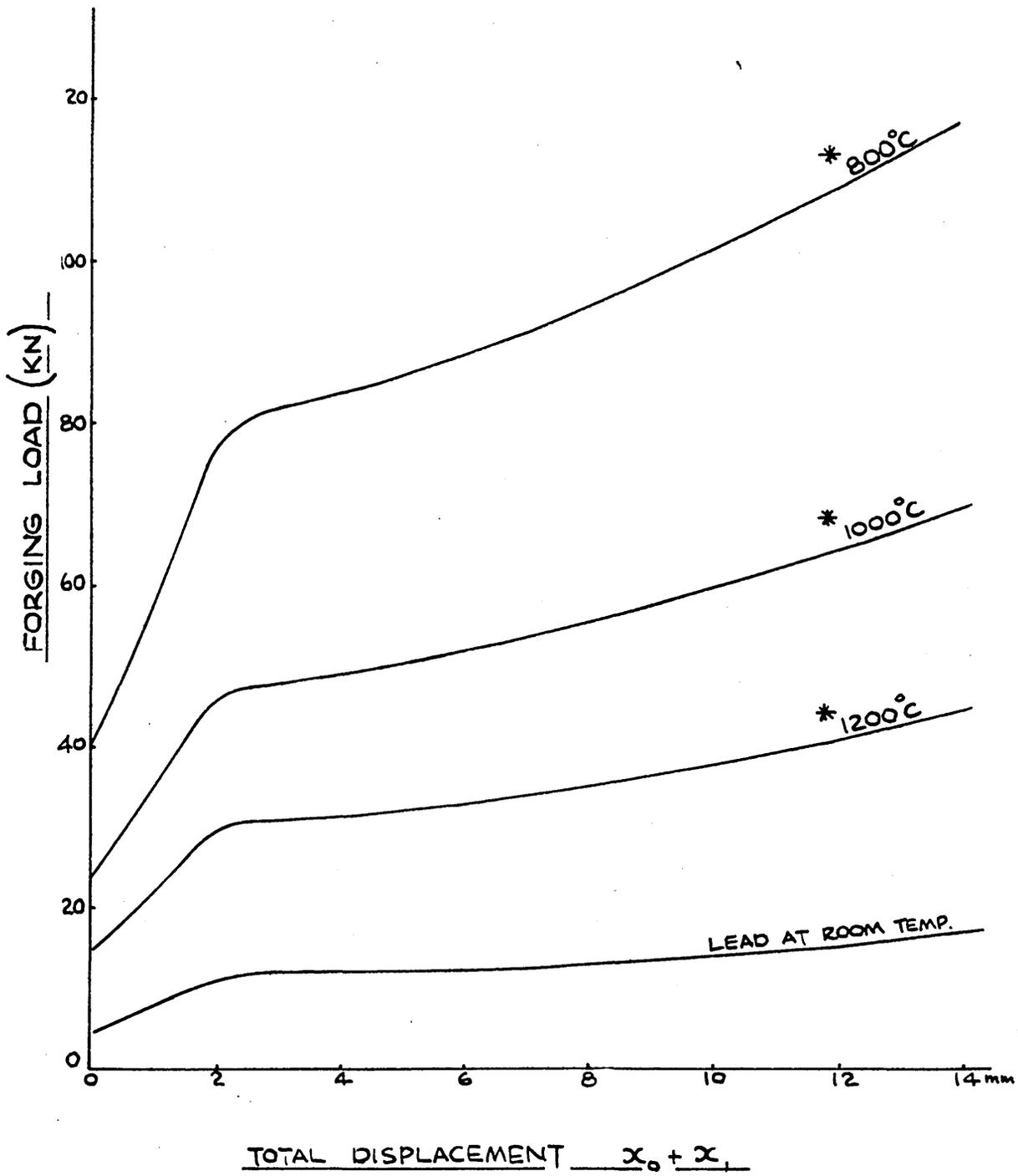
* 0.08 % CARBON STEEL

FORGING LOAD v. TOTAL DISPLACEMENT

FIG.92

175

THEORETICAL CURVES

BOSS DIA. = 14 mm L_o = 24 mm
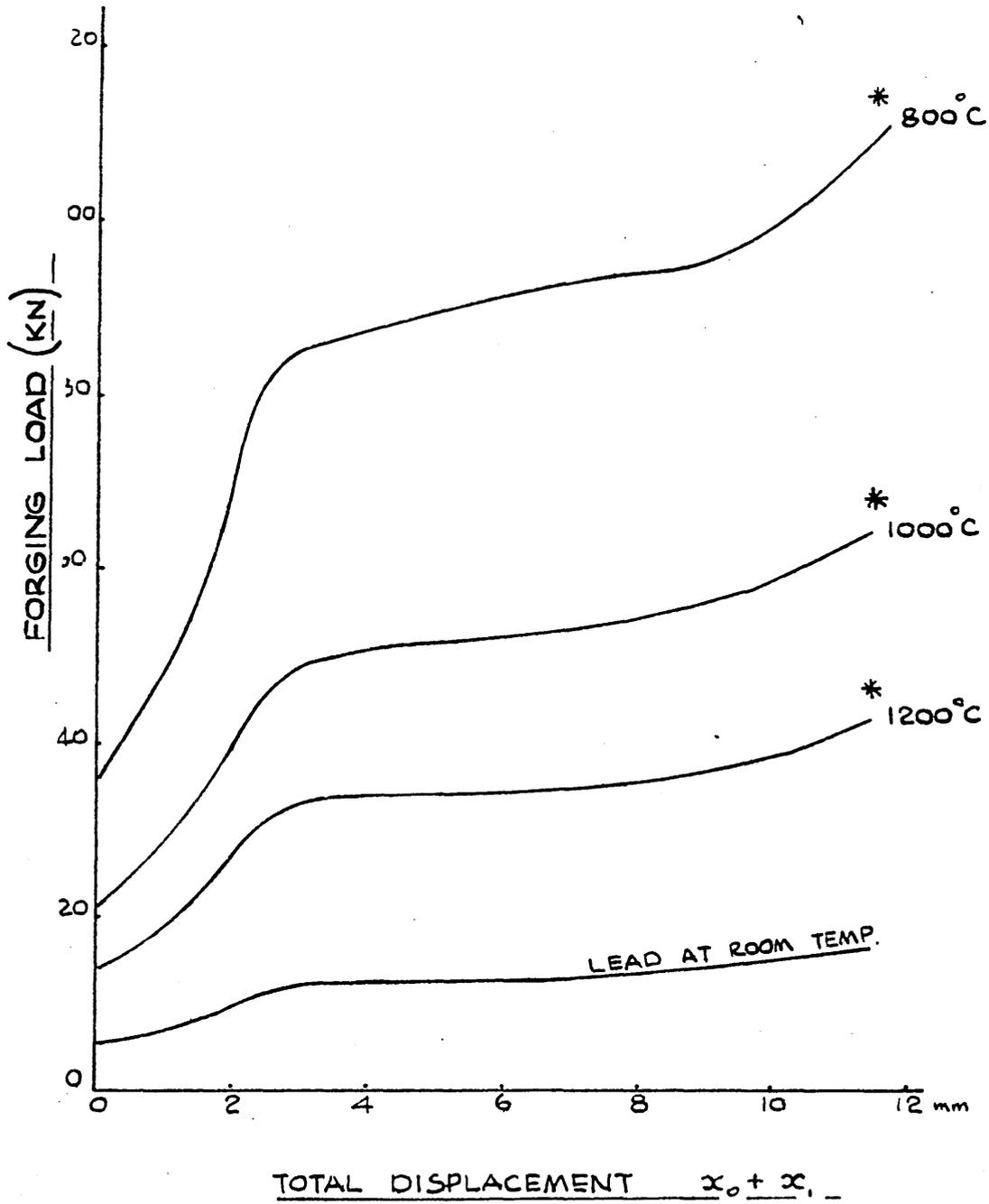
* 0.08 % CARBON STEEL
       10

FORGING LOAD v. TOTAL DISPLACEMENT

FIG. 93

176

THEORETICAL CURVES

BOSS DIA = 16mm $L_0 = 24$ mm

* 0.08% CARBON STEEL

* 800°C

* 1000°C

* 1200°C

LEAD AT ROOM TEMP.

FORGING LOAD $\left(\underline{KN}\right)$ —

TOTAL DISPLACEMENT $x_0 + x_1$

FORGING LOAD v. TOTAL DISPLACEMENT

FIG. 94

177

THEORETICAL CURVES

BOSS DIA = 18 mm L_o = 24 mm

* 0.08 % CARBON STEEL

FORGING LOAD v. TOTAL DISPLACEMENT

FIG. 95

178

THEORETICAL CURVES

BOSS DIA = 20mm L_o = 24 mm.

*0.08 %/10 CARBON STEEL

TOTAL DISPLACEMENT $x_o + x_1$

FORGING LOAD v. TOTAL DISPLACEMENT

FIG. 96   179.

THEORETICAL / EXPERIMENTAL CURVES

BOSS DIA = 9mm   Y = 17 N/mm²

THEORETICAL CURVE

X EXPERIMENTAL
RESULTS
STATIC LUBRICATED.

TOTAL ENERGY ABSORBED $\left(\frac{N_m}{}\right)$ —

TOTAL DISPLACEMENT $x_0 + x_1$
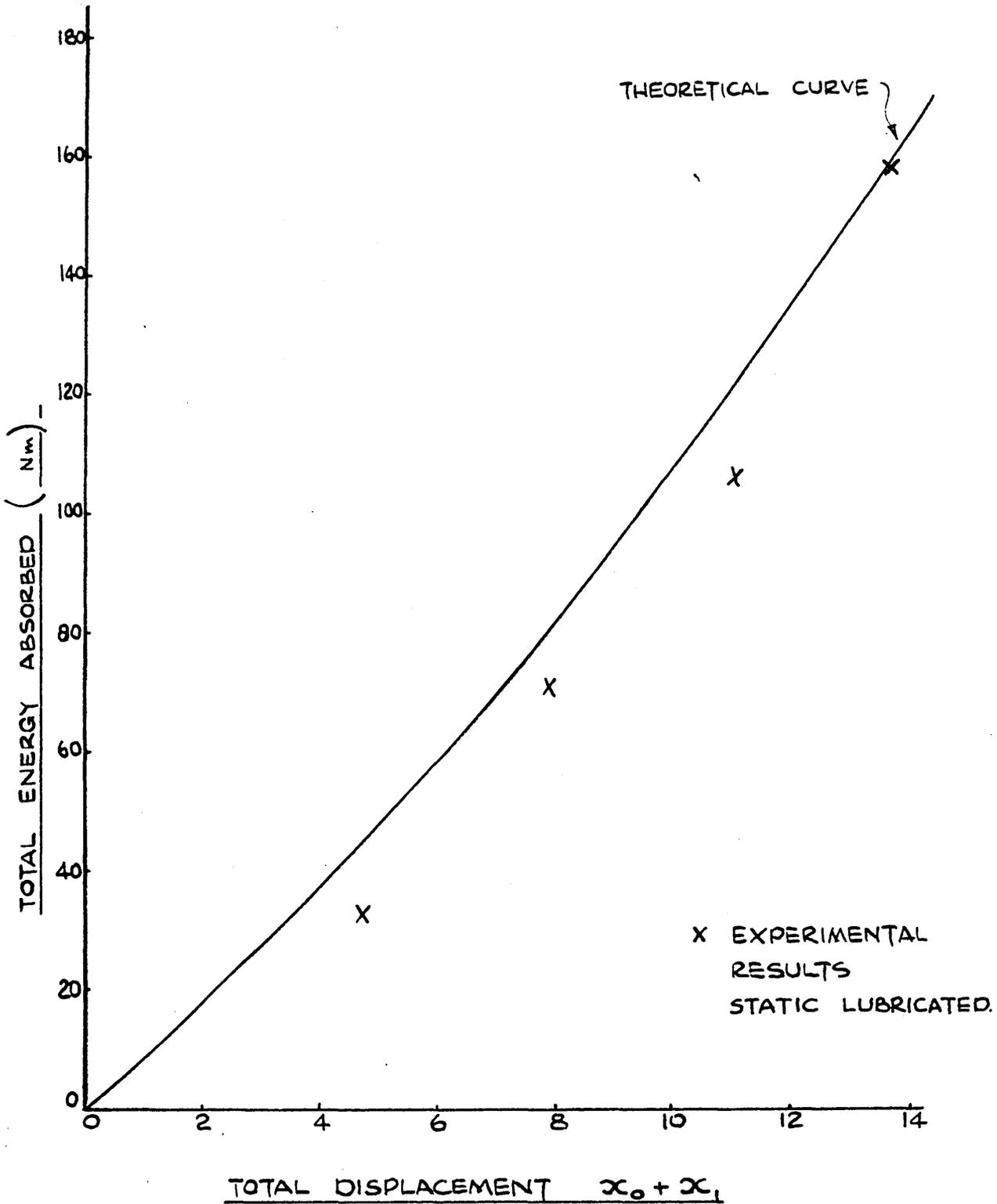
TOTAL ENERGY ABSORBED v. TOTAL DISPLACEMENT.

FIG. 97.   180

THEORETICAL / EXPERIMENTAL CURVES

BOSS DIA. = 12 mm $Y = 17 \underline{N}/mm^2$.

THEORETICAL CURVE

X   EXPERIMENTAL
    RESULTS.
    STATIC LUBRICATED.

TOTAL DISPLACEMENT $x_0 + x_1$

TOTAL ENERGY ABSORBED v. TOTAL DISPLACEMENT.

FIG. 98.   181

THEORETICAL / EXPERIMENTAL CURVES

BOSS DIA = 18 mm $Y = 17 \, N/mm^2$

THEORETICAL CURVE

X EXPERIMENTAL
RESULTS.
STATIC LUBRICATED.

TOTAL DISPLACEMENT $x_0 + x_1$.

TOTAL ENERGY ABSORBED v. TOTAL DISPLACEMENT.

FIG.99   182

THEORETICAL/EXPERIMENTAL CURVES

BOSS DIA = 9mm $Y = 17 \, N/mm^2$

TOTAL ENERGY ABSORBED v. TOTAL DISPLACEMENT.

FIG. 100   183

THEORETICAL / EXPERIMENTAL CURVES

BOSS DIA.= 12 mm $Y = 17 \, N/mm^2$

Legend:

EXPERIMENTAL RESULTS (DROP HAMMER) — X

EXPERIMENTAL RESULTS (QUASI-STATIC) — ●

THEORETICAL RESULTS (STATIC)

THEORETICAL RESULTS (DYNAMIC)

Y-axis: TOTAL ENERGY ABSORBED (Nm)

X-axis: TOTAL DISPLACEMENT $x_0 + x_1$

TOTAL ENERGY ABSORBED v. TOTAL DISPLACEMENT.

FIG. 101

184

THEORETICAL / EXPERIMENTAL CURVES

BOSS DIA = 18 mm $Y = 17 \ N/mm^2$

EXPERIMENTAL RESULTS
(DROP HAMMER) ——— — ·· — ·· —×—

EXPERIMENTAL RESULTS
(QUASI-STATIC) -------●------

THEORETICAL RESULTS ——— (STATIC)

THEORETICAL RESULTS ——— · ——— (DYNAMIC)

TOTAL DISPLACEMENT $x_0 + x_1$

TOTAL ENERGY ABSORBED v. TOTAL DISPLACEMENT.

FIG. 102   185
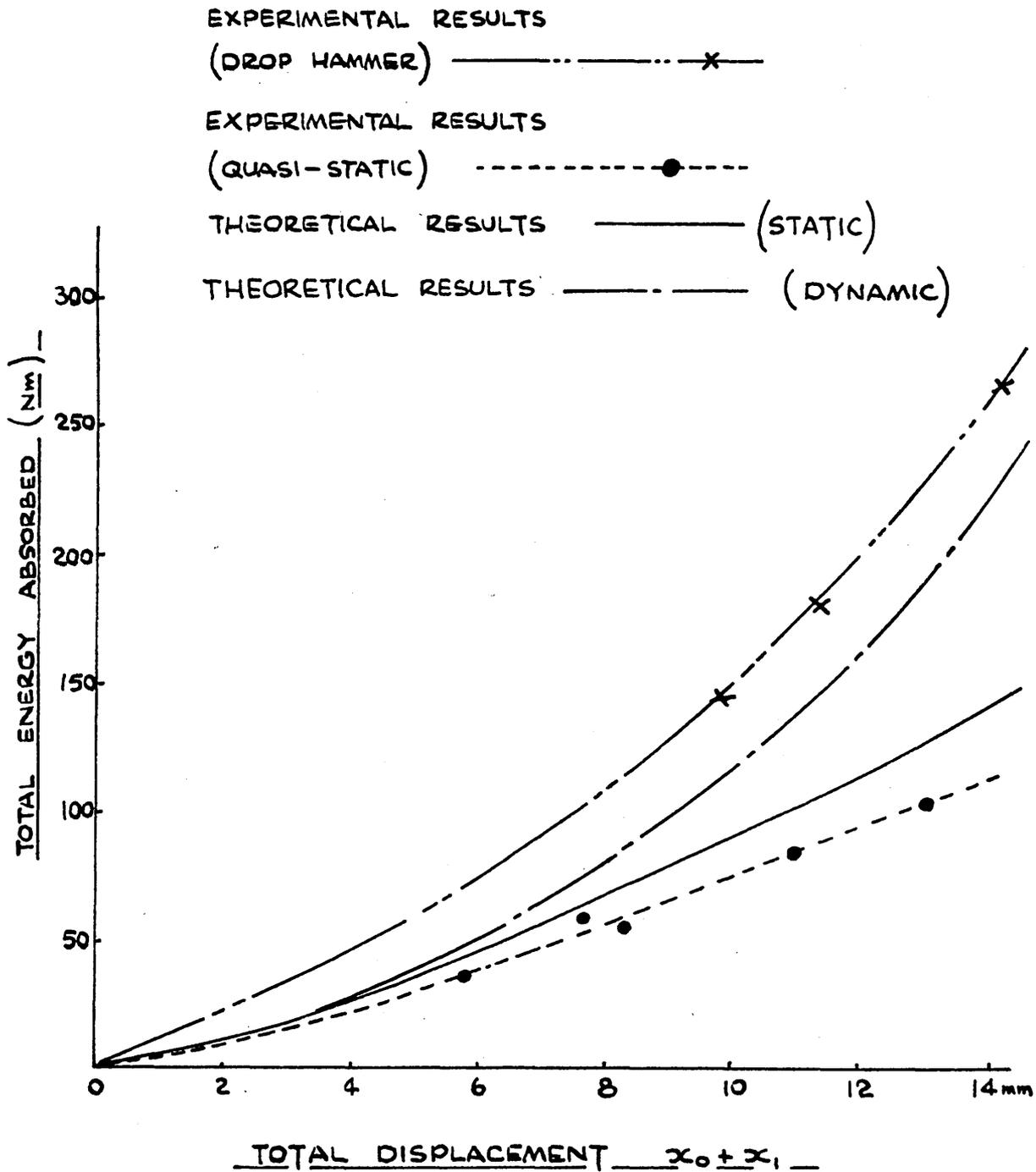
DISPLACEMENT MODE   COPPER BILLETS

FIG. 103.

DOUBLE ENDED EXTRUSION $D_c = 18mm$ $L_o = 24mm$ $Y = 17 \frac{N}{mm^2}$

THEORY BASED ON TEST PIECE $L_o = 12mm$
(SINGLE ENDED EXTRUSION)

ENERGY v. DISPLACEMENT

FIG. 104.

DOUBLE ENDED EXTRUSION $D_c = 18$ $L_0 = 24\,mm$ $Y = 17\,N/mm^2$

THEORY BASED ON TEST PIECE $L_0 = 12\,mm$
(SINGLE ENDED EXTRUSION)

THEORY ———————

EXPERIMENTAL STATIC LUBRICATED. △
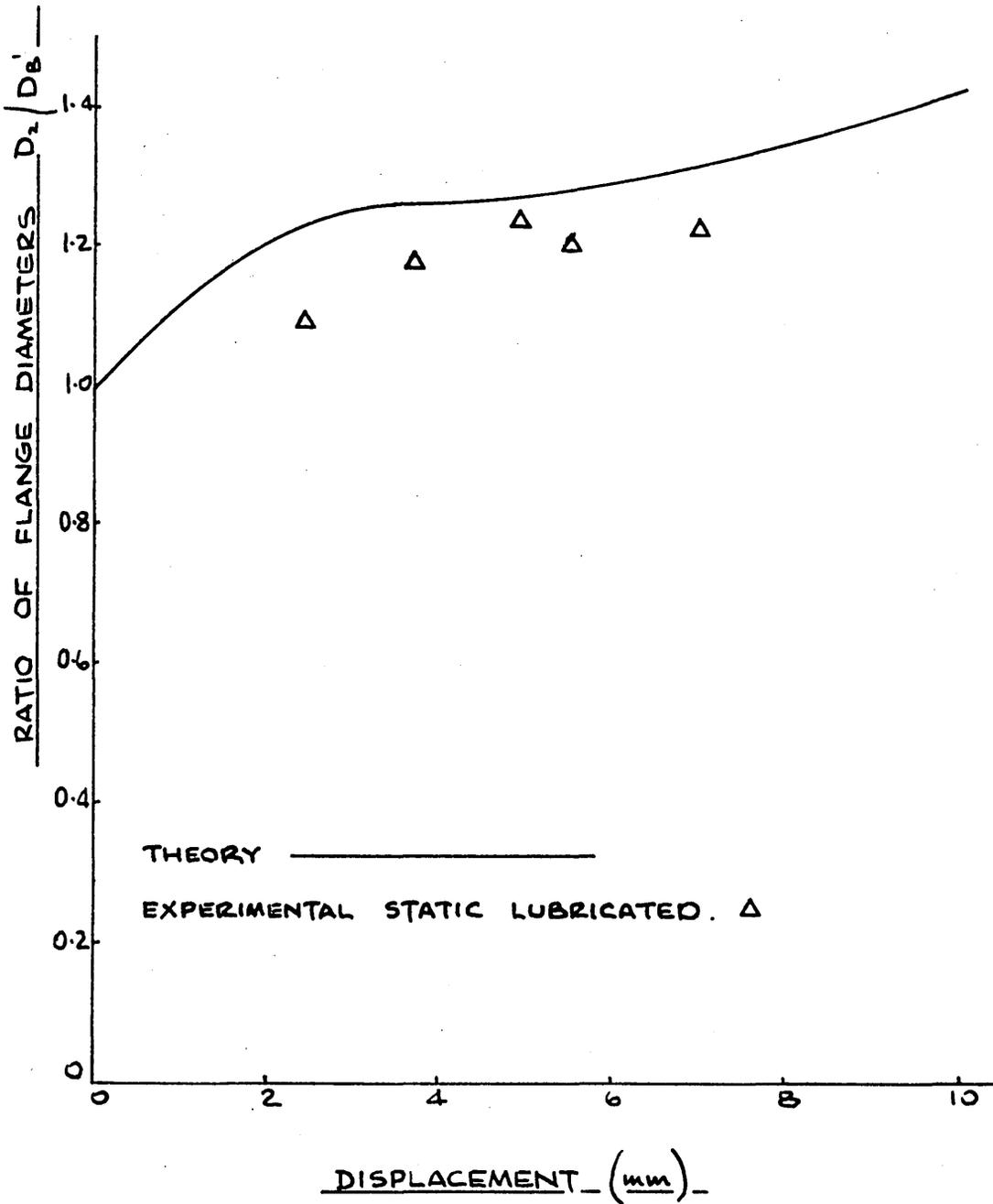
RATIO OF FLANGE DIAMETERS v. TOTAL DISPLACEMENT.

FIG. 105.   188

DOUBLE ENDED EXTRUSION $D_c = 18mm$ $L_o = 2+mm$ $Y = 17 N/mm^2$

THEORY BASED ON TEST PIECE $L_o = 12mm$
(SINGLE ENDED EXTRUSION)
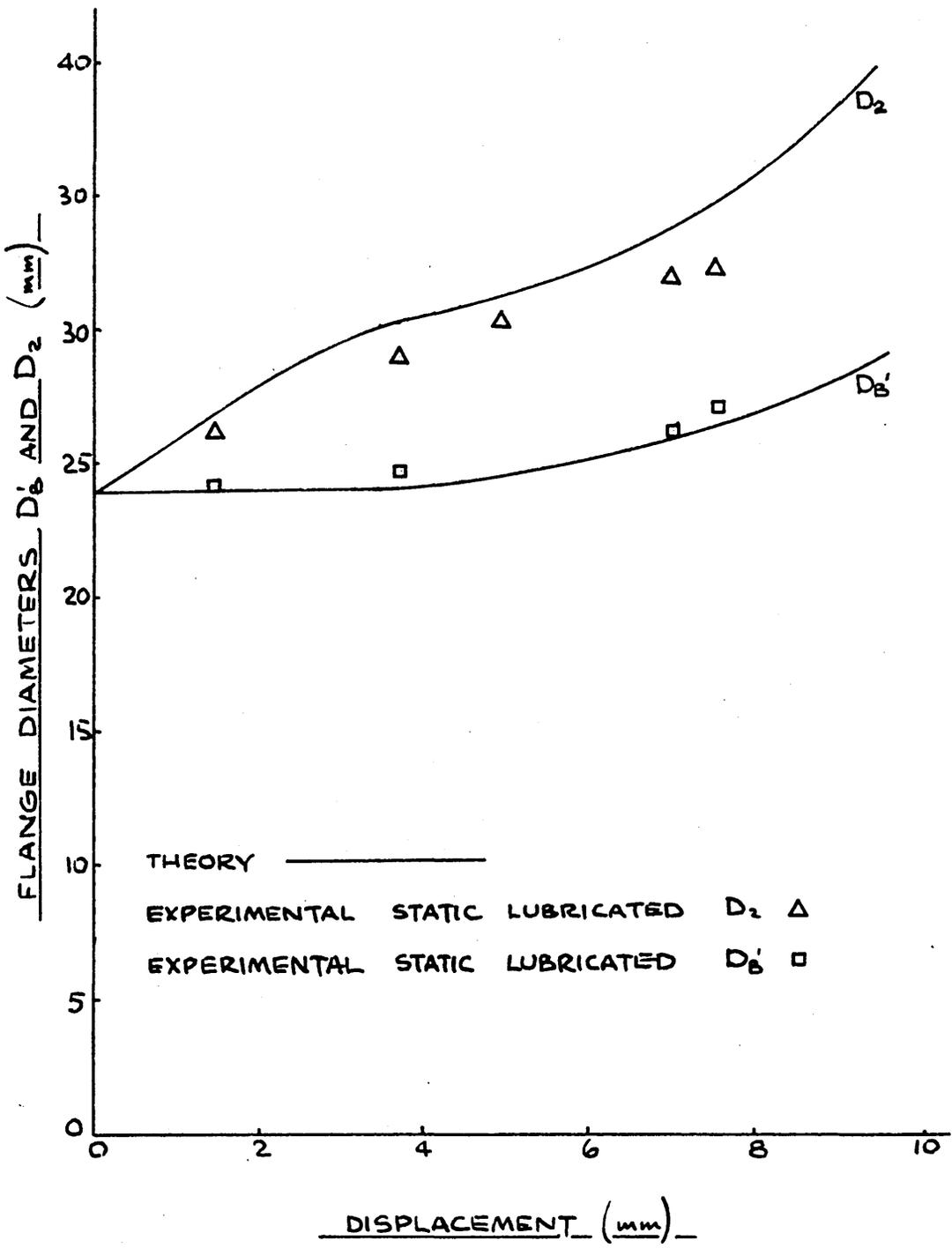
FLANGE DIAMETERS v. DISPLACEMENT.

FIG. 106.   189

DISPLACEMENT MODE DOUBLE ENDED EXTRUSION

FIG. 107.

DISPLACEMENT MODE   DOUBLE ENDED EXTRUSION
ALUMINIUM COPPER AND LEAD.

FIG. 108.

DOUBLE ENDED EXTRUSION. UNEVEN PROFILE
SHOWN IN LEAD AND ALUMINIUM BILLETS.

FIG. 109.

THEORETICAL AND EXPERIMENTAL RESULTS

$m = 1.0$ $L_o = 24 mm$

EXPERIMENTAL RESULTS
△ $D_c = 18 mm.$
□ $D_c = 12 mm.$

A	$D_c = 21 mm$
B	$D_c = 18$ "
C	$D_c = 15$ -
D	$D_c = 12$ -

PERCENTAGE TOTAL HEIGHT.

PERCENTAGE DEFORMATION

PERCENTAGE TOTAL HEIGHT v PERCENTAGE DEFORMATION

FIG 110

193
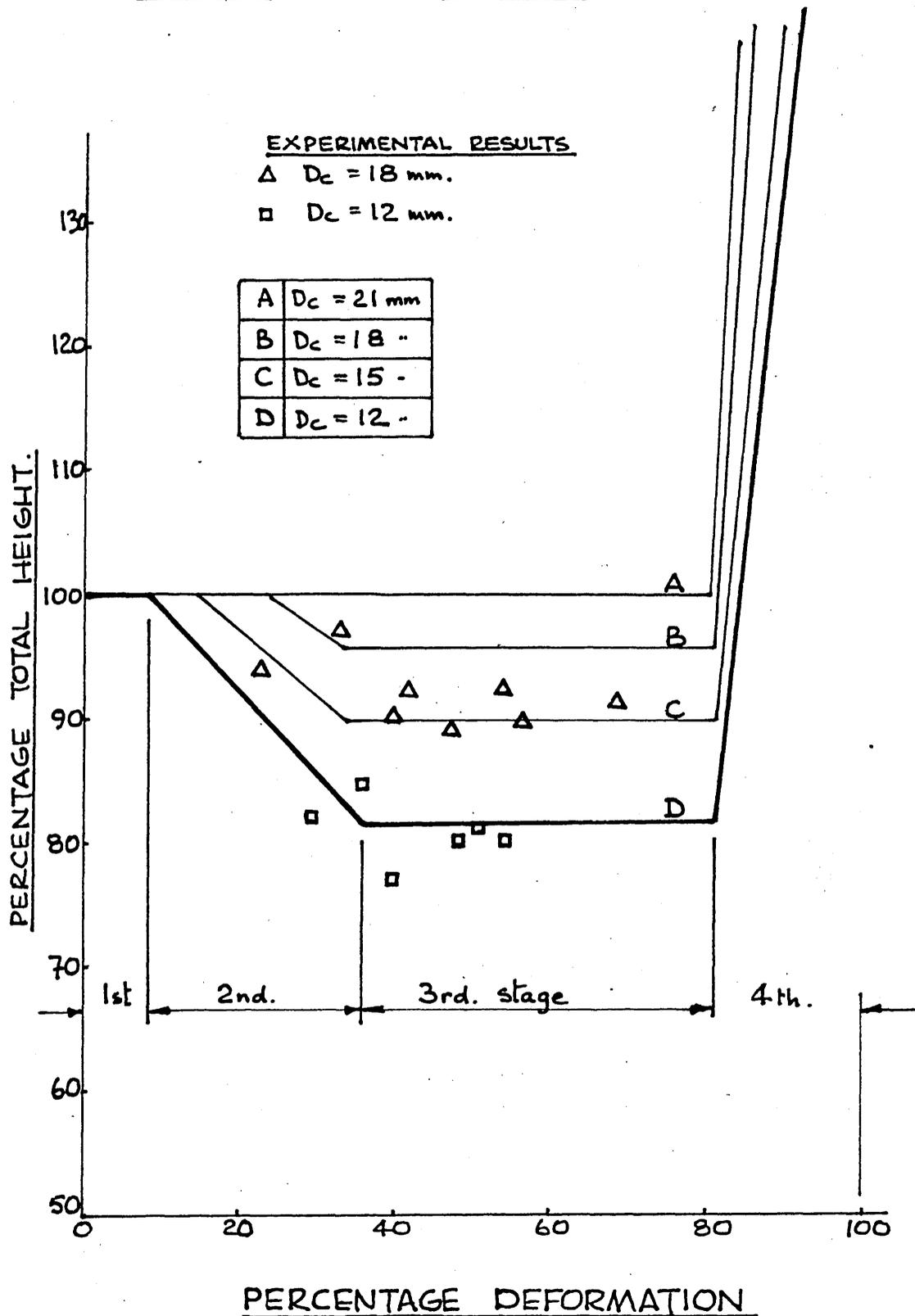
THEORETICAL RESULTS

m = 0.5 L_o = 24 mm

PERCENTAGE TOTAL HEIGHT v. PERCENTAGE DEFORMATION.

FIG.111

194
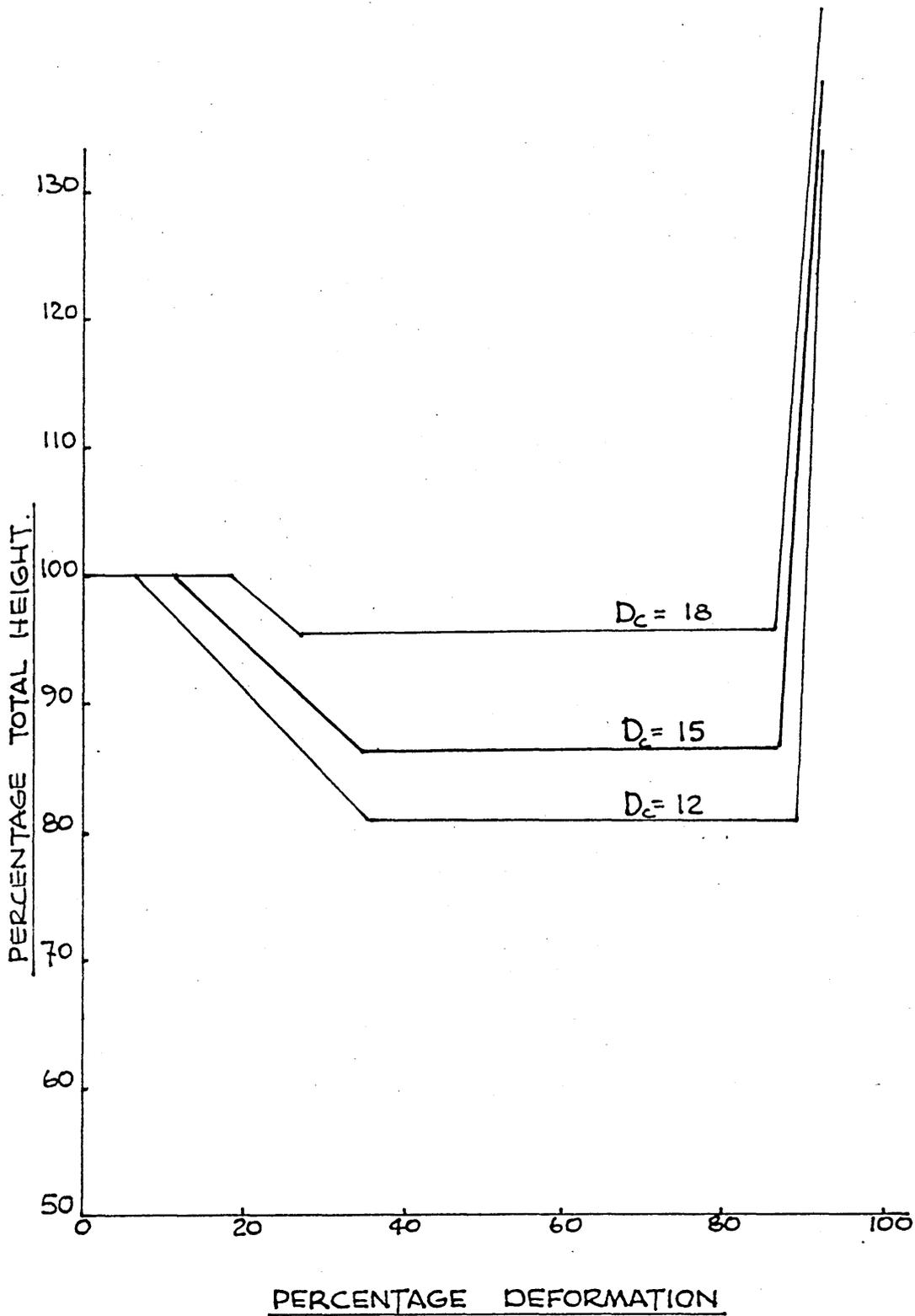
THEORETICAL AND EXPERIMENTAL RESULTS.

$D_c = 12 \, mm$ $L_o = 24 \, mm$
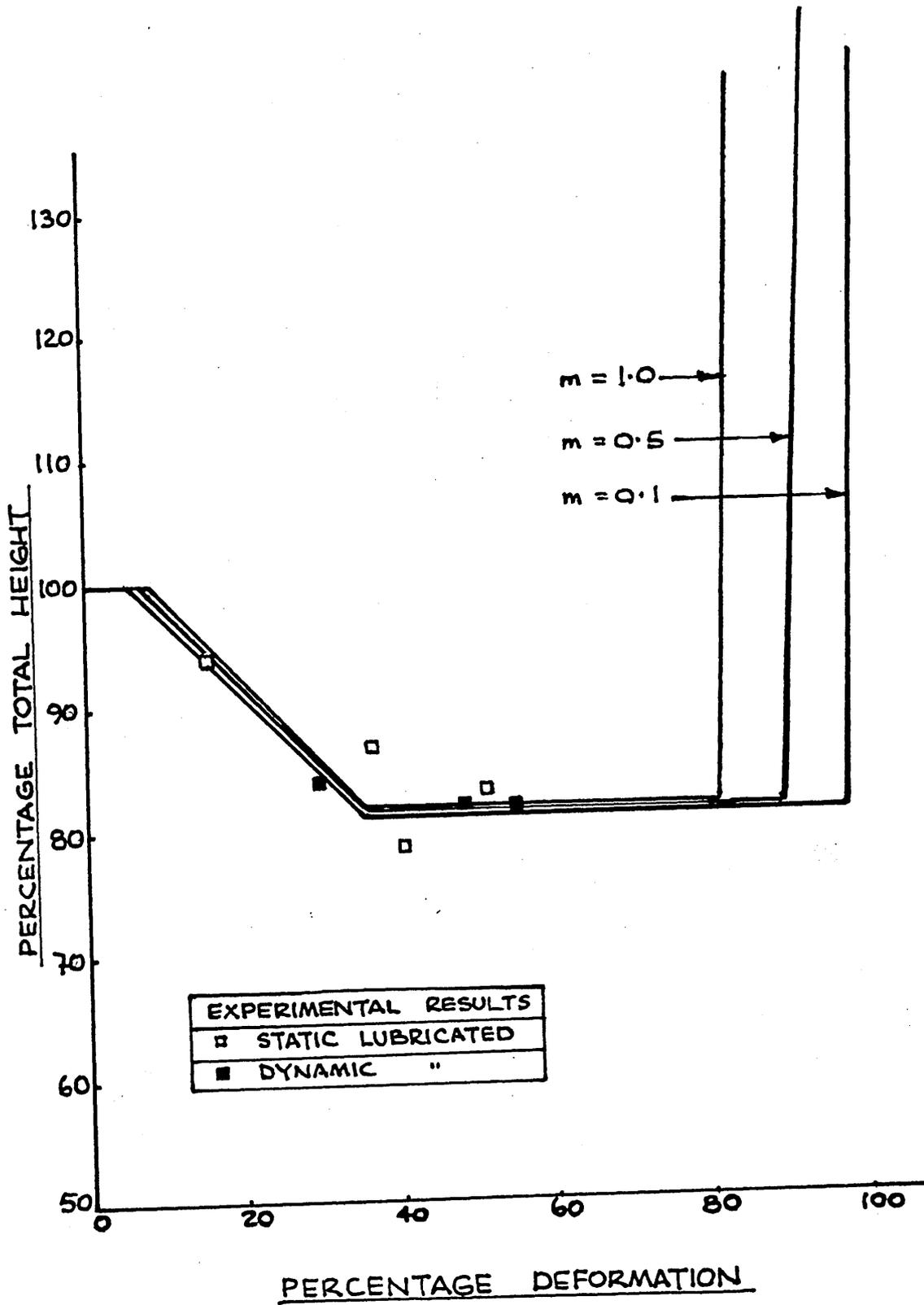
PERCENTAGE TOTAL HEIGHT v PERCENTAGE DEFORMATION

FIG 112

195

THEORETICAL AND EXPERIMENTAL RESULTS

$D_c = 12\,mm$ $L_0 = 24\,mm$
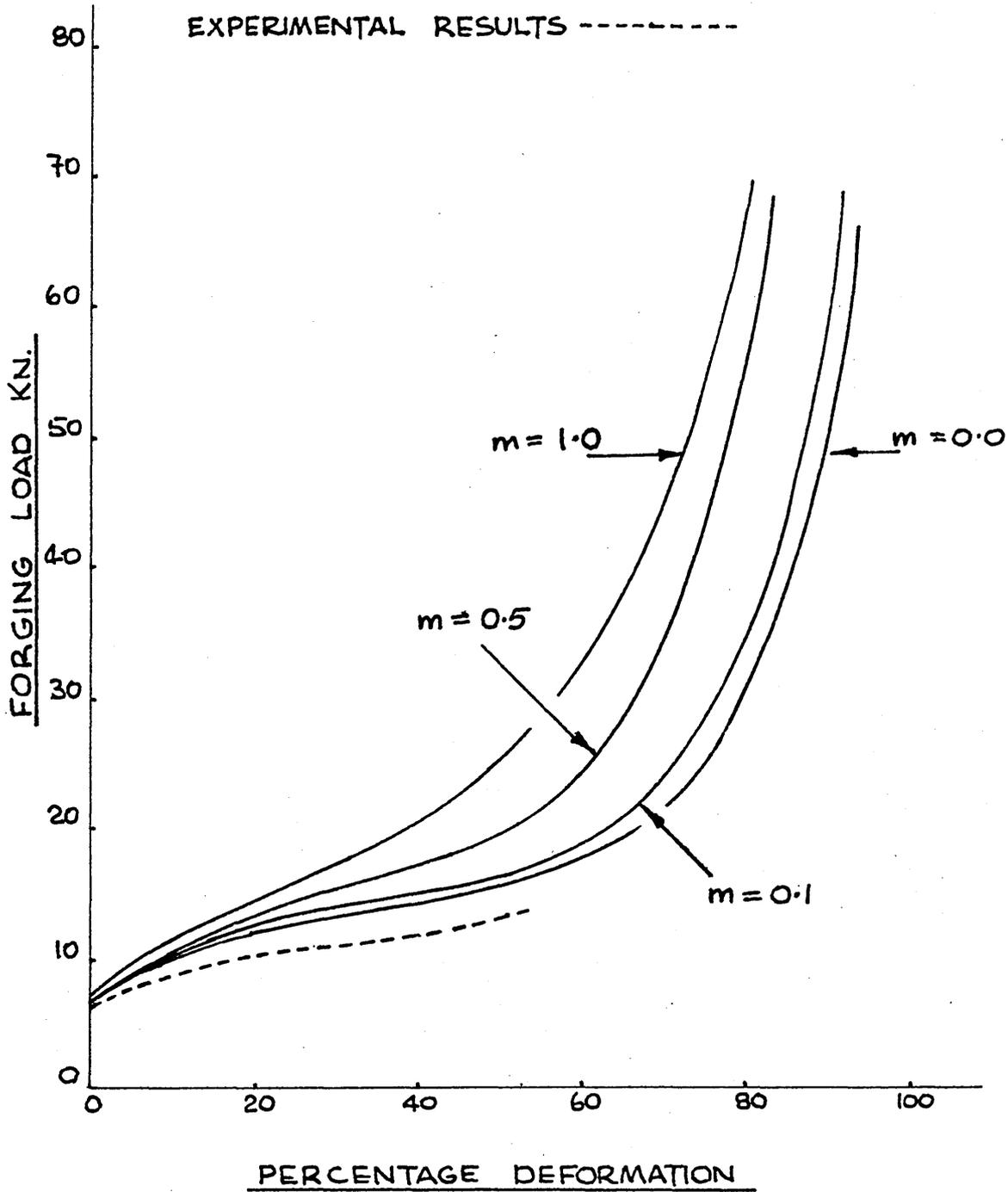
FORGING LOAD v. PERCENTAGE DEFORMATION

FIG 113.

196

CHAPTER 7

CONCLUSIONS AND SUGGESTIONS FOR FURTHER WORK

197

7.1 Conclusions

The laboratory drop hammer proved to be an effective means of providing variable impact velocities required for dynamic extrusion forging.

Despite the short forging impact time, less than 10 msec, there was no difficulty in storing, digitally, load/time and displacement time data for later analysis.

When the deformation mode of the billet was not obscured by dies the high speed camera proved very useful for recording the change in shape of the billet.

Lead is an ideal material for simulating the hot-working of steel the one drawback being the difficulty of preparing 'deformed' test pieces so that their grain flow can be observed.

For both simple upsetting and closed die forging, inclusion of the strain rate sensitivity effect in the analysis (numerical technique) greatly improved the accuracy in predicting the load, energy requirements and deformation profiles.

In extrusion forging the deformation profile of the billet is very much influenced by the billet to boss diameter ratios as well as the length of the billet.

The boss height obtainable for a given billet diameter is dependent on the diameter of the boss.

The theory developed provides a useful tool for

predicting the deformation profile of extrusion forged specimens with reasonable accuracy, formed under both dynamic and static conditions. This is one of the most important aspects of the present work which the works of references (61) and (62) did not deal with at all. The forging load predictions agree closely with those obtained from the static tests and also with those obtained from dynamic tests when modified flow properties of the material are incorporated in the theory.

The deformation profile of the billet under extrusion forging conditions appears to be independent of material property, especially the tapering effect, until the fourth stage commences.

7.1.1 The Effect of Friction

It has been seen that the radial flow of metal within a die cavity will be restrained by friction. The extent to which this will occur will depend upon the type of lubricant used and the surface finish of the die. Also, as the metal flow resembles that of a liquid rather than a solid, the influence of friction is more when the metal is flowing through a thin section than through a thick section. The flow situation is further complicated by the fact that the channel through which the metal has to flow is constantly changing due to the relative movement of the dies. From the tests conducted friction was found to modify the shape of the deformed billet

and to increase the energy required for unit
displacement.

With the extrusion forging of axisymmetrical shapes
friction can have a considerable effect on the amount
of metal actually extruded, particularly when large
percentage displacements occur; the higher the
coefficient of friction, the earlier the fourth
deformation mode will occur.

7.1.2   The Effect of Strain Rate

If the material being formed is a rigid-perfectly
plastic and non rate sensitive material then the
rate at which it is deformed will not affect the
forces involved, apart from the material inertia
effect. But many materials are rate sensitive
in that the faster they are deformed the greater the
force required to produce the deformation. This has
been clearly demonstrated in the drop hammer tests
where the high initial strain rates, 400 sec^{-1} maximum,
can double the forces that would be required for
quasi-static tests.

7.2   Suggestions for Further Work

7.2.1   The Equipment

Providing bolt-on sections to increase the mass of
the tup would widen the range of tests and would
provide more energy capacity.

The die cavity could be modified to include different draft angles and corner radii.

7.2.2 Experimental Work

It would be useful to undertake another series of tests to examine further the existing analysis. Possible tests are: Dynamic and quasi-static tests on billets of different materials and different lengths at room temperature:

(a) single ended extrusion forging to include deformation under fourth mode,

(b) double ended extrusion forging with identical and unequal boss diameters.

Similar tests with steel at hot forging temperatures, would provide useful data to compare with the existing analysis.

7.2.3 The Analysis

Modification of the existing analysis to include the effect of material inertia and strain rate should greatly improve the correlation between theoretical and experimental results. This applies particularly to the dynamic tests on strain-rate sensitive materials. The existing analysis can be used for 'double ended' extrusion of cylindrical billets, where the boss diameters are identical. A further modification to embrace boss diameters of unequal size would widen the application of the analysis.

REFERENCES

1. T.A. SCHEY 'Principles of forging design IITR1 review
    for the American Iron and Steel Inst.

2. A. GELEJI 'Forge equipment, rolling mills and access-
    ories' Akademiai Kiado, Budapest 1967

3. T. ALTAN and R.J. FIORENTINO 'Prediction of loads and
    stresses in closed-die forging J of Eng for Industry
    May 1971

4. Technical handbook on forging and drop forging
    M.V. Storozhev, Moscow 1959

5. L.G. DRABING 'Forging production seminar' Published
    by Alfred Herbert Limited, Coventry 1966

6. S.A. BALOGUN 'Die loads and stresses in press
    forging' PhD thesis University of Aston Birmingham 1971

7. F. NEUBERGER and S. PANNASCH 'Werkstoffverbrauch beim
    Gesenkschmieden von Stahl' Fertigungstechnik und
    Betrieb Vol 12 1962

8. 'Counterblow hammers - type EK-A' Trade publication
    by Technsinpex Hungary

9. F. NEUBERGER et alia 'Prediction of energy consumption
    in drop forging' Fertigungstechnik und Betrieb Part 1
    January 1960

10. H. MAKELT 'Ermittlung des Kraft - und Arbeitsbedarfs fur
    das Stauchen und Gesenkschmieden' Werkstatt und Betrieb
    Part 6 1958

11. DROP FORGING RESEARCH ASSOCIATION MEMTRB CONTRACT
    KA/72C/327/CB/A72C Annex No 2 LOAD AND ENERGY
    ESTIMATION IN FORGING Final Report

12. E. SIEBEL 'The Plastic forming of metals' Steel
    Oct 16 1933 to May 7 1934

13. W. SCHROEDER and D.A. WEBSTER 'Press forging thin
    sections: effect of friction, area and thickness on
    pressure required' J App Mechanics September 1949

14. J. FOSTER 'The high speed mechanical forging press'
    Metal Treatment and Drop Forging December 1963.

15. T.A. DEAN 'The mechanics of flash in drop forging -
    temperature and speed effects'

16. R.L. DIETRICH and G. ANSEL 'Calculation of press
    forging pressures and application to magnesium forgings'
    Trans ASM vol 38 1947

17. S.K. BISWAS and B.W. ROOKS 'Application of a modular
    approach to estimate load and energy in closed die
    forging' Proc 15th MTDR Conference, Birmingham,
    September 1974

18. T. ALTAN et alia 'The use of analytical methods in
    predicting load and stresses in closed die forging'. A
    study of themechanics of closed die forging, First
    report Battelle Mem Inst 1969

19. R.P. McDERMOTT 'An Introduction to the upper bound
    elemental technique (UBET) as applied to axisymmetric
    forgings' PhD Thesis Leeds Univ 1974

20. J.D. LUBAHN J. Appl. Physics, 1949, 14, 229

21. H.I. FUSFELD J. Appl. Physics, 1949, 20, 1052

22. H.R. LOW, Jr, and F. GAROFALO, Proc. Soc. Exper.
     Stress Analysis, 1947, 4, (2), 16.

23. J.E. DORN, P. PIETROKOWSKY, and T.E. TIETZ, Trans.
     Amer. Inst. Min. Met. Eng., 1950, 188, 933.

24. J.F. ALDER and V.A. PHILLIPS 'The Effect of strain rate
     and temperature on the resistance of Aluminium, Copper
     and Steel to compression', J. Inst Metals 1954, 83, 80.

25. H. KUDO 'An upper bound approach to plane strain forging
     and extrusion', Int. J. Mech Science Vol 1, 1960

26. P. LUDWIK "Elemente der technologischen Mechanik" 1909:
     Berlin (Springer)

27. L.D. SOKOLOV, Doklady Akad. Nauk S.S.S.R., 1949, 67, 459

28. L.D. SOKOLOV, ibid, 1947, 17, 543

29. L.D. SOKOLOV, ibid, 1948, 18, 93

30. L.D. SOKOLOV, Doklady Akad, Nauk S.S.S.R., 1949, 67, 459

31. L.D. SOKOLOV, ibid, 1950, 70, 839

32. F. SEITZ, A.W. LAWSON and P. MILLER, O.S.R.D. Rep, 1942,
     (495)(NDRC A41)

33. F. SEITZ, A.W. LAWSON and P. MILLER, ibid, 1942 (619)
     (NDRC A63)

34. F. SEITZ, ibid, 1942 (1388)(NDRC A174)

35. O.C. SIMPSON, E.L. FIREMAN and J.S. KOEHLER, ibid, 1944 (3330)(NDRC A257)

36. G.H. WINSLOW and W.H. BESSEY, ibid, 1945 (5039)(NRDC A324)

37. D.W. GINNS, J. Inst. Metals, 1937, 61, 61.

38. C.F. ELAM, Proc. Roy. Soc., 1938 [A], 165, 568.

39. P.G. JONES and H.F. MOORE, Proc. Amer. Soc. Test. Mat., 1940, 40, 610

40. R.A.C. SLATER, W. JOHNSON and S.Y. AKU Experiments in the fast upsetting of short pure lead cylinders and a tentative analysis Int. J. Mech. Sci 1968 Int. J. Mech. Sci 10, 143

41. P.M. COOK True stress-strain curves for steel compression at high temperature and strain rates. 1957 Proc. Conf. Prop at high rates of strain, Inst. Mech. Engrs. Paper 2.

42. L.E. MALVERN Experimental studies of strain rate effects and plastic wave propagation in annealed aluminium. Proc. ASME Coll on Behaviour of materials under dynamic loading 1965 p.81.

43. S.K. SAMANTA Resistance to dynamic compression of low carbon steel and alloy steels at elevated temperatures and at high strain rates. 1968 Int. of J. Mech. Sci, 10, 613

44. H. SUZUKI, et al Studies on the flow stress of metals and alloys, Report Institute of Industrial Sciences, Univ. of Tokyo, 1968, Vol 18, No 3

45. S.K. SAMANTA On relating the flow stress of aluminium and copper to strain, strain rate and temperature 1969 Int. J. Mech. Sci, 11, 433

46. S.K. SAMANTA The dynamic compression testing of steel at elevated temperatures. 1970, Proc 11th Int MTDR Conf p.827

47. C.E.N. STURGESS and A.N. BRAMLEY The use of impact-forming device to obtain dynamic stress-strain data. Proc. 11th Int MTDR Conf p.803

48. B. LENGYEL and M MOHITPUR Dynamic stress-strain data to large strains 1972 J. Inst. Metals p 100

49. M. MOHITPUR and B. LENGYEL A method of obtaining iso-thermal, constant high strain rate stress-strain data, Proc 16th Int MTDR 1975 MTDR Conf p 503

50. G.L. BARAYA, W. JOHNSON and R.A.C. SLATER The dynamic compression of circular cylinders of super-pure aluminium at elevated temperatures 1965 Int. J. Mech. Sci. 7, 621

51. S.C. JAIN and A.N. BRAMLEY Speed and frictional effects in hot forging 1968, Proc. Instn. of Mech Engrs, Vol 182, 78

52. T.A. DEAN The influence of billet inertia and die friction in forging processes - A simple energy approach. 1970, 11th Int. MTDR Conf. p.761

53. R.P. McDERMOTT and A.N. BRAMLEY An elemental upper-bound technique for general use in forging analysis. 1974 Proc. 15th Int. MTDR Conf, p 437.

54. T.A. DEAN The mechanics of flash in drop forging - temperature and speed effect. 1976 Proc. Inst. Mech. Engrs. Vol 190-33/76 p.457.

206

55. M.S.J. HASHMI and F.B. KLEMZ The effect of friction
    in simple upsetting of cylindrical billets of elastic-
    plastic and elastic-strain hardening material: A
    numerical technique 1976 Proc 17th Int MTDR Conf
    p 597

56. F.B. KLEMZ and M.S.J. HASHMI Simple upsetting of
    cylindrical billets: Experimental investigation and
    theoretical prediction 1977 Proc 18th Int MTDR Conf
    p 323

57. M.S.J. HASHMI A numerical technique for analysing simple
    upsetting of cylindrical billets of strain rate
    sensitive material. 1977 Proc 18th Int MTDR Conf p 27

58. M.S.J. HASHMI and F.B. KLEMZ Closed die forging of
    axisymmetric shapes from cylindrical billets of strain
    hardening and strain rate sensitive material:
    Experimental results and theoretical predictions
    1978 Proc 19th Int MTDR Conf p 61

59. J. DANCKERT and T. WANHEIM Model-Material Technique
    Applied in the Analysis of the Forging of a Specimen
    of Complicated Shape 1977 Scandinavian Journal of
    Metallurgy 6 185-190

60. A.T. MALE and M.G. COCKROFT (1964) A method for
    determination of the coefficient of friction of metals
    under conditions of bulk plastic deformation. J. Inst.
    of Metals Vol 93 p 38

61. S.C. JAIN, A.N. BRAMLEY, C.H. LEE and SHIRO KOBYASHI.
    Theory and Experiment in Extrusion Forging. Proc. 11th
    Int MTDR Conf 1970 p 1097

62. J.A. NEWNHAM and G.W. ROWE. An analysis of Compound
    Flow of Metal in a simple extrusion/forging process

63. W. JOHNSON Extrusion through square dies of large
    reduction. J. Mech. Phys. Solids 4, 191, 1955

APPENDIX 1

QUASI-STATIC COMPRESSION OF A SHORT CYLINDER OF PERFECTLY PLASTIC MATERIAL

If a short circular cylinder of rigid-perfectly plastic material whose height to radius ratio, h/a is less than 3, is compressed between rigid parallel dies at a speed less than 150 m/s then all inertia and wave effects can be neglected.

Let the coefficient of friction between the flat end faces of the cylinders and the dies be μ.

Let the three normal stresses be σ_r, σ_θ and σ_z and assume that they are independent of z and that they are principal stresses.

The equation of equilibrium for an element of the cylinder see Fig. 114, is

$$\frac{\sigma_r - \sigma_\theta}{r} + \frac{\partial \sigma_r}{\partial r} = - \frac{2\mu\sigma_z}{h} \qquad (1)$$

If volume constancy is assumed then it can be shown that $d\varepsilon_\theta = d\varepsilon_r$, and since the elastic components of strain are negligible by comparison with plastic components then through the Levy-Mises equation, $\sigma_\varepsilon = \sigma_r$ then (1) becomes:

$$\frac{d\sigma_r}{dr} = - \frac{2\mu\sigma_z}{h} \qquad (2)$$

Using Tresca's yield criterion, where σ_r, $\sigma_\theta > \sigma_z$, then
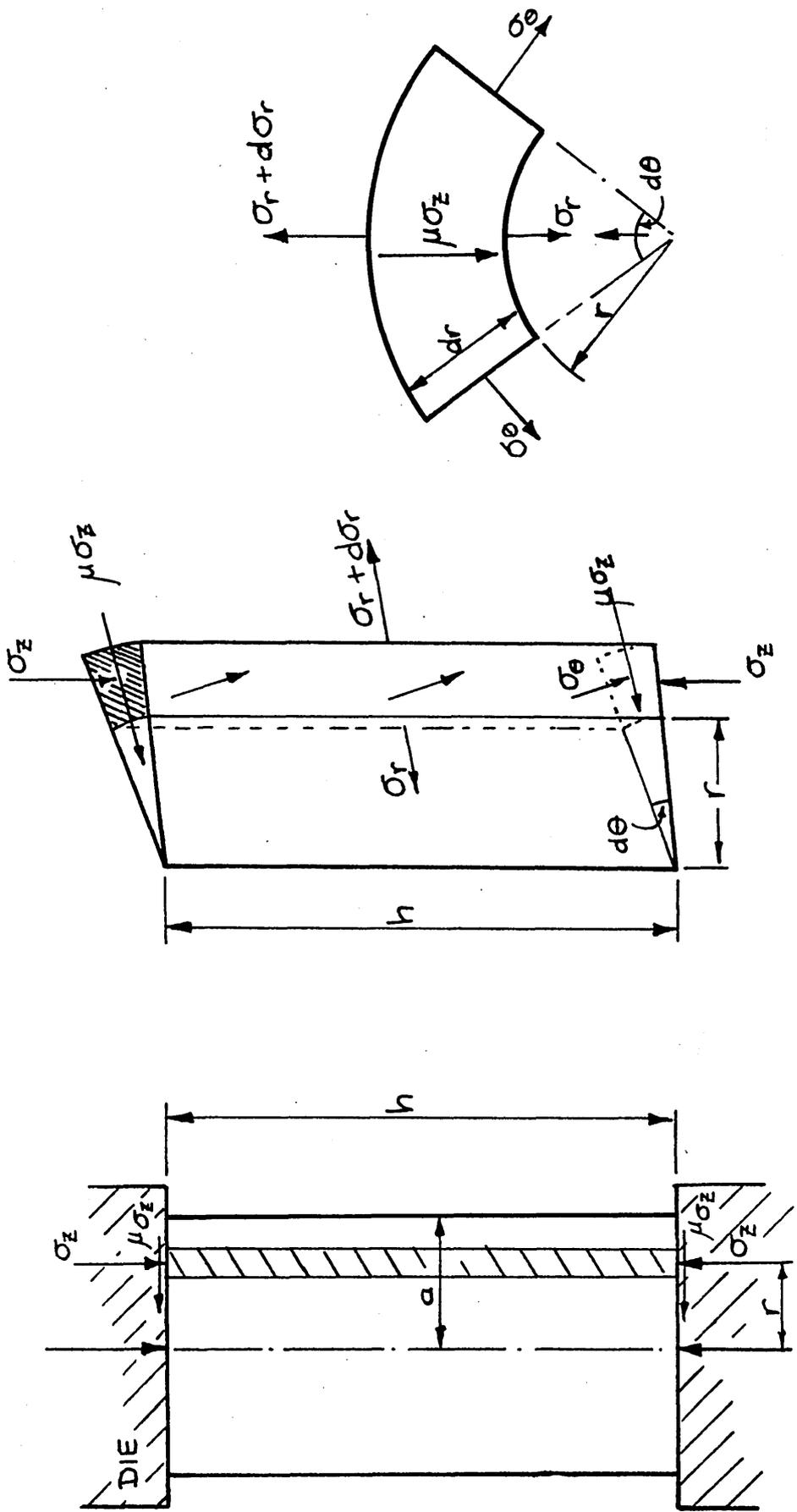
SMALL ELEMENT

FIG.114   QUASI-STATIC COMPRESSION OF A SHORT CYLINDER OF PERFECTLY PLASTIC MATERIAL

A1·2

$(\sigma_r - \sigma_z) = Y$ or $d\sigma_r = d\sigma_z$, where Y is the uniaxial yield stress of the material. Substituting for $d\sigma_r$ in (2) and integrating

$$\ln\sigma_z = -\frac{2\mu}{h}r + C \quad \text{------------------------------ (3)}$$

at $r = a$, $\sigma_r = 0$ and $\sigma_z = -Y$
equation (3) becomes

$$-\sigma_z = Y\exp[2\mu(a - r)/h]$$

replacing $-\sigma_z$ by p

$$p = Y\exp[2\mu(a - r)/h]$$

and since μ is small

$$p \cong Y[1 + \frac{2\mu(a - r)}{h}] \quad \text{------------------------ (4)}$$

A1·3

FAST COMPRESSION OF A SHORT CYLINDER

To assess the influence of speed in simple compression consider the case of the frictionless compression of a short circular cylinder by an upper die moving at constant speed v, the lower die being at rest.

Fig. 115 shows an upper die descending with speed v; u_r and f_r denote radial speed and acceleration, which are assumed to be independent of z at a given time.

The equation for constancy of volume is,

$$v\pi r^2 = 2\pi rhu_r$$

or
$$u_r = \frac{rv}{2h} \hspace{4cm} (5)$$

Also

$$f_R = \frac{du_r}{dt} = \frac{\partial r}{\partial t}\frac{v}{2h} + \frac{r}{2h}\frac{\partial v}{\partial t} - \frac{rv}{2h^2}\frac{\partial h}{\partial t}$$

$$= \frac{u_r v}{2h} + \frac{r \dot{v}}{2h} + \frac{rv^2}{2h^2} \quad , \text{ since } \frac{\partial h}{\partial t} = -v$$

and using (5)

$$f_r = \frac{rv^2}{4h^2} + \frac{r\dot{v}}{2h} + \frac{rv^2}{2h^2}$$

$$= \frac{3rv^2}{4h^2} + \frac{r\dot{v}}{2h} \hspace{3cm} (6)$$

Thus the radial acceleration f_r is $\frac{3rv^2}{4h^2}$ for a constant speed upper die.

The equation of radial motion of an element, see Fig. 115 is

$$d(rd\theta h\sigma_r) - \sigma_\theta hdrd\theta = rd\theta hdr\rho f_r \quad\text{———————} \quad (7)$$

where ρ is the density of the cylinder.

Equation (7) reduces to

$$\frac{\sigma_r - \sigma_\theta}{r} + \frac{\partial \sigma_r}{\partial r} = \rho f_r$$

Assuming $\sigma_r = \sigma_\theta$ and replacing f_r by $3rv^2/4h^2$ equation (7) becomes

$$\frac{\partial \sigma_r}{\partial r} = \frac{3\rho v^2 r}{4h^2}$$

or

$$\sigma_r = \frac{3\rho v^2 r^2}{4h^2 . 2} + C \quad\text{——————————} \quad (8)$$

since $\sigma_r = 0$ when $r = a$ equation (8) becomes

$$\sigma_r = \frac{3\rho v^2}{8h^2} (r^2 - a^2)$$

In the absence of acceleration parallel to the axis of the cylinder (if $\dot{v} \neq 0$, then equation (8) should be modified) and using the Tresca yield criterion as

$$\sigma_r - \sigma_z = Y$$

the compressive stress in the dies p, is given by

$$p = -\sigma_z = Y - \sigma_r$$
$$= Y + \frac{3\rho v^2}{8h^2} (a^2 - r^2)$$
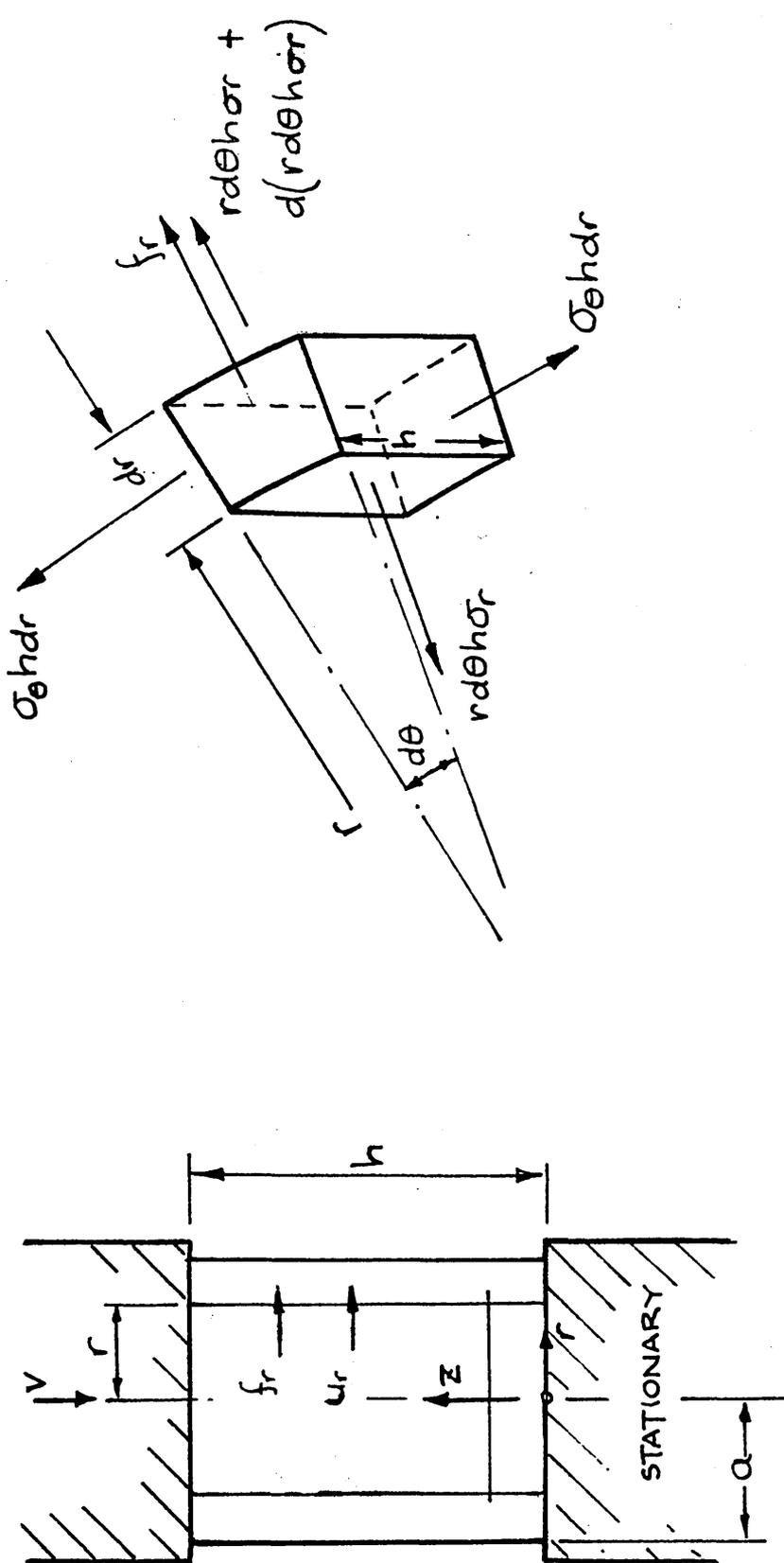
FIG.115   FAST COMPRESSION OF A SHORT CYLINDER

A2·3

THEORETICAL RESULTS

$D_B = 24\,mm$ $L_0 = 24\,mm$ $Y = 17\,N/mm^2$

$D_C = 18\,mm$ $x_0 = 3.405$

$W_p\,(\text{1st STAGE}) = 14.22\,Nm.$

x mm	W_T Nm	P_2 KN	h_b mm	h_f mm
1.25	32.24	13.81	3.95	19.35
2.5	45.9	13.99	4.50	18.10
3.75	59.86	14.20	5.04	16.85
5.0	74.23	14.47	5.59	15.6
6.25	89.08	14.80	6.14	14.35
7.5	104.62	15.19	6.68	13.1
10.0	138.6	16.26	7.77	10.6
12.0	170.0	17.5	8.65	8.6

THEORETICAL RESULTS

$D_B = 24$ mm $\qquad L_0 = 24$ mm $\qquad Y = 17$ N/mm^2

$D_C = 12$ mm $\qquad x_0 = 0.886$ mm

$\underline{W_P \left(1\text{ST STAGE} \right) = 5.22 \text{ Nm}}$

x mm	W_T Nm	P_2 KN	h_b mm	h_f mm
1.25	17.8	11.29	1.21	21.86
2.5	30.1	11.64	1.53	20.61
3.75	42.9	12.0	1.86	19.36
5.0	56.3	12.44	2.18	18.1
6.25	70.35	12.91	2.5	16.86
7.5	85.23	13.45	2.83	15.6
10.0	11.81	14.7	3.48	13.1
12.0	14.85	16.1	4.0	11.1

A3.2

THEORETICAL RESULTS

$D_B = 24\,mm$ $L_o = 24\,mm$ $Y = 17\,N/mm^2$

$D_c = 9\,mm$ $x_o = 0.335$

$W_p\,(\text{1st STAGE}) = 2.31\,Nm$

x_1 mm	W_T Nm	P_2 KN	h_b mm	h_f mm
1.25	13.52	9.98	0.57	22.4
2.5	28.52	10.38	0.81	21.2
3.75	40.62	10.8	1.05	19.9
5.0	53.3	11.27	1.29	18.66
6.25	66.8	11.79	1.52	17.41
7.5	81.12	12.36	1.76	16.16
10.0	11.3	13.7	2.24	13.67
12.0	14.25	15.07	2.61	11.66

A3.3

THEORETICAL RESULTS

$D_B = 24$ mm $L_0 = 30$ mm $Y = 17$ N/mm^2

$D_c = 18$ mm $x_0 = 3.405$ mm

W_P (1ST STAGE) $= 14.22$ Nm

x mm	W_T Nm	P_2 KN	h_b mm	h_f mm
1.25	32.6	14.4	3.83	25.35
2.5	46.61	14.54	4.25	24.1
3.75	60.8	14.7	4.67	22.9
5.0	75.27	14.9	5.1	21.6
6.25	90.0	15.1	5.52	20.3
7.5	105.3	15.4	5.94	19.1
10.0	137.43	16.0	6.79	16.6
12.0	146.4	16.7	7.46	14.6

A3.4

THEORETICAL RESULTS

$D_B = 24$ mm $L_0 = 18$ mm $Y = 17$ N/mm^2

$D_C = 18$ mm $x_0 = 3.405$ mm

W_P (1ST STAGE) $= 14.22$ Nm.

x mm	W_T Nm	P_2 KN	h_b mm	h_f mm
1.25	31.56	12.73	4.17	13.35
2.5	44.61	12.96	4.95	12.1
3.75	58.11	13.27	5.72	10.86
5.0	72.28	13.7	6.49	9.6
6.25	87.43	14.27	7.26	8.35
7.5	104.0	15.04	8.03	7.1
10.0	145.2	17.59	9.57	4.6
12.0	195.77	21.80	10.2	2.6

A3.5

THEORETICAL RESULTS

$D_B = 24$ mm $L_0 = 18$ mm $Y = 17$ N/mm²

$D_c = 9$ mm $x_0 = 0.335$

W_P (1st STAGE) = 2.31 Nm.

x mm	W_T Nm	P_2 KN	h_b mm	h_f mm
1.25	13.6	10.0	0.65	16.4
2.5	25.3	10.58	0.97	15.2
3.75	37.9	11.2	1.29	13.91
5.0	51.44	11.99	1.6	12.66
6.25	66.2	12.7	1.93	11.41
7.5	82.5	13.64	2.24	10.16
10.0	121.4	16.1	2.88	7.66
12.0	162.5	19.0	3.39	5.66

A3.6

```
10   REM  EXTRUSION FORGING
20   INPUT "BILLET DIAMETER";DB
30   INPUT "BOSS DIAMETER";DC
40   INPUT "BILLET HEIGHT, FRICTION FACTOR";LO,FM
45   DIM M2(30),M3(30)
47   I = 1
50   PI = 3.1416:YO = 17.
60   D1 = SQR((DB ↑ 2 + DC ↑ 2):HO = DC / 2.:D3 = D1 - DC:D4 = DB - DC

70   FB = D1 ↑ 2 - DC ↑ 2:FC = DB ↑ 2 - DC ↑ 2:FF = 1. + FM * DB / 6. /
     LO
74   I = 1
80   FO = PI * FC * FF * YO / 4.:P1 = PI * DB ↑ 2 * YO * FF / 4.:P5 = F
     1.
90   PRINT "D1=";D1;"PO=";PO;"P1=";P1
100  INPUT X
110  MP = PI * YO * FC * (FB * ( LOG (FB) - 1. - LOG (FC)) + FC) / 8.
     / D1
     C
115  MP = MP + PI * YO * FM * (D1 ↑ 2 + DB ↑ 2 - 2. * DC ↑ 2) * (D1 -
     DB) / 16.
120  RC = 2. * (PO + P1) / PI / DC / YO - HO:CC = 4. * MP / PI / DC /
     YO
130  XO = ( SQR (BC ↑ 2 + 4. * CC) - BC) / 2.:X1 = XO:ETA = 0:L1 = LO
     - XO
140  PRINT "XO=";XO
150  PRINT "2ND MODE STARTS"; PRINT
170  INPUT "INCREMENT";DX
180  X1 = X1 + DX
185  BETA = LOG (L1 / (L1 - DX)):ETA = ETA + BETA
187  CDC = DC * EXP (BETA / 2.)
190  M1 = PI * FC * (HO + XO) * YO * ( LOG (L1 / (L1 - DX))) / 4.
200  M2 = PI * DC * YO * DX * (HO - HO * DX / 2. / L1) / 2.
```

```
210 W3 = ( LO - XO - HO ) * PI * DB ↑ 2 * YO * ( LOG ( L1 / ( L1 - DX ) ) ) / 4.
215 W4 = PI * DC ↑ 2 * YO * ( DDC - DC ) / 8.
220 D2 = D3 * EXP ( ETA / 2 ) + DC:DDB = D4 * EXP ( ETA / 2 ) + DC
230 WT = PI * YO * ( D2 - D1 ) * ( D2 ↑ 2 + D1 ↑ 2 - 2 * DC ↑ 2 ) / 16. * FM
240 WB = PI * YO * ( DDB - DB ) * ( DDB ↑ 2 + DB ↑ 2 ) / 16. * FM
250 T2W = W1 + W2 + W3 + W4 + WT + WB
260 W1 = PI * FC * LO * YO * DETA / 4.
270 W2 = PI * YO * DX * ( L1 - DX / 2. ) / 2.
280 T3W = W1 + W2 + WT + WB
290 PRINT " T2W=";T2W;" T3W=";T3W
310 P4 = PI * DDB ↑ 2 * YO * ( 0.8 + 3.0 * LOG ( D2 / DC ) ) / 4.
320 IF T2W > T3W THEN GOTO 402
325 J = 5
340 S1H = LO - XO - HO
350 H2 = DC * ( 1. - ( X1 - XO ) / L1 ) / 2.
360 S2H = S1H * ( L1 - ( X1 - XO ) ) / L1
370 HB = ( XO + DC * ( X1 - XO ) / 2. / ( LO - XO ) )
380 HF = LO - X1
390 HT = HB + HF
392 P2 = T2W / DX
395 PRINT : PRINT " P2= " P2= ";P2; PRINT
400 GOTO 500
402 P3 = T3W / DX
405 IF P4 < P3 THEN GOTO 460
410 PRINT "THIRD STAGE BEGIN"
412 IF J = 5 THEN GOTO 420
414 HB = XO + DX
```

```
416 HF = LO - XO - DX
418 HT = LO
419 GOTO 445
420 HB = HB + DX
430 HF = HF - DX
440 HT = HT
445 PRINT : PRINT "P3=";P3: PRINT
450 GOTO 500
460 PRINT "FOURTH STAGE BEGIN"
461 M2(I) = D2;M3(I) = DDR
462 P4 = PI * M3(I) ^ 2 * YO * (0.8 + 3 * LOG (M2(I) / DC)) / 4.0
466 XL = M2(I) ^ 2 / DC ^ 2 * X
467 PRINT "DISP VOL=";XL: PRINT
468 HB = HB + XL
469 PRINT "BILLET DIA=";M2(I)
475 I = I + 1
480 HF = HF - DX
490 HT = HB + HF
495 PRINT : PRINT "P4=";P4: PRINT
500 PRINT "BOSS HT=";HB;" FLANGE HT=";HF;" TOTAL HT=";HT: PRINT
503 PHT = HT * 100 / 24.
505 PRINT "PERCENTG TOTAL HT=";PHT: PRINT
510 PRINT " TOTAL COMPN.=";X1 * 100. / LO;" PERCENT": PRINT
520 D1 = D2;DB = DDB
522 L1 = LO - X1
540 PRINT " TYPE '1' TO REPEAT,'2' TO END"
545 INPUT X
550 IF X = 1 THEN GOTO 180
560 END
```

A4.3

THE EFFECT OF FRICTION IN SIMPLE UPSETTING OF CYLINDRICAL BILLETS OF ELASTIC-PLASTIC AND ELASTIC-STRAIN HARDENING MATERIAL: A NUMERICAL TECHNIQUE

M. S. J. HASHMI and F. B. KLEMZ

Department of Mechanical and Production Engineering, Sheffield
Polytechnic

SUMMARY

This paper describes a numerical technique for analysing simple
upsetting of cylindrical billets, which incorporate the effects of
interface friction, axial inertia and strain hardening property of the
billet material. This method essentially uses a lumped mass model for
the actual billet. The procedure amounts to expressing the dynamic
force equilibrium equation for each mass point in finite-difference
form and relating the displacement of each mass point to the strain in
the corresponding link after each time increment. The stress in each
link, and hence the axial force, is then calculated from the material
stress-strain characteristics which may be elastic-plastic or elastic-
strain hardening.
This theoretical approach enables the billet profile, the tup
load, and velocity to be determined at any stage during the in-process
time. The stress and strain-time history at any point within the
billet can also be determined. Three different values of the friction
coefficient - 0, 0.25 and 0.5 have been considered.

TRODUCTION

In recent years high energy rate
rming processes have received consider-
le attention, firstly since it has proved
be an effective method of producing
mplex components to a high degree of
curacy and secondly, because of difficul-
es arising from the shortening of tool
fe caused by the complex forcing function
the die-billet interface. It has been
tablished [1-3] that high rates of
rming also enhances the effect of
terial inertia, strain-rate sensitivity,
ress wave propagation and friction in
e interface.

A great deal of experimental and
eoretical work has already been carried
t to investigate various aspects of high
ergy-rate forming as applied to forging
d simple upsetting operations. Compre-
nsive surveys of previous work appeared
references [1] to [7] and will not be
peated in this paper.

It is, however, worth noting that
st of the theoretical methods developed
viously have so far contributed towards
derstanding the in-process variation of
e tup load and billet height, often
ploying complicated and sometimes cum-
rsome analytical expressions. The
thors felt that a simpler theoretical
proach, capable of incorporating the
terial inertia and strain-hardening
fect and also the effect of elastic and
astic stress wave propagation could be
veloped enabling further understanding
the behaviour of the billet during the
-process time.

The present paper describes a numer-
ical technique for analysing simple up-
setting of cylindrical billets which in-
corporates the effects of billet-tup
interface friction, radial inertia and
strain hardening properties of the billet
material. This method essentially uses a
lumped mass model for the actual billet
and operates on the following assumptions,

(i) the billet could be idealized to be
made up of a number of concentrated
masses connected to each other by
massless links of circular cross-
section which possess the same
strength properties as the material
of the billet,

(ii) the plane sections remain plane
throughout the deformation process,

(iii) uniform axial straining occurs with-
in each individual link,

(iv) the frictional stress in the billet-
tup interface is proportional to the
normal stress in the face of the
billet,

(v) the radial expansion of each conn-
ecting link is governed by the con-
dition of volume constancy, and

(vi) there is no resistance to radial
expansion of any link from the
neighbouring link except for the
links in contact with the top and
the bottom platens in which case
interface frictional force resists
radial expansion.

A5·1

The procedure amounts to expressing the dynamic force equilibrium equations for each concentrated mass point in finite-difference form and relating the displacement of each masspoint to the strain in the corresponding link after each time increment. The stress in each link, and hence the axial force, is then determined from the material stress-strain characteristics which may be elastic-plastic or elastic-strain hardening. This theoretical approach enables prediction of the instantaneous and final shape of the billet, the variation in tup load and velocity, and the stress and strain-time history at any point within the billet.

The influence of the frictional force at the billet-die interface was also taken into account considering three different values for the coefficient of friction, $\mu = 0.0$, 0.25 and 0.5.

NOMENCLATURE

A   layer area in the cross-section model
E   elastic modulus
F   external force per unit length
N   axial force
R   current billet radius
m   mass per unit length
Δs link length in the numerical model
Δt time increment
u,v   displacement
x,y   co-ordinate axis
ϵ engineering strain
σ stress

Subscripts

i   this refers to the masspoint number and the preceeding link
j   time position
l   refers to the sublayer number
r   refers to the layer number

Superscripts

m   modified value
t   trial value

ANALYSIS

The general equation of motion for an element of the billet, soon after the tup strikes the top face, can be derived by considering the internal and external forces acting on the element as shown in Fig.1(a) and is given by

$$\frac{\partial (N)}{\partial x} + F_x - m\ddot{u} = 0 \qquad (1)$$

where m denotes mass per unit length and (¨) denotes double differentiation with respect to time.

Figure 1(b) shows the lumped parameter model for the element in Fig.1(a) and equation (1) could be written in finite-difference form to correspond to this model. This model replaces the actual billet by a mass-link system. The mass of each element of the billet is represented by a concentrated mass connected to

other masses by massless links which can transmit axial force. Under the action of the external and internal forces therefore, the position of each mass in the model identifies the position of the corresponding element of the actual billet.

The finite-difference equation for the element at the ith location of the model in Fig.1(b) is given by

$$N_{i+1} - N_i + F_x\left(\frac{\Delta s_i + \Delta s_{i+1}}{2}\right) - m_i\ddot{u}_i = 0 \qquad (2)$$

Equation (2) as it applies to all the mass points along the billet gives the instantaneous values of $u_{i,j+1}$ for any time t_{j+1} when coupled with the following relationship between the acceleration and displacement in finite-difference notation,

$$u_{i,j+1} = \ddot{u}_{i,j}(\Delta t)^2 + 2u_{i,j} - u_{i,j-1} . \qquad (3)$$

The time increment Δt is defined through

$$\Delta t = t_{j+1} - t_j \qquad (4)$$

The change in length of each link is given by the change of location of each mass point and hence the axial strain in each link is obtained. A constitutive relationship is next used to calculate the stress at any section which in turn gives the value of the axial force.
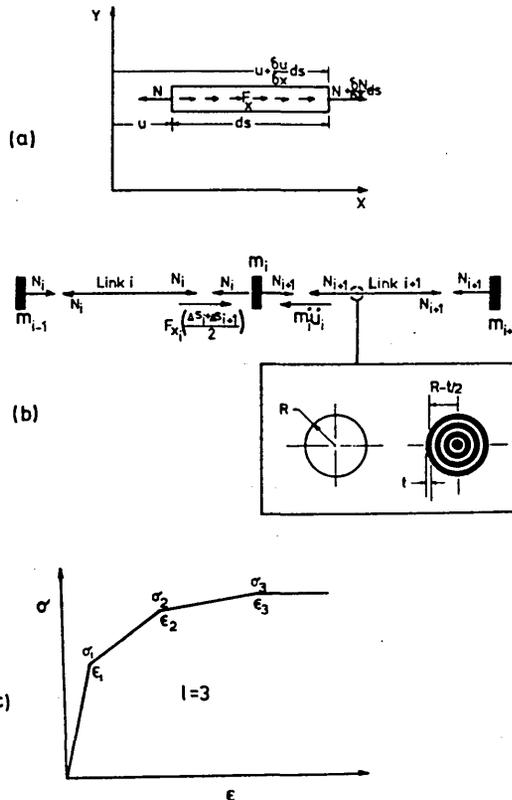

Fig.1. (a) An element of the billet
        (b) Equivalent finite-difference model
        (c) Approximated polygonal stress-strain diagram

In order to facilitate the calculation of stress which may vary across the cross-section of the billet, it is necessary to idealize the actual cross-section to an equivalent cross-section model which consists of a number of layers across each of which the stress is assumed to be uniform. The circular cross-section of the billet is assumed to consist of n discrete, evenly spaced tubular cross-sectional area layers of material which can carry normal stresses. These layers are considered to be separated by a material which can not carry any normal stress but has infinite shear rigidity.

With this simplified model the stress in the billet can be defined by the individual normal stresses at the n separate layers without having to contravene the assumption that plane sections remain plane throughout the deformation process. The cross-sectional area of each tubular layer can be calculated by equating the fully plastic pure axial load carrying ability, with those of the actual cross-section of the billet. A typical circular section and the corresponding idealized section model are shown in the inset in Fig.1(b).

In order to describe the elastic-plastic stress state in a layer of the section-model further idealization is made and each layer is assumed to consist of sublayers the number of which is determined by the number of positive sloped sides in the approximated polygonal stress-strain diagram shown in Fig.1(c). For example, the polygonal stress-strain diagram for an elastic linearly strain hardening material consists of two positive sloped sides and hence two sublayers to each layer are required. Each sublayer can only carry stresses not exceeding the sublayer yield stress.

The sublayer area $A_{\ell r}$ is related to the layer area A_r by

$$A_{\ell r} = A_r (E_\ell - E_{\ell+1})/E \qquad (5)$$

here

$$E_\ell = \frac{\sigma_\ell - \sigma_{\ell-1}}{\varepsilon_\ell - \varepsilon_{\ell-1}}$$

is the ℓth slope of the polygonal stress-strain diagram, σ_ℓ is the stress and ε_ℓ is the corresponding engineering strain as illustrated in Fig.1(c).

The change in length $\delta(\Delta s)$ of the link s_i at time t_j gives the strain increment in each layer of ith link as,

$$\delta\varepsilon_{ir,j} = \frac{\delta(\Delta s)_{i,j}}{\Delta s_{i,o}} \qquad (6)$$

here $\Delta s_{i,o}$ is the original length of the link.

Knowing the sublayer stress $\sigma_{ir\ell,j-1}$ at time t_{j-1}, at the ℓth sublayer of the rth layer at the ith link and the strain increment $\delta\varepsilon_{ir,j}$ at time t_j at the rth layer of the ith link, the sublayer stress $\sigma_{ir\ell,j}$ at time t_j, at the ℓth sublayer is determined as follows.

First a trial value $\sigma^t_{ir\ell,j}$ of the sublayer stress $\sigma_{ir\ell,j}$ is calculated by assuming an elastic path, thus

$$\sigma^t_{ir\ell,j} = \sigma_{ir\ell,j-1} + E\delta\varepsilon_{ir,j} \qquad (7)$$

Once the trial value is calculated, the correct value could be ascertained by using the following conditions: Let $\sigma_{y\ell}$ be the sublayer yield stress and be given by $\sigma_{y\ell} = E\varepsilon_\ell$, where ε_ℓ is the strain defining the ℓth corner of the polygonal stress-strain diagram. Denoting $\sigma_{ir\ell,j}$ as σ_ℓ for convenience,

$$\left. \begin{array}{lll} \text{If } -\sigma_{y\ell} \leqslant \sigma^t_\ell \leqslant \sigma_{y\ell} & \text{then } \sigma_\ell = \sigma^t_\ell \\[2mm] \text{If } \sigma^t_\ell < -\sigma_{y\ell} & \text{then } \sigma_\ell = -\sigma_{y\ell} \\[2mm] \text{If } \sigma^t_\ell > \sigma_{y\ell} & \text{then } \sigma_\ell = \sigma_{y\ell} \end{array} \right\} (8)$$

This procedure is applied to all sublayers of each layer for all the links.

The values of the sublayer stresses for the links in immediate contact with the tup and the anvil are then modified, to take into account the interface friction, by using the equation,

$$\sigma = \sigma_0 [1 + 2\mu(R-r)/h] \quad \ldots \ldots \qquad (9)$$

given in reference [8] where σ_0 is the uniaxial flow stress, h, R and r are the current billet height, outer radius and intermediate radius respectively. Following the terminology applied to the numerical model this equation could be written as

$$\sigma^m_{\ell,j} = \sigma_{\ell,j} [1 + 2\mu(R_i - R_{ir})/h] \qquad (10)$$

where μ is the interface friction coefficient, and $\sigma_{\ell,j}$ is the sublayer stress determined by equations (8). After this modification, the axial forces $N_{i,j}$ in each link are then obtained from the equation,

$$N_{i,j} = \sum_{r=1}^{n} \sum_{\ell=1}^{k} \sigma_{ir\ell,j} A_{\ell,j} \quad \ldots \ldots \qquad (11)$$

where $A_{\ell,j}$ is the current sublayer area.

If the links could be assumed to have the same mass density as the billet, then further modification to the values of the sublayer stresses could be made, to take into account the effect of radial inertia of the billet material, by using the equation

$$\sigma = 3\rho v^2 (R^2 - r^2)/8h^2 \qquad (12)$$

given in reference [8], where ρ is the material density, v is the rate of straining, h, R and r are the current billet height, outer radius and intermediate radius respectively. The above equation only applies when the velocity v is constant, a condition which is assumed to be satisfied when deformation of each individual link during very small time interval Δt is considered.
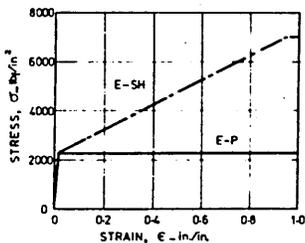
A5·3

In the present numerical approach the time increment cannot be chosen arbitrarily. The value of the time increment should be less than the time needed for the elastic stress wave to propagate through the length of the link. For detailed information about this method the reader is referred to Ref. [9].

RESULTS AND DISCUSSIONS

To illustrate the effectiveness of the present numerical method, a simple upsetting operation similar to the one considered in reference [3], was chosen. This enabled a direct comparison to be made between the theoretical method presented in reference [3] and the present work in predicting the relationship between axial deformation, tup load and velocity. A billet of 2 in. diameter and 2 in. height and a tup weighing 500 lbf impinging on to it with a velocity of 100 ft/sec was considered. For the elastic-plastic (E-P) model the yield stress of 22400 lbf/in^2 and Young's modulus of 10 x 10^6 lbf/in^2 and for the elastic-strain hardening (E-SH) model, the stress-strain characteristics shown in Fig.2(b) were adopted. Three values of the interface friction, µ, equal to zero, 0.25 and 0.5 were considered. The billet in actual loading configuration and its corresponding numerical model is shown in Fig.2(a).

The present method enabled the prediction of the instantaneous shape of the billet, the outer profiles of which were obtained by joining the mid-peripheral points of the thin elements. Fig.3 shows a series of changing profiles of a billet of elastic-plastic material having interface coefficient of friction, µ, equal to (a) zero and (b) 0.5. It is evident from careful inspection of this figure, that with the onset of the process, the deformation begins with the billet increasing in diameter in the area immediately adjacent to the tup. This size change takes the form of a slightly mushroomed profile which soon progresses along the length of the billet and is reflected at the anvil, thus reversing the initial mushroomed shape. The reflected plastic front then progresses upwards and is again reflected at the tup. The billet continues to deform in this manner, alternating the mushroomed shape, until the plastic deformation ceases. The instantaneous profiles for zero interface friction in Fig.3(a) shows no significant barrelling effect which, however, is very much evident in the profiles shown in Fig.3(b) for the interface friction, µ, equal to 0.5.

Fig.4 shows the comparison of the variation in tup velocity with billet deformation for billets of elastic-plastic and elastic-strain hardening material. In both cases the interface friction coefficient of 0.5 was considered. The result predicted in reference [3] for a rigid-plastic material of yield stress
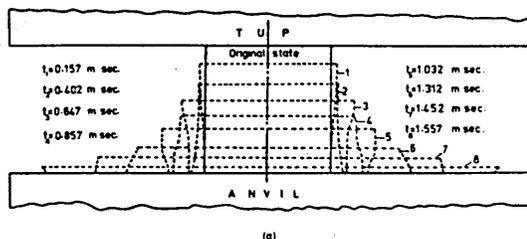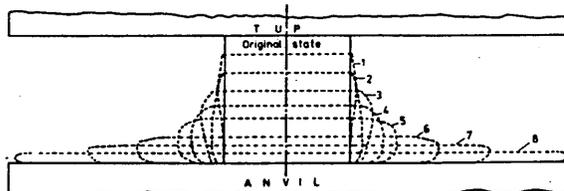

(a)

(b)

Fig.2. (a) Billet in its actual loading configuration and its corresponding numerical model
(b) Polygonal stress-strain diagrams for E-P and E-SH model

(a)

(b)

Fig.3. Showing successive deformation pattern of a billet of elastic plastic material
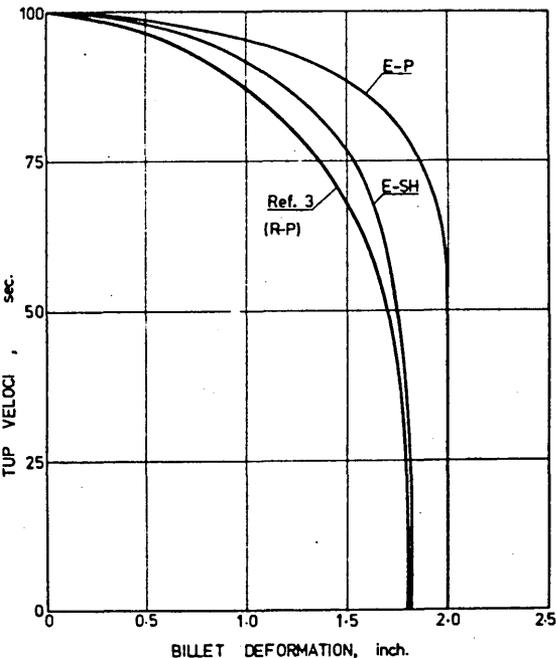(a) without friction µ = 0 and
(b) with friction, µ = 0.5

Fig.4. Variation in tup velocity Vs def-
ormation (μ= 0.5)
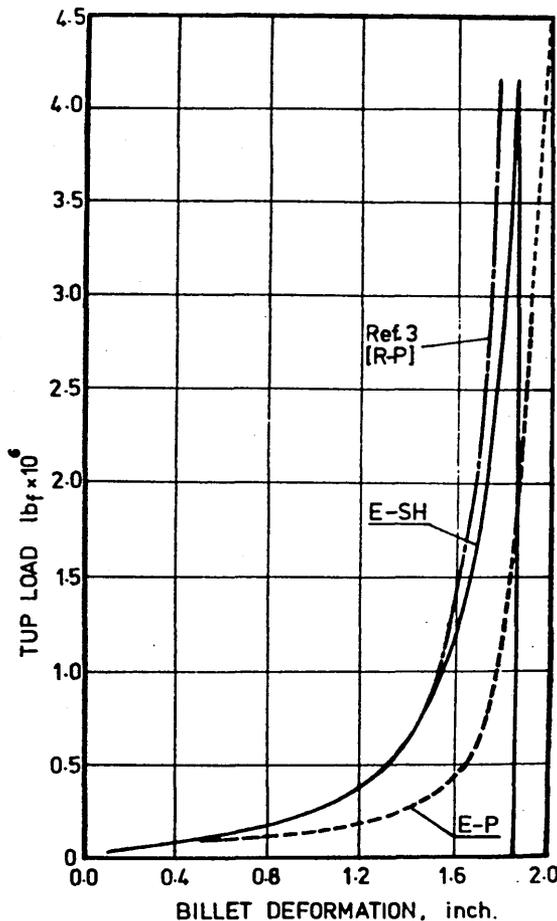
Fig.5. Variation in tup load with def-
ormation (μ= 0.5) showing the
effect of billet material properties

2400 lbf/in^2 is also included in the same
igure for comparison. It is seen that the
up velocity does not change appreciably
til near the end of the deformation
rocess, when the velocity decreases
uickly. It should be noted, however, that
e curve predicted for rigid-plastic
terial in reference [3]differ consid-
rably from that predicted using the pres-
nt method.

The variation in tup load during the
eformation process is one of the import-
nt parameters of interest in an upsetting
peration. This is shown in Fig.5 for
illets of E-P and E-SH model with friction
oefficient of O.5. A tup-load vs
eformation curve from reference [3] for
igid-plastic material is also included
n the same figure. The effect of
terial property on the tup load is
learly evident from this figure. It is
een that a much higher tup-load for a
iven extent of deformation is predicted
n reference [3].

The effect of interface friction on
e variation of tup load with deformation
or a billet of E-SH material is shown in
ig.6 which shows tup load vs billet de-
ormation curves for coefficients of fric-
ion of zero and O.5. The effect of the
aterial property on the deformation
rocess can be seen from Fig.7 which shows
e variation in billet height with in-
rocess time for E-P and E-SH material, in
oth cases zero interface friction was

considered. Fig.8 compares the rate of
consumption of the initial kinetic energy
possessed by the tup in deforming billets
of E-P and E-SH material having zero
interface friction. A more rapid absorp-
tion of energy by the E-SH model is clearly
evident from this figure. The effect of
interface friction on the rate of consump-
tion of tup-energy is demonstrated in
Fig.9, which shows percentage kinetic
energy absorbed vs billet deformation
curves for a billet of E-P material having
interface friction of zero, 0.25 and O.5.

The presence of friction in the tup-
billet interface restricts the material at
the interface from spreading freely and
causes barrelling of the deformed billet.
The effect of friction on the extent of
spread at the interface for a billet of
E-SH material is shown in Fig.10, which
shows the percentage change in diameter
at the tup-billet interface with billet
deformation for interface friction co-
efficients of zero, 0.25 and O.5. When
friction is present, the restricted mater-
ial spread at the interface results in

Fig.6. Variation in tup load with def-
ormation (E - SH) showing the eff-
ect of interface friction
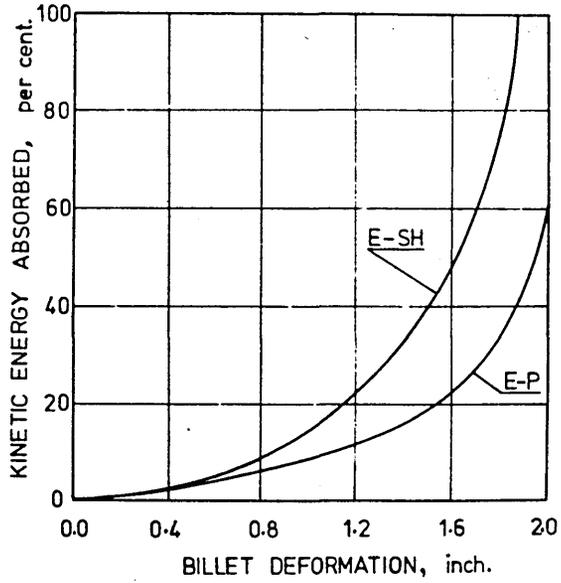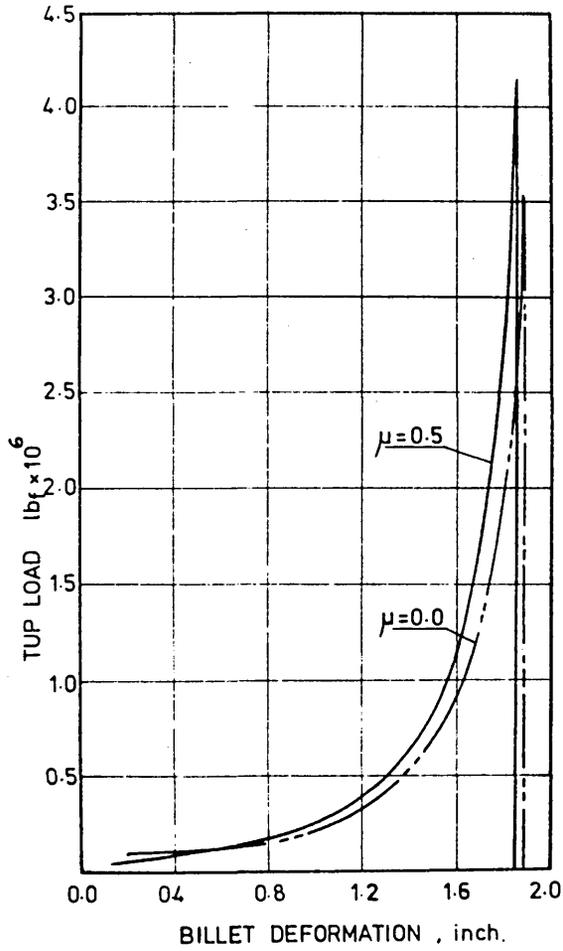
Fig.8. Showing the rate of K.E. absorption
with deformation for E-P and E-SH
material (μ = O)

Fig.7. Effect of material property on the
time variation of the billet height
(μ = O)
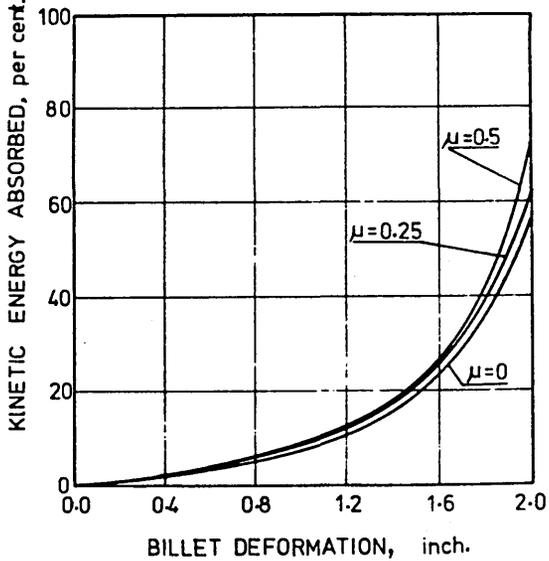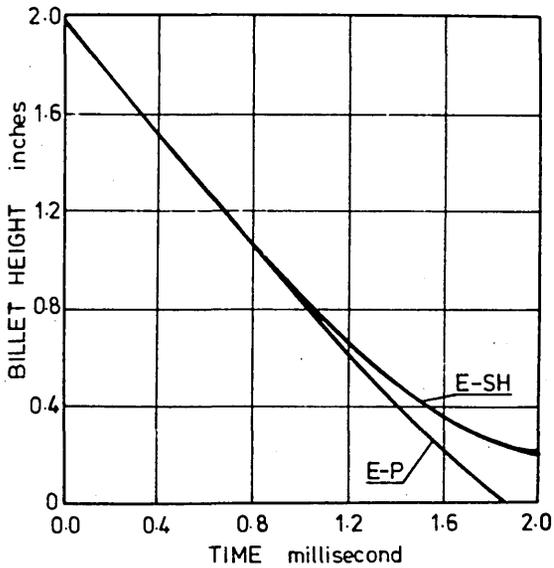
Fig.9. Variation in the kinetic energy
absorbed with different values of
friction coefficient. (E - SH)

CHANGE IN DIAMETER , per cent.

μ = 0

μ = 0.25

μ = 0.5

BILLET DEFORMATION, inch.
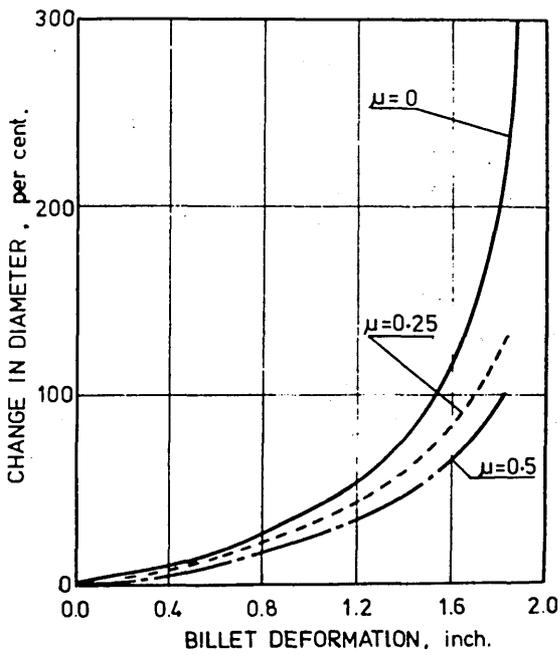
g.10.Percentage change in billet diameter
at the tup-billet interface with tup
displacement (E - SH)

sser-axial strain to the layer of
llet material adjacent to the tup than
e layer at mid section. However, equal
ial straining within the billet is
pected if there is no interface friction.
g.11 shows the variation in axial strain
the top interface and middle section of
billet of E-SH material during the in-
ocess time for friction coefficients of
) zero and (b) 0.5.
The radial velocity of the billet
terial at the top and bottom face was
edicted using the present numerical
thod and is shown in Fig.12 for a
llet of E-SH material having zero inter-
ce friction. It is evident from this
gure that the radial velocity changes
th in-process deformation time in a
clic manner. A phase difference,
wever, is present between the radial
locity curves for top and bottom face.
is could perhaps be explained as the
sult of the propagation of and reflection
the stress wave fronts in between the
p and the anvil while deformation
ogresses.
The magnitude of the radial velocity
s predicted to reach about four times the
itial tup velocity at the final stages of
formation. The radial inertia, however,
found to have insignificant effect on
e tup load for the range of tup velocity
nsidered in this work.

AXIAL STRAIN

top face   mid section

(μ=0)   (a)

AXIAL STRAIN

mid section   top face

(μ=0.5)   (b)

TIME millisecond
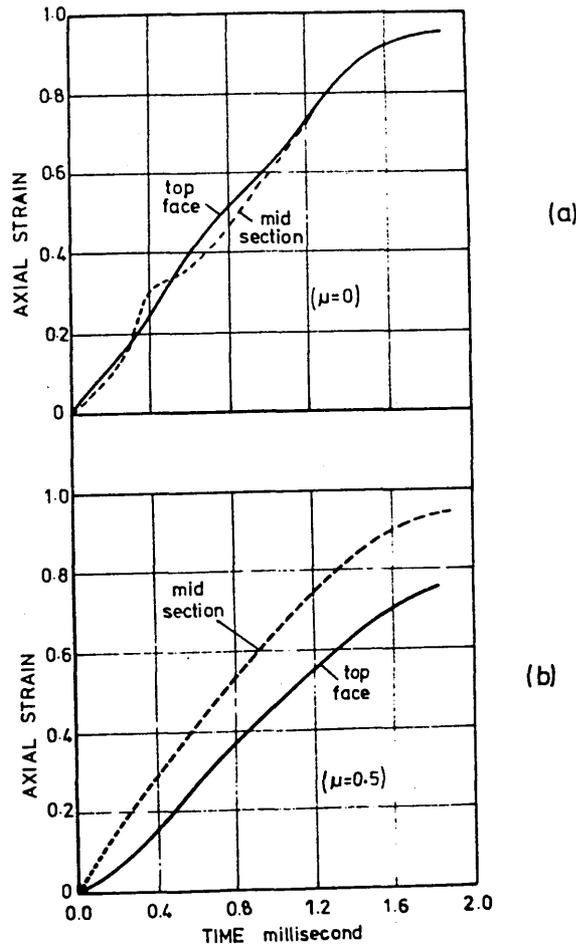
Fig.11.Time variation of the axial strain
at the top and middle section (E-SH)

RADIAL VELOCITY in/sec ×10⁻³

bottom face

top face

TIME, milliseconds.
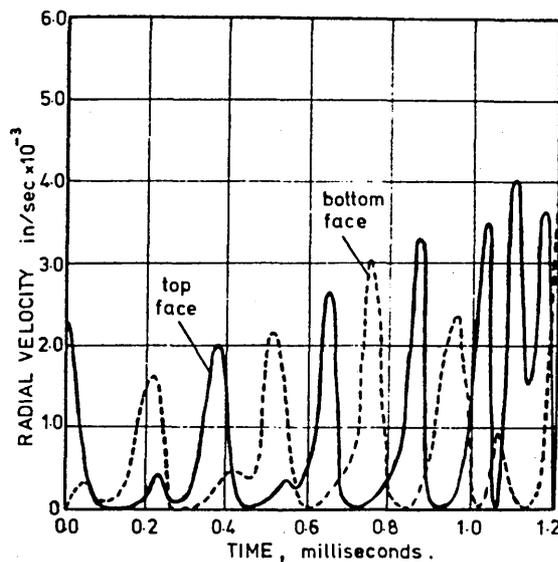
Fig.12.Time variation of the radial velocity
of the billet material at the tup and
anvil interface of the billet
(μ = 0, E-SH)

A5.7

CONCLUSIONS

The results predicted using the present numerical method compare well with those using other methods [3]. However, further experimental evidence is needed to verify the practical significance of these approaches.

The presence of friction at the tup-billet interface is seen to have considerable effect on the tup load, shape of the deforming billet, and strain and stress distribution during the deformation process.

The present method provides a comprehensive picture of the mechanics of deformation during the upsetting process, thus facilitating the analysis of the behaviour of the billet at any stage during its in-process time.

REFERENCES

1. W.SCHROEDER and D.A.WEBSTER (1949) Press Forging Thin Sections: Effect of Friction, Area and Thickness on Pressures Required.   J.App.Mech. p.289

2. J.B.HADDOW (1965) On the Compression of Thin Disc, Int.J.Mech.Sci. 7, p.657

3. H.LIPPMAN (1966) On the Dynamics of Forging, Proc.7th Int.M.T.D.R.Conf. p.53

4. R.A.C.SLATER, W.JOHNSON and S.Y.AKU (1968) Experiments in the Fast Upsetting of Short Pure Lead Cylinders and a Tentative Analysis. Int.J.Mech.Sci. 9. p.169

5. S.K.SAMANTA (1968) Resistance to Dynamic Compression of Low-Carbon Steel and Alloy Steels at Elevated Temperature and at High Strain Rates, Int.J.Mech.Sci. 10, p.613

6. T.A.DEAN (1970) The Influence of Billet Inertia and Die Friction in Forging Processes, Proc.11th Int.M.T.D.R.Conf, p.761

7. C.E.N.STURGESS and A.N.BRAMLEY (1970) The use of Impact-Forming Devices to obtain Dynamic Stress-Strain Data.   Proc.11th Int.M.T.D.R. Conf. p.803

8. W.JOHNSON (1972) Impact Strength of Materials, Edward Arnold, London, p.153-154

9. M.S.J.HASHMI (1972) Study of Elastic-Plastic Response of Structures to Dynamic Load. PhD.Thesis, University of Manchester Institute of Science and Technology

SIMPLE UPSETTING OF CYLINDRICAL BILLETS: EXPERIMENTAL INVESTIGATION AND THEORETICAL PREDICTION

F.B. KLEMZ and M.S.J. HASHMI
Department of Mechanical and Production Engineering
Sheffield City Polytechnic, Sheffield

SUMMARY

Experiments were carried out by deforming cylindrical billets under a free falling tup in an experimental drop-hammer unit. Load-time variation was measured experimentally using a load cell incorporated in the anvil. High speed photographs were used to obtain instantaneous and final profiles of the billet and also the data giving tup velocity-time curves after the onset of the deformation process.

In order to study the effect of friction, billets were tested under lubricated and dry condition. Experimental results were then compared with those predicted using a numerical technique (1), incorporating elastic-strain hardening stress-strain characteristics of the billet material obtained from quasi-static compression test.

ODUCTION

the advent of high energy rate
ing processes in recent years, con-
rable effort has been devoted,
tly, to the estimation of the
stance of metals to deformation at
rates of strain and secondly, to
understanding of the complex forcing
tion which prevails during the def-
tion process due to material inertia,
strain rate, stress wave propog-
n and interface friction. To this
simple upsetting of cylindrical
ets provided the most convenient
simple means of carrying out exper-
tal as well as analytical studies.

ished literature on the subject
s that most of the experimental
ies were aimed at establishing emp-
al equations of some sort relating
ic flow stress, strain and strain
(2-13). A number of other stu-
have also been carried out putting
ard analytical methods for predic-
the load-deformation behaviour of
ets of material having stress-strain
acteristics following one or other
he relations established in earlier
ies, some of these incorporated
tion and material inertia (16).
ver, most of these analyses appear
e cumbersome and involve lengthy
vations.

More recently, in reference (1) the
authors presented a numerical technique
for predicting load and deformation be-
haviour of a billet of elastic-strain
hardening material incorporating inter-
face friction and material inertia. It
was also suggested in reference (1) that
the billet deforms in a mode dominated
by elastic-plastic stress wave propog-
ation through the billet until deforma-
tion ceases. This effect was found to
be more dominant when interface friction
was negligible.

The purpose of this study is to obtain
experimental results by carrying out
tests on a cylindrical billet and compare
with those predicted using the above men-
tioned numerical technique, thus facilit-
ating verification of its effectiveness.
In this study, tests were carried out on
commercially pure lead and aluminium
alloy cylindrical billets by deforming
them under a free falling tup in an exper-
imental drop hammer designed, constructed
and instrumented for this purpose. The
reason for using lead and aluminium alloy
as the billet material is that lead is hot
worked at room temperature and is highly
strain-rate sensitive. On the other hand
aluminium alloy at room temperature is
known to be non strain rate sensitive for
strains of the order of $10^2 sec^{-1}$. Tests

A5·9

on billets of these different materials
would, hopefully, provide experimental res-
ults with and without the influence of
strain rate sensitivity. The theoretical
prediction for both cases would be without
taking strain rate sensitivity into account.

Two types of frictional condition were
studied, one, using a paste of graphite in
petroleum jelly as lubricant to induce low
friction and, the other, without any lubric-
ant to induce dry friction condition. High
speed photographs were used to obtain exper-
imental data giving instantaneous billet pro-
files and tup-displacement-time curves.
Elastic strain-hardening stress-strain char-
acteristics of the billet material were obt-
ained from quasi-static compression tests and
were incorporated in the numerical technique
the details of which are given in reference
(1) and will not be repeated in this paper.

EXPERIMENTAL EQUIPMENT AND PROCEDURE

Simple upsetting of commercially pure
lead cylindrical billets having diam-
eter of 1.00 in and height of 0.95 in
and aluminium alloy cylindrical billets
of 0.75 in diameter and 0.75 in height,
was performed at room temperature using
an experimental drop hammer.   The
force time variations were obtained by
using a hardened tool steel load-cell
which was incorporated in the anvil
unit of the drop hammer.   Output sig-
nals generated from the load-cell were
fed to a storage oscilloscope through a
transient recorder and a built in filter.
The traces displayed on the screen were
then photographed by means of a Polaroid
camera to produce records for further
analysis.   The tup velocity just before
impact was measured using an electronic
counter which is activated and stopped by
means of a photocell unit which also tri-
ggers the oscilloscope.

The energy required to produce plastic
deformation of the billet was provided by
a tup which could fall freely from any
desired height up to a maximum of 15 ft.
The mass of the tup was variable but
during the present tests it was maintained
constant at 35.5 lb.   Fig.1. shows a
schematic diagram of the lower part of the
drop hammer showing the anvil unit, load
cell, tup, billet and velocity measuring
arrangement.   The load cell was calibra-
ted using a 50 tonf compression machine
and then incorporated into the anvil unit.

High speed photographs were taken at a
speed of 2400 frames/sec using a Hi-cam
high speed camera.   The processed film
was then projected on to a screen using a
16 mm cine-projector with single frame
movement facilities and analysed for inst-
antaneous profiles and tup-displacement-
time curves.
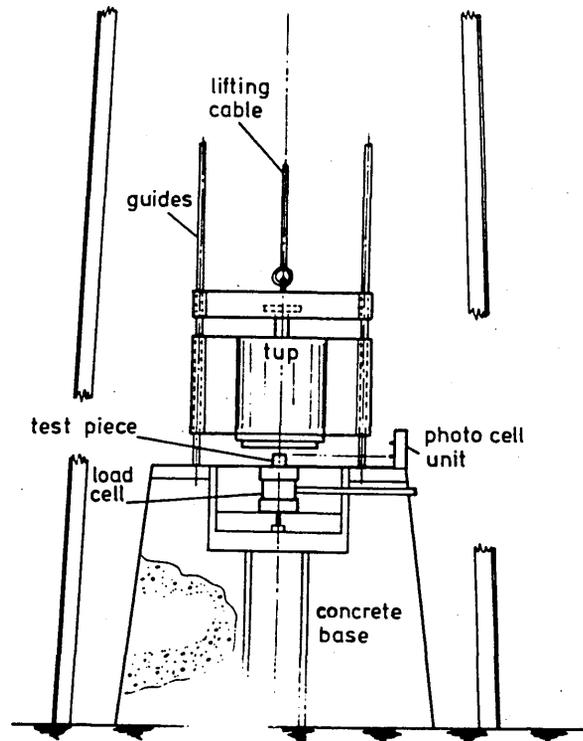
Fig.1.   Schematic diagram showing the
loading arrangement of the
billet.

The lead billets were annealed in boiling
water for 30 minutes while the aluminium
alloy billets were annealed at 350°C for
15 minutes in an oven before testing.

RESULTS AND DISCUSSIONS

Experimental results were obtained from
tests carried out on lead and aluminium
alloy billets under lubricated and dry
frictional conditions.   In all cases the
tup weighing 35.5 lbf was allowed to fall
freely on to the billet from a height of
15 ft.   Experimentally measured tup vel-
ocity was found to be 30 ft/sec.

The load-time variation was obtained
from the tracings recorded in the oscill-
oscope.   A typical photograph of such a
trace for aluminium billet is shown in
Fig.2.   The distinct kink in the shape
of the trace was present in every test
with aluminium alloy billets.

A5·10

→ 0·5 msec/cm

.2. Photograph showing a typical
    load-time trace for aluminium
    billet.
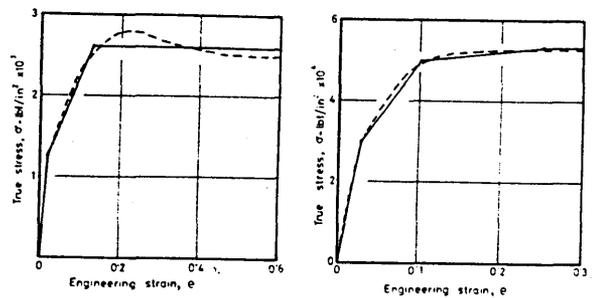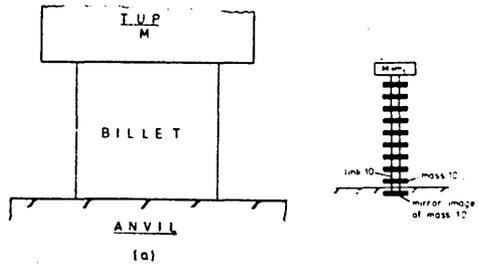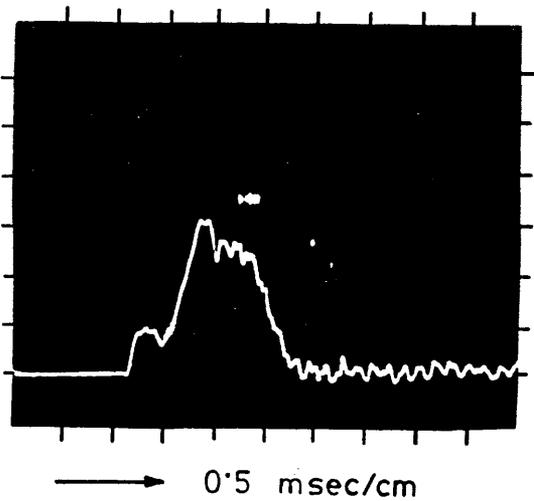
Fig.3a. Actual loading configuration
        and the corresponding numerical
        model.

    b. Stress-strain characteristics
       for lead and

    c. Stress-strain characteristics
       for aluminium

lyses were undertaken for lead and
 inium alloy billets, each loaded
er lubricated and dry conditions. The
ults predicted were then compared with
se obtained experimentally.   For the
ricated test condition where a paste of
phite in petroleum jelly was used as
ricant, it was assumed in the analysis
t a constant frictional coefficient
0.06 existed for both lead and alumin-
 billets.   This value of μ was thought
 e a reasonable estimate of what graph-
 in petroleum jelly would induce.   No
empt was made to actually determine
ctional coefficient.   For dry test con-
ions the value for μ= 0.577 was incor-
ated in the analysis for lead billets
) while for aluminium billets μ = 0.18
 used (14).

 actual loading configuration and its
ivalent numerical model, applied to
  the lead and aluminium billets, is
n in Fig.3(a).   The quasi-statically
ained stress-strain characteristics
 their polygonal approximation, as
uired by the numerical technique, for
  and aluminium used in this study
 shown in Fig.3(b) and (c) respect-
ly.

 instantaneous profiles of a lead
let, obtained using high speed pho-
aphs, at various instants of time
er the onset of the process are
ı in Fig.4(a).   This test was
ied out under lubricated conditions.
is seen that the billet deforms in a
er such that the profile shape

remains right cylindrical throughout the
deformation process.   The theoretically
predicted instantaneous profiles for the
same billet are shown in Fig.4(b) which
shows profile shapes having either up-
wards or downwards directed slightly
tapered sides.   Slight barrelling also
becomes apparent in the profiles corres-
ponding to higher reductions in billet
height.

The instantaneous profiles shown in Fig.
5(a) for a lead billet deformed under
dry condition are seen to compare reas-
onably well with those in Fig.5(b), pre-
dicted using a numerical technique.
The die load obtained experimentally was
plotted in Fig.6(a) and (b) against red-
uction in billet height measured off the
high speed photographs for lead and alum-
inium billets respectively, both tests
carried out under lubricated condition.
The theoretically predicted curves are
also included in the respective figures
for comparisons.   It can be seen that
for the lead billet a much lower die
load is predicted; less than 50% for 60%
reduction in billet height.   On the
other hand the die load predicted for
the aluminium alloy billet is comparable
with those obtained experimentally,
being slightly higher during the initial
part of the deformation and slightly
lower thereafter.
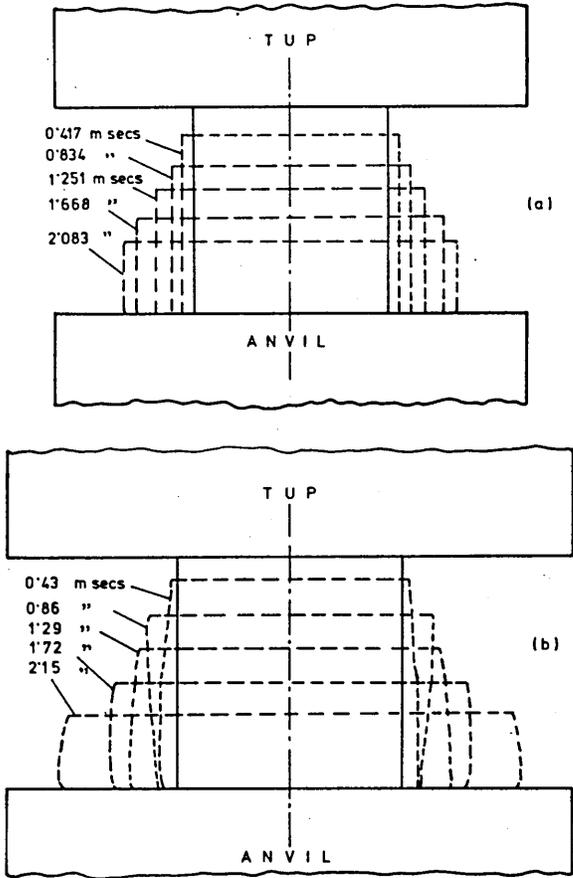
Fig.4a. Showing the instantaneous pro-
files of a lead billet defor-
med under lubricated test con-
dition, and

b. Corresponding instantaneous pro-
files predicted theoretically.
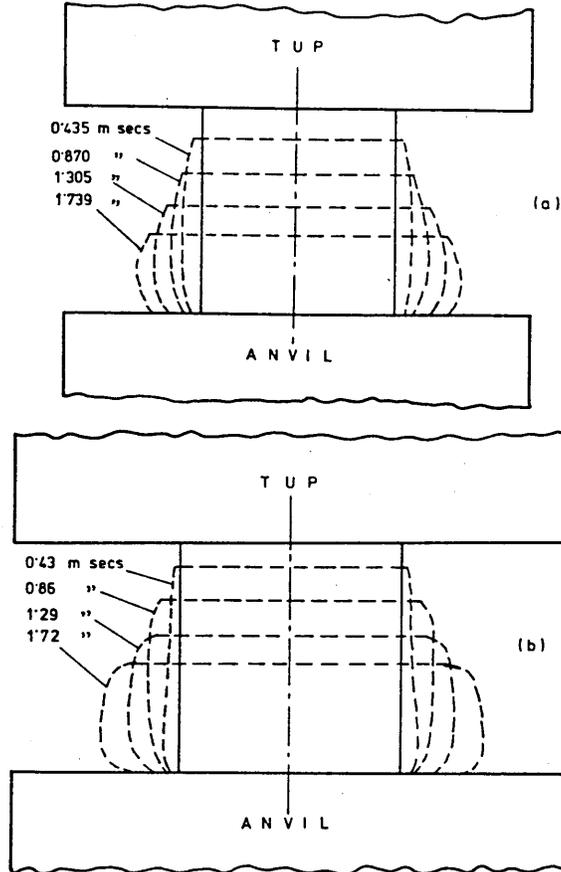
Fig.5a. Showing the instantaneous pro-
files of a lead billet deformed
under dry test condition, and

b. Corresponding instantaneous pro-
files predicted theoretically.

The prediction of a much lower die load
for lead billets points out the inad-
equacy of the present technique when
applied to strain rate sensitive mat-
erial.   For a non strain rate sensit-
ive material this method provides a
satisfactory means of predicting load
deformation characteristics.   In order
to compare the effect of end friction
the die load /deformation curves obt-
ained experimentally for aluminium
billets under lubricated and dry test
conditions are plotted in Fig.7.   The
corresponding predicted curves are also
shown in this figure.   It is seen that

a maximum increase in die load of less
than 10% occurs for reductions of billet
height of up to 16%.   The increase in
die load due to friction as predicted
using the numerical technique is slight-
ly less than that obtained experiment-
ally.

The increase in friction, when the
billet is deformed under dry test con-
ditions, results in increased barrell-
ing of the billet.   Fig.8. shows the
increase in radii at mid and top section
of the aluminum billet.   The extent

A5·12

Fig.7.   Comparing die load vs. deform-
          ation curves for aluminium
          billet deformed under lubrica-
          ted and dry test conditions.

g.6.   Variation in die load with def-
        ormation obtained experiment-
        ally and predicted theoretic-
        ally for (a) lead and (b)
        aluminium billets deformed
        under lubricated test condition.

barrelling can easily be estimated
om this figure.   The theoretically
edicted results suggest slightly less
rrelling of the billet.

p displacement-time curves were
tained using high speed photographs
ich upon graphical differentiation
ve velocity-time curve and hence
netic energy of the tup still unused
any time instant during the deform-
ion process.

Fig.8.   Showing the increase in radius
          at mid and top section with
          deformation for aluminium billet
          under dry test condition.

A5·13

Fig.9. Percent kinetic energy absorbed
vs. deformation curves for (a)
lead and (b) aluminium billets
deformed under lubricated test
condition.

Fig.10. Showing variation in billet
height during the in process
time for (a) lead and (b) alum
inium billets under lubricated
test conditions.

Fig.9. shows the
variation in percentage kinetic energy
absorbed with deformation for (a) lead
and (b) aluminium alloy billets both
deformed under lubricated test condit-
ions.   Tht theoretical curve for the
lead billet shows much less energy is
required when more than 55%reduction in
height is obtained.   This is again a
gross underestimation of the actual
energy requirement.   The analysis, by
neglecting strain rate sensitivity,
assumes low resistance of the billet to
deformation and hence predicts less

energy requirement for deformation.   On
the other hand, it is evident from Fig.
9(b), which shows similar kinetic energy
vs. deformation curves for the alumin-
ium alloy billet, that there is close
agreement between the experimental res-
ults of predictions obtained theoret-
ically.

Finally, the deformation vs. time curves
for lead and aluminium alloy billets
deformed under lubricated test conditi-
ons are shown in Fig.10(a) and (b) res-
pectively.

A5·14

It is seen that the exper-
ental and theoretical correlation is
ery good for lead billets for up to
5% deformation.   For aluminium billet
lose agreement exists during the whole
f the deformation process.

NCLUSIONS

periments were carried out on lead and
uminium alloy billets under a free
lling tup.   Results obtained from die
ad measurement and high speed photo-
aphs were compared with those predic-
d using numerical technique outlined
 reference (1).

was shown that the technique is inad-
uate for predicting load and energy
quirements for deforming lead billets,
t provide satisfactory predictions for
uminium alloy billets.   It is sugg-
ted that neglect of strain rate sens-
ivity in the analysis caused the dis-
epancy in the results for lead billets.

KNOWLEDGEMENTS

e authors gratefully acknowledge the
sistance given by Messrs.D.McKay,
.Fletcher and R.M.Wilkinson of the
partment of Mechanical and Production
gineering for making, commissioning
d instrumenting the drop hammer unit
d preparing test specimens.   They
so express their thanks to Mr.P.
scher of Visual Aids Unit for his
lp with high speed photography and
production of diagrams.   Thanks are
so due to Miss J.M.Webster for typing
e manuscript.

FERENCES

M.S.J.HASHMI and F.B.KLEMZ (1976).
The effect of friction in simple
upsetting of cylindrical billets of
elastic-plastic and elastic-strain
hardening material: A numerical
technique.   Proc.17th Int.MTDR Conf.
p-597

J.F. ALDER and K.A.PHILIPS (1954).
The effect of strain-rate and temp-
erature on the resistance of alu-
minium, copper and steel to comp-
ression. J.Inst.Metals, 83, p.80.

P.M.COOK, (1957). True stress-
strain curves for steel compress-
ion at high temperature and strain
rates. Proc.Conf.Prop at high
rates of strain, Inst.Mech.Engrs.
Paper 2.

L.E.MALVERN, (1965). Experimental
Studies of strain rate effects and
plastic wave propogation in annea-
led aluminium. Proc.ASME Coll. on
Behaviour of materials under dynam-
ic loading. p-81.

5. R.A.C.SLATER, S.Y.AKU and W.JOHN-
    SON (1968). Experiments in the
    fast upsetting of short pure lead
    cylinders and a tentative analysis.
    Int.J.Mech.Sci. vol 10, p-143.

6. S.K.SAMANTA (1968). Resistance to
    dynamic compression of low carbon
    steel and alloy steels at elev-
    ated temperatures and at high
    strain rates. Int.J.Mech.Sci.
    vol.10. p-613.

7. H.SUZUKI, et al (1968). Studies
    on the flow stress of metals and
    alloys, Report.Institute of Indus-
    trial Science, University of
    Tokyo. Vol.18 No.3.

8. S.K.SAMANTA (1969). On relating
    the flow stress of aluminium and
    copper to strain, strain-rate and
    temperature. Int.J.Mech.Sci.vol.
    11, p-433.

9. S.K.SAMANTA (1970). The dynamic
    compression testing of steels at
    elevated temperatures. Proc.11th
    Int.MTDR Conf. p-827.

10. C.E.N.STURGESS and A.N.BRAMLEY.
    (1970). The use of impact-forming
    device to obtain dynamic stress-
    strain data. Proc.11th Int.MTDR.
    Conf. p-803.

11. B.LENGYEL and M.MOHITPUR (1972)
    Dynamic stress-strain data to
    large strains, J.Inst.Metals. 100

12. M.MOHITPUR and B.LENGYEL (1975) A
    method of obtaining isothermal,
    constant high strain rate stress-
    strain data, Proc.16th Int.MTDR
    Conf. p-503.

13. G.L.BARAYA, W.JOHNSON and R.A.C.
    SLATER. (1965). The dynamic compress-
    ion of circular cylinders of super-
    pure aluminium at elevated temper-
    atures. Int.J.Mech.Sci. Vol.7.
    p-621.

14. A.T.MALE and M.G.COCKROFT (1964)
    A method for determination of the
    coefficient of friction of metals
    under conditions of bulk plastic
    deformation. J.Inst. of Metals.
    Vol.93. p-38.

15. S.C.JAIN and A.N.BRAMLEY. (1968)
    Speed and frictional effects in hot
    forging. Proc.Instn.of Mech.Engrs.
    Vol.182 p-783.

16. T.A.DEAN (1970). The influence of
    billet inertia and die friction in
    forging processes - A simple energy
    approach. 11th Int.MTDR.Conf. p-761

A5.15

CLOSED DIE FORGING OF AXISYMMETRIC SHAPES FROM CYLINDRICAL BILLETS OF STRAIN HARDENING AND STRAIN RATE SENSITIVE MATERIAL: EXPERIMENTAL RESULTS AND THEORETICAL PREDICTIONS

M. S. J. HASHMI and F. B. KLEMZ

Department of Mechanical and Production Engineering, Sheffield City Polytechnic

SUMMARY

Cylindrical lead billets were forged into axisymmetric shapes using dry and lubricated closed dies under a laboratory drop hammer. The experimental results were compared with those predicted theoretically using a numerical technique previously presented by the authors in references (17, 18). In this numerical technique the elastic strain hardening plastic and strain rate sensitive material property of the billet was incorporated. Effects of material inertia and die-billet interface friction on the tup load and product shape were also taken into account.

INTRODUCTION

In recent years a great deal of experimental and theoretical work has been carried out to investigate various aspects of high-energy rate forming in general and closed die forging and simple upsetting processes in particular. Published literature on the subject shows that most of the experimental studies were aimed at establishing dynamic stress-strain characteristics (1 - 12). Some other studies have been carried out putting forward analytical methods for predicting load-deformation behaviour and other aspects in simple upsetting and closed die forging incorporating, in some cases the effects of friction, material inertia and flash (13 - 16). However, almost all of these analyses involved very cumbersome and lengthy derivation in some approximate form.

In references (17, 18) the authors presented a finite-difference numerical technique for predicting load and deformation behaviour in simple upsetting of elastic-strain hardening plastic and strain rate sensitive material. The effects of material inertia and interface friction were also incorporated. In this study experiments were carried out under a laboratory drop hammer, forging cylindrical lead billets into simple axisymmetric shapes using dry and lubricated closed dies. The forging load initial impact velocity and tup-displacement were measured experimentally. The above mentioned numerical technique was then used to theoretically predict the deformation behaviour of the billet incorporating material inertia, strain rate sensitivity and die-billet interface friction. These predicted results were compared with those obtained experimentally. The detailed description of the numerical technique has previously been given in references (17, 18) and hence will not be repeated in this paper.

EXPERIMENTAL EQUIPMENT AND PROCEDURE

Initially, simple upsetting tests were carried out to establish the dynamic stress-strain properties of the lead under consideration. It was found that the lead showed considerable strain hardening effect for strain rates between about 1 to 500 per second, the quasi-statically obtained stress-strain curve showed no such strain hardening effect. Similar observations were also made in reference (4) for pure lead.

These experimentally determined dynamic stress-strain curves were found to fit closely the strain rate sensitivity equation $\sigma = \sigma_1[1 + (\frac{\dot{e} - \dot{e}_1}{D})^{1/p}]$ where σ is the dynamic flow stress corresponding to strain rates, $\dot{e}_1$ of up to 500 per second and σ_1 is the flow stress corresponding to strain rate $\dot{e}_1$ equal to 1 per second. The constants of strain rate sensitivity D and p were found to be 100 s^{-1} and 0.65 respectively. These experimentally established static and dynamic stress-strain curves are shown in Fig 1.
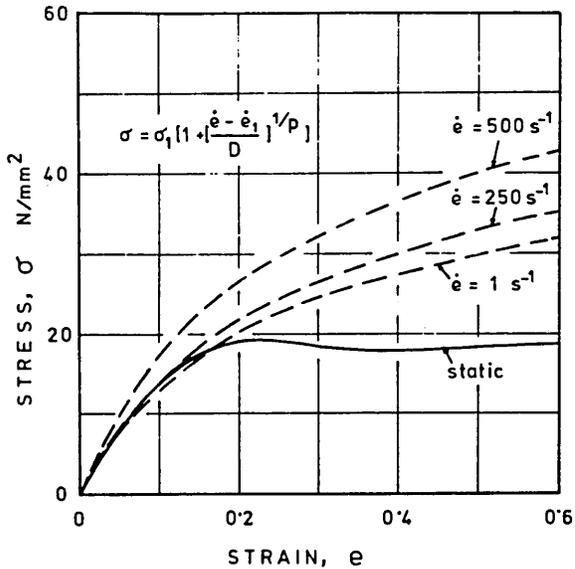
Fig 1   Static and dynamic stress-strain curves for commercially pure lead.

Fig 2   Showing (a) cylindrical lead billet and (b) final deformed shape.

Commercially pure lead cylindrical billets, 24 mm in diameter and 46 mm in height, were forged into axisymmetric shape as shown in Fig 2, using a laboratory drophammer. The schematic diagram in Fig 3 shows the loading arrangement of the billet under the drop hammer. The die-billet assembly was placed on top of the "strain gauge incorporated" tool steel load-cell and the load time trace was recorded using transient recorder CRO and/or a X - Y graph plotter. The tup velocity just before impact and the tup displacement time trace were also recorded simultaneously using transient recorder, photo-cell unit and electronic counters.
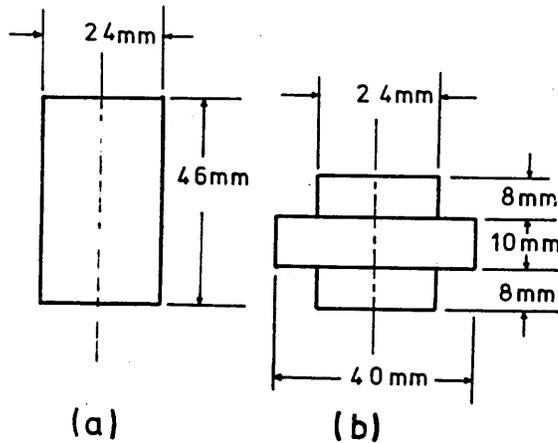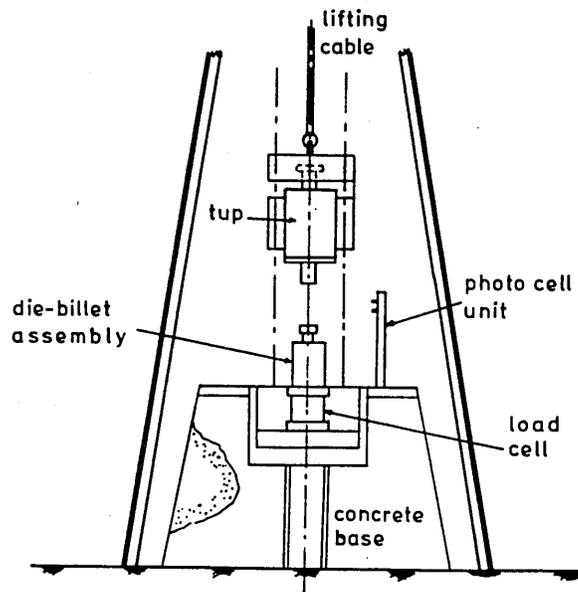
Fig 3   Schematic diagram showing the loading arrangement under the drop hammer.

A5·17

RESULTS AND DISCUSSION

Experimental results were obtained from forging tests carried out on lead billets under lubricated and dry friction conditions. In both cases the tup of mass 17 Kg was allowed to fall freely on top of the die-billet assembly giving equivalent impact velocity of 9 m/s.

Analysis was undertaken for each loading situation using the numerical technique described in references (17, 18). The stress-strain properties depicted in Fig 1 were incorporated into the analysis. The effects of material inertia and interface friction at the die-billet constraint were also taken into account. The die-load, instantaneous billet profiles, die pressure and strain rate within the billet were predicted theoretically and compared with experimental results where appropriate.

The actual loading configuration of the billet is shown in Fig 4 (a) and the equivalent numerical model is shown in Fig 4 (b). The instantaneous profiles of the billet were predicted theoretically or both the lubricated and dry friction orging conditions. In the analysis, he friction factor for dry friction ondition was taken as unity whilst for ubricated condition it was taken as

zero along any die-billet interface. For shearing friction within the billet at the die-billet constraint the friction factor was again taken as unity rendering sticking friction. Fig 5 (a) shows theoretically predicted instantaneous profiles at various times during the deformation process for a billet forged under lubricated condition. The instantaneous profiles for a billet forged under dry friction conditions are shown in Fig 5 (b). It was not possible to record the experimental instantaneous profiles due to the nature of the forming process. Therefore, only the corresponding experimentally obtained final profiles are shown in these figures. It is clearly evident that forging under dry friction condition gives rise to considerable barrelling of the billet during the deformation process. This causes the billet material to get into the flash land relatively earlier than under lubricated forging condition.
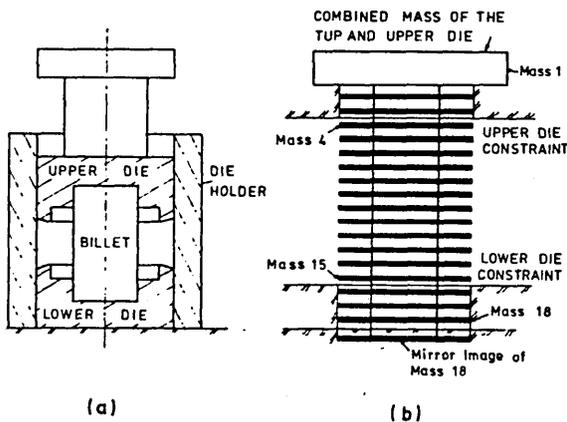

(a)

(b)

(a)

(b)

ig 4   Showing (a) actual loading configuration of the billet and (b) corresponding equivalent numerical model.
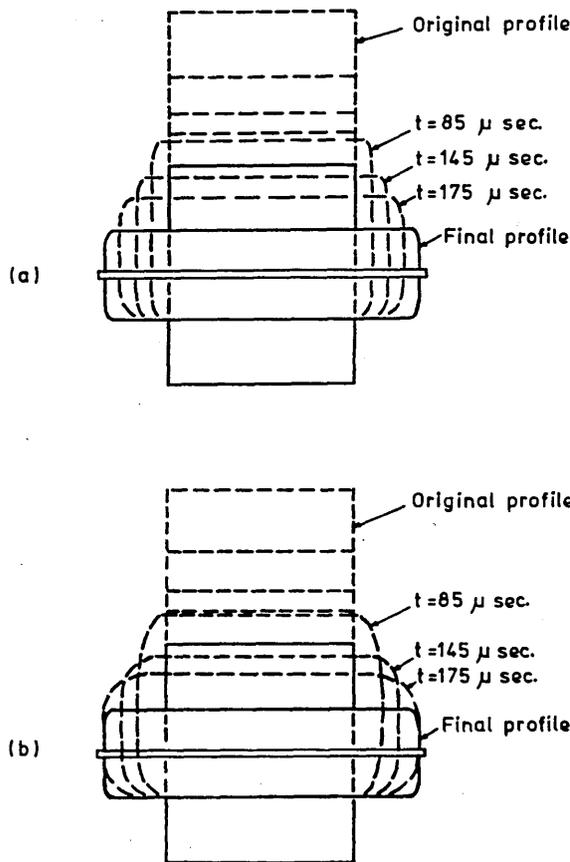
Fig 5   Theoretically predicted instantaneous profiles under (a) lubricated and (b) dry friction condition.

In Fig 6 the variations in forging loads with tup displacement measured experimentally are compared with those predicted theoretically for forging under lubricated and dry friction condition. The effects of strain rate and material inertia on the forging load was found to be .significant when the experimentally established dynamic stress-strain properties shown in Fig 3 were incorporated in the analysis. The agreement between the theoretical and experimental forging load under both frictional conditions show close agreement. Fig 6 also shows quasi-static forging load under dry friction condition. This static load is seen to be considerably lower than both the experimental and theoretically predicted dynamic forging loads. This discrepancy may be explained by the apparent strain hardening of lead under consideration under dynamic loading conditions.
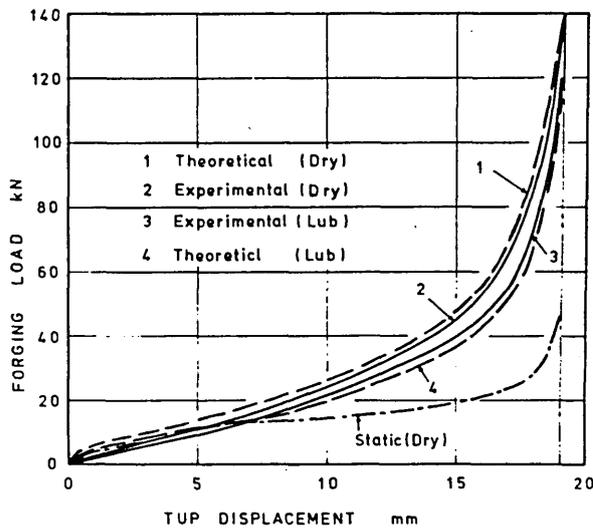

Fig 6   Comparison of experimental and theoretical forging load Vs tup-displacement curves.

The instantaneous profiles in Fig 5 (a) and (b) showed barrelling of the billet in a qualitative manner. In Fig 7 this is shown in a quantitative manner in terms of the variation in the billet radius at mid-section and at the die-billet constraints. It is clearly evident from this figure that forging under dry friction condition causes the billet radius at mid-span to increase at relatively faster rate with deformation than under lubricated forging condition. This may result in appreciable loss of material as flash.

The theoretically predicted variation in strain rate at mid-section and at the section along the die-billet constraint is shown in Fig 8 for lubricated and dry friction conditions. This figure shows that during most of the deformation process the maximum strain rate within
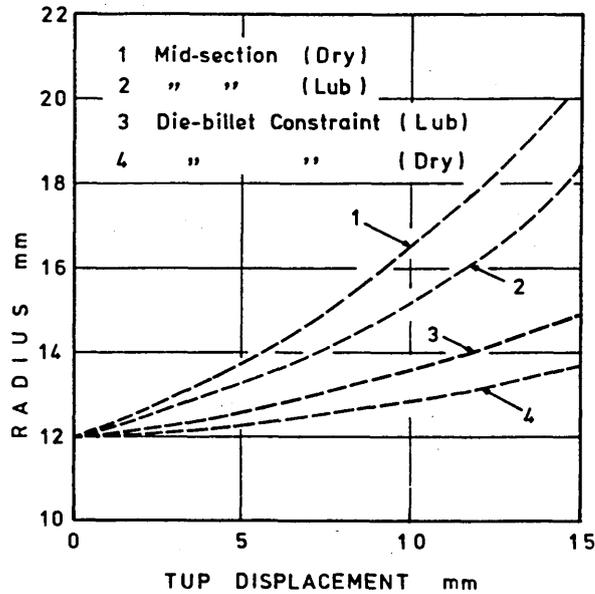

Fig 7   Variation in billet radius with tup-displacement at mid-section and die-billet constraint.
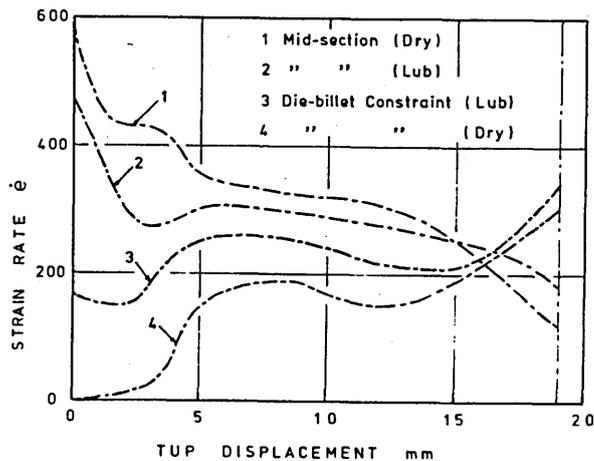

Fig 8   Variation in strain rate with tup-displacement at mid-section and die-billet constraint.

the billet remains below about 350 per
second for impact velocity of 9 m/s and
hence makes no appreciable difference in
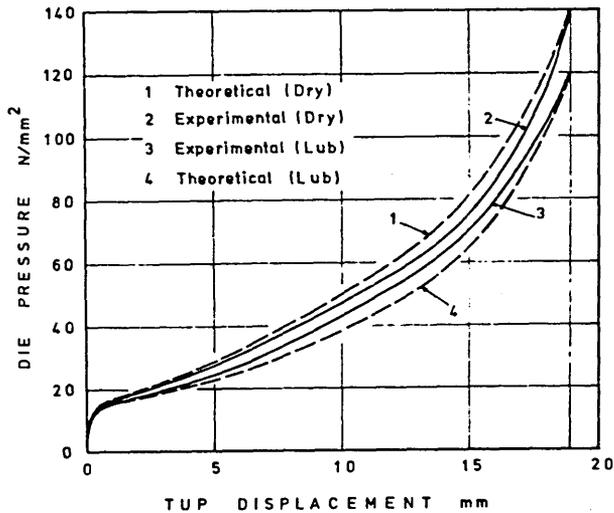the forging load at later stages of
deformation.

Fig 9   Showing die-pressure Vs tup-
         displacement curves predicted
         theoretically and obtained
         experimentally.

Finally, comparison of the theoretically
estimated die pressures with those
obtained experimentally as shown in Fig 9
shows close agreement under both forging
conditons. It is evident, however, that
in the case of dry friction, the theoret-
ically predicted die pressure is slightly
greater than that obtained experiment-
ally whilst this trend is reversed in the
case of lubricated forging condition.
The main reason for this behaviour could
be the fact that for dry friction condition
the friction factor was taken as unity
and for lubricated friction conditions
its value was taken as zero in the
theoretical calculations.

In actual forging situations it is most
unlikely that these limiting frictional
conditions were exactly the same, although
great care was taken to meet these
conditions as closely as possible.
"Graphite in petroleum jelly" was used
as lubricant for lubricated forging
operations.

CONCLUSIONS

Cylindrical lead billets were forged
into axisymmetric shapes using closed
dies under dry friction and lubricated
condition. Experimentally obtained
forging loads were compared with those
predicted theoretically using a numerical
technique previously outlined in
references (17, 18). The effects of
material inertia and strain rate were
incorporated into the analysis and the
predicted results showed close
agreement with those obtained experiment-
ally.

REFERENCES

1. J.F. ALDER and K A PHILLIPS (1954).
     The effect of strain-rate and
     temperature on the resistance of
     aluminium, copper and steel to
     compression. J Inst Metals, 83,
     p 80.

2.   P M COOK, (1957). True stress-
     strain curves for steel compress-
     ion at high temperature and strain
     rates. Proc Conf Prop at high
     rates of strain, Inst Mech Engrs.
     Paper 2.

3.   L E MALVERN, (1965). Experimental
     Studies of strain rate effects and
     plastic wave propogation in
     annealed aluminium. Proc ASME
     Coll on Behaviour of materials
     under dynamic loading. P-81.

4.   R A C SLATER, S Y AKU and
     W JOHNSON (1968). Experiments in
     the fast upsetting of short pure
     lead cylinders and a tentative
     analysis. Int J Mech Sci Vol 10,
     p 143.

5.   S K SAMANTA (1968). Resistance to
     dynamic compression of low carbon
     steel and alloy steels at
     elevated temperatures and at high
     strain rates. Int J Mech Sci,
     Vol 10, p 613.

6.   H SUZUKI, et al (1968). Studies
     on the flow stress of metals and
     alloys, Report Institute of
     Industrial Science, University of
     Tokyo. Vol 18, No 3.

7.   S K SAMANTA (1969). On relating
     the flow stress of aluminium and
     copper to strain, strain-rate and
     temperature. Int J Mech Sci,
     Vol 11, p 433.

8.   S K SAMANTA (1970). The dynamic
     compression testing of steel at
     elevated temperatures. Proc 11th
     Int MTDR Conf, p 827.

9.   C E N STURGESS and A N BRAMLEY
     (1970). The use of impact-forming
     device to obtain dynamic stress-
     strain data. Proc 11th Int MTDR
     Conf, p 803.

10. B LENGYEL and M MOHITPUR (1972).
     Dynamic stress-strain data to
     large strains. J Inst Metals, 100.

11. M MOHITPUR and B LENGYEL (1975).
     A method of obtaining isothermal,
     constant high strain rate stress-
     strain data, Proc 16th, Int MTDR
     Conf, p 503.

12. G L BARAYA, W JOHNSON and
     R A C SLATER. (1965). The dynamic
     compression of circular cylinders
     of super-pure aluminium at elevated
     temperatures. Int J Mech Sci, Vol 7
     p 621.

13. S C JAIN and A N BRAMLEY, (1968).
     Speed and frictional effects in hot
     forging. Proc Instn of Mech Engrs,
     Vol 182, p 783.

14. T A DEAN (1970). The influence of
     billet inertia and die friction in
     forging processes - A simple energy
     approach. 11th Int MTDR Conf, p 761.

15. R P McDERMOTT and A N BRAMLEY (1974).
     An elemental upper-bound technique
     for general use in forging analysis.
     Proc 15th Int MTDR Conf, P 437.

16. T A DEAN (1976). The mechanics of
     flash in drop forging - temperature
     and speed effect. Proc Inst Mech
     Engrs, Vol 190-33/76, p 457.

17. M S J HASHMI and F R KLEMZ (1976).
     The effect of friction in simple
     upsetting of cylindrical billets of
     elastic-plastic and elastic-strain
     hardening material : A numerical
     technique. Proc 17th Int MTDR
     Conf, p 597.

18. M S J HASHMI (1977). A numerical
     technique for analysing simple
     upsetting of cylindrical billets
     of strain rate sensitive material.
     Proc 18th Int MTDR Conf, p 27.

A5·21